At the heart of the universe is a steady, insistent beat: the sound of cycles in sync. It pervades nature at every scale from the nucleus to the cosmos. Every night along the tidal rivers of Malaysia, thousands of fireflies congregate in the mangrove and flash in unison, without any leader or cue from the environment. Trillions of electrons march in lockstep in a superconductor, enabling electricity to flow through it with zero resistance. In the solar system, gravitational synchrony can eject huge boulders out of the asteroid belt and toward Earth; the cataclysmic impact of one such meteor is thought to have killed the dinosaurs. Even our bodies are symphonies of rhythm, kept alive by the relentless, coordinated firing of thousands of pacemaker cells in our hearts. In every case, these feats of synchrony occur spontaneously, almost as if nature has an eerie yearning for order.

Strogatz, 2003

University of Alberta

Characterisation of the sleep-related slow oscillation in the neocortical – entorhinal – hippocampal bidirectional circuit

by

Trisha Denise Wolansky

A thesis submitted to the Faculty of Graduate Studies and Research
in partial fulfillment of the requirements for the degree of

Doctor of Philosophy

Centre for Neuroscience

Fall 2009
Edmonton, Alberta

Examining Committee

Dr. Clayton T. Dickson, Psychology, Physiology, and Centre for Neuroscience

Dr. Christopher B. Sturdy, Psychology and Centre for Neuroscience

Dr. John J. Greer, Physiology and Centre for Neuroscience

Dr. Kelvin E. Jones, Physical Education and Centre for Neuroscience

Dr. Jeremy B. Caplan, Psychology and Centre for Neuroscience

Dr. C. Andrew Chapman, Psychology and Centre for Studies in Behavioural Neurobiology, Concordia University, Montréal, Québec, Canada

Abstract

Our ability to recall information and events is astounding and dependent on the medial temporal lobe (MTL) memory system. The synaptic interconnections between the neocortex (nCTX), entorhinal cortex (EC), and hippocampus (HPC) are the anatomical basis of this memory system. The electrophysiological basis of memory formation in this system is largely unknown, but the activity patterns that occur during slow wave sleep (SWS) are thought to play an important role. One prominent activity pattern that occurs during SWS is the slow oscillation (SO). It is a large-amplitude rhythm of ~1Hz that was first described in the nCTX and only occurs during SWS and deep anaesthesia. Using the urethane-anaesthetised rat, I provide the first description of the SO in the HPC in *Chapter 2*. I found that the SO in the HPC was dynamically coordinated with that in the nCTX. Because the EC is the anatomical interface between the nCTX and HPC, I hypothesised that it could be responsible for this coordination. *Chapter 3* characterises the SO in the EC and its coordination with both the nCTX and HPC. My results suggested that the synaptic interconnections between the nCTX and HPC via the EC were not solely responsible for SO coordination across these structures. Another possibility is that SO coordination across the nCTX, EC, and HPC occurs via the nucleus reuniens thalami (NReu). In *Chapter 4*, I delivered trains of electrical stimulation to the frontal cortex (fCTX) to enhance the SO in the nCTX and assess any effect in the HPC. In addition, I delivered the same stimulation trains directly to the medial prefrontal cortex (mpfCTX) and NReu. I found that repeated stimulation in each structure entrained the hippocampal SO. I also found

that repeated stimulation of the fCTX and mpfCTX enhanced SO coordination across the nCTX and HPC, but repeated stimulation of the NReu did not. My results suggested that SO coordination across the nCTX and HPC occurs via both the EC and NReu. Understanding the coordination of SO activity across these structures will provide insight to the electrophysiological basis of the MTL memory system and the role of SWS in its function.

Acknowledgements

I would like to acknowledge the time, energy, and support of my supervisor, Dr. Clayton T. Dickson, as well as that given by the rest of my supervisory committee: Dr. Christopher B. Sturdy and Dr. John J. Greer. Thank you to Dr. Kelvin E. Jones, Dr. Jeremy B. Caplan, and Dr. C. Andrew Chapman for participating in my thesis defence. I would also like to thank all members of the Brain Rhythms Lab, past and present for their hard work and dedication. Finally, I would like to acknowledge the love and support of my family and friends – I could not have done this without you.

Chapter 1: This study was supported by a Natural Science and Engineering Research Council (NSERC: Canada) grant RGPIN 249861 to CTD. CTD is an Alberta Heritage Foundation for Medical Research (AHFMR) Scholar. SRP was supported by NSERC and AHFMR summer studentships. Multi-channel silicon probes were kindly provided by the University of Michigan Center for Neural Communication Technology, sponsored by NIH/NCRR grant P41-RR09754.

Chapters 2 and 3: This study was supported by a Canadian Institutes of Health Research (CIHR) grant MOP77625 to CTD. CTD is an AHFMR Senior Scholar. TW was supported by an NSERC post-graduate studentship.

Table of Contents

List of Tables

Chapter 3: The Slow Oscillation is a Feature of Both the Input and Output Layers of the Entorhinal Cortex

List of Figures

Chapter 1: Introduction

Chapter 2: Hippocampal Slow Oscillation: A Novel EEG State and Its Coordination with Ongoing Neocortical Activity

Chapter 3: The Slow Oscillation is a Feature of Both the Input and Output Layers of the Entorhinal Cortex

Chapter 4: Slow-Frequency Stimulation of the Neocortex Entrains the Slow Oscillation in the Hippocampus

List of Abbreviations

Acetylcholine	ACh
Alveus	Alv
Autocorrelation	AC
Average	Avg
Cornu ammonis 1	CA1
Cornu ammonis 2	CA2
Cornu ammonis 3	CA3
Cross-correlation	X-Corr
Current source density	CSD
Dentate gyrus	DG
Electroencephalogram	EEG
Electromyogram	EMG
Entorhinal cortex	EC
Deep	deep EC
Layer II	LII
Layer III	LIII
Layer V	LV
Superficial	supEC
Eserine	eser
Experiment	Exp
Frontal cortex	fCTX
Deep	fCTX deep
Superficial	fCTX sup
γ – aminobutyric acid	GABA
Hippocampal fissure	fiss
Hippocampus	HPC
Intraperitoneal	*i.p.*
Intravenous	*i.v.*

Large-amplitude irregular activity	LIA
Left	L
Local field potential	LFP
Low-voltage fast activity	LVFA
Medial prefrontal cortex	mpfCTX
Medial temporal lobe	MTL
Minimum alveolar concentration	MAC
Multiprobe channel	MP Ch
Multiunit	MU
Neocortex	nCTX
Non-rapid eye movement	non-REM
Not significant	NS
Parahippocampal cortex	Para
Perforant path	PP
Perirhinal cortex	Peri
Positive	Pos
Posterior cortex	pCTX
Potassium	K^+
Rapid eye movement	REM
Rectified	rect
Respiration	resp
Retrosplenial cortex	RSP cortex
Right	R
Slow oscillation	SO
Slow wave sleep	SWS
Sodium	Na^+
Spike-triggered average	STA
Spontaneous	spon
Stimulation	stim/STIM
Stratum granulosum	SGran

Stratum lacunosum moleculare	SLM
Stratum lucidum	SLu
Stratum moleculare	SMol
Stratum oriens	SOr
Stratum pyramidale	SPyr
Stratum radiatum	SRad
Subiculum	Subic
Theta	TH
Triggered-average	TA

Chapter 1:

Introduction

Part 1: General Introduction

The ultimate goal of neuroscience is to understand how behaviour is related to brain function. One of the most intriguing elements of this relationship is memory – the ability of the brain to retain relevant information and apply it at a later time.

The medial temporal lobe memory system. The entorhinal cortex (EC) and hippocampus proper (HPC) are part of a mnemonic system that is critical for the encoding and retrieval of declarative or episodic long-term memories – those for facts and events. Much of what is known about the episodic memory system, including the roles of the HPC and EC, somehow stems from the famous patient H.M.

H.M. underwent surgery for intractable epilepsy; he received a bilateral removal of his medial temporal lobe (MTL) including all or parts of: the HPC, amygdala, perirhinal cortex, and EC. Following extensive assessment of H.M., several observations and conclusions were made regarding the function of this brain region. First, severe damage to the MTL resulted in anterograde amnesia – the inability to acquire new long-term memories for facts and events. It also resulted in a temporally graded retrograde amnesia – the inability to remember past events such that memories of events occurring close to the time of lesion are more susceptible to loss as compared to memories of distant events (**Figure 1-01**). This suggested that the MTL is not a permanent storage site for episodic mnemonic information. Second, H.M. exhibited no loss in other cognitive or perceptual abilities suggesting that episodic memory is an entirely dissociable

cognitive ability. Finally, MTL damage did not impair short-term or other forms of long-term learning and memory suggesting that the mnemonic function of the MTL is limited to the long-term episodic type (Scoville, 1954; Scoville and Milner, 1957; Milner, 1972).

Squire and Zola-Morgan formally defined the MTL memory system to consist of the HPC, dentate gyrus (DG), subiculum (Subic), EC, perirhinal cortex, and parahippocampal cortex in 1991 (**Figure 1-02**). They also reiterated its involvement in the acquisition and retention of long-term episodic memories. The interconnections among these structures are the anatomical substrates of this memory system. Briefly, neocortical sensory association areas (*red*) funnel multimodal information into the EC via the parahippocampal and perirhinal cortices (*green*). The EC transmits processed information into and receives processed information from the HPC (*blue*) and sends it back to the neocortical association areas from which it was originally received (**Figure 1-02**).

Sleep. Evidence suggests that the processing and eventual storage of episodic mnemonic information is dependent on brain activity that occurs during sleep (reviewed in: Buzsáki, 1998; Hasselmo, 1999; Peigneux et al., 2001; Tononi and Cirelli, 2001; Ribeiro and Nicolelis, 2004; Walker and Stickgold, 2004; Rauchs et al., 2005). The general behavioural state of sleep in mammals can be roughly be broken down into rapid eye movement (REM) and non-REM. Non-REM sleep can be further broken down into several distinct brain states (**Figure 1-03**) observable in the electroencephalogram (EEG).

Low-voltage fast activity (LVFA) in the neocortical EEG is gradually replaced by higher amplitude lower frequency activity such as alpha (8 to 12Hz) and spindles (7 to 14Hz) in stages 1 and 2 of non-REM sleep. As sleep deepens in stages 3 and 4, delta (1 to 4Hz) and the slow oscillation (SO; ≤ 1Hz) dominate the EEG. REM is the deepest stage of sleep but the EEG is characterised by wake-like LVFA in the neocortex (nCTX) and theta (3 to 12Hz) in the HPC. Throughout a night of sleep, brain activity alternates between these stages several times. In the early night, more time is spent in stage 4 – deep slow wave sleep (SWS). Later in the night, more time is spent in REM sleep (**Figure 1-03**).

Thesis background. One analogy I like to use to describe my research is two-way radios: multiple people can communicate over long distances using them as long as each radio is on the same channel (i.e., frequency). The same principal can be applied to the brain: different parts of the brain can communicate if they're "on the same channel" or oscillating at the same frequency. Fast frequencies tend to synchronize over relatively short distances and slow frequencies tend to synchronize over longer distances. Therefore, if structures are spread out in the brain (e.g., the nCTX, EC, and HPC), they are more likely to communicate via slow frequencies.

Neuronal synchronisation is a critical factor in synaptic plasticity (Lynch et al., 1977; McNaughton et al., 1978; Levy and Steward, 1979; Barrionuevo and Brown, 1983; Bramham and Srebro, 1987; Stanton and Sejnowski, 1989; Dan and Poo, 2004). Synchronised interactions across distant brain areas at slow frequencies could then be a suitable platform for synaptic plasticity across the

nCTX, EC, and HPC. Rhythmic slow frequency (≤ 1Hz) oscillations only occur naturally during SWS, but are also observed during anaesthesia. In fact, sleep is the most commonly used metaphor for anaesthesia (Shafer, 1995).

There are several similarities between the behavioural states of sleep and anaesthesia including: a subjective loss of consciousness, reduced sensory sensitivity, and reduced behavioural responsiveness. There are also several obvious differences; for example, one can be roused from sleep but not from anaesthesia. Many anaesthetic agents induce a unitary deactivated brain state rather than cyclic alternations similar to those that occur during sleep. Urethane is a highly toxic, but commonly used veterinary anaesthetic (Koblin, 2002). It is thought to induce anaesthesia by increasing leak conductance and decreasing neuronal excitability (Sceniak and Maciver, 2006). One of the main advantages of using urethane experimentally is that it is metabolised very slowly, inducing a state of anaesthesia that can last several hours. Another advantage is that brain states spontaneously alternate in a manner that is virtually identical to natural sleep (Wolansky et al., 2006; Clement et al., 2008). Many other physiological correlates of sleep are also comparable between the two behavioural conditions (Clement et al., 2008).

Thesis overview. I used urethane anaesthesia as a model of natural sleep to explore the potential presence and coordination of slow oscillatory brain rhythms across the nCTX, EC, and HPC. We found that the neocortical SO during the deactivated state of urethane anaesthesia was accompanied by a similar oscillation of ~1Hz in the HPC. This hippocampal SO modulated the activity in the majority

of neurons we recorded and modulated the occurrence of other deactivated state-related rhythms. It was dynamically coordinated with activity in the nCTX and was largest near the hippocampal fissure where one of the main entorhinal inputs to the HPC terminates. Based on this and the broader organisation of the neocortical – entorhinal – hippocampal loop, we speculated that the EC may play an important role in the coordination of the SO across the HPC and nCTX.

We found that the SO was present in the EC during the deactivated state and was coordinated with similar activity in the HPC and nCTX. It was largest in the superficial layers (which contain the cells giving rise to hippocampal input) but was more coherent with the hippocampal SO in the deep layers (which receive the bulk of hippocampal output). In addition, cellular activity in the deep layers was modulated by the SO more robustly than that in the superficial layers. These data indicated that the SO is a significant feature of both the input to and output from the HPC. They also suggest that the EC is not the sole mediator of neocortical – hippocampal SO coordination.

The coordination of the SO could also be mediated via a poorly studied neocortical – midline thalamic – hippocampal pathway. This pathway begins in the medial prefrontal cortex (mpfCTX), and passes through the nucleus reuniens thalami (NReu) before sending projections to both the HPC and EC. The termination zones of this pathway are the same regions where the SO was observed to be largest. Potentially, this is a compelling hypothesis of SO coordination since the neocortical SO is thought to arise preferentially from the frontal cortex (fCTX) (Massimini et al., 2004; Murphy et al., 2009).

We compared the effects of electrical stimulation across the surface of the fCTX, direct stimulation of the mpfCTX, and direct stimulation of the NReu. In general, we found that trains of low amplitude and slow frequency stimulation across the fCTX enhanced the SO power in the HPC but identical trains delivered to the mpfCTX and NReu did not. Repeated trains of stimulation in each of the fCTX, mpfCTX, and NReu appeared to entrain the hippocampal SO. However, SO coordination between the HPC and nCTX was only enhanced during repeated fCTX and mpfCTX stimulation. Our data suggest that the hippocampal SO can be entrained by both the fCTX – EC – HPC and mpfCTX – NReu – HPC synaptic circuits but that these circuits differentially mediate SO coordination across the nCTX and HPC.

Figure 1-01:

Retrograde versus anterograde amnesia

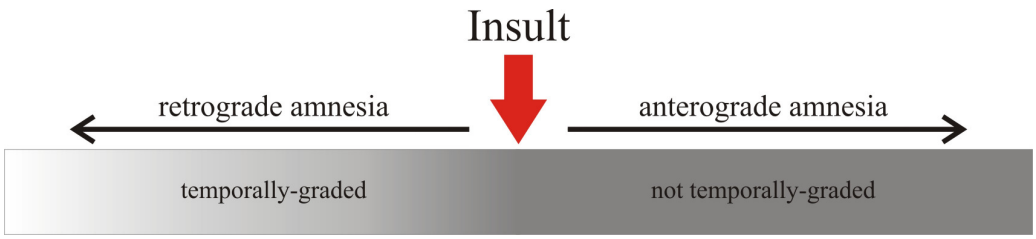

Damage to the HPC results in two different types of amnesia: retrograde and anterograde. Retrograde amnesia refers to a loss of episodic memories that were acquired prior to hippocampal damage. Memories for events that occurred close to the time of insult are more susceptible to loss as compared to those for events farther back in time, thus retrograde amnesia is referred to as temporally-graded. Anterograde amnesia refers to an inability to acquire new episodic memories following hippocampal damage. Abbreviations: hippocampus (HPC)

Figure 1-02:

The medial – temporal lobe memory system

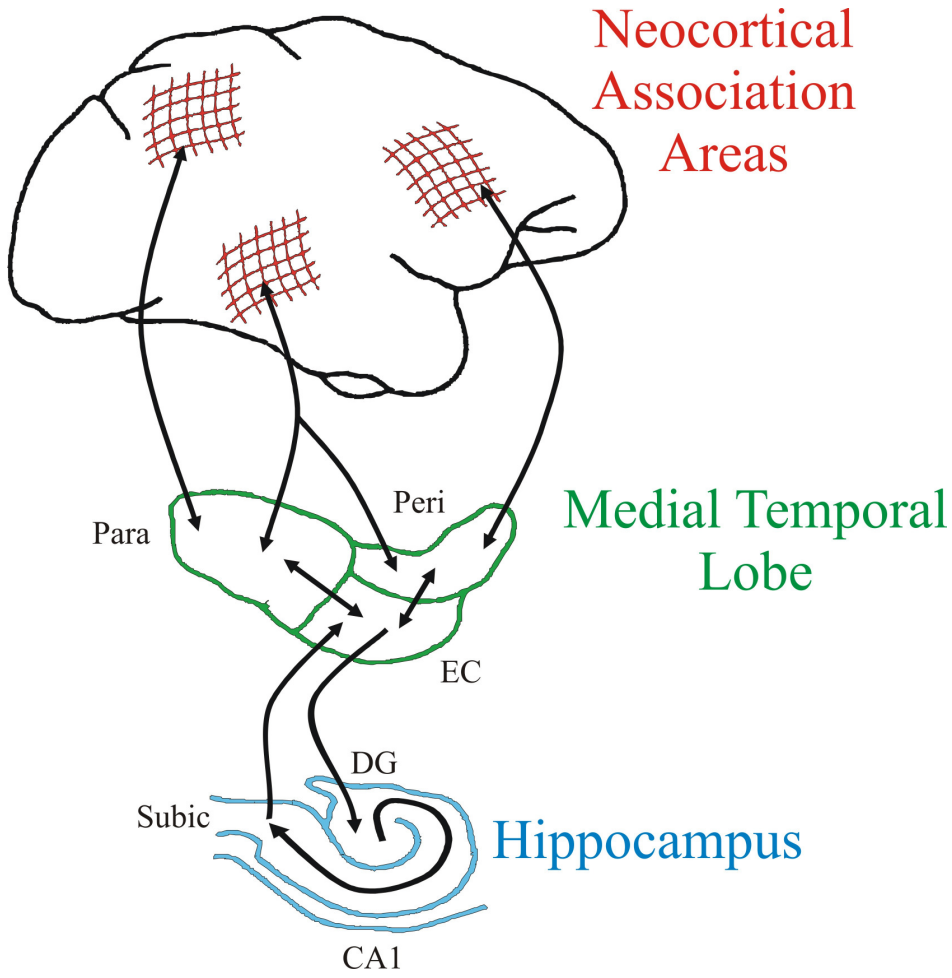

Figure 1-02 Caption:

The MTL memory system was coined by Squire and Zola-Morgan in 1991. The interconnections between these structures are the anatomical substrates of this memory system. Neocortical sensory association areas (*red*) funnel multimodal information into the EC via the parahippocampal and perirhinal cortices (*green*). The EC transmits processed information into and receives processed information from the HPC (*blue*) and sends it back to the neocortical association areas from which it was originally received. Adapted from: Squire and Zola-Morgan, 1991. Abbreviations: cornu ammonis 1 (CA1), dentate gyrus (DG), entorhinal cortex (EC), medial temporal lobe (MTL), parahippocampal cortex (Para), perirhinal cortex (Peri), subiculum (Subic)

Figure 1-03:

The General Structure of Sleep

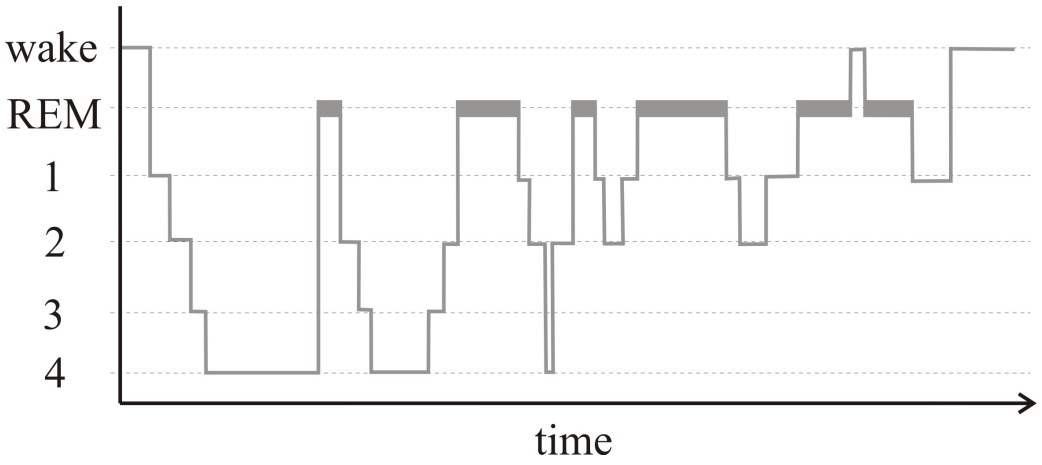

The EEG during stages 1 and 2 of sleep is characterised by higher amplitude lower frequency activity such as alpha (8 to 12Hz) and spindles (7 to 14Hz). As sleep deepens in stages 3 and 4, delta (1 to 4Hz) and the SO (≤ 1Hz) dominate the EEG. REM is the deepest stage of sleep but the EEG is characterised by wake-like low amplitude high frequency activity in the nCTX and theta (3 to 12Hz) in the HPC. Throughout a night of sleep, brain activity alternates across these stages several times. In the early night, more time is spent in stage 4 – SWS. Later in the night, more time is spent in REM sleep. Abbreviations: electroencephalogram (EEG), hippocampus (HPC), neocortex (nCTX), rapid eye movement (REM), slow oscillation (SO), slow wave sleep (SWS)

Part 2: Anatomy and Physiology of the Hippocampal and Entorhinal Cortices

The HPC and EC are the two structures at the heart of the MTL memory system (**Figure 1-02**) – a larger neural network that also consists of the parahippocampal and perirhinal cortices. The anatomy and physiology of these structures individually as well as their synaptic interconnections are pivotal to their function in the MTL memory system.

Highly processed, multimodal sensory information from neocortical association areas is funnelled into the MTL. This information is processed through multiple stages of a (mostly) unidirectional loop beginning with the EC, passing through the major subdivisions of the HPC, and eventually back to the EC which returns the original cortical projection. This circuit will be described further below.

Hippocampus

The brain structure we now know as the HPC was originally named by the anatomist Arantius (1587) because of its structural resemblance to a sea horse; in Greek, *hippos* meaning "horse" and *kampos* meaning "sea monster" (as cited in: Amaral and Lavenex, 2007).

Gross Anatomy. In humans, the HPC sits at the inner surface of the MTL (*top panel* of **Figure 4**) and in rats, it accounts for a large proportion of the total brain mass (*bottom panel* of **Figure 4**). Slicing through the HPC in the transverse plane reveals that it appears as an interlocking "C" and "V". The cornu ammonis

(CA) and Subic subdivisions make up the "C" and the "V" is the DG. Based on connectivity and cytoarchitectural differences, region CA can be further subdivided into regions CA3, CA2, and CA1 (summarised in: Amaral and Witter, 1995; Amaral and Lavenex, 2007). **Figure 1-05** is a diagrammatical representation of: the DG (*red*) and hilus (*light blue*), CA3 (*dark blue*), CA2 (*not shown*), CA1 (*green*), and Subic (*orange*).

Cytoarchitecture. Hippocampal neurons fall into one of two general categories: principal neurons and interneurons. The principal neurons of the HPC are pyramidal neurons and the principal neurons of the DG are granule cells (**Figures 1-06**). In region CA, the cell bodies of pyramidal neurons are located in stratum pyramidale (SPyr). Their apical dendrite extends superficially toward the hippocampal fissure, branching in stratum radiatum (SRad) and stratum lacunosum – moleculare (SLM). SLM is the most superficial lamina of the HPC and lies adjacent to the hippocampal fissure. The basal dendrites of CA pyramids are located dorsally in stratum oriens (SOr). Their axons primarily travel via the alveus (Alv) – a thin layer of white matter that lies immediately ventral to the nCTX. The alveus is composed of both hippocampal afferent and efferent fibres.

The cell bodies of granule cells are located in stratum granulosum (SGran) which makes up the "V" of the DG (**Figure 1-06**). Their dendrites extend superficially towards the hippocampal fissure or the ventricular surface into stratum moleculare (SMol). Inside the "V" of SGran lies the hilus – a polymorphic cell layer composed mostly of inhibitory interneurons. To summarise, the hippocampal laminae progressing from dorsal to ventral through a

coronal section of dorsal CA1 are (**Figure 1-06B**): the alveus, SOr, SPyr, SRad, SLM and then across the hippocampal fissure into the DG. In the DG, the laminae from dorsal to ventral are: SMol, SGran, and the hilus.

There are multiple subtypes of interneurons positioned within each of the hippocampal laminae. They modulate the activity of both principal neurons and other local interneurons. The local field potential (LFP; *see below* and *Appendix A*) and multiunit (MU) activity are two representations of the net interactions between principal neurons and interneurons.

Intrinsic connections. As mentioned above, information flows through the MTL in a (mostly) unidirectional manner (**Figure 1-07**). Input from the superficial layers of the EC (supEC) to the DG (perforant path; *see below)* is transmitted from the DG to CA3, from CA3 to CA1, and from CA1 to Subic or back to the deep layers of the EC (deep EC; *green*). Input from the supEC to CA1 (temporoammonic path; see below) is transmitted from CA1 to Subic or directly back to the deep EC. The Subic also sends projections to the deep EC (*orange*). The axons of dentate granule cells make up the mossy fibre pathway (*red*; **Figure 1-07**) which projects to stratum lucidum of CA3 – an additional lamina exclusive to CA3 not mentioned previously (**Figure 1-06**). The axons of CA3 pyramids make up both the CA3 associational network which terminates in SRad of CA3 (*not shown*) and the Schaffer collateral pathway which terminates in SRad of CA1 (*blue*; **Figure 1-07**). The extensive associational network in CA3 is the major example of non-unidirectional information flow in the HPC; there is also a very weak associational network in CA1 (Tamamaki et al., 1987; Amaral et al., 1991).

Pyramidal neurons in CA3 send commissural projections to CA3, CA2, and CA1 in the contralateral HPC (Blackstad, 1956; Fricke and Cowan, 1978). A small number of CA1 pyramids may also project to the contralateral HPC (van Groen and Wyss, 1990).

Extrinsic connections. The main cortical input to the HPC is from the supEC, but it also receives cortical inputs from the perirhinal cortex and postrhinal cortex. Briefly, information from neocortical association areas funnels through the supEC and follows two main pathways into the HPC: the perforant pathway and the temporoammonic pathway (**Figure 1-07**). The perforant pathway (*yellow*) includes the projection from entorhinal layer II to both SMol of the DG and to SLM of CA3 (**Figure 1-07**). The temporoammonic path (*pink*) is the projection from entorhinal layer III to SLM of CA1. Following intrinsic processing, hippocampal output is sent back to neocortical association areas from region CA1 and Subic via the deep EC (Swanson and Cowan, 1977; Finch and Babb, 1980, 1981; Witter et al., 1988; van Groen and Wyss, 1990; Naber et al., 2001; Kloosterman et al., 2003a).

The HPC receives subcortical inputs from the septal nuclei, brainstem, hypothalamus, and NReu. The septal projection is heaviest in the DG (SMol and hilus) and is composed of cholinergic (Wainer et al., 1984; Amaral and Kurz, 1985; Wainer et al., 1985), γ – aminobutyric acid (GABA) – ergic (Kohler et al., 1984a), and glutamatergic (Colom et al., 2005) fibres. The septal projection to the HPC terminates in SOr and SRad; it is organised for excitation of principal neurons and inhibition of interneurons (Mosko et al., 1973; Baisden et al., 1984;

Amaral and Kurz, 1985; Wainer et al., 1985; Nyakas et al., 1987; Freund and Antal, 1988) suggesting that the net effect of septal input to the HPC is excitatory.

The HPC receives projections from several brainstem nuclei. Noradrenergic fibres from the locus coeruleus terminate in the hilus of the DG, SLu of CA3, and superficial SLM in CA3 and CA1 and have a net excitatory effect on hippocampal activity (Pickel et al., 1974; Swanson and Hartman, 1975; Koda et al., 1978a; Koda et al., 1978b; Moore et al., 1978; Haring and Davis, 1983, 1985a, 1985b; Loughlin et al., 1986). Serotonergic fibres from the median and dorsal raphé nuclei terminate in the hilus of the DG and diffusely within CA3 and have a net inhibitory effect on hippocampal activity (Conrad et al., 1974; Moore and Halaris, 1975; Kohler and Steinbusch, 1982; Halasy et al., 1992; Vertes et al., 1999). Dopaminergic fibres from the ventral tegmental area innervate the HPC extremely sparsely. Dopamine has both excitatory and inhibitory effects on hippocampal activity (Sealfon and Olanow, 2000).

Projections from the posterior hypothalamus are (mostly) glutamatergic (Kiss et al., 2000), terminate in SMol, the hilus, and close to SPyr, and have a net excitatory effect on hippocampal activity (Haglund et al., 1984; Kohler et al., 1985; Magloczky et al., 1994). Finally, the NReu projects to SLM of CA1 at all septo-temporal levels of the HPC. It synapses asymmetrically onto pyramidal cell spines, suggesting that its net effect is excitatory (Herkenham, 1978; Wouterlood et al., 1990).

Not all subdivisions of the HPC send output extrinsically. The only output of the DG is to CA3. Region CA3 sends output to contralateral CA3, CA2, and

CA1 (Blackstad, 1956; Fricke and Cowan, 1978), ipsilateral CA1, and bilaterally to the lateral septal nucleus (Swanson and Cowan, 1977; Swanson et al., 1980). Region CA2 also sends output to CA1 (Ishizuka et al., 1990); little else is known about CA2. The outputs of CA1 are much more substantial than those of the other subdivisions of the HPC. Besides projections to the deep EC, CA1 sends output to the: lateral septal nucleus, nucleus of the diagonal band of Broca, retrosplenial and perirhinal cortices, prelimbic region of the medial fCTX, anterior olfactory nucleus, olfactory bulb, nucleus accumbens, basal nucleus of the amygdala, as well as the anterior and dorsomedial hypothalamus (Jay et al., 1989; van Groen and Wyss, 1990).

Entorhinal Cortex

The EC has not been studied as extensively as other structures in the hippocampal formation, although Ramón y Cajal suggested that what the remainder of the hippocampal formation is doing depends on what the EC has already done (as paraphrased in: Amaral and Lavenex, 2007).

Cytoarchitecture. There are two schemes currently used to describe the cortical lamination of the EC: one originally suggested by Cajal and one by Lorente de Nó. I will use the Cajalian scheme in which the EC consists of four cellular layers (II, III, V, and VI) and two acellular layers (I and IV or the lamina dissecans). Layer I is at the pial surface and layer VI is deep, adjacent to the angular bundle (**Figure 1-08**). Using this scheme, the EC can be divided up into

superficial and deep regions: layers I, II, and III are considered to be the supEC and layers V and VI are considered to be the deep EC.

Cytoarchitecture and laminar characteristics are often used to delineate the different subdivisions of the EC rather than simply location. In the medial EC (*purple* region in **Figure 1-09**), layer II cells are dispersed in an even layer, the deep layers are clearly differentiated, and the lamina dissecans is sharply defined. In the lateral EC (*green* region in **Figure 1-09**), layer II cells are densely packed and clustered into "islands", the deep layers are less differentiated, and the lamina dissecans is less clear. Between the lateral and medial subdivisions of the EC there is a transitional region that shares characteristics of both the lateral and medial subdivisions that is sometimes referred to as the intermediate EC (*grey* region in **Figure 1-09**) (Steward, 1976; Steward and Scoville, 1976; Wyss, 1981). Other researchers have specified additional entorhinal subfields in both primates (Amaral et al., 1987) and rodents (Uva et al., 2004).

The EC has a rich variety of both excitatory and inhibitory cell types (**Figure 1-10A**) (Amaral and Witter, 1995; Amaral and Lavenex, 2007). Layer I has very few, widely dispersed stellate-shaped and horizontal neurons (**1**) that contribute to the perforant path both directly (via synaptic projections) and indirectly (via synaptic connections on the dendrites of layer II neurons that project to the DG). Layer I also contains many transversely oriented fibres. Layer II contains medium – large stellate neurons (**2**) and a population of relatively small pyramidal neurons (**3**). The stellate and pyramidal neurons in layer II (**Figure 1-10B**) are the origin of the perforant path to the DG and CA3. They are

also the origin of extensive longitudinal associational connections to layer II neurons in other parts of the EC; they do not extend many connections to the deep layers. Multipolar (**4**) and horizontal (**5**) neurons in layer II also directly contribute to the perforant path projection. Finally, there is a population of axo-axonic interneurons (**6**) in layers II and III. Pyramidal cells (**7**) are the most numerous cell type in layer III (**Figure 1-10B**); they are the source of the temporoammonic path to CA1 and Subic. Axon collaterals from these pyramids are distributed mainly in layers I and III; few collaterals are distributed in layers II and V. Layer III also contains multipolar, stellate, fusiform, horizontal, and bipolar neurons (*not shown*) that contribute to the temporoammonic pathway.

Layer IV of the EC is also called the lamina dissecans. It is generally considered acellular, but it does contain the basal dendrites of layer III pyramids (**7**), scattered fusiform (inhibitory) and pyramidal (excitatory) cells whose dendrites project up to layer I and whose axons project down to the white matter (*not shown*). Layer V can be divided into two sub-layers: Va and Vb. Layer Va is typically characterised by large pyramidal neurons (**8**) whose dendrites ascend into the superficial regions of layer II and into layer I where they branch out into a tuft (**Figure 1-10B**). Their axons descend into the white matter and smaller axon collaterals ascend into the supEC (Lingenhöhl and Finch, 1991). Relatively small horizontal (**9a**), multipolar (**9b**), and stellate (**9c**) cells can also be observed in layer Va. The neurons in layers Vb and VI can be divided into 3 groups: 1) those that mainly influence local neurons in layers Vb and VI (**10**), 2) those that influence cells in the supEC through highly collateralised axons (**11**), and 3) those

that are likely to be projection neurons because their axons descend into the deep white matter (**12**). Additional small GABA immunopositive neurons (inhibitory) can be observed in all layers of the EC (*not shown*), although they are most abundant in the supEC. Interestingly, there is evidence that some GABA immunopositive neurons in layers II and III project to the DG (Amaral and Witter, 1995; Amaral and Lavenex, 2007).

Intrinsic connections. The EC has an extensive network of associational connections; cells tend to innervate cells in the same or more superficial layers. It is not known, however, whether the axon collaterals from the deep EC that reach the supEC terminate on the same neurons that give rise to the perforant and temporoammonic pathways. It is also not known whether these associational connections are excitatory, inhibitory, or some combination of the two.

In addition to the ipsilateral associational connections, commissural projections from all entorhinal regions terminate in the homotypic region of the contralateral EC, primarily in layers I and II (Kohler, 1986, 1988).

Extrinsic connections. Neocortical inputs terminate on entorhinal neurons in both the superficial (I through III) and the deep (V and VI) layers. The inputs to the supEC are organised topographically and those in the deep EC terminate diffusely. This is significant because it suggests that neocortical output is being integrated with *both* hippocampal input and hippocampal output. Perirhinal and postrhinal cortices also provide topographically organised multimodal input to the EC. The perirhinal cortex projects mainly to layers I and III in the lateral EC and the postrhinal cortex projects mainly to layers I and III in the medial EC. The

majority of deep EC output projections to the nCTX are directed at higher order associational and multimodal regions.

Similarly to the HPC, subcortical inputs to the EC come from the medial septum, brainstem, hypothalamus, and NReu. The medial septal afferents terminate mostly in the lamina dissecans (and less densely in layer II) of the medial region of the medial and lateral subdivisions of the EC (Beckstead, 1978; Alonso and Kohler, 1984; Gage et al., 1984; Milner and Amaral, 1984; Saper, 1985). Inputs arrive at multiple levels within the EC from various regions of the brainstem such as the ventral tegmental area (Fallon et al., 1978; Swanson, 1982), the central and dorsal raphé nuclei (Azmitia and Segal, 1978), and the locus coeruleus (Moore et al., 1978). Inputs from the supramammillary nucleus (Haglund et al., 1984), the tuberomammillary nucleus (Wyss et al., 1979; Kohler, 1985; Saper, 1985), and the lateral hypothalamic area (Kohler et al., 1984b) also arrive at various levels within the EC. Finally, a population of neurons from the NReu terminates densely in layers I and III (Herkenham, 1978; Wouterlood et al., 1990; Wouterlood, 1991).

Entorhinal projections to the HPC (i.e., perforant and temporoammonic paths; **Figure 1-07**) are organised topographically in both the longitudinal (i.e., septotemporal) (**Figure 1-11**) and transverse axes (*not shown*). The most lateral and caudal regions of the EC that lie close to the rhinal sulcus (*purple*) project to the septal half (dorsal region) of the HPC (*purple*). Progressively more medial and rostral regions of the EC project to progressively more temporal (or ventral) regions of the HPC (*grey* and *green* regions) (Ruth et al., 1982, 1988; Witter et

al., 1989; Dolorfo and Amaral, 1998). In CA1, projections from the medial and lateral divisions of the EC terminate throughout the full depth of SLM.

CA1 is the first hippocampal region to return projections to the EC. Hippocampal output projections to the EC are topographically organised in the same manner as entorhinal inputs to the HPC (i.e., EC – HPC interconnections are topographically reciprocal). The organisation of these synaptic connections, in addition to the associational connections from the deep to superficial entorhinal layers are the anatomical basis for point to point reverberating circuits (Kloosterman et al., 2003b; Kloosterman et al., 2004), beginning and ending in the EC.

Figure 1-04:

The hippocampus in the human and the rat brains

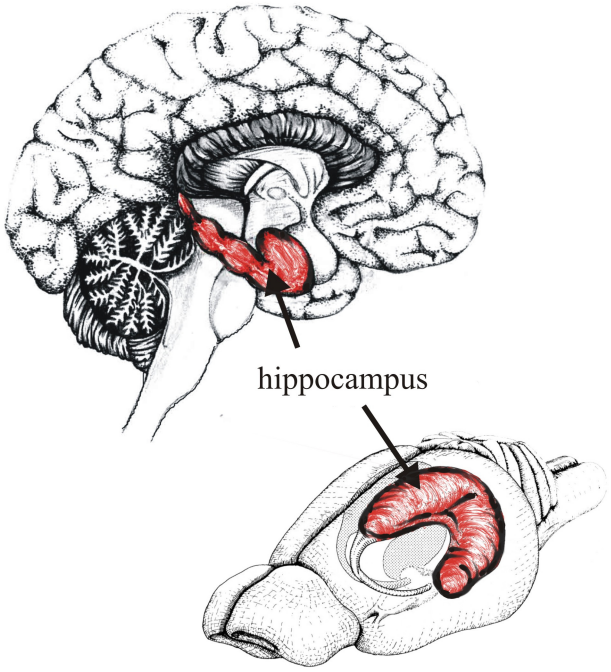

The hippocampus (*red*) is a paired structure that lies on the inner surface of the medial temporal lobe in the human brain. In rats, it constitutes a large portion of the total brain mass.

Figure 1-05:

Subdivisions of the hippocampus

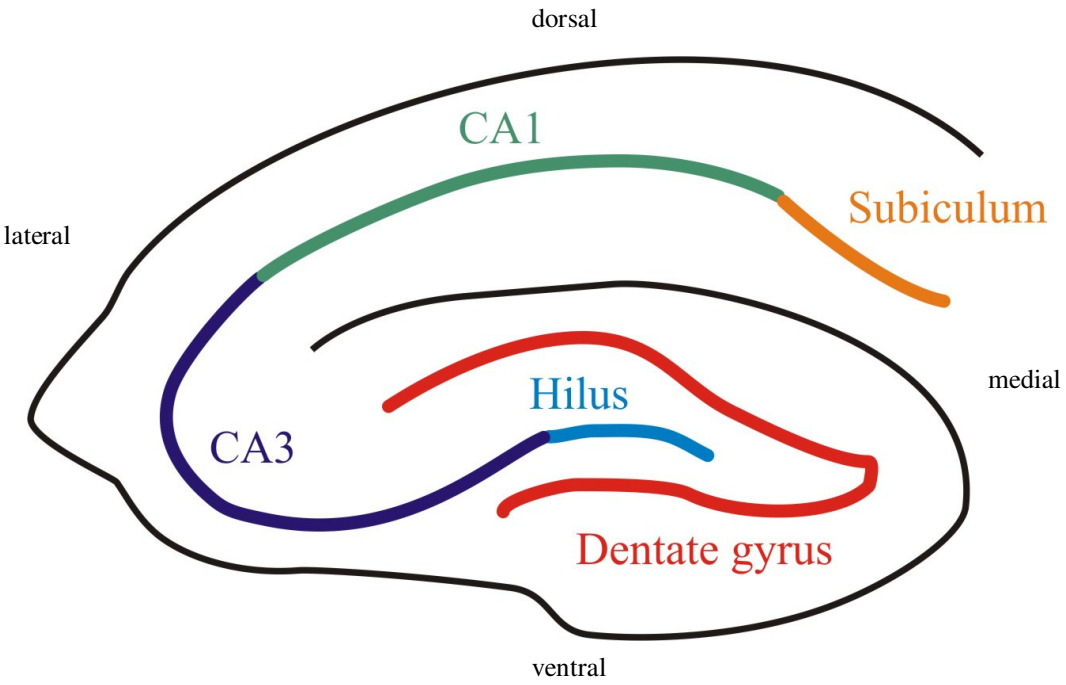

The HPC has several main subdivisions: the dentate gyrus (DG; *red*), the hilus (*light blue*), cornu ammonis 3 (CA3; *dark blue*), cornu ammonis 2 (CA2; *not shown*), cornu ammonis 1 (CA1; *green*), and subiculum (Subic; *orange*).

Figure 1-06:

Summary of the hippocampal laminae

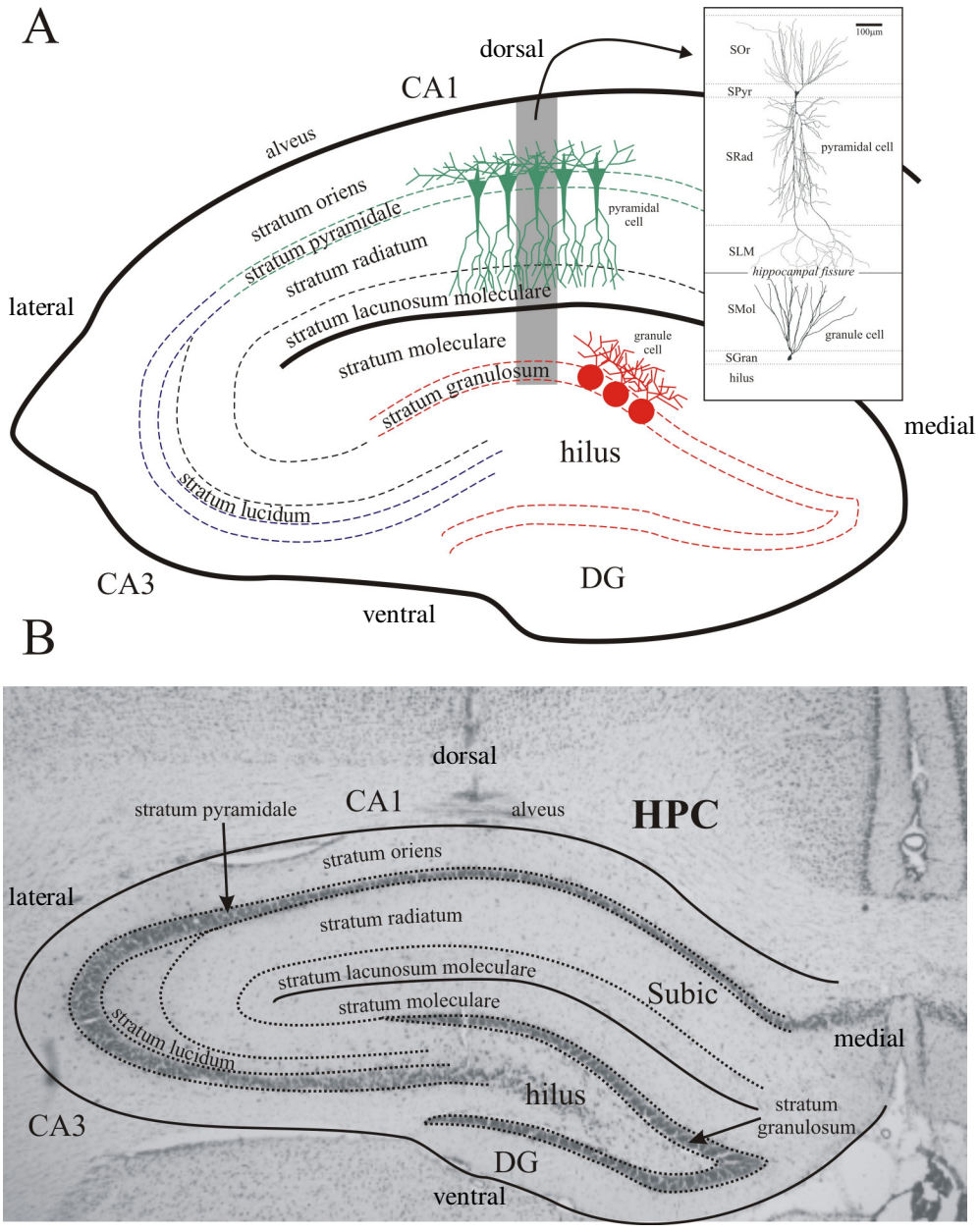

Figure 1-06 Caption:

As depicted in the pictorial representation and inset in **A**, and the coronal section in **B**, the deepest region of the HPC is SOr. It is relatively acellular, but contains the axons from the principal neurons located in SPyr. Just superficial to SPyr in region CA3 is SLu – the region of CA3 where the terminals from the mossy fibre pathway terminate (see **Figure 1-09**). Superficial to SLu in CA3 and immediately superficial to SPyr in both CA2 and CA1 is SRad. In CA3, this lamina contains the terminals of the CA3 to CA3 associational connections. In CA1, this lamina contains the terminals of the Schaffer collaterals. SLM is the most superficial lamina of the HPC. In CA3, it contains the terminals of the perforant path inputs and in CA1 it contains the terminals from both the temporoammonic path inputs as well as midline thalamic afferent inputs. The DG lies immediately ventral to the hippocampal fissure. The most superficial lamina in the DG is SMol which contains the dendrites of granule cells, several different types of interneurons, perforant path inputs, and mossy cell inputs. SGran lies deep to SMol and it is the principal cell layer of the DG. The deepest layer of the DG is the hilus. It is a region composed of multiple subtypes of interneurons. Adapted from: Claiborne et al., 1990; Ishizuka et al., 1995; Amaral and Lavenex, 2007. Abbreviations: cornu ammonis 1 (CA1), cornu ammonis 3 (CA3), dentate gyrus (DG), hippocampus (HPC), stratum granulosum (SGran), stratum lacunosum moleculare (SLM), stratum lucidum (SLu), stratum moleculare (SMol), stratum oriens (SOr), stratum pyramidale (SPyr), stratum radiatum (SRad)

Figure 1-07:

Information flow through the medial temporal lobe is unidirectional

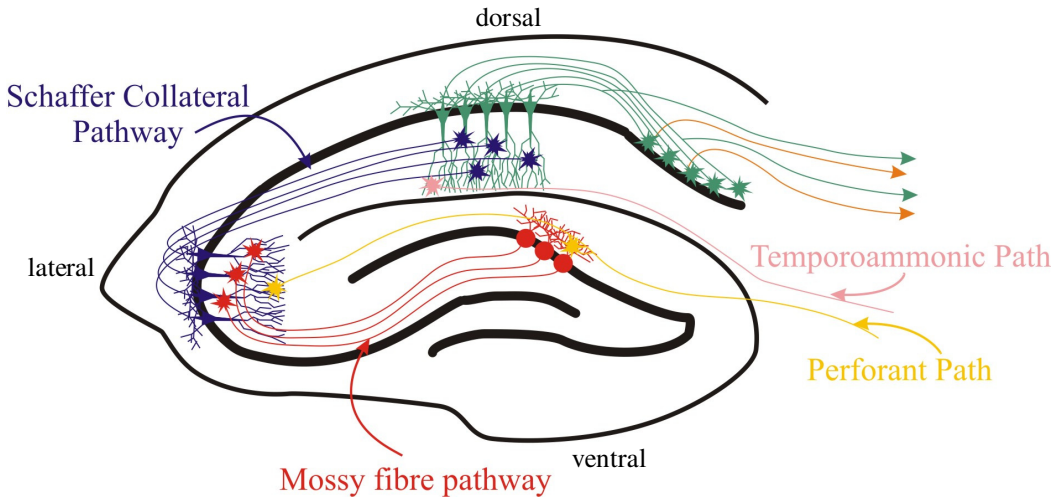

Information flows from the supEC to the HPC via the perforant (*yellow*) and temporoammonic (*pink*) paths, from the DG to CA3 via the mossy fibre pathway (*red*), from CA3 to CA1 via the Schaffer Collateral pathway (*blue*), and from CA1 to Subic or the deep EC (*green*). The Subic also sends projections to the deep EC (*orange*). Abbreviations: cornu ammonis 1 (CA1), cornu ammonis 3 (CA3), deep entorhinal cortex (deep EC), dentate gyrus (DG), entorhinal cortex (EC), hippocampus (HPC), subiculum (Subic), superficial EC (supEC)

Figure 1-08:

Summary of the entorhinal laminae and surrounding anatomy

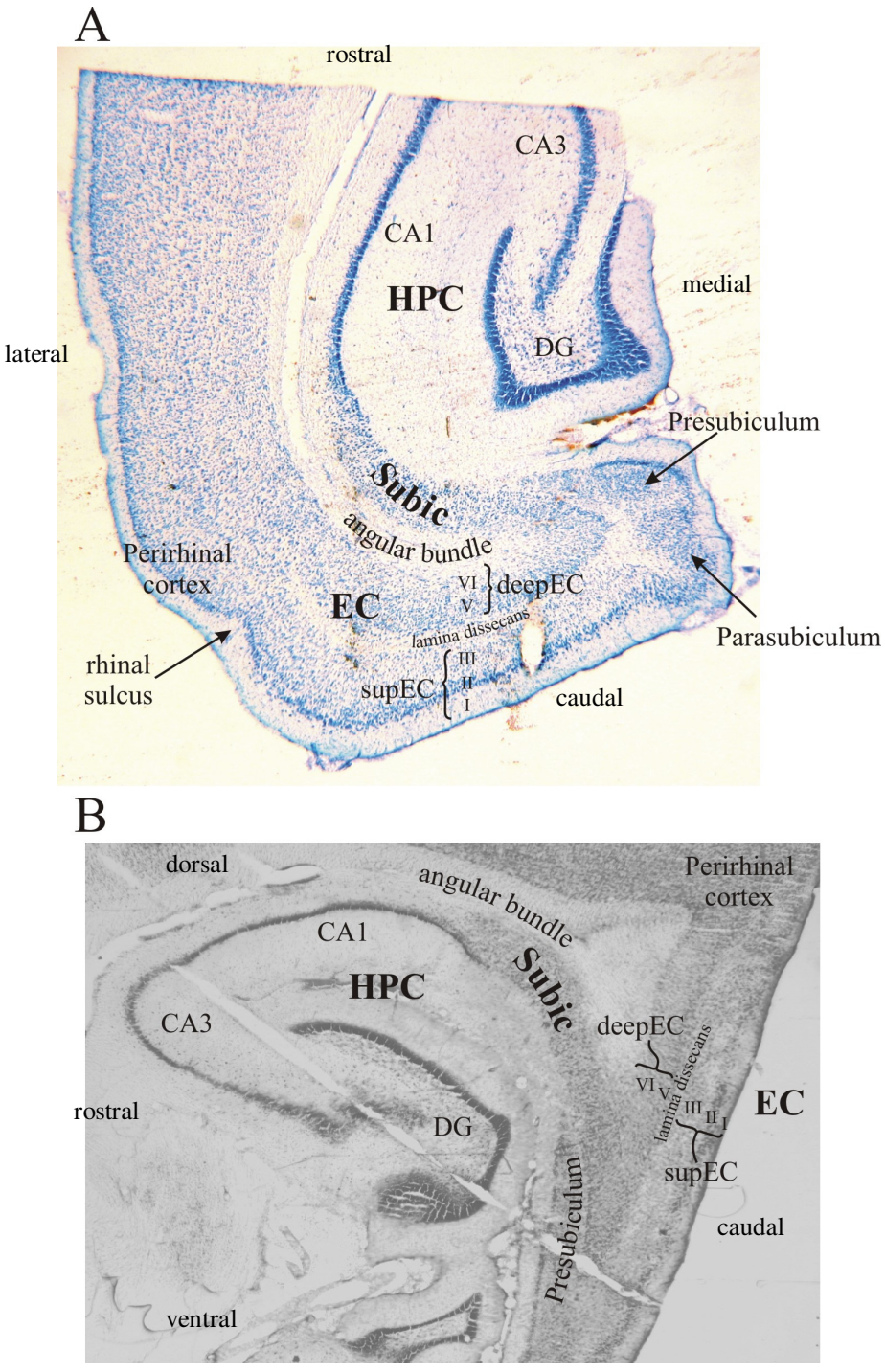

Figure 1-08 Caption:

The entorhinal laminae and surrounding anatomy are evident in both the horizontal (**A**) and sagittal (**B**) planes. The EC is bordered by the perirhinal cortex, parasubiculum, presubiculum, and Subic. Layer I lies adjacent to the pial surface, layers III and V are located on either side of the lamina dissecans, and layer VI is located adjacent to the angular bundle. Abbreviations: cornu ammonis 1 (CA1), cornu ammonis 3 (CA3), deep entorhinal cortex (deep EC), dentate gyrus (DG), entorhinal cortex (EC), hippocampus (HPC), subiculum (Subic), superficial entorhinal cortex (supEC)

Figure 1-09:

Two major subdivisions of the entorhinal cortex: lateral and medial

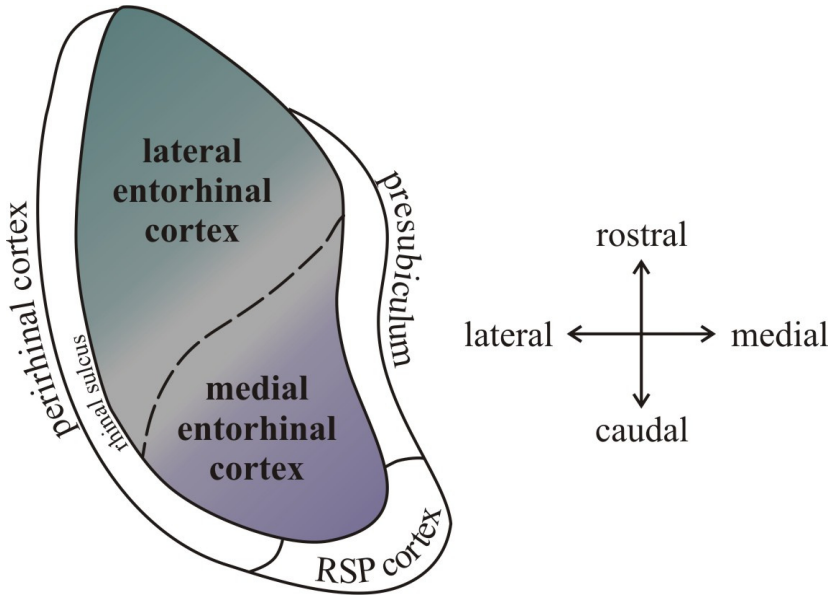

Layer II cells are dispersed in an even layer, the deep layers are clearly differentiated, and the lamina dissecans is sharply delineated in the medial EC (*purple* region). Layer II cells are densely packed and clustered into "islands", the deep layers are less differentiated, and the lamina dissecans is less clear in the lateral EC (*green* region). There is a transitional region that shares characteristics of both the lateral and medial subdivisions between the lateral and medial subdivisions of the EC. This region is sometimes referred to as the intermediate EC (*grey* region). Abbreviations: retrosplenial cortex (RSP cortex)

Figure 1-10:

Summary of the different types of neurons in the entorhinal cortex

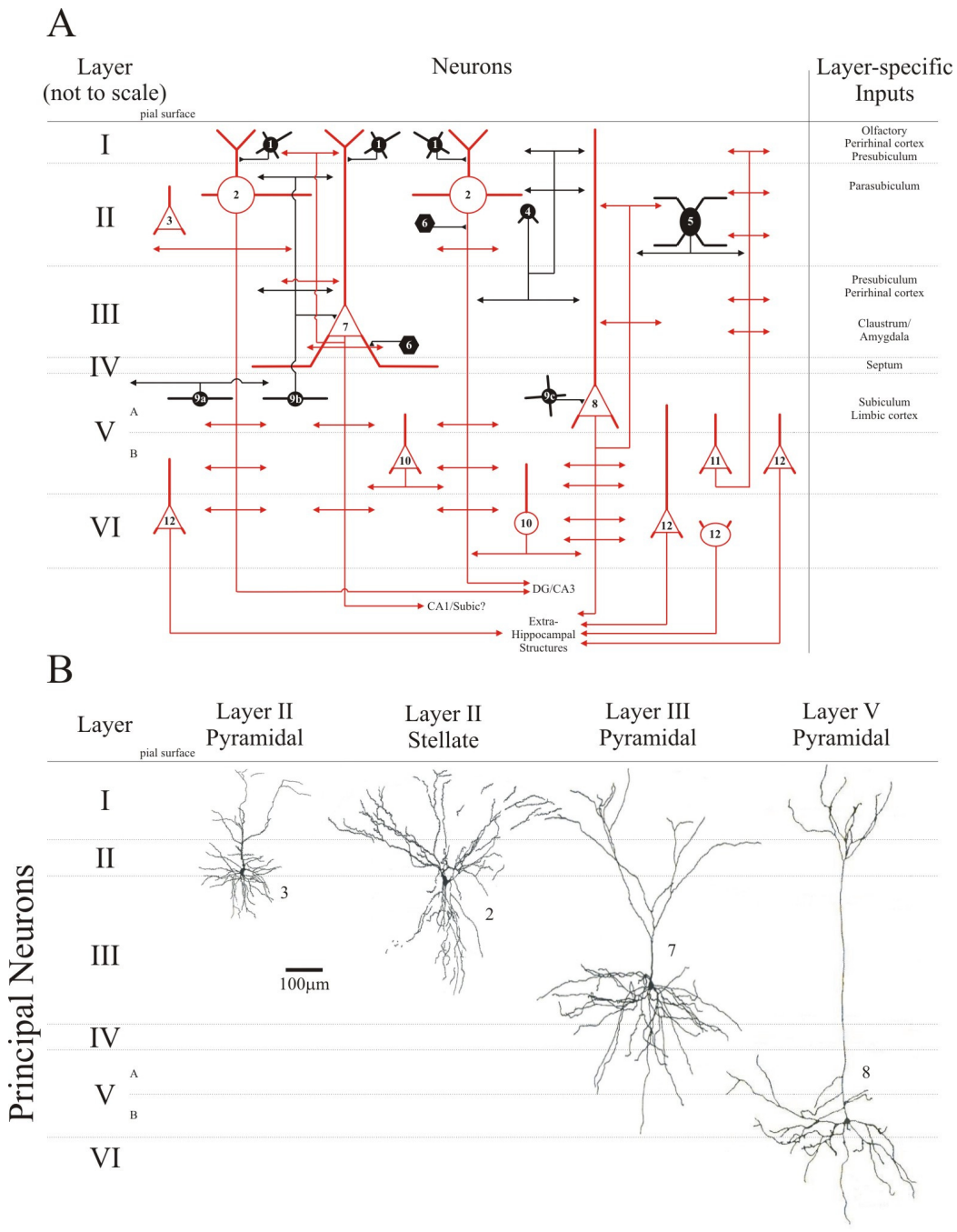

Figure 1-10 Caption:

(**A**) Neurons shown in *red* are excitatory and those shown in *black* are inhibitory. Layer I has very few, widely dispersed stellate and horizontal neurons (**1**) that contribute to the perforant path as well as many transversely oriented fibres. Layer II contains medium – large stellate neurons (**2** and **B**) and a population of relatively small pyramidal neurons (**3** and **B**). Multipolar (**4**) and horizontal (**5**) neurons in layer II also directly contribute to the perforant path projection. Finally, there is a population of axo-axonic interneurons (**6**) in layers II and III. Layer III pyramidal cells (**7** and **B**) are the source of the temporoammonic path to CA1 and Subic. Layer III also contains multipolar, stellate (**B**), fusiform, horizontal, and bipolar neurons (*not shown*) that contribute to the temporoammonic pathway. Layer IV of the EC is the lamina dissecans. It is generally considered acellular, but it does contain scattered fusiform and pyramidal cells. Layer V can be divided into two sub-layers: Va and Vb. Layer Va is typically characterised by large pyramidal neurons (**8** and **B**) whose dendrites ascend into the superficial regions of layer II and into layer I. Relatively small horizontal (**9a**), multipolar (**9b**), and stellate (**9c**) cells can also be observed in layer Va. There are 3 groups of neurons in layers Vb and VI: 1) those that mainly influence local neurons (**10**), 2) those that influence cells in the supEC (**11**), and 3) those that are likely to be projection neurons (**12**). Adapted from: Amaral and Witter, 1995; Amaral and Lavenex, 2007. Abbreviations: cornu ammonis 1 (CA1), cornu ammonis 3 (CA3), dentate gyrus (DG), subiculum (Subic)

Figure 1-11:

Topographical organisation of entorhinal – hippocampal projections

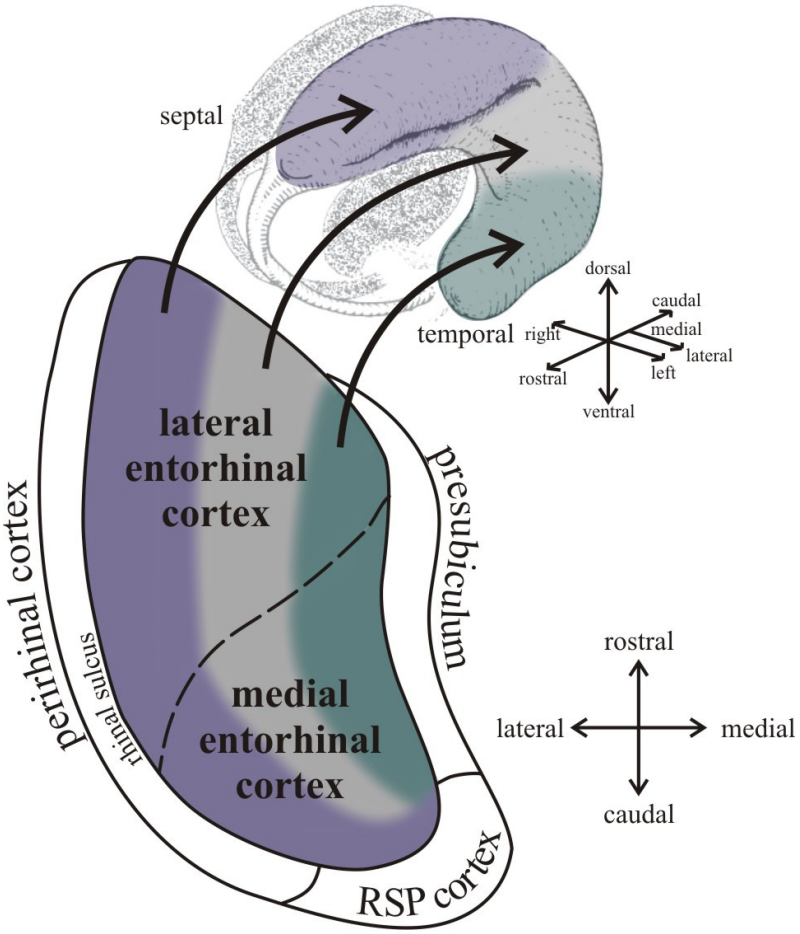

Figure 1-11 Caption:

Layer II projections to the HPC are organised topographically in both the longitudinal (i.e., septotemporal) and transverse axes (*not shown*). The most lateral and caudal regions of the EC that lie close to the rhinal sulcus (*purple*) project to the septal half (dorsal region) of the HPC (*purple*). Progressively more medial and rostral regions of the EC project to progressively more temporal (or ventral) regions of the HPC (*grey* and *green* regions). Adapted from: Amaral and Witter, 1995; Dolorfo and Amaral, 1998. Abbreviations: retrosplenial cortex (RSP cortex)

Part 3: State – Dependent Activity in the Hippocampal and Entorhinal Cortices

Different types of behaviour are typically associated with different types of brain activity (or mental arousal) which can be documented from the general structure of the EEG. For example, LVFA dominates the EEG of an awake and alert subject when the brain is actively responding to the environment. At the other extreme, very slow frequency, high amplitude activity is observed in a comatose patient when the brain is not responding to the environment. This "state – dependent activity" can be measured across the brain as a whole using scalp EEG or in localised regions of the brain using the LFP recorded from implanted electrodes (*see Appendix A*). If the activity of a neuronal network is rhythmic and recurring, the result is an oscillation (*see Appendix B*).

The relationship between the state – dependent activity of a neuronal network and the behaviour of neurons within that network is reciprocal: brain state is determined by the neuronal activity within a particular network and the behaviour of neurons within that network is constrained by the overall brain state. Therefore, we can make inferences regarding the neuronal activity in a particular network (i.e., information processing) based on the overall state – dependent activity occurring within it.

Overview. The state-dependent activity of the HPC and EC can be roughly divided into both rhythmic and non-rhythmic states. Rhythmic states have traditionally included: theta (3 to 12Hz) (**Figure 1-12A**), gamma (25 to 80Hz), and ripples (100 to 200Hz). Non-rhythmic states include large-amplitude irregular

activity (LIA) (**Figure 1-12B**) and small irregular activity (SIA) (O'Keefe, 2007). For the purpose of my thesis, I will be characterising the theta oscillation as the "activated" state and LIA as part of the "deactivated" state. Under urethane anaesthesia, the activated and deactivated states roughly correspond to REM and non-REM sleep, respectively (Clement et al., 2008).

Theta (3 to 12Hz). The theta rhythm (**Figure 1-12A**) was first discovered in the HPC of the rabbit in 1938 by Jung and Kornmuller (as cited in: O'Keefe, 2007). Green and Arduini (1954) later showed that this rhythm was correlated with arousal and cortical desynchronisation (i.e., activation). It is a near sinusoidal oscillation that can be observed in the rat HPC (and EC) during exploratory movements and during REM sleep (Whishaw and Vanderwolf, 1973; Vanderwolf, 2001). The *top panel* of **Figure 1-12A** shows a sample of theta recorded in the HPC of a urethane-anaesthetised rat. It has a power peak (*middle panel*) and rhythmic autocorrelation (AC; *bottom panel*) at 3.5Hz. Theta is thought to be relatively synchronous across the entire hippocampal network (Mitchell and Ranck, 1980; Fox et al., 1986; Bullock et al., 1990; but see: Lubenov and Siapas, 2009) and has been implicated in synaptic function and plasticity (Pavlides et al., 1988; O'Keefe and Recce, 1993; Huerta and Lisman, 1995; Skaggs et al., 1996; Holscher et al., 1997; Hyman et al., 2003; Hasselmo, 2005). Finally, hippocampal theta is dependent on input from both the medial septum and the EC (Bland and Oddie, 2001; Buzsáki, 2002).

Large-amplitude irregular activity. Traditionally, large-amplitude irregular activity (LIA) has been characterised as the activity pattern in the rat

HPC during low arousal when theta is not present; during stereotypical behaviours such as eating or grooming, as well as during quiet sitting and non-REM sleep (Whishaw and Vanderwolf, 1973; Vanderwolf, 2001). The *top panel* of **Figure 1-12B** shows a sample of LIA recorded in the urethane-anaesthetised rat. It has high power at several frequencies (*middle panel*) and is non-rhythmic (*bottom panel*). Hippocampal "sharp waves" – the extracellular result of synchronous bursts in CA3 pyramids that have summated in CA1, occur coincidently with hippocampal ripples – synchronous bursts of action potentials in most theta-related interneurons and some pyramidal neurons, during LIA (Buzsáki et al., 1992). Inhibitory dentate spikes – synchronous bursts of action potentials in dentate mossy cells, have also been shown during LIA (Bragin et al., 1995). Unlike theta, LIA is not dependent on the medial septum (Bland et al., 1996). Hippocampal activity during LIA may strengthen recent synaptic modifications (i.e., hippocampal sharp wave/ ripple complexes) (Buzsáki, 1989) or be involved in transferring information from the HPC to the nCTX (Siapas and Wilson, 1998).

Figure 1-12:

Traditional hippocampal activated and deactivated states

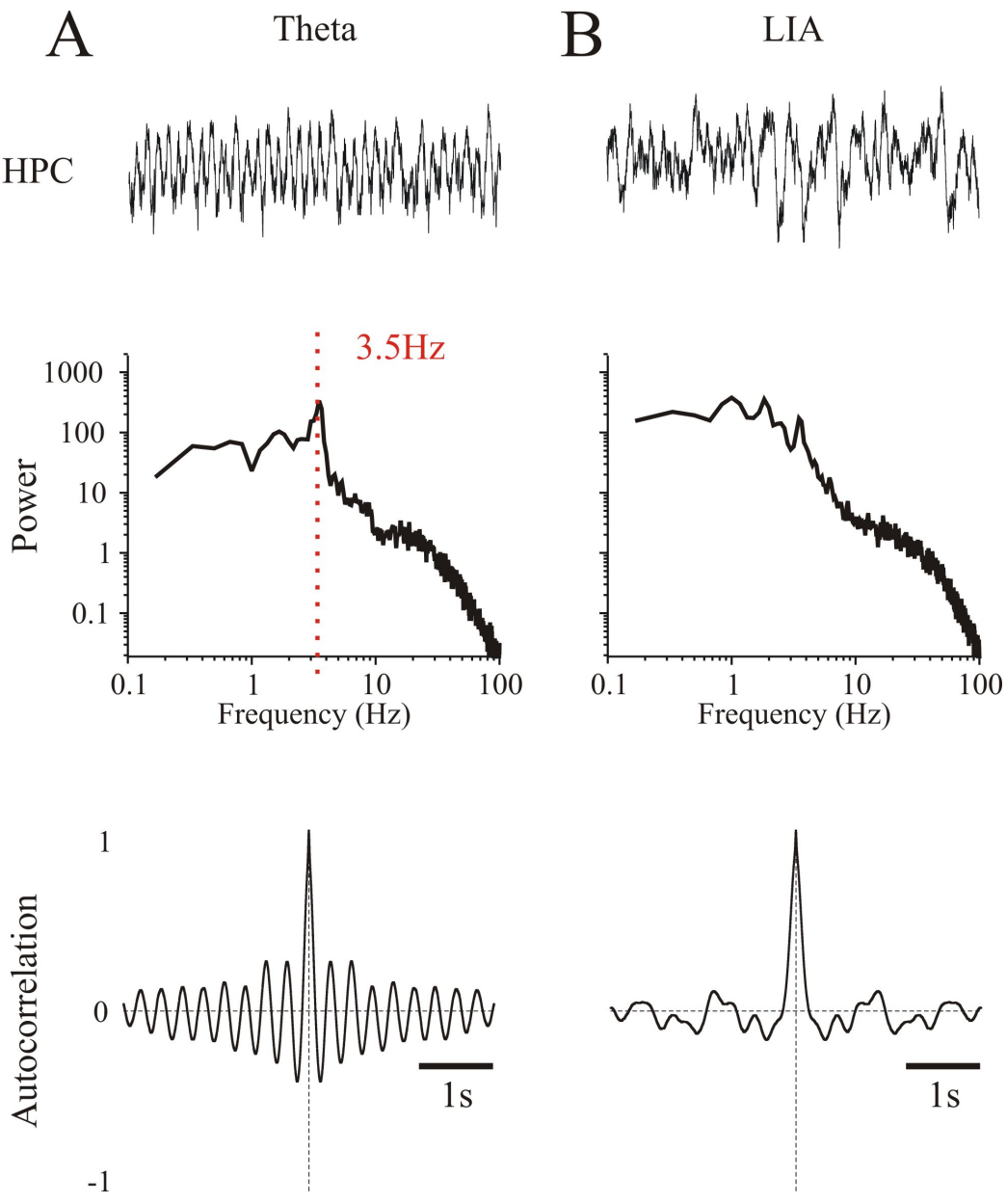

Figure 1-12 Caption:

Hippocampal and entorhinal state-dependent activity can be divided into activated and deactivated states. The prominent oscillation during the activated state is theta (**A**). It is a near sinusoidal 3 to 12Hz oscillation that can be observed in the rat HPC during cortical activation. This includes during exploratory movements and during REM sleep. The power spectrum (*middle panel*) of the theta sample clearly shows a power peak at 3.5Hz. The autocorrelation (*bottom panel*) is also rhythmic at 3.5Hz. (**B**) Traditionally, the prominent activity during the deactivated state is LIA. It can be observed during times of low arousal such as quiet sitting and non-REM sleep. As shown in the *middle* and *bottom panels* of **B**, LIA has high power at several frequencies and a non-rhythmic autocorrelation. Abbreviations: hippocampus (HPC), large-amplitude irregular activity (LIA), non-rapid eye movement (non-REM), rapid eye movement (REM)

Part 4: The Slow Oscillation

Sleep is a well-conserved state of unconsciousness. It is a common venue to study state – dependent activity because all brain activity during sleep is generated and organised internally (i.e., there is minimal incoming sensory information to influence neural activity). As mentioned previously, the various stages of sleep are characterised by the presence of different oscillatory patterns in the EEG. Stage 1 is characterised by the development of cortical alpha and theta, stage 2 by spindles and K-complexes, stage 3 by spindles and delta, and finally stage 4 is characterised by delta and the slow rhythm. Alpha, spindles, and delta are all considered "thalamocortical oscillations" – those that are generated through synaptic interactions between the thalamus and the nCTX. A common function for these thalamocortical oscillations is the gating of sensory information from the thalamus to the nCTX (Buzsaki, 2006).

Delta (1 to 4Hz). Thalamocortical neurons are bistable – they exhibit two main activity states. When the membrane potential is depolarised, they generate sodium-dependent action potentials in a tonic mode. When the membrane potential is hyperpolarised, they generate rhythmic calcium-dependent oscillations at delta frequencies that are accompanied by bursts of sodium-dependent spikes (oscillatory mode) (McCormick and Pape, 1990). The thalamocortical delta oscillation can be observed in the nCTX during the neocortical DOWN state (Nunez et al., 1992).

Spindles (7 to 14Hz). Spindles are generated and synchronised in the reticular nucleus of the thalamus, but reticular neurons do not project directly to

the nCTX. Reticular neurons generate a burst of action potentials (i.e., spindle) which is transmitted to dorsal thalamic nuclei. The dorsal nuclei neurons initially hyperpolarise and then rebound and exhibit a low-threshold calcium-dependent spike, sometimes accompanied by sodium-dependent spikes (similar to the delta oscillation; *see above*). These spikes are transmitted to both the nCTX for spindle expression and back to the reticular nucleus for spindle reinforcement (Bal and McCormick, 1996; Timofeev et al., 1996).

K-complexes. Spindles are preceded by large population bursts in neocortical neurons called K-complexes. They are triggered by the simultaneous DOWN – UP shift in membrane potential in large numbers of cortical neurons during the SO (*see below*) (Amzica and Steriade, 1997) and are transmitted from the nCTX to the reticular thalamus where spindles are generated. Therefore, if K-complex occurs while the reticular thalamus is in its depolarised state, a spindle could be initiated and transmitted back to the nCTX. If a K-complex occurs while the thalamus is in a hyperpolarised state, delta oscillations can be transmitted back to the nCTX.

The slow oscillation (≤ 1Hz). Steriade et al. (1993a) provided the first description of the SO in the nCTX of the anaesthetised and naturally-sleeping cat and naturally-sleeping human. They stated that "…*the slow oscillation consisted of long-lasting depolarizations, with superimposed full somatic action potentials or presumed dendritic spikes, separated by long periods of neuronal silence*" (Steriade et al., 1993a; page 3255). The simultaneous change in the membrane potential of many neocortical pyramidal neurons from a hyperpolarised "DOWN"

state to a depolarised "UP" state generates the SO in the LFP. It was shown that this pattern of activity occurred in the majority of cortical neurons, occurred at a frequency ≤ 1Hz (Steriade et al., 1993a), and was independent of thalamocortical projections (Steriade et al., 1991; Contreras and Steriade, 1995).

The SO only occurs during deep anaesthesia and SWS. Accordingly, it can be blocked by stimulation of either the cholinergic pedunculopontine tegmentum or the noradrenergic locus coeruleus (Steriade et al., 1993b). Slow waves are generated in distinct areas of the nCTX, most often in the more anterior regions, and propagate across the nCTX. In addition, the cortical region of generation and the direction of propagation may vary from wave to wave (Massimini et al., 2004).

The SO biases the occurrence of other sleep-related rhythms (Steriade et al., 1993c). As mentioned above, the DOWN – UP transition in membrane potential triggers a K-complex which can initiate a spindle in the reticular nucleus of the thalamus if the thalamus is in a depolarised state. When the thalamus is in a hyperpolarised state, the K-complex can induce the expression of delta oscillations during the down state of the SO. The observable sleep EEG is the net result of delta, spindles, and K-complexes all grouped by the SO.

Aside from the nCTX, the SO or UP – DOWN membrane potential transitions have been observed in several other brain structures including: the striatum (Mahon et al., 2001; Tseng et al., 2001), amygdala (Crane et al., 2009), EC, and Subic (Isomura et al., 2006). It is not clear whether the SO is an element of hippocampal electrographic activity. If so, the relationship(s) between the HPC

and other structures of the MTL memory system during the SO will be an important avenue of research towards the integration and understanding of episodic mnemonic processing and SWS.

Figure 1-13

UP and DOWN states of the slow oscillation

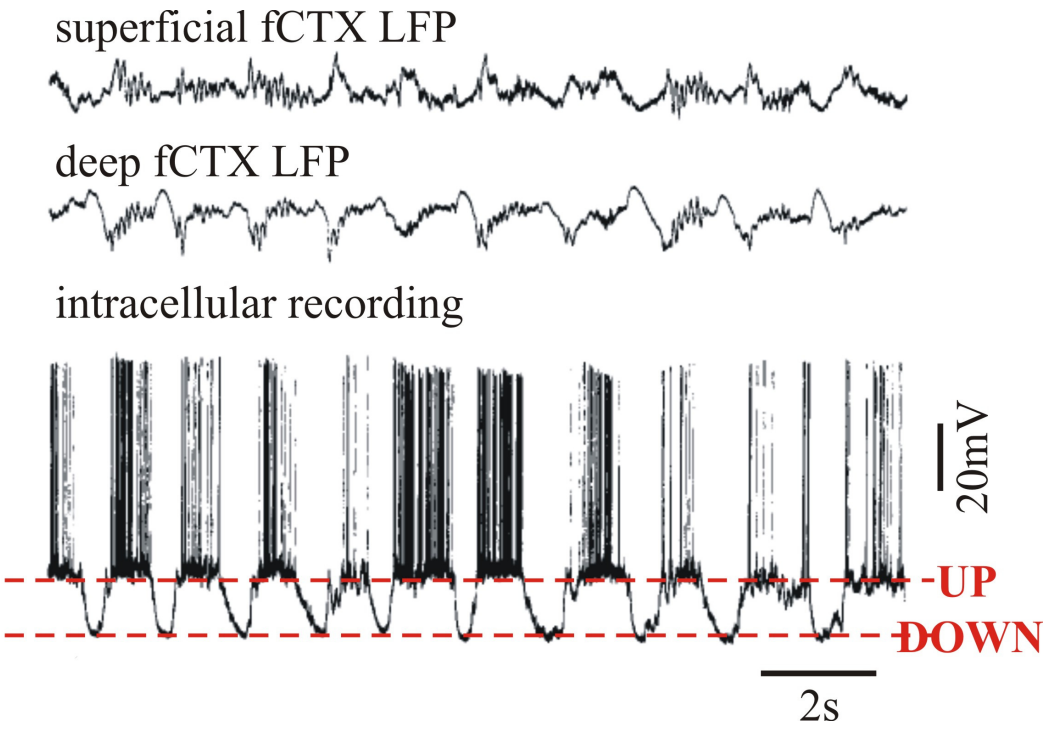

"*…the slow oscillation consisted of long-lasting depolarizations, with superimposed full somatic action potentials or presumed dendritic spikes, separated by long periods of neuronal silence*" (Steriade et al., 1993a; page 3255). The simultaneous change in the membrane potential of many neocortical pyramidal neurons from a hyperpolarised "DOWN" state to a depolarised "UP" state generates the SO in the LFP. Adapted from: Steriade et al., 1993a. Abbreviations: frontal cortex (fCTX), local field potential (LFP)

Introduction References

Alonso A, Kohler C (1984) A study of the reciprocal connections between the septum and the entorhinal area using anterograde and retrograde axonal transport methods in the rat brain. J Comp Neurol 225:327-343.

Amaral DG, Kurz J (1985) An analysis of the origins of the cholinergic and noncholinergic septal projections to the hippocampal formation of the rat. J Comp Neurol 240:37-59.

Amaral DG, Witter MP (1995) Hippocampal Formation. In: The Rat Nervous System, Second Edition (Paxinos G, ed), pp 443-493. USA: Academic Press.

Amaral DG, Lavenex P (2007) Hippocampal Neuroanatomy. In: The Hippocampus Book (Anderson P, Morris R, Amaral DG, Bliss T, O'Keefe J, eds), pp 37 - 114. New York, New York: Oxford University Press.

Amaral DG, Insausti R, Cowan WM (1987) The entorhinal cortex of the monkey: I. Cytoarchitectonic organization. J Comp Neurol 264:326-355.

Amaral DG, Dolorfo C, Alvarez-Royo P (1991) Organization of CA1 projections to the subiculum: a PHA-L analysis in the rat. Hippocampus 1:415-435.

Amzica F, Steriade M (1997) The K-complex: its slow (<1-Hz) rhythmicity and relation to delta waves. Neurology 49:952-959.

Azmitia EC, Segal M (1978) An autoradiographic analysis of the differential ascending projections of the dorsal and median raphe nuclei in the rat. J Comp Neurol 179:641-667.

Baisden RH, Woodruff ML, Hoover DB (1984) Cholinergic and non-cholinergic septo-hippocampal projections: a double-label horseradish peroxidase-acetylcholinesterase study in the rabbit. Brain Res 290:146-151.

Bal T, McCormick DA (1996) Mechanisms of oscillatory activity in guinea-pig nucleus reticularis thalami *in vitro*: a mammalian pacemaker. J Physiol (Lond) 468:669-691.

Barrionuevo G, Brown TH (1983) Associative long-term potentiation in hippocampal slices. Proc Natl Acad Sci U S A 80:7347-7351.

Beckstead RM (1978) Afferent connections of the entorhinal area in the rat as demonstrated by retrograde cell-labeling with horseradish peroxidase. Brain Res 152:249-264.

Blackstad TW (1956) Commissural connections of the hippocampal region in the rat, with special reference to their mode of termination. J Comp Neurol 105:417-537.

Bland BH, Oddie SD (2001) Theta band oscillation and synchrony in the hippocampal formation and associated structures: the case for its role in sensorimotor integration. Behav Brain Res 127:119-136.

Bland BH, Trepel C, Oddie SD, Kirk IJ (1996) Intraseptal microinfusion of muscimol: effects on hippocampal formation theta field activity and phasic theta-ON cell discharges. Exp Neurol 138:286-297.

Bragin A, Jando G, Nadasdy Z, van Landeghem M, Buzsáki G (1995) Dentate EEG spikes and associated interneuronal population bursts in the hippocampal hilar region of the rat. J Neurophysiol 73:1691-1705.

Bramham CR, Srebro B (1987) Induction of long-term depression and potentiation by low- and high-frequency stimulation in the dentate area of the anesthetized rat: magnitude, time course and EEG. Brain Res 405:100-107.

Bullock TH, Buzsáki G, McClune MC (1990) Coherence of compound field potentials reveals discontinuities in the CA1-subiculum of the hippocampus in freely-moving rats. Neurosci 38:609-619.

Buzsaki G (2006) Cycle 7: The Brain's Default State - Self-Organized Oscillations in Rest and Sleep. In: Rhythms of the Brain, pp 175 - 205. New York, New York: Oxford University Press.

Buzsáki G (1989) Two-stage model of memory trace formation: A role for "noisy" brain states. Neurosci 31:551-570.

Buzsáki G (1998) Memory consolidation during sleep: a neurophysiological perspective. J Sleep Res 7 Suppl 1:17-23.

Buzsáki G (2002) Theta oscillations in the hippocampus. Neuron 33:325-340.

Buzsáki G, Horvath Z, Urioste R, Hetke J, Wise K (1992) High-frequency network oscillation in the hippocampus. Science 256:1025-1027.

Claiborne BJ, Amaral DG, Cowan WM (1990) Quantitative, three-dimensional analysis of granule cell dendrites in the rat dentate gyrus. J Comp Neurol 302:206-219.

Clement EA, Richard A, Thwaites M, Ailon J, Peters S, Dickson CT (2008) Cyclic and sleep-like spontaneous alternations of brain state under urethane anaesthesia. PLoS ONE 3:e2004.

Colom LV, Castaneda MT, Reyna T, Hernandez S, Garrido-Sanabria E (2005) Characterization of medial septal glutamatergic neurons and their projection to the hippocampus. Synapse 58:151-164.

Conrad LC, Leonard CM, Pfaff DW (1974) Connections of the median and dorsal raphe nuclei in the rat: an autoradiographic and degeneration study. J Comp Neurol 156:179-205.

Contreras D, Steriade M (1995) Cellular basis of EEG slow rhythms: a study of dynamic corticothalamic relationships. J Neurosci 15:604-622.

Crane JW, Windels F, Sah P (2009) Oscillations in the basolateral amygdala: aversive stimulation is state dependent and resets the oscillatory phase. J Neurophysiol.

Dan Y, Poo MM (2004) Spike timing-dependent plasticity of neural circuits. Neuron 44:23-30.

Dolorfo CL, Amaral DG (1998) Entorhinal cortex of the rat: organization of intrinsic connections. J Comp Neurol 398:49-82.

Fallon JH, Koziell DA, Moore RY (1978) Catecholamine innervation of the basal forebrain. II. Amygdala, suprarhinal cortex and entorhinal cortex. J Comp Neurol 180:509-532.

Finch DM, Babb TL (1980) Neurophysiology of the caudally directed hippocampal efferent system in the rat: projections to the subicular complex. Brain Res 197:11-26.

Finch DM, Babb TL (1981) Demonstration of caudally directed hippocampal efferents in the rat by intracellular injection of horseradish peroxidase. Brain Res 214:405-410.

Fox SE, Wolfson S, Ranck JB, Jr. (1986) Hippocampal theta rhythm and the firing of neurons in walking and urethane anesthetized rats. Exp Brain Res 62:495-508.

Freund TF, Antal M (1988) GABA-containing neurons in the septum control inhibitory interneurons in the hippocampus. Nature 336:170-173.

Fricke R, Cowan WM (1978) An autoradiographic study of the commissural and ipsilateral hippocampo-dentate projections in the adult rat. J Comp Neurol 181:253-269.

Gage FH, Bjorklund A, Stenevi U (1984) Cells of origin of the ventral cholinergic septohippocampal pathway undergoing compensatory collateral sprouting following fimbria-fornix transection. Neurosci Lett 44:211-216.

Green JD, Arduini AA (1954) Hippocampal electrical activity in arousal. J Neurophysiol 17:533-557.

Haglund L, Swanson LW, Kohler C (1984) The projection of the supramammillary nucleus to the hippocampal formation: an immunohistochemical and anterograde transport study with the lectin PHA-L in the rat. J Comp Neurol 229:171-185.

Halasy K, Miettinen R, Szabat E, Freund TF (1992) GABAergic interneurons are the major postsynaptic targets of median raphe afferents in the rat dentate gyrus. Eur J Neurosci 4:144-153.

Haring JH, Davis JN (1983) Topography of locus ceruleus neurons projecting to the area dentata. Exp Neurol 79:785-800.

Haring JH, Davis JN (1985a) Differential distribution of locus coeruleus projections to the hippocampal formation: anatomical and biochemical evidence. Brain Res 325:366-369.

Haring JH, Davis JN (1985b) Retrograde labeling of locus coeruleus neurons after lesion-induced sprouting of the coeruleohippocampal projection. Brain Res 360:384-388.

Hasselmo ME (1999) Neuromodulation: acetylcholine and memory consolidation. Trends Cogn Sci 3:351-359.

Hasselmo ME (2005) What is the function of hippocampal theta rhythm?--Linking behavioral data to phasic properties of field potential and unit recording data. Hippocampus 15:936-949.

Herkenham M (1978) The connections of the nucleus reuniens thalami: Evidence for a direct thalamo-hippocampal pathway in the rat. J Comp Neurol 177:589-610.

Holscher C, Anwyl R, Rowan MJ (1997) Stimulation on the positive phase of hippocampal theta rhythm induces long-term potentiation that can be depotentiated by stimulation on the negative phase in area CA1 in vivo. J Neurosci 17:6470-6477.

Huerta PT, Lisman JE (1995) Bidirectional synaptic plasticity induced by a single burst during cholinergic theta oscillation in CA1 in vitro. Neuron 15:1053-1063.

Hyman JM, Wyble BP, Goyal V, Rossi CA, Hasselmo ME (2003) Stimulation in hippocampal region CA1 in behaving rats yields long-term potentiation when delivered to the peak of theta and long-term depression when delivered to the trough. J Neurosci 23:11725-11731.

Ishizuka N, Weber J, Amaral DG (1990) Organization of intrahippocampal projections originating from CA3 pyramidal cells in the rat. J Comp Neurol 295:580-623.

Ishizuka N, Cowan WM, Amaral DG (1995) A quantitative analysis of the dendritic organization of pyramidal cells in the rat hippocampus. J Comp Neurol 362:17-45.

Isomura Y, Sirota A, Ozen S, Montgomery S, Mizuseki K, Henze DA, Buzsaki G (2006) Integration and segregation of activity in entorhinal-hippocampal subregions by neocortical slow oscillations. Neuron 52:871-882.

Jay TM, Glowinski J, Thierry AM (1989) Selectivity of the hippocampal projection to the prelimbic area of the prefrontal cortex in the rat. Brain Res 505:337-340.

Kiss J, Csaki A, Bokor H, Shanabrough M, Leranth C (2000) The supramammillo-hippocampal and supramammillo-septal glutamatergic/aspartatergic projections in the rat: a combined [3H]D-aspartate autoradiographic and immunohistochemical study. Neuroscience 97:657-669.

Kloosterman F, Witter MP, Van Haeften T (2003a) Topographical and laminar organization of subicular projections to the parahippocampal region of the rat. J Comp Neurol 455:156-171.

Kloosterman F, van Haeften T, Lopes da Silva FH (2004) Two reentrant pathways in the hippocampal-entorhinal system. Hippocampus 14:1026-1039.

Kloosterman F, Van Haeften T, Witter MP, Lopes Da Silva FH (2003b) Electrophysiological characterization of interlaminar entorhinal connections: an essential link for re-entrance in the hippocampal-entorhinal system. Eur J Neurosci 18:3037-3052.

Koblin DD (2002) Urethane: help or hindrance? Anesth Analg 94:241-242.

Koda LY, Schulman JA, Bloom FE (1978a) Ultrastructural identification of noradrenergic terminals in rat hippocampus: unilateral destruction of the locus coeruleus with 6-hydroxydopamine. Brain Res 145:190-195.

Koda LY, Wise RA, Bloom FE (1978b) Light and electron microscopic changes in the rat dentate gyrus after lesions or stimulation of the ascending locus coeruleus pathway. Brain Res 144:363-368.

Kohler C (1985) Intrinsic projections of the retrohippocampal region in the rat brain. I. The subicular complex. J Comp Neurol 236:504-522.

Kohler C (1986) Intrinsic connections of the retrohippocampal region in the rat brain. II. The medial entorhinal area. J Comp Neurol 246:149-169.

Kohler C (1988) Intrinsic connections of the retrohippocampal region in the rat brain. III. The lateral entorhinal area. J Comp Neurol 271:208-228.

Kohler C, Steinbusch H (1982) Identification of serotonin and non-serotonin containing neurons of the mid-brain raphe projecting to the entorhinal area and the hippocampal formation. A combined immunohistochemical and fluorescent retrograde tracing study in the rat brain. Neuroscience 7:951-975.

Kohler C, Chan-Palay V, Wu J-Y (1984a) Septal neurons containing glutamic acid decarboxylase immunoreactivity project to the hippocampal region. Anat Embriol 169:41-44.

Kohler C, Haglund L, Swanson LW (1984b) A diffuse alpha MSH-immunoreactive projection to the hippocampus and spinal cord from individual neurons in the lateral hypothalamic area and zona incerta. J Comp Neurol 223:501-514.

Kohler C, Swanson LW, Haglund L, Wu J-Y (1985) The cytoarchitecture, histochemestry and projections of the tuberomammillary nucleus in the rat. Neuroscience 16:85-110.

Levy WB, Steward O (1979) Synapses as associative memory elements in the hippocampal formation. Brain Res 175:233-245.

Lingenhöhl K, Finch DM (1991) Morphological characterization of rat entorhinal neurons in vivo: soma-dendritic structure and axonal domains. Exp Brain Res 84:57-74.

Loughlin SE, Foote SL, Grzanna R (1986) Efferent projections of nucleus locus coeruleus: morphologic subpopulations have different efferent targets. Neuroscience 18:307-319.

Lubenov EV, Siapas AG (2009) Hippocampal theta oscillations are travelling waves. Nature 459:534-539.

Lynch GS, Dunwiddie T, Gribkoff V (1977) Heterosynaptic depression: a postsynaptic correlate of long-term potentiation. Nature 266:737-739.

Magloczky Z, Acsady L, Freund TF (1994) Principal cells are the postsynaptic targets of supramammillary afferents in the hippocampus of the rat. Hippocampus 4:322-334.

Mahon S, Deniau JM, Charpier S (2001) Relationship between EEG potentials and intracellular activity of striatal and cortico-striatal neurons: an in vivo study under different anesthetics. Cereb Cortex 11:360-373.

Massimini M, Huber R, Ferrarelli F, Hill S, Tononi G (2004) The sleep slow oscillation as a traveling wave. J Neurosci 24:6862-6870.

McCormick DA, Pape H-C (1990) Properties of a hyperpolarization-activated cation current and its role in rhythmic oscillation in thalamic relay neurones. J Physiol (Lond) 431:291-318.

McNaughton BL, Douglas RM, Goddard GV (1978) Synaptic enhancement in fascia dentata: cooperativity among coactive afferents. Brain Res 157:277-293.

Milner B (1972) Disorders of learning and memory after temporal lobe lesions in man. Clin Neurosurg 19:421-446.

Milner TA, Amaral DG (1984) Evidence for a ventral septal projection to the hippocampal formation of the rat. Exp Brain Res 55:579-585.

Mitchell SJ, Ranck JBJ (1980) Generation of theta rhythm in medial entorhinal cortex of freely moving rats. Brain Res 189:49-66.

Moore RY, Halaris AE (1975) Hippocampal innervation by serotonin neurons of the midbrain raphe in the rat. J Comp Neurol 164:171-183.

Moore RY, Ziegler B, Bayer SA (1978) Monoamine neuron innervation of the hippocampal formation: alteration by neonatal irradiation. Exp Neurol 60:318-326.

Mosko S, Lynch G, Cotman CW (1973) The distribution of septal projections to the hippocampus of the rat. J Comp Neurol 152:163-174.

Murphy M, Riedner BA, Huber R, Massimini M, Ferrarelli F, Tononi G (2009) Source modeling sleep slow waves. Proc Natl Acad Sci U S A 106:1608-1613.

Naber PA, Lopes da Silva FH, Witter MP (2001) Reciprocal connections between the entorhinal cortex and hippocampal fields CA1 and the subiculum are in register with the projections from CA1 to the subiculum. Hippocampus 11:99-104.

Nunez A, Curro Dossi R, Contreras D, Steriade M (1992) Intracellular evidence for incompatibility between spindle and delta oscillations in thalamocortical neurons of cat. Neuroscience 48:75-85.

Nyakas C, Luiten PG, Spencer DG, Traber J (1987) Detailed projection patterns of septal and diagonal band efferents to the hippocampus in the rat with emphasis on innervation of CA1 and dentate gyrus. Brain Res Bull 18:533-545.

O'Keefe J (2007) Hippocampal Neurophysiology in the Behaving Animal. In: The Hippocampus Book (Anderson P, Morris R, Amaral DG, Bliss T, O'Keefe J, eds), pp 475-548. New York, New York: Oxford University Press.

O'Keefe J, Recce ML (1993) Phase relationship between hippocampal place units and the EEG theta rhythm. Hippocampus 3:317-330.

Pavlides C, Greenstein Y, Grudman M, Winson J (1988) Long-term potentiation in the dentate gyrus is induced preferentially on the positive phase of theta-rhythm. Brain Res 439:383-387.

Peigneux P, Laureys S, Delbeuck X, Maquet P (2001) Sleeping brain, learning brain. The role of sleep for memory systems. Neuroreport 12:A111-124.

Pickel VM, Segal M, Bloom FE (1974) A radioautographic study of the efferent pathways of the nucleus locus coeruleus. J Comp Neurol 155:15-42.

Rauchs G, Desgranges B, Foret J, Eustache F (2005) The relationships between memory systems and sleep stages. J Sleep Res 14:123-140.

Ribeiro S, Nicolelis MA (2004) Reverberation, storage, and postsynaptic propagation of memories during sleep. Learn Mem 11:686-696.

Ruth RE, Collier TJ, Routtemberg A (1982) Topography between the entorhinall cortex and the dentate septotemporal axis in rats. I. Medial and intermediate entorhinal projecting cells. J Comp Neurol 209:69-78.

Ruth RE, Collier TJ, Routtemberg A (1988) Topographical relationship between the entorhinal cortex and the septotemporal axis of the dentate gyrus in rats. II. Cells projecting from lateral entorhinal subdivisions. J Comp Neurol 270:506-516.

Saper CB (1985) Organization of cerebral cortical afferent systems in the rat. II. Hypothalamocortical projections. J Comp Neurol 237:21-46.

Sceniak MP, Maciver MB (2006) Cellular actions of urethane on rat visual cortical neurons in vitro. J Neurophysiol 95:3865-3874.

Scoville WB (1954) The limbic lobe in man. J Neurosurg 11:64-66.

Scoville WB, Milner B (1957) Loss of recent memory after bilateral hippocampal lesions. J Neurol Neurosurg Psychiat 20:11-21.

Sealfon SC, Olanow CW (2000) Dopamine receptors: from structure to behavior. Trends Neurosci 23:S34-40.

Shafer A (1995) Metaphor and anesthesia. Anesthesiology 83:1331-1342.

Siapas AG, Wilson MA (1998) Coordinated interactions between hippocampal ripples and cortical spindles during slow-wave sleep. Neuron 21:1123-1128.

Skaggs WE, McNaughton BL, Wilson MA, Barnes CA (1996) Theta phase precession in hippocampal neuronal populations and the compression of temporal sequences. Hippocampus 6:149-172.

Squire LR, Zola-Morgan S (1991) The medial temporal lobe memory system. Science 253:1380-1386.

Stanton PK, Sejnowski TJ (1989) Associative long-term depression in the hippocampus induced by hebbian covariance. Nature 339:215-218.

Steriade M, Dossi RC, Nunez A (1991) Network modulation of a slow intrinsic oscillation of cat thalamocortical neurons implicated in sleep delta waves: cortically induced synchronization and brainstem cholinergic suppression. J Neurosci 11:3200-3217.

Steriade M, Nunez A, Amzica F (1993a) A novel slow (< 1 Hz) oscillation of neocortical neurons in vivo: depolarizing and hyperpolarizing components. J Neurosci 13:3252-3265.

Steriade M, Amzica F, Nunez A (1993b) Cholinergic and noradrenergic modulation of the slow (approximately 0.3 Hz) oscillation in neocortical cells. Journal of Neurophysiology 70:1385-1400.

Steriade M, Nunez A, Amzica F (1993c) Intracellular analysis of relations between the slow (< 1 Hz) neocortical oscillation and other sleep rhythms of the electroencephalogram. J Neurosci 13:3266-3283.

Steward O (1976) Topographic organization of the projections from the entorhinal area to the hippocampal formation of the rat. J Comp Neurol 167:285-314.

Steward O, Scoville SA (1976) The cells of origin of entorhinal afferents to the hippocampus and fascia dentata of the rat. J Comp Neurol 169:347-370.

Strogatz SH (2003) SYNC: How Order Emerges from Chaos in the Universe, Nature, and Daily Life. New York, New York.

Swanson LW (1982) The projections of the ventral tegmental area and adjacent regions: a combined fluorescent retrograde tracer and immunofluorescence study in the rat. Brain Res Bull 9:321-353.

Swanson LW, Hartman BK (1975) The central adrenergic system. An immunofluorescence study of the location of cell bodies and their efferent connections in the rat utilizing dopamine-beta-hydroxylase as a marker. J Comp Neurol 163:467-505.

Swanson LW, Cowan WM (1977) An autoradiographic study of the organization of the efferent connections of the hippocampal formation in the rat. J Comp Neurol 172:49-84.

Swanson LW, Sawchenko PE, Cowan WM (1980) Evidence that the commissural, associational and septal projections of the regio inferior of the hippocampus arise from the same neurons. Brain Res 197:207-212.

Tamamaki N, Abe K, Nojyo Y (1987) Columnar organization in the subiculum formed by axon branches originating from single CA1 pyramidal neurons in the rat hippocampus. Brain Res 412:156-160.

Timofeev I, Contreras D, Steriade M (1996) Synaptic responsiviness of cortical and thalamic neurones during various phases of slow sleep oscillation in cat. J Physiol 494:265-278.

Tononi G, Cirelli C (2001) Some considerations on sleep and neural plasticity. Arch Ital Biol 139:221-241.

Tseng KY, Kasanetz F, Kargieman L, Riquelme LA, Murer MG (2001) Cortical slow oscillatory activity is reflected in the membrane potential and spike trains of striatal neurons in rats with chronic nigrostriatal lesions. J Neurosci 21:6430-6439.

Uva L, Gruschke S, Biella G, De Curtis M, Witter MP (2004) Cytoarchitectonic characterization of the parahippocampal region of the guinea pig. J Comp Neurol 474:289-303.

van Groen T, Wyss JM (1990) Extrinsic projections from area CA1 of the rat hippocampus: olfactory, cortical, subcortical, and bilateral hippocampal formation projections. J Comp Neurol 302:515-528.

Vanderwolf CH (2001) The hippocampus as an olfacto-motor mechanism: were the classical anatomists right after all? Behav Brain Res 127:25-47.

Vertes RP, Fortin WJ, Crane AM (1999) Projections of the median raphe nucleus in the rat. J Comp Neurol 407:555-582.

Wainer BH, Levey AI, Rye DB, Mesulam MM, Mufson EJ (1985) Cholinergic and non-cholinergic septohippocampal pathways. Neurosci Lett 54:45-52.

Wainer BH, Bolam JP, Freund TF, Henderson Z, Totterdell S, Smith AD (1984) Cholinergic synapses in the rat brain: a correlated light and electron microscopic immunohistochemical study employing a monoclonal antibody against choline acetyltransferase. Brain Res 308:69-76.

Walker MP, Stickgold R (2004) Sleep-dependent learning and memory consolidation. Neuron 44:121-133.

Whishaw IQ, Vanderwolf CH (1973) Hippocampal EEG and behavior: changes in amplitude and frequency of RSA (theta rhythm) associated with spontaneous and learned movement patterns in rats and cats. Behav Biol 8:461-484.

Witter MP, Griffioen AW, Jorritsma-Byham B, Krijnen JLM (1988) Entorhinal projections to the hippocampal CA1 region in the rat: an underestimated pathway. Neurosci Lett 85:193-198.

Witter MP, Groenewegen HJ, Lopes da Silva FH, Lohman AHM (1989) Functional organization of the extrinsic and intrinsic circuitry of the parahippocampal region. Prog Neurobiol 33:161-253.

Wolansky T, Clement EA, Peters SR, Palczak MA, Dickson CT (2006) Hippocampal slow oscillation: a novel EEG state and its coordination with ongoing neocortical activity. J Neurosci 26:6213-6229.

Wouterlood FG (1991) Innervation of entorhinal principal cells by neurons of the nucleus runiens thalami. Anterograde PHA-L tracing combined with retrograde fluorescent tracing and intracellular injection with lucifer yellow in the rat. Eur J Neurosci 3:641-647.

Wouterlood FG, Saldana E, Witter MP (1990) Projection from the nucleus reuniens thalami to the hippocampal region: light and electron microscopic tracing study in the rat with the anterograde tracer Phaseolus vulgaris-leucoagglutinin. J Comp Neurol 296:179-203.

Wyss JM (1981) An autoradiographic study of the efferent connections of the entorhinal cortex in the rat. J Comp Neurol 199:495-512.

Wyss JM, Swanson LW, Cowan WM (1979) A study of subcortical afferents to the hippocampal formation in the rat. Neuroscience 4:463-476.

Chapter 2:

Hippocampal Slow Oscillation:

A Novel EEG State and its Coordination with

Ongoing Neocortical Activity

Trish Wolansky[2], Elizabeth A. Clement[2], Steven R. Peters[2], Michael A. Palczak[2], and Clayton T. Dickson[1, 2]

[1]Department of Psychology, and [2]Centre for Neuroscience,

University of Alberta, Edmonton, Canada

Published in:

Journal of Neuroscience, June 7, 2006

26 (23): 6213 – 6229

Introduction

The role of the HPC and associated parahippocampal regions in certain memory processes is well documented (Scoville and Milner, 1957; Cohen and Squire, 1980; Zola-Morgan et al., 1986; Squire and Zola-Morgan, 1991; Squire, 1992; Corkin et al., 1997; Stefanacci et al., 2000). Bilateral damage to this area elicits a profound anterograde and a temporally graded retrograde amnesia, suggesting that its operation is temporarily necessary for the permanent formation of new long-term memories. The final repository of memory traces is believed to be located in modality-specific regions of the nCTX and the transfer of mnemonic information to these sites is known as consolidation (McGaugh, 2000). Consolidation is likely to involve synaptic plasticity promoted by activity-dependent interactions of hippocampal and neocortical neuronal ensembles mediated through their interconnections via parahippocampal structures (Squire and Alvarez, 1995; Eichenbaum, 2000; Lavenex and Amaral, 2000; Witter et al., 2000; Frankland and Bontempi, 2005) (c.f. (Nadel and Moscovitch, 1997).

Sleep may play an important role in both hippocampal-dependent and -independent memory consolidation (Marr, 1970, 1971; Pavlides and Winson, 1989; Karni et al., 1994; Smith and MacNeill, 1994; Wilson and McNaugghton, 1994; Plihal and Born, 1997; Maquet et al., 2000; Walker et al., 2002; Peigneux et al., 2003; Huber et al., 2004; Ribeiro et al., 2004). For recent reviews see: (Buzsáki, 1998; Hasselmo, 1999; Peigneux et al., 2001; Tononi and Cirelli, 2001; Ribeiro and Nicolelis, 2004; Walker and Stickgold, 2004; Rauchs et al., 2005); for an opposing view, see: (Vertes and Eastman, 2000). State – dependent rhythmic

neuronal population synchrony during different sleep stages is a candidate mechanism by which the activity of hippocampal and neocortical ensembles could be coordinated, and may also be a way to promote synchronisation-dependent synaptic plasticity (Buzsáki, 1989; Buzsáki, 1996; Siapas and Wilson, 1998; King et al., 1999; Steriade, 1999; Sirota et al., 2003; Dan and Poo, 2004; Siapas et al., 2005). Therefore, the coordination of brain rhythms across the HPC and the nCTX could be a platform for the transfer of mnemonic codes, leading to the permanent formation of the engram.

In the rodent HPC, state – dependent activity during sleep has been traditionally divided into two mutually exclusive categories based upon their spectral characteristics and occurrence in specific sleep states. The activated state consists of prominent 3 to 12Hz rhythmical activity known as theta or RSA (Vanderwolf et al., 1978; Buzsáki et al., 1983; Bland, 1986; Buzsáki, 2002). Theta is co-expressed with a faster gamma rhythm (25 to 80Hz), and appears during rapid eye movement (REM) sleep and under some general anaesthetics. During REM sleep, hippocampal theta is correlated with an activated (low-voltage fast) EEG in the nCTX and is similarly dependent upon ascending cholinergic inputs (Robinson et al., 1977; Usui and Iwahara, 1977; Vanderwolf et al., 1977; Stewart and Vanderwolf, 1987).

The deactivated state of hippocampal population activity is believed to consist of a non-rhythmical, broadband signal that is known as LIA. Intermittent, large-amplitude (> 2mV) transients (30 to 120ms) called hippocampal “sharp waves” or “spikes” (Jouvet et al., 1959a; Buzsáki, 1986; Suzuki and Smith, 1987)

are characteristic of this state. Sharp waves are correlated with population bursts of hippocampal neurons and localised fast frequency field oscillations (ripple: 125 to 250Hz) (O'Keefe and Nadel, 1978; Buzsáki et al., 1983; Buzsáki, 1986; Suzuki and Smith, 1988b; Ylinen et al., 1995). LIA occurs during non-REM, is typically present under most general anaesthetics, and is usually correlated with the presence of deactivated (large-amplitude slow) neocortical activity patterns. Conversely to theta, LIA appears to be induced by treatments that block ascending cholinergic influences on the HPC.

Here we describe a novel, and previously overlooked, deactivated pattern of spontaneous hippocampal activity in the naturally sleeping and urethane-anaesthetised rat, which bears a remarkable similarity to the previously described slow rhythm in the nCTX (Steriade et al., 1993c; Amzica and Steriade, 1997). Based upon its spectral (frequency) characteristics, its cellular correlates, and its dynamic coordination with the neocortical slow rhythm, we propose that it constitutes a novel, and previously unreported state of hippocampal neural activity that we have called the hippocampal SO. We also suggest that the dynamic coordination of the SO across hippocampal- and neo-cortices could constitute a vehicle for the consolidation of hippocampal-dependent memory processes. Preliminary descriptions of these results have appeared in abstract form (Grams et al., 2003; Wolansky et al., 2004; Dickson et al., 2005).

Materials and Methods

Data were obtained from 139 (chronic n = 12; acute n = 127) male Sprague-Dawley rats weighing 184.8 to 502.5g (average ± SEM: 270.4 ± 5.1g). All methods conformed to the guidelines established by the Canadian Council on Animal Care, the Society for Neuroscience, and were approved by the Biosciences Animal Policy and Welfare Committee of the University of Alberta.

Chronic (Behaving) Preparation

Anaesthesia and surgery. Animals were initially induced with gaseous isoflurane (4 minimum alveolar concentration or MAC) in an enclosed anaesthetic chamber. Following loss of righting reflexes, they were administered an intraperitoneal (*i.p.*) injection of a ketamine/xylazine cocktail (90 and 10mg/kg, respectively). Supplements of the ketamine/xylazine cocktail (10% of original dose) were administered as necessary to maintain the animal's level of anaesthesia. Rats were given a subcutaneous injection of atropine methyl nitrate (0.05 mg/kg) to prevent respiratory complications. Following anaesthesia, body temperature was maintained at 37°C using a servo driven system connected to a heating pad and rectal probe (TR-100, Fine Sciences Tools; Vancouver, BC, Canada).

Using antiseptic stereotaxic techniques, animals were implanted with unilateral neocortical (from bregma: **AP**: +0.3, **ML**: +1.0, **DV**: -0.2 or -1.5mm) and bilateral hippocampal (from bregma: **AP**: -3.3, **ML**: ±2.0, **DV**: -2.8 to -3.3mm) electrodes. An additional uninsulated electrode implanted vertically in the

frontal nCTX (verified to be electrically neutral by comparison to ground) served as an indifferent electrode. All intracerebral electrodes were manufactured by Plastics One (Roanoke, VA). Bipolar EMG electrodes were constructed from Teflon insulated stainless steel (bare diameter of 125µm: A-M Systems Inc.; Carlsborg, WA) and were implanted in the neck musculature as described elsewhere (Whelan, 2003). A wire soldered to a skull screw placed over the cerebellum served as ground. All wires and connector assemblies were fixed to the skull using jeweller's screws and dental acrylic. Following implantation, the scalp was cleaned and sutured, and the animal was placed in a clean cage.

Animals were allowed to recover for a minimum of one week prior to any recording. During this time, they were handled on a daily basis and habituated to the recording apparatus for at least two hours each day during the light cycle. During the habituation procedure, all leads were connected to suspended wires and animals were allowed to freely behave in the recording chamber which was contained in a Faraday cage and housed in a quiet room. Adequate habituation ensured that animals slept during recording sessions.

Multi-site field and occasionally field and multiunit, recordings were made simultaneously during ongoing (spontaneous) behaviour for a variable time period (1 to 8 hours) daily. Continuous observation or video monitoring ensured that samples for analysis were taken during periods when the animal was sleeping. To be qualified as sleep, the animal had to be in a resting posture, with the head and body down and the eyes closed. During sleep, REM and non-REM episodes could be differentiated by the presence or absence of activated patterns of EEG in the

nCTX (LVFA) and HPC (theta), respectively. Further confirmation was obtained with electromyogram (EMG) recordings; a decrease in EMG tone was concomitant with non-REM to REM alternations. Further details of electrical recording procedures are described below. Following adequate samples of natural sleep, rats were prepared for acute anaesthetised recordings as described in the subsequent section. Recordings were taken using the same connector pins used for naturally sleeping recordings.

Acute (Anaesthetised) Preparation

Anaesthesia and surgery. Animals were initially induced with gaseous isoflurane (4 MAC) in an enclosed anaesthetic chamber. Following loss of righting reflexes, they were maintained on isoflurane (2.0 to 2.5 MAC) via a nose cone and implanted with a jugular catheter. Isoflurane was discontinued and general anaesthesia was achieved using slow intravenous (*i.v.*) administration of urethane (0.8g/ml; final dosage 1.3 ± 0.01g/kg) via the jugular vein. Body temperature was maintained at 37°C using a servo driven system connected to a heating pad and rectal probe (FST) for the remainder of the surgical and recording procedures. Level of anaesthesia was assessed throughout the experiment by monitoring reflex withdrawal to a hindpaw pinch. If any visible withdrawal occurred, the animal was administered a supplemental dose (0.01ml) of urethane.

Stereotaxic placement of fixed recording and indifferent electrodes was conducted for frontal neocortical, hippocampal, and entorhinal sites as previously described for the chronic preparation. Recording electrodes were constructed from

Teflon-coated stainless steel wire (bare diameter 125µm: A-M Systems Inc.). These electrodes were aimed at the frontal (**AP**: +0.3, **ML**: ±1.0mm), and posterior (**AP**: -4.5, **ML**: ±1.5mm) neocortices, either in superficial (**DV**: -0.1 to -0.25mm; *fCTX sup*) or deep (**DV**: -1.0 to -1.5mm; *fCTX deep*) layers; the hippocampal fissure of the dorsal HPC (**AP**: -3.3, **ML**: ±2.0, **DV**: -2.8 to -3.3mm; *HPC fiss*); and the supEC (**AP**: -8.5, **ML**: ±4.5, **DV**: -5.5 to -8.0mm). An indifferent electrode, consisting of either an electrically connected pair of thick Teflon insulated wires (200µm: A-M Systems Inc.) staggered by 1.5mm or a single wire of the same type scraped bare to a distance of at least 1.5mm, was implanted in the frontal hemisphere (verified to be electrically neutral by comparison to ground). The stereotaxic apparatus was connected to ground. Following implantation, all static electrodes were fixed to the skull using jeweller's screws and dental acrylic.

Recording Procedures

Field recordings. All field potential recordings were amplified at a gain of 1000 and filtered between 0.1 to 500Hz using a differential AC amplifier (Model 1700, A-M Systems Inc.). All single electrode signals were referenced to the implanted indifferent electrode. In some cases, signals were recorded using alternate configurations of the reference (including ground) and comparisons of the different configurations did not reveal any gross differences in the signals (**Figure 2-01**). Following recording sessions, small lesions were made at the tips of active electrodes by passing 0.1 to 1mA of D.C. current for 5s using an isolated

constant current pulse generator (Model 2100, A-M Systems Inc.) allowing us to specify their location during histological procedures (*see below*).

Multiunit recordings. Multiunit recordings were made using the same electrodes as described for field recordings above. Signals were amplified at a gain of 1000 and bandpass filtered between 0.5 to 5kHz. Offline digital filtering (*see below*) allowed us to extract both the LFPs and simultaneous multiunit activity from these traces. As with field electrodes, small electrolytic lesions were made at the electrode tips to localise their intracerebral position.

Single-unit recordings. Single-unit activity was recorded using fine glass micropipettes (inner diameter: 1.12mm; outer diameter: 1.5mm; A-M Systems Inc.) filled with 0.5M sodium chloride or sodium acetate mixed with 2% pontamine sky blue (resistance ranging from 5 to 30MΩ). Micropipettes were mounted on a single axis fine hydraulic micromanipulator (FHC; Bowdoinham, ME) that was positioned over the brain with a coarse 3-axis manipulator (FST). Signals were initially amplified using a DC amplifier (Neurodata IR-283, Cygnus Technology, Inc.; Delaware Water Gap, PA) at a gain of 10, split, and further amplified using two channels of an AC amplifier (Model 2100, A-M Systems Inc.). One of these channels was amplified at a gain of 1000 and bandpass filtered between 0.5 to 10kHz for unit activity and the other was amplified at a gain of 100 and bandpass filtered between 0.1 to 500Hz for local field activity. Comparison of the glass micropipette's local field signal to the contralateral fixed hippocampal electrode (amplitude, frequency composition, and phase) aided in determining the vertical position of the glass micropipette tip. At the end of the

recording session, pontamine sky blue was iontophoresed by 250 to 300ms pulses of 1mA positive current applied at a frequency of 1Hz for 5 to 10 minutes to the position of the electrode tip.

Linear multiprobe recordings. Multi-channel field recordings were made using 16-contact silicon multiprobes arranged in a vertical linear array with a contact separation of 100µm (Center for Neural Communication Technology, University of Michigan; Ann Arbour, MI). Signals from the probe were amplified at a final gain of 1000 and wide-band filtered between 0.7Hz to 10kHz via a 16-channel headstage (unity gain) and amplifier system (Plexon Inc.; Dallas, TX). All signals from the multiprobe were referenced to stereotaxic ground. Simultaneous extracellular voltage profiles were taken at spatial intervals of 0.5mm from the surface of the brain to a final depth of 4.5mm using the coordinates contralateral to the dorsal HPC reference electrode described above (**AP**: -3.3, **ML**: ±2.0mm). The signal from the first (deepest) channel on the probe was audio amplified and sent to a speaker. The well established electrophysiological profile of theta field activity (Bland and Bland, 1986), robust increases in multiunit activity, and the distribution of evoked potentials via afferent stimulation (*see below*) aided in the determination of the vertical position of the probe.

In order to make the multiprobe track visible for histological purposes, the probe was moved slightly in two horizontal planes at its most ventral position.

The position of the probe track in every experiment was verified by comparing the histology to a laminar profile of the ongoing field potentials.

Evoked potentials. Bipolar stimulating electrodes were constructed from a twisted pair of thick Teflon insulated wires (200µm: A-M Systems Inc.), with tips vertically staggered by 0.5 to 1.0mm. Electrodes were aimed at the contralateral ventral hippocampal commissure (**AP**: -0.9, **ML**: ±0.5, **DV**: -3.9 to -4.2mm), the ipsilateral perforant path (**AP**: -7.3, **ML**: ±5.0, **DV**: -2.4 to -2.7mm), and/or contralateral CA3 (**AP**: -3.8, **ML**: ±3.75, **DV**: -2.6 to -2.9mm). Profiles were generated by passing a biphasic pulse of 50 to 200µA of D.C. current for 0.2 to 0.5ms using an isolated constant current pulse generator (Model 2100, A-M Systems Inc.).

Electromyogram recordings. Potentials from bipolar EMG electrodes were referenced to each other, amplified at a gain of 10000 and bandpass filtered between 10 to 500Hz.

Respiration. In some anaesthetised animals, a thermocouple wire (30 gauge Type K; Thermo Electric Co., Inc.; Brampton, ON, Canada) was placed just inside the nasal passage and its signal amplified at a gain of 10000 and filtered between 0.1 and 500Hz. This method yielded a continuous representation of the respiratory cycle due to the temperature difference between inspired and expired air (Chaput and Holley, 1980).

Data storage. Field and EMG activity was sampled at 1kHz, multiunit activity at 10kHz, and single-unit activity at 20kHz. All signals were digitised

with a Digidata 1322A A-D board connected to a Pentium PC running the AxoScope acquisition program (Axon Instruments; Union City, CA). Most experiments were digitised online but some multi-channel field experiments were initially recorded on tape using a 4-channel DAT recorder (CDAT4; Cygnus Technology Inc.) at a sampling frequency of 2.5kHz before being digitised.

Euthanasia and Histology.

At the end of anaesthetised recording sessions, rats were perfused transcardially, initially with physiological saline, and then with 4% paraformaldehyde in saline. Brains were extracted and stored overnight in 30% sucrose in 4% paraformaldehyde. The tissue was frozen with compressed CO_2 and sliced at 48μm with a rotary microtome (Leica 1320 Microtome; Vienna, Austria). Slices were then mounted on gel-coated slides, allowed to dry for a minimum of 24 hours, subsequently stained using cresyl violet or thionin, and cover-slipped. Microscopic inspection of stained slices was used to verify recording loci. Digital photomicrographs (Canon Powershot S45; Tokyo, Japan) were taken on a Leica DM LB2 (Buffalo, NY) microscope, imported using Canon Remote Capture 2.7 software (Tokyo, Japan) and processed with Corel PhotoPaint (Ottawa, ON, Canada).

Data Processing and Analysis

Raw signals were first examined visually using AxoScope (Axon Instruments) and segments for further analysis were chosen. Subsequent analyses were conducted using Matlab Version 5.1 or 5.3 (Mathworks; Natick, MA) and visualised using Origin Version 6.0 (Microcal Software Inc.; Northampton, MA).

These analyses included: digital filtering, single and dual-channel spectral analyses, and auto- and cross-correlations for field signals, spike triggered averaging, autocorrelation, and phase cycle preference for unit and multiunit signals. Single and dual-channel spectral analyses were performed to confirm the EEG state of visually-selected data segments prior to further analysis (*see below* and **Figure 2-06**). Our digital filtering technique was confirmed to elicit zero phase distortion by both spectral and cross-correlation analyses (**Figure 2-02**).

Field recordings. Autopower, crosspower, cross phase, and coherence spectra were computed and plotted for field signals and signal pair combinations. Spectra were computed from data segments whose length depended upon the type and stationarity of the signal. For segments of activated patterns with higher frequency components such as theta, segments were at least 30s. For deactivated patterns with lower frequency components such as LIA and slow oscillations, segments were at least 60s. Using Welch's periodogram method, spectra were estimated from a series of 6s long, sequential Hanning windowed samples from these data segments with 2s overlap. Spectral values were averaged across a peak frequency bandwidth (peak frequency ± 1/6Hz) and compared across EEG states. Spectral profiles for theta and slow oscillatory activity recorded with the linear multiprobe were also constructed in this way by comparing each trace from the probe against a fixed (hippocampal or cortical) reference and extracting peak frequency values. Because of the differences in the frequency responsiveness of the two amplification systems used, we corrected for potential phase distortion of simultaneously recorded signals between them by performing a spectral phase

analysis of pure sine input ranging from 0.1Hz to 30 Hz and mathematically accounting for any frequency-dependent discrepancies in all subsequent analyses (**Figure 2-03**).

Spectrograms were computed from even longer data segments (several minutes) in which spontaneous state alternations took place. A sliding windowing procedure was adopted that allowed discrete spectra to be calculated for specific time points across the entire data segment. Windows were 24s in duration and were moved across the data segment in increments of 6s. Spectral analysis of these individual windows was identical to the methods described above, although estimates of coherence were based on smaller (2s) Hanning windowed segments.

The range of time lags for auto- and cross-correlations of field activity depended on the peak power frequency as computed by autospectral analysis. For frequencies $\leq$ 1Hz, we used a window size of 2.5s while for frequencies $\geq$ 3Hz, we used a window size of 1s. Sliding cross-correlations of larger data segments were conducted using a sliding windowing procedure similar to that for spectrograms. Windows were 5s in duration and were moved across the original data segment in increments of 1 to 2.5s.

Single unit activity. Spike rates, inter-spike intervals, and autocorrelation histograms (10-100ms bin size) were computed to analyse spike train dynamics. The relationship between EEG and unit activity was assessed by spike-triggered averaging (STA) of simultaneously recorded field potentials. The preferred phase of unit spiking to rhythmic field activity was assessed separately by filtering the contralateral reference hippocampal field in a specific bandwidth (0.5 to 1.5Hz for

the SO and 3 to 6Hz for theta) and then computing the time points of negative to positive zero crossings. Unit activity was binned (bin size: 18°) according to the phase of the field cycle from 0 to 360° (i.e., one zero crossing to the next).

Current source density analysis. Current source density (CSD) analysis was conducted on spontaneous or averaged field profiles recorded using the linear multiprobe following the assumptions of Freeman and Nicholson (1975), Nicholson and Freeman (1975), Rodriguez and Haberly (1989), and Ketchum and Haberly (1993). Spontaneous multiprobe traces were lowpass filtered at 10Hz prior to CSD computation. Comparison of filtered and unfiltered CSD profiles revealed no gross differences aside from fast frequency sink-source alternations. Briefly, CSD was computed by estimating the second spatial derivative of voltage traces derived from the multiprobe. This estimate was calculated using a three-point difference (differentiation grid size of 300μm) on the voltage values across spatially adjacent traces:

$$CSD = [f(p_{i-1})-2f(p_i)+f(p_{i+1})]/d^2$$

Where $f(p_i)$ is the field signal from probe channel i (i = 2, 3, …, 14) and d is the distance between adjacent channels (0.1mm).

Multiunit, gamma, dentate spike, and ripple activity. Multiunit activity was extracted from wide-band recorded signals by digital filtering of the original signal (0.5 to 5kHz). Gamma (25-80Hz), dentate spiking (70-140Hz) and ripple (140-220Hz) activity were extracted using a similar procedure. In order to analyse the relationship of these forms of activity to the SO, they were rectified and

subjected to a similar set of analyses as previously specified for single unit activity.

Statistics. All comparisons across conditions for the same datasets were made using one-tailed pair-wise *t*-tests ($p < 0.05$). As most tests were specified *a priori*, this was also the case for datasets with more than two conditions. For remaining situations, data were analysed using ANOVA. A Scheffé correction was made for subsequent post-hoc pair-wise tests.

The significance of the time series analyses conducted were assessed through comparisons with the 95% confidence limits of either the estimation procedure or a randomised distribution computed on the same datasets. Randomised coherence distributions were computed by shuffling the time windows of one signal versus another from the same data set used for the original coherence estimation. In all cases, the distribution of these randomised coherence values (random $n \geq 144$) varied between 0 and 0.025 across all frequencies. Randomised cross-correlation distributions were also computed using this same time window shuffling procedure from the same data set used for the original cross-correlation computation. Since the distribution of randomised values (random $n = 100$) varied systematically across different lag values, the 95% confidence limits were extracted from the randomised distribution as a function of lag and compared to the actual cross-correlation function. For strongly correlated signals, the maximal value of this randomised distribution was a small fraction (2.5 to 10%) of the first (near zero lag) peak. Autocorrelation function significance was assessed by comparison to a distribution of 100 different

autocorrelograms computed on lowpass (3Hz) filtered noise. The spectrum of this filtered noise represents a random phase approximation of a typical EEG spectrum. The significance of spike-triggered averages (STAs) was computed by comparison to the distribution of STAs computed using a series (n = 100) of randomised (shuffled) spike trains derived from the original data. The shuffling of spike trains was conducted through random assignments based on the actual inter-spike intervals computed for the original spike train. The resulting distribution of STAs had a variance which was proportional to the amplitude of the original field signal but which was lower than the original fluctuations for signals with a strong correspondence.

The significance of autocorrelation histograms derived from point processes (unit activity) was assessed by computing the average bin value and their fluctuations within a randomised distribution (random n = 100). Confidence limits were computed as the average value ± 2*SEM. Any units with autocorrelation histograms demonstrating systematic and periodic fluctuations beyond this window were classified as rhythmic. This technique has been noted to eliminate problems using either spectral or Gabor fitting analyses (Samonds and Bonds, 2005). The frequency of any periodicity was assessed by Fourier transformation of the autocorrelogram. Phase histograms were statistically evaluated using the Rayleigh statistic for circular data (Zar, 1999).

Drugs and Chemicals

Atropine methyl nitrate, atropine sulfate, eserine, lidocaine, oxotremorine, scopolamine, thionin, and urethane were all purchased from Sigma (St. Louis,

MO). Pontamine sky blue was purchased from Avocado Research Chemicals (Heysham, Lancaster, UK). Isoflurane and ketamine were purchased from Bimeda-MTC (Animal Health Inc.; Cambridge, ON). Cresyl violet was purchased from Acros Organics (Morris Plains, NJ), paraformaldehyde from Fisher Scientific (Toronto, ON), and xylazine from Bayer Inc. (Toronto, ON).

Results

The hippocampal slow oscillation: a novel state in normal sleep and under anaesthesia

In preliminary recordings of hippocampal EEG under naturally sleeping and urethane-anaesthetised conditions, we noted a large-amplitude, highly rhythmic slow activity that was spontaneously and periodically apparent in both conditions (**Figure 2-04**). This wave pattern appeared visually and spectrally different from other previously described forms of hippocampal state – dependent EEG observed during sleep or anaesthesia (such as theta or LIA) and had distinct behavioural correlates. Under freely behaving conditions, this slow rhythmical activity only emerged during prominent SWS episodes within non-REM sleep. Under urethane, the spontaneous appearance of this activity (and its regularity/rhythmicity) appeared to be dependent upon the level of anaesthesia; increasing anaesthetic dosage moderately increased the proportion of time spontaneously spent in the slow oscillatory state (correspondingly decreasing the amount of time spontaneously spent in theta). Conversely, experiments conducted under lower levels of anaesthesia, or in which the level of anaesthesia became gradually lighter (partial metabolism over a time period greater than 1hr) showed the opposite relationship. In addition, the slow rhythmic wave pattern was abolished by robust sensory stimulation in both sleeping (auditory stimulation) and anaesthetised (hindpaw or tail pinch) conditions. Based upon these observations and the fact that the slow, rhythmic activity in the HPC appeared to be related to a similar form of activity in the nCTX, we elected to name this novel

hippocampal state the hippocampal SO, in keeping with nomenclature already established for slow neocortical activity (Steriade et al., 1993c; Amzica and Steriade, 1997).

The spontaneous evolution of the hippocampal SO was remarkably similar in both naturally sleeping and anaesthetised recordings conducted in the same animals (n = 12) as shown in **Figure 2-04 A** and **B**. As described by previous researchers (Rimbaud et al., 1955; Jouvet et al., 1959b; Winson, 1972; Robinson et al., 1977; Vanderwolf et al., 1977), hippocampal EEG alternated between activated and deactivated patterns in concert with activated (LVFA) and deactivated (slow wave) patterns in the nCTX during sleep, expressed during REM and non-REM, respectively (**Figure 2-04A**). Specifically in the HPC, spontaneous alternation between REM and non-REM involved a gradual EEG state transition from theta, to LIA, and finally to the SO. The alternation from non-REM back to REM was characterised by a relatively abrupt change from the SO to theta, which could involve a brief transition through LIA. Remarkably, the same electrographic elements could be observed during spontaneous state changes under urethane anaesthesia, and their evolution followed a highly similar pattern (**Figure 2-04B**).

Classically, LIA has been regarded as the deactivated state in the HPC (Vanderwolf, 1969; Leung et al., 1982; Buzsáki et al., 1983; Leung, 1985; Buzsáki, 1986, 1996) and is characterised by a non-rhythmic, broadband signal with large-amplitude transients (see *raw trace expansions*, *autocorrelation functions*, and *spectra* in **Figure 2-04 A** to **F**). While the SO also appeared during

deactivated stages, it could be differentiated from LIA as a clearly rhythmic, ~1Hz signal of very high amplitude (power at ~1Hz during sleep/LIA: 14.62 ± 1.89 versus sleep/SO: 44.96 ± 8.41 and urethane/LIA: 11.69 ± 5.09 versus urethane/SO: 42.11 ± 13.66mV^2 were significantly different in the HPC; *t-test: $p < 0.05$; see **Figure 2-04 E** and **F**). Based upon both their electrographic signatures and their differential expression during the evolution of EEG states, LIA and the SO appeared to represent clearly distinct states, apparent even when the concurrent neocortical field had a strong ~ 1Hz component (power at ~1Hz during sleep/LIA: 9.32 ± 0.41 versus sleep/SO: 10.4 ± 0.78 and urethane/LIA: 24.65 ± 9.80 versus urethane/SO: 27.54 ± 10.5mV^2 were not significantly different in the nCTX; t-test: $p > 0.05$; see *spectra* in **Figure 2-04 E** and **F**).

One difference between the expression of the hippocampal SO during sleep versus urethane anaesthesia had to do with its longevity and stability. During sleep, the SO was only apparent during deep SWS episodes and was frequently interrupted by short arousals, during which the SO was replaced by irregular (LIA-like) activity or, if a movement occurred, an activated (theta) pattern. An SO episode under urethane was highly stereotyped, lasting a predictable amount of time, could be (briefly) interrupted by segments of LIA, but was very rarely interrupted by EEG activation (i.e., theta).

Simultaneous field and multiunit recordings from verified hippocampal sites (those shown are from the DG in SGran) suggested that hippocampal neuronal populations tended to generate action potentials in a phase-related manner to the ongoing SO in both natural sleep and urethane anaesthesia (**Figure**

2-04 G and **H**). In order to determine whether this state modulated ongoing cellular dynamics in the HPC and to conclusively demonstrate that the SO is a truly distinct state from LIA, we performed simultaneous single-unit and field recordings in the HPC of urethane-anaesthetised animals. In order to be analysed, adequate continuous and stationary samples of spontaneous theta (≥ 30s), and the SO (≥ 60s) states were required. In most cases, an additional 60s of LIA was also obtained. Under these conditional limitations, we obtained and analysed data from 38 single neurons from twenty animals in a variety of hippocampal subfields.

The SOr unit shown in **Figure 2-05** demonstrated a significant (*t-test: $p < 0.01$) change in its mean firing rate (**Figure 2-05G**) and its pattern of discharge (**Figure 2-05 B** and **C**) across spontaneous state changes from theta to LIA and the SO (see **Figure 2-05A**). Notably, this unit demonstrated a rhythmic spike pattern that was phase related to ongoing field oscillations in the contralateral HPC during both theta and the SO (*left* and *right-most panels* in **Figure 2-05C**), but the preferred phase of spiking to the field reversed polarity across the two states (theta: 82°; Rayleigh z = 211, n = 926, $p < 0.01$; SO: 288°; Rayleigh z = 150, n = 2004, $p < 0.01$; *left* and *right-most panels* in **Figure 2-05 B**, **D**, and **E**). Spectral and autocorrelational analyses of the field signals for each state verified that the field states were truly different (*grey shaded area* represents 95% confidence interval; **Figure 2-05F**).

Of all units recorded (n = 38; SOr/SPyr n = 14; SRad n = 5; SLM n = 8; SMol/SGran n = 10; SGran/hilus n = 1), 34/38 (89%) showed a significant change in spike train dynamics during the SO. 25/38 (66%) generated rhythmic and

phase-related action potentials during the hippocampal SO, 23/38 (61%) showed a significant (*t-test: $p < 0.05$) change in their firing rate during LIA as compared to the SO, and 16/38 (42%) showed both. Of the remaining 13/38 (34%) neurons that were not rhythmic during the SO, only 10 were recorded with adequate samples of LIA for a full comparison. Significant changes in spike rates were observed in 7/10 of these neurons when comparing across LIA and the SO (*t-test: $p < 0.01$). Therefore, the vast majority of hippocampal neurons sampled showed definitive, yet diverse changes in spike train dynamics during the SO.

Most of the neurons that generated rhythmic action potentials during the SO also did so during theta (21/25: 84%). Interestingly, 15/21 (71%) of the neurons that were rhythmic during both the SO and theta (including that shown in **Figure 2-05**) demonstrated a change in the polarity of their preferred phase to the field oscillation when comparing across the two states regardless of their anatomical location (SOr/SPyr n = 6/8: 75%; SRad n = 3/4: 75%; SLM n = 2/3: 67%; SMol/SGran n = 3/5: 60%; SGran/hilus n = 1/1: 100%). In general, most theta-related cells (Bland and Colom, 1993) appeared to be modulated by both hippocampal theta and the SO (32/35: 91%), however, neither firing rates nor spike train dynamics during theta predicted spiking behaviour during the SO.

Coordination of the hippocampal and neocortical slow rhythms

Due to the highly stereotyped fashion in which the SO repetitively emerged under urethane anaesthesia, we examined the temporal correspondence of the SO across the two structures in finer detail using this preparation; an

example is shown in **Figure 2-06**. By examining temporally expanded traces taken in succession across the extended-duration field recordings from the HPC and nCTX, and by computing a spectrogram for the entire episode, the evolution of the SO and the unique pattern of its coordination across the two cortical regions could be observed more explicitly. In 52 animals, we observed a total of 343 spontaneous evolutions of the hippocampal SO comprised of the basic pattern described above (theta – LIA – SO – LIA – theta). In a further 13 animals, the anaesthetic level was at a depth which prevented spontaneous alternations into the activated state. In most of these cases (n = 8), evidence of fluctuations between LIA and the SO could be observed.

As shown in the raw traces (**Figure 2-06A**), spectrograms (**Figure 2-06B**), and spectra (**Figure 2-06C**), the SO typically appeared first in the nCTX and was correlated with the appearance of LIA in the HPC. When the SO eventually appeared in the HPC, it was only transiently coordinated with the SO in the nCTX (*raw trace expansions* in **Figure 2-06A**). Slow rhythms in the nCTX typically outlasted the SO in the HPC, but only for a brief amount of time.

Not surprisingly, the spectral coherence of the SO across cortical and hippocampal sites for the above experiments only tended to be moderate (~0.5) and variable within and across any given episode. To verify that this level of coherence was a genuine feature of the hippocampal-neocortical interaction, we performed additional experiments in which we recorded from two distant neocortical sites simultaneously with the hippocampal site (n = 7) or from two homotypic hippocampal sites simultaneously with a single neocortical site (n = 6)

in the urethane-anaesthetised animal (**Figure 2-07**). In these experiments, the coherence of the SO computed between intracortical (0.9 ± 0.01) and inter-hippocampal (0.9 ± 0.02) sites was consistently high, but only intermediate for cortical to HPC sites (0.5 ± 0.06 in **A**; 0.6 ± 0.06 in **B**; **t*-test: $p < 0.01$; *lower panels* of **Figure 2-07 A** and **B**).

To investigate the hippocampal-neocortical dynamics of SO coordination over time, we performed sliding cross-correlation analyses of hippocampal and neocortical activity across single SO evolutions in the urethane-anaesthetised animal. Individual cross-correlations at successive (**Figure 2-08C**) and specific times (**Figure 2-08D**) during the evolution of the SO showed that both the first (~0s lag) and second (~1s lag) peak correlation values tended to increase significantly over time, although there was a systematic and periodic fluctuation in both correlation and coherence values (**Figure 2-08E**). The periodicity of the cross-correlation fluctuations overlapped extensively and consistently across all SO evolutions (minimum of 3 used) within the same animal, as well as across all experiments (n = 7; 17.2 ± 0.6s; ~0.05Hz; **Figure 2-08F**).

Previous studies have suggested that there may be a functional relationship between respiration and the slow oscillatory EEG activity in medial temporal cortices under urethane or ketamine/xylazine anaesthesia (Fontanini et al., 2003; Manns et al., 2003; Fontanini and Bower, 2005). We assessed if any such relationship existed in our own experiments (n = 5) by performing spectral analysis between the respiratory cycle and both hippocampal and neocortical EEG signals (see **Figure 2-09**).We found that the SO EEG signal (regardless of site)

had a completely different peak frequency from the respiratory rhythm (HPC: 1.33 ± 0.08; nCTX: 1.33 ± 0.08; respiration: 2.17 ± 0.15Hz; *t-test: $p < 0.01$), and was also non-coherent with it (HPC versus respiration: 0.19 ± 0.03; nCTX versus respiration: 0.14 ± 0.02). SO power and hippocampal-neocortical coherence (0.57 ± 0.03) were consistent with our previous findings (**Figure 2-07**).

Cholinergic modulation of the slow oscillation

In naturally sleeping conditions, the ascending cholinergic system has been shown to play a role in the activation of forebrain regions: activated patterns of the EEG are correlated with elevated levels of acetylcholine (ACh) as compared to deactivated patterns (Jasper and Tessier, 1971; Kametani and Kawamura, 1990; Day et al., 1991; Williams et al., 1994). As well, exogenous activation of cholinergic receptors induces the activated state in the nCTX and HPC, and muscarinic antagonists induce the deactivated state (Bland, 1986; Vanderwolf, 1988; Steriade et al., 1993b). In order to confirm that the SO in the HPC of urethane-anaesthetised rats followed a similar dependence, we performed systemic manipulations of cholinergic neurotransmission. Consistent with prior findings, both the hippocampal and the neocortical SO were abolished by systemic administration of eserine (n = 5) or oxotremorine (n = 5) (**Figure 2-10B**) and were enhanced by atropine (n = 6) (**Figure 2-10C**). The frequency composition of spontaneous activity and pharmacologically-induced hippocampal theta (F (2, 17) = 4.1, $p > 0.05$) and SO (t-test: $p > 0.05$), in addition to the peak frequency power of spontaneous activity as compared to pharmacologically-

induced theta (F (2, 11) = 1.6, $p > 0.05$) and SO (t-test: $p > 0.05$) were highly similar (see **Figure 2-10 D**, **E**, and **F**). The ability of muscarinic antagonism to promote the SO at both hippocampal and neocortical sites was consistent for experiments in which atropine was administered alone or following cholinergic agonism in the same animal (n = 4). In all cases, spontaneous state changes were completely abolished following either muscarinic agonism or antagonism.

Laminar profile analysis of the hippocampal slow oscillation

It is clear that while the slow oscillatory activity in the HPC and nCTX are somewhat independent, they are also coupled. One possible coupling mechanism could be through cortico-hippocampal synaptic interactions mediated via the EC (Collins et al., 1999; Lavenex and Amaral, 2000; Witter et al., 2000). We performed laminar profile and CSD analyses of field activity using the linear multiprobe through both the nCTX and dorsal HPC of urethane-anaesthetised rats. We recorded samples of both spontaneous SO and theta field activity at sequential 0.5mm depth intervals, to a final depth of 4.5mm ventral to the pial surface (n = 12). At every position, we computed the spectral profile (autospectral power, cross phase, and coherence) for each channel of the probe across the two states (14 channels across 1.4mm in each recording). Power values were averaged across a 0.3Hz bandwidth centered on the peak power frequency (peak frequency ± 1/6Hz; 0.7 to 1.3Hz for the SO: 1.1 ± 0.01Hz and 3.2 to 4.7Hz for theta: 3.9 ± 0.03Hz) and were normalised to power values at the stationary HPC electrode. Phase and coherence values between probe sites, the stationary neocortical

electrode (for the SO), and the stationary hippocampal electrode (for theta) were averaged across the same frequency ranges. All values were arranged by relative depth, plotted and verified against the topography of the histological probe track as shown in **Figure 2-11 A** and **B**.

The profile for theta rhythm (*black lines*; **Figure 2-11B**) was consistent with that of previous reports (reviewed in Bland, 1986). No dipole was observed in the nCTX, although one was observed in the HPC. A null zone was located just below SPyr in the inner portion of SRad, at a depth of 2.6mm in the experiment shown (2.6 ± 0.02mm). This depth corresponded to the location of the phase reversal and to a significant drop in the coherence of the theta signal in all animals. In addition, theta was maximal at a depth of 3.0mm (3.1 ± 0.03mm), which was established to be at the level of SLM and the hippocampal fissure based on previous descriptions (Winson, 1974; Bland and Whishaw, 1976; Buzsáki et al., 1986) (reviewed in Bland, 1986) and histological verification.

The profile for SO (*red lines*; **Figure 2-11B**) is shown superimposed upon the theta profile. Across all experiments, there was an obvious SO field dipole in the nCTX. This is consistent with previous research on the neocortical SO (Amzica and Steriade, 1998). The neocortical SO phase reversal and a significant drop in the coherence of the signal as compared to the static cortical site occurred at a depth which corresponded to layer IV or V (0.9mm; 0.86 ± 0.01mm) (**Figure 2-11B**). Although no null zone was observed in the HPC for the SO, a power maximum and a phase shift of ~20 degrees (22.3 ± 1.1º) existed at a depth of 2.9 to 3.0mm (3.1 ± 0.02mm). This phase shift reflects an average time difference of

56 ± 3ms for hippocampal versus neocortical activity at 1Hz. In all 12 experiments and as depicted in **Figure 2-11B**, the power value at this level was even larger (459.7 ± 21.8%) than those recorded at the maximal neocortical site. The location of the SO power maximum and phase shift reliably corresponded to the position of the maximal power value of theta (SLM/fissure). Finally, with the exception of the reversal point in the nCTX, the coherence throughout the SO profile was high (near 1.0), although values throughout the HPC tended to be lower and more variable (0.6-0.9).

Expanded raw traces of laminar profile recordings at the levels indicated (*blue box/numbers*) in **Figure 2-11B** demonstrate the above-mentioned features for both theta (**Figure 2-11C**) and the SO (**Figure 2-11D**). The null (reversal) point for theta is clearly seen in trace #5 (inner SRad) while the maximum is present at trace #9 (SLM/fissure). Although the rhythmicity of the SO is less clear, the maximal amplitude is observed at same level (trace #9: SLM/fissure) as for theta. Interestingly, fast transient events could also be observed to reverse at or near this level. By averaging 32 1.5s long segments of phase-matched, filtered (10Hz lowpass) SO activity, we constructed an average voltage profile through the HPC that clearly demonstrates the SO phase shift within the HPC (**Figure 2-11E**). CSD analysis on this averaged voltage profile revealed a large sink at the point of SO maximum (trace #9: SLM/fissure) and smaller sinks straddling trace #6 (SRad).

In order to verify the laminar location of recording sites along the multiprobe, averaged evoked potentials to single electrical shocks of known

hippocampal afferent pathways (contralateral CA3: n = 4; ventral hippocampal commissure: n = 3; perforant path: n = 4), along with samples of spontaneous field activity during theta and the SO, were mapped along each sequential positioning of the multiprobe and later compared to the histological track. CSD profiles for averaged evoked potentials and for continuous EEG recordings of spontaneous rhythms are shown in **Figure 2-12** aligned to a diagrammatical representation of the histological track.

As previously described (Buzsáki et al., 1986; Brankack et al., 1993; Bragin et al., 1995b), the CSD profiles of evoked potentials showed characteristic patterns of sinks and sources, which were used to delineate the various laminae within the HPC. Commissural (*not shown*) and contralateral CA3 stimulation produced the most massive sink in SRad of CA1 (*left panel* of **Figure 2-12A**). Perforant path stimulation evoked an early and large sink well below SRad of CA1 that spanned the molecular layer of the DG (*right panel* of **Figure 2-12A**).

CSD profiles for continuous samples of spontaneous theta (**Figure 2-12C**) were highly similar to those previously described using averaged phase-locked potentials (Buzsáki et al., 1986; Brankack et al., 1993; Bragin et al., 1995b). The largest amplitude sink-source alternations occurred at a depth that corresponded to SLM. CSD profiles for continuous samples of spontaneous SO (**Figure 2-12D**) also showed prominent sink-source alternations at ~1Hz at the same level (SLM). The amplitude of sink-source fluctuations at the level of the SLM was confirmed to be the largest using spectral analysis.

As SLM is the level of termination of the temporoammonic pathway, this suggests that entorhinal input may play an important role in the phasing, coordination, and possibly generation of the SO within the HPC. In support of this idea, we have made preliminary recordings of supEC field and multiunit activity (n = 3) in urethane-anaesthetised rats, which indicate that SO activity is also a prominent feature of the electrographic activity of the EC (**Figure 2-13**). Multiunit activity tended to occur rhythmically at ~1Hz (**Figure 2-13A**) and slightly before the negative phase (Rayleigh z = 41, n = 3053, $p < 0.01$) of the hippocampal field potential.

Although the largest amplitude sink-source alternations occurred in SLM, intermittent (but somewhat rhythmic) current flow was also observed in SRad during the SO (**Figures 2-11E** and **2-12D**). Some of this activity may represent passive current flow generated by active zones at the level of SLM since it tended to be of lower amplitude, opposing direction, and appeared temporally correlated to the latter. However, based upon their location, these events may also reflect hippocampal sharp waves (Buzsáki et al., 1983; Buzsáki, 1986; Suzuki and Smith, 1987) that are timed to the occurrence of the SO. To test this idea, we performed an analysis of the temporal relationship between the SO and hippocampal ripples (125 to 250Hz) (O'Keefe and Nadel, 1978; Buzsáki et al., 1983; Buzsáki, 1986; Suzuki and Smith, 1988b; Ylinen et al., 1995) that frequently co-occur with sharp waves. By triggering on SPyr ripple activity, we assessed any possible phase relationship between ripples and the slow component of the SLM CSD (**Figure 2-14 A** to **D**). Ripple-triggered CSD waveform averages (**Figure 2-14D)** and phase

histograms (**Figure 2-14C**) confirmed no significant phase preference existed (Rayleigh z = 6.7, n = 334, $p > 0.05$). This was not due to a reduction in overall ripple activity during the SO since the total ripple current flow was not significantly (*t*-test: $p > 0.05$) different between LIA (1.13 ± 0.4) and the SO (1.24 ± 0.5).

In CSD profiles that straddled the hippocampal fissure and included the molecular layer of the DG (SMol), sporadic current flow in concert with the SO was also observed (*not shown*). As these events appeared to be localised to the outer two-thirds of the molecular layer, this activity may represent dentate spikes (Bragin et al., 1995a). Current flow corresponding to dentate spiking tended to occur more during the SO (10.2 ± 3.3mV^2/mm^2) than during LIA (9.2 ± 3.5mV^2/mm^2), however, this difference was not significant (*t*-test: $p > 0.05$). Phase analysis of SMol dentate spikes in relation to the SO-filtered SLM CSD (**Figure 2-14 E** to **H**) revealed that they tended to occur during or just after the maximal sink in SLM (Rayleigh z = 65, n = 729, $p < 0.01$; **Figure 2-14G**) and occurred rhythmically at ~1Hz (**Figure 2-14H**).

In single electrode recordings (**Figures 2-04**, **2-05**, **2-06**, and **2-10**) and laminar profiles (**Figure 2-11D**), we noted that other high frequency components were elevated during the SO. By triggering on gamma (25 to 80Hz) activity, we assessed any possible phase relationship between SLM gamma and the slow component of the SLM CSD (**Figure 2-14 I** to **L**). Gamma-related current flow tended (not significant; *t*-test: $p > 0.05$) to be greater during the SO (81.2 ± 45) than during LIA (40.8 ± 12) at the level of SLM. In addition, gamma-related

activity fluctuated rhythmically at ~1Hz (**Figure 2-14L**) in phase with the maximal SO sink in SLM (Rayleigh z = 51, n = 732, $p < 0.01$; **Figure 2-14K**).

Discussion

The hippocampal slow oscillation as a novel state

Collectively, our data suggest that the rodent HPC demonstrates a previously undescribed, deactivated EEG state consisting of a rhythmic slow (≤ 1Hz) oscillation similar to, and coordinated with, the previously described neocortical SO (Steriade et al., 1993c). Although this type of activity would have historically been categorised as slow delta, our terminology follows the interpretation of Amzica & Steriade (1997).

As previously shown for the neocortical SO (Steriade et al., 1993a, 1993c; Steriade et al., 2001; Timofeev et al., 2001), the hippocampal SO is a spontaneous and similar feature of both SWS and urethane anaesthesia. Its unique temporal and spectral properties, its dynamic correspondence with the neocortical SO, and the differential activity of hippocampal units are all highly similar across both states and clearly demonstrate that the SO represents a different, and more deactivated state than LIA. One characteristic difference was the sporadic and transient appearance of the SO during sleep, whereas it tended to last longer and was more stereotyped under urethane anaesthesia. A similar phenomenon has been noted for the neocortical SO (Steriade et al., 1993c).

An important question concerns why this activity has never been previously reported or characterised. To a large extent, this is likely due to the disproportionate attention paid to the hippocampal “activated” (i.e., theta) state, although brief descriptions of a slow oscillatory state in the HPC under urethane anaesthesia (Leung, 1985; Suzuki and Smith, 1988a) and during sleep (Jouvet et

al., 1959a) do exist. Recent attention has been directed towards transient synchronised hippocampal patterns occurring during sleep (Buzsáki, 1986, 1996) and especially to their relationship(s) to ongoing neocortical activity (Siapas and Wilson, 1998; Sirota et al., 2003; Battaglia et al., 2004). These patterns have been considered without reference to the hippocampal SO. This may be for a number of reasons: 1) the lack of stationarity of the SO, especially during natural sleep (Steriade et al., 1993c), 2) the erroneous interpretation of the hippocampal SO as volume conducted potentials from overlying nCTX, 3) elimination of the SO signal due to intrahippocampal bipolar electrode arrangements and differential amplification (Robinson, 1980; Bland, 1986), and 4) elimination of the SO signal due to the common practice of hipass filtering ≥ 1Hz to reduce electrical artefacts in freely behaving animals (Steriade et al., 1993c).

Hippocampal cellular activity during the slow oscillation

As was suggested by one of the first paired single unit recording studies in the HPC during sleep (Noda et al., 1969a, 1969b), slow synchronisation between hippocampal units appears to be a prominent feature of the deactivated state. During the SO under urethane anaesthesia, hippocampal multiunit activity from both CA1 and dentate subfields appeared to be phase-related to the ongoing SO field and a high proportion of single units showed differential spike train dynamics during this field state.

The characteristics of single unit activity during the SO did not seem to be predicted by their behaviour during theta. Neither the classification of units as

theta-on or theta-off nor the classification of units as being phase related to theta (phasic or tonic) as described by Bland and Colom (1993), reliably provided any systematic indication of subsequent firing behaviour during the SO. Our data imply that the theta and SO states impose a distinct and overlapping influence on the dynamics of the hippocampal network and provide further evidence that different EEG activities reflect different functional processing states.

Coordination of the hippocampal and neocortical slow oscillations

One of the most striking and perhaps most important findings of this study concerned the dynamic coordination of the SO between the HPC and nCTX. The SO was often observed in the nCTX without concomitant activity in the HPC, although the converse was not true. This suggests that the regulation of the SO state across hippocampal- and neo-cortices is dependent on activity in ascending activating systems (likely cholinergic), and also that it is not directly paced from a common source. The coordination of the SO within the nCTX and HPC was consistently strong, whereas the coordination between these areas was variable and often only transient. These data strongly suggest that the neocortical and hippocampal SO phenomena are independently regulated; yet somehow coupled.

A likely mechanism for the coordination of neocortical and hippocampal SO is through synaptic interactions mediated via the EC. The bulk of neocortical input to the HPC arrives via the superficial layers (II and III) of the EC and the bulk of the hippocampal output returns to the nCTX via the deep layers (V and VI) of the EC (Lavenex and Amaral, 2000; Witter et al., 2000). Our hippocampal

CSD, EC field and EC multiunit recordings implicate the temporoammonic pathway (EC layer III to the apical dendritic zone of CA1; i.e., SLM) as providing robust, rhythmic, excitatory input at slow frequencies during the SO. In support of this, the SO has been previously noted in the EC of both the ketamine/xylazine anaesthetised and naturally sleeping cat (Collins et al., 1999; Collins et al., 2001) as well as the urethane-anaesthetised rat (Isomura et al., 2005). Furthermore, preliminary evidence from our laboratory (Dickson et al., 2005) suggests that lesions of the perforant pathway also affect the hippocampal SO.

Another possibility for regulation of hippocampal-cortical coordination comes from a thalamic input via the reuniens nucleus which also terminates in the SLM (Wouterlood et al., 1990) and is known to have feed-forward excitatory and inhibitory influences upon pyramidal cells in CA1 (Dolleman-Van der Weel et al., 1997; Bertram and Zhang, 1999). This input may be another, less direct pathway for cortical influences to be mediated in the HPC since the nCTX is known to modulate the SO in a variety of thalamic nuclei (Steriade et al., 1993d; Timofeev and Steriade, 1996). Future experiments should address the role of this structure in the coordination of neocortical and hippocampal SO.

Relationship of the slow oscillation to other hippocampal synchronised ensemble patterns

During non-REM sleep and anaesthesia, two transient and irregularly occurring population events have been previously described in the HPC: sharp waves co-expressed with ripple oscillations (~200Hz) (O'Keefe and Nadel, 1978;

Buzsáki, 1986; Suzuki and Smith, 1987; Buzsáki et al., 1992; Ylinen et al., 1995), and dentate spikes (Bragin et al., 1995a). Since CA1 ripples are known to be weakly correlated with slow neocortical activity during sleep (Siapas and Wilson, 1998; Sirota et al., 2003; Battaglia et al., 2004), we were interested to know whether they were also related to the hippocampal SO. Although some weak ripple-SO coupling was observed, dentate spikes were far more consistently phase-related to the SO. Since dentate spikes have been shown to be dependent upon superficial entorhinal input (Bragin et al., 1995a), this provides further evidence that neocortical and hippocampal SO coordination may be mediated via the EC. At a minimum, our data suggest that the hippocampal SO plays a selective role in shaping transient population dynamics throughout the trisynaptic pathway.

Although the gamma rhythm (25 to 80Hz) has been typically associated with the theta state (Bragin et al., 1995b), we also observed a large increase in this bandwidth during the SO. This gamma power increase appeared to be the largest in the SLM region and was phase related to the ongoing SO (maximal during the SO sink in SLM). We also observed a phase-related increase in gamma power at a similar position during ongoing theta. Although we can only speculate, this fast activity could be due to either: 1) fast synchronisation of inputs to SLM, or 2) a locally reverberating network in SLM.

Effects of pharmacological agents on hippocampal slow oscillation: Implications for its generation and dependence upon neural activity in ascending activating systems

The control of hippocampal activation during sleep and urethane anaesthesia is known to occur solely via ascending cholinergic influences, unlike that in freely-moving animals (reviewed in: Bland, 1986; Vanderwolf, 1988). Pharmacological challenges that promote muscarinic neurotransmission abolished the SO and resulted in an activated (theta) state. Conversely, muscarinic antagonism abolished the activated (theta) state and produced the SO. Parallel results have previously been reported for the neocortical SO (Steriade et al., 1993b). The hippocampal SO, like its neocortical counterpart (Sanchez-Vives and McCormick, 2000; Timofeev et al., 2000), appears to represent a spontaneous activity state allowed by a reduction in tone of the ascending activating system.

Another question that remains is whether the hippocampal SO can be elicited by other anaesthetics, which have been shown to elicit the neocortical SO. For example, the neocortical SO is a prominent feature of ketamine/xylazine, but not barbiturate, anaesthesia (Steriade et al., 1993c). Preliminary experiments in our laboratory using *i.v.* injections of these compounds have suggested that the same is true of the hippocampal SO (Lo, A., Clement, E.A., Mah, E., and Dickson, C.T., unpublished data).

Functional relevance of the hippocampal slow oscillation

Transient synchronisation of neuronal elements across and within networks could facilitate synaptic modifications during sleep (Buzsáki, 1998; Hasselmo, 1999; Peigneux et al., 2001; Tononi and Cirelli, 2001; Ribeiro and Nicolelis, 2004; Walker and Stickgold, 2004; Rauchs et al., 2005). We believe that the SO state presents an ideal platform for modification of synaptic weights in the bi-directional neocortico-hippocampal circuit that is considered to be the brain's hardware for declarative memory formation. It is well known that neuronal synchronisation is a critical factor in synaptic plasticity. Robust synchrony between pre- and post-synaptic neurons enhances, while a lack of synchrony decreases, synaptic efficacy (Lynch et al., 1977; McNaughton et al., 1978; Levy and Steward, 1979; Barrionuevo and Brown, 1983; Bramham and Srebro, 1987; Stanton and Sejnowski, 1989; Dan and Poo, 2004).

A link between SWS, the regulation of site-specific slow oscillatory activity, and memory consolidation has been recently shown for a procedural learning task (Huber et al., 2004), as well as for a hippocampal-dependent navigation task (Peigneux et al., 2004). In both studies, an increase in slow-wave activity during post-training sleep was correlated with a subsequent enhancement of performance. This suggests that memory consolidation may occur during SWS episodes. Although our observations do not allow for a direct link between the SO and hippocampal-dependent memory consolidation, it is of interest to note that recent studies have specifically implicated the temporoammonic pathway in this process (Remondes and Schuman, 2004; Brun et al., 2005). Since the present

study shows that the coordination of the hippocampal and neocortical SO appears to rely on the temporoammonic pathway, it is intriguing to suggest that the regulation of the SO is the neurophysiological platform by which hippocampal-dependent memory consolidation occurs.

Figure 2-01:

Neocortical indifferent electrode versus stereotaxic ground reference during urethane anaesthesia

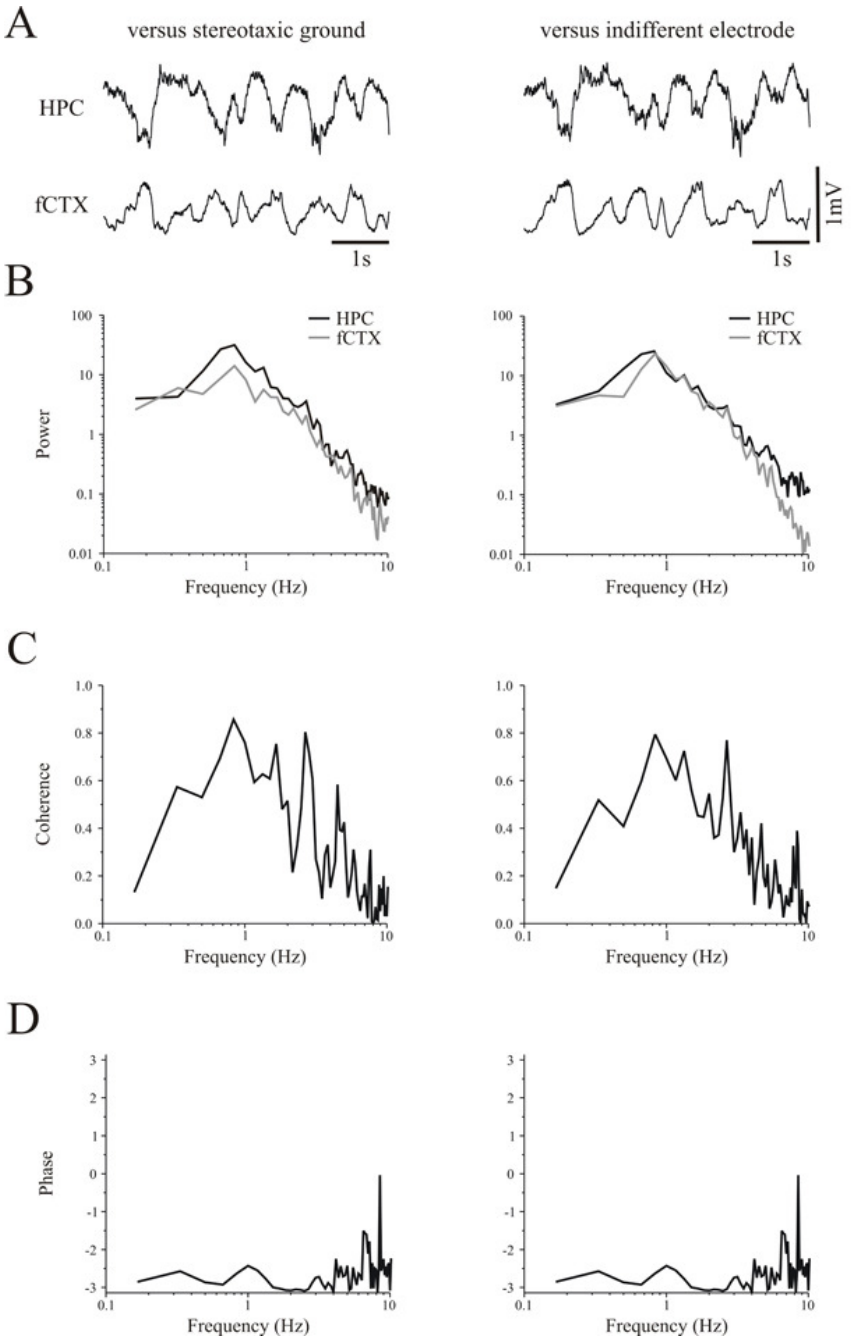

Figure 2-01 Caption:

(**A**) Raw signals recorded from the HPC and fCTX referenced to stereotaxic ground (*left panel*) and the neocortical indifferent electrode (*right panel*) appear very similar and are comparable to traces shown in the other figures of the manuscript. Spectral analysis of the signals reveals that (**B**) the peak frequency was the same in both the HPC and fCTX (0.83Hz) and the maximum power was not significantly (*t*-test: $p > 0.05$) different in either the fCTX (versus ground 10.4 ± 1.9; versus indifferent electrode 16.8 ± 3.3mV^2) or the HPC (versus ground 24.9 ± 4.6; versus indifferent electrode 19.1 ± 4.0mV^2) across the two referencing conditions. (**C**) The coherence at the peak frequency across the HPC and fCTX was comparable to our other measurements (versus ground 0.75 ± 0.05; versus indifferent electrode 0.69 ± 0.06), and was not significantly (*t*-test: $p > 0.05$) different across the two conditions. (**D**) Finally, there was no difference (*t*-test: $p > 0.05$) in the phase angle of the two signals (versus ground: -2.7 ± 0.1rad; versus indifferent electrode: -2.6 ± 0.2rad) across the two conditions. Abbreviations: frontal cortex (fCTX), hippocampus (HPC)

Figure 2-02:

Spectral analysis of digitally filtered signals during urethane anaesthesia

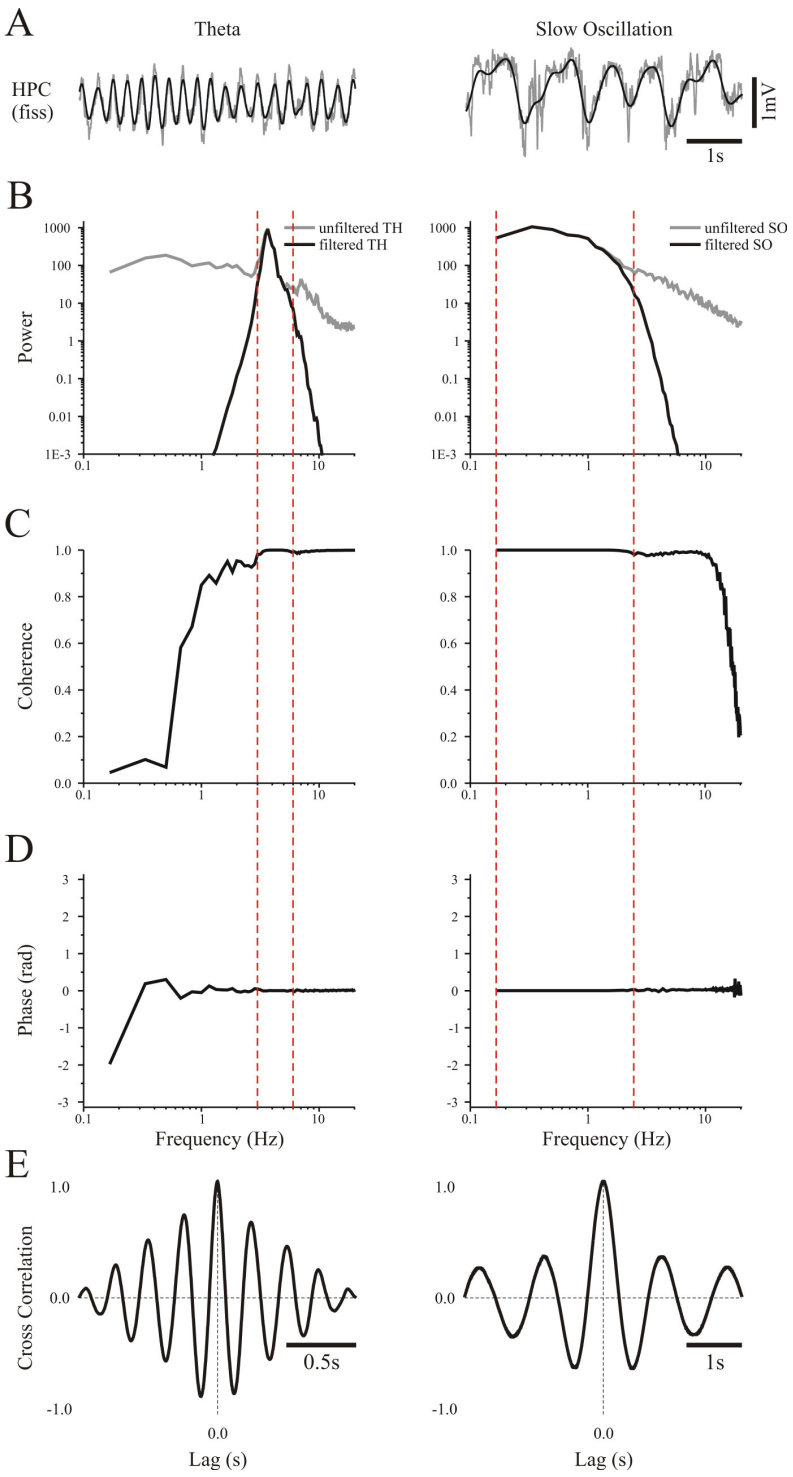

Figure 2-02 Caption:

(**A**) Overlaid samples of raw (*grey*) and digitally filtered (*black*) theta (*left panel*) and SO (*right panel*) activity and (**E**) cross-correlation analysis demonstrate that filtering did not phase-distort the signals. Theta traces were bandpass filtered from 3 to 6Hz (3^{rd} order) and SO traces were lowpass filtered at 2.5Hz (3^{rd} order) (*red lines* represent filter bandwidths). Spectral analysis of the signals reveals identical power peak frequencies (**B**), perfect coherence (**C**), and zero phase shift (**D**) within filter frequency ranges. Abbreviations: hippocampal fissure (fiss), hippocampus (HPC), slow oscillation (SO), theta (TH)

Figure 2-03:

Sine wave input/output analysis of Plexon amplifier system during urethane anaesthesia

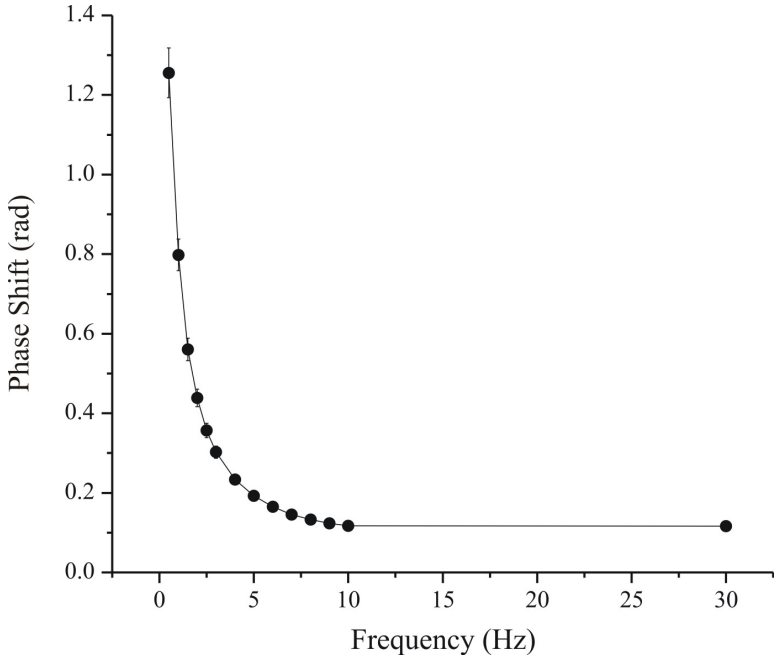

A frequency-dependent phase shift was observed in the output of the amplifier system in response to stationary sin wave input (0.1 to 30Hz). The values of the phase shifts in radians are shown plotted against input frequency. Though the phase shift at 1Hz is significant (1.26 ± 0.06rad; 72.19 ± 3.44deg), we mathematically incorporated this shift into our phase values prior to subsequent analysis.

Figure 2-04:

Slow oscillatory field activity in the hippocampus is a feature of the deactivated state of both natural sleep and urethane anaesthesia

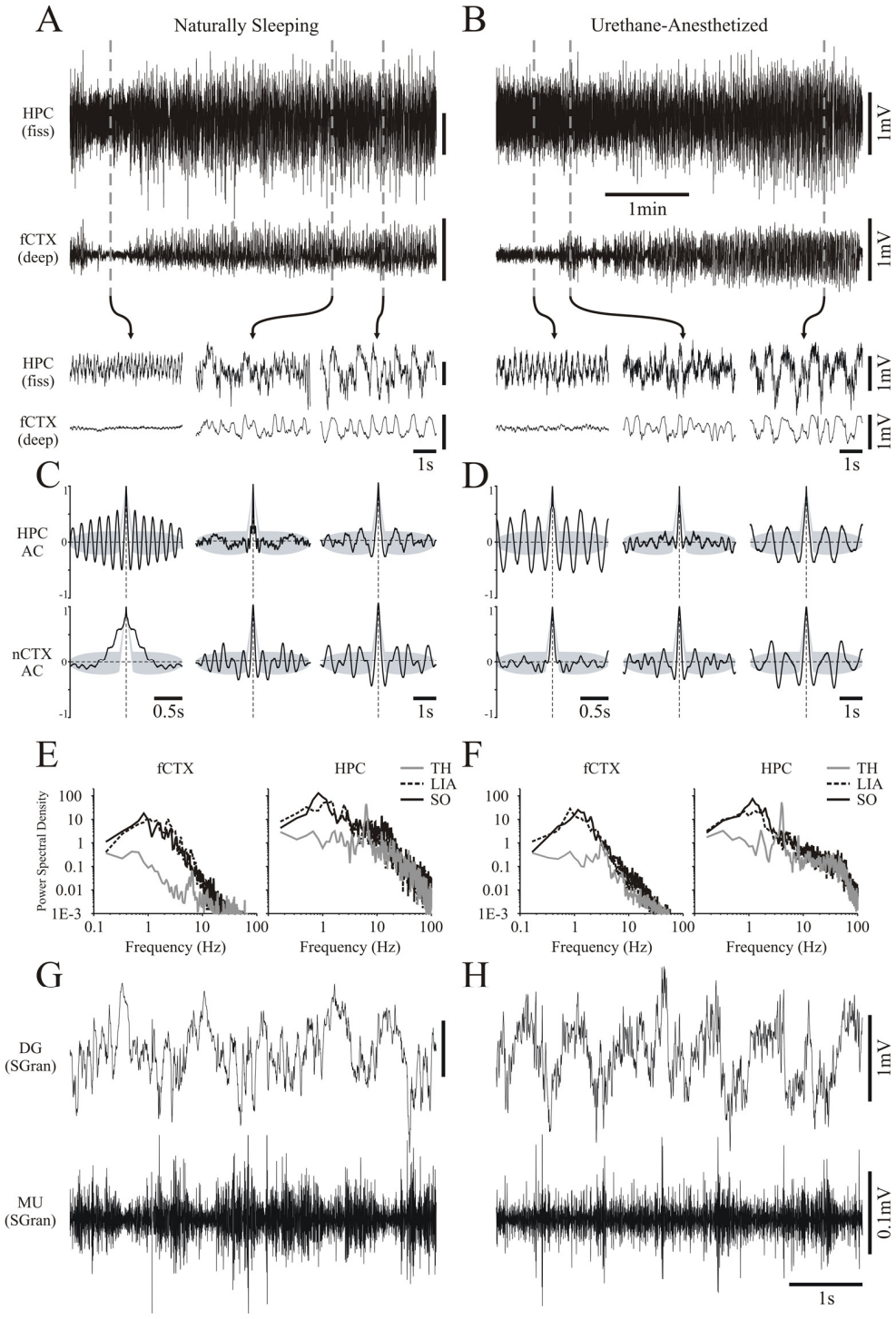

Figure 2-04 Caption:

Long-duration recordings of hippocampal (*top*) and neocortical (*bottom*) field activity during natural sleep (**A**) and urethane-anaesthesia (**B**) in the same animal. Both demonstrate spontaneous shifts from activated to deactivated EEG states of which the fine temporal features are highlighted in the expansions below. Note that across this state shift, hippocampal field activity was gradually transformed from theta to a large-amplitude SO that was similar to slow activity in the nCTX. This transformation occurred through a state characterised by irregular hippocampal activity. Corresponding autocorrelation functions (significant values are those outside *grey shaded area*) and power spectra for each recording site across the three states are shown for natural sleep (**C** and **E**) and for anaesthesia (**D** and **F**). A strong power peak and slow rhythmical activity was observed in the cortical signal during the entire deactivated state across the two conditions. This was only the case in the HPC at later stages of the deactivated state. DG (SGran) field and multiunit activity recorded in another animal during the SO suggested phase locking of unit activity to the local field oscillations in both sleeping (**G**) and anaesthetised (**H**) conditions. Abbreviations: autocorrelation (AC), deep layers (deep), dentate gyrus (DG), frontal cortex (fCTX), hippocampal fissure (fiss), hippocampus (HPC), large-amplitude irregular activity (LIA), multiunit (MU), slow oscillation (SO), theta (TH)

Figure 2-05:

Three distinct states of hippocampal field and unit activity during urethane anaesthesia

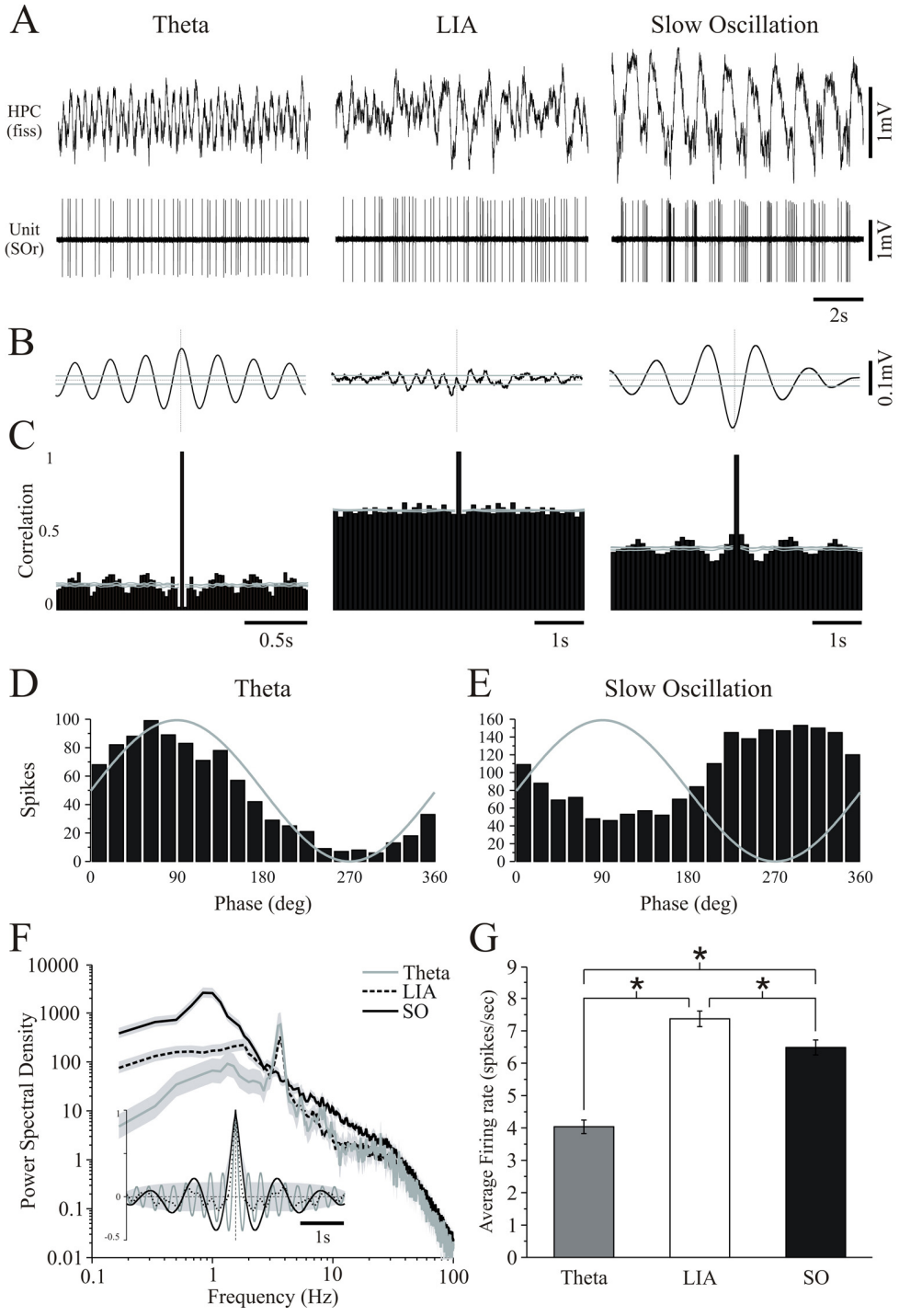

Figure 2-05 Caption:

(**A**) Hippocampal field (*top*) and SOr single-unit (*bottom*) activity at three separate instances during a single recording episode. Representative traces are plotted for theta, LIA, and the SO. Each state was characterised by distinct patterns of field waveforms, spike trains, and field-unit correlations. (**B**) Spike triggered averages of field activity and spike train autocorrelation histograms (**C**) for the three respective hippocampal states shown in **A**. *Grey lines* in **B** & **C** represent 95% confidence intervals. Phase histograms for this unit during theta (**D**) and the SO (**E**) demonstrate significant state-dependent phase-related preferences which changed across states. Both phase histograms were significantly non-uniform. (**F**) Power spectra and autocorrelation functions of hippocampal field activity demonstrate the differences in frequency components and rhythmicity across all three states (*grey shaded area* represents 95% confidence interval). The SO was characterised by a dramatic increase in rhythmic power and a shift of peak frequency values to a lower range (~1Hz and below). (**G**) Average firing rates of the same cell for a 60s episode in each state showing significant differences between all three states. Abbreviations: hippocampal fissure (fiss), hippocampus (HPC), large-amplitude irregular activity (LIA), slow oscillation (SO), stratum oriens (SOr)

Figure 2-06:

Differential evolution of hippocampal and neocortical slow oscillatory states during urethane anaesthesia

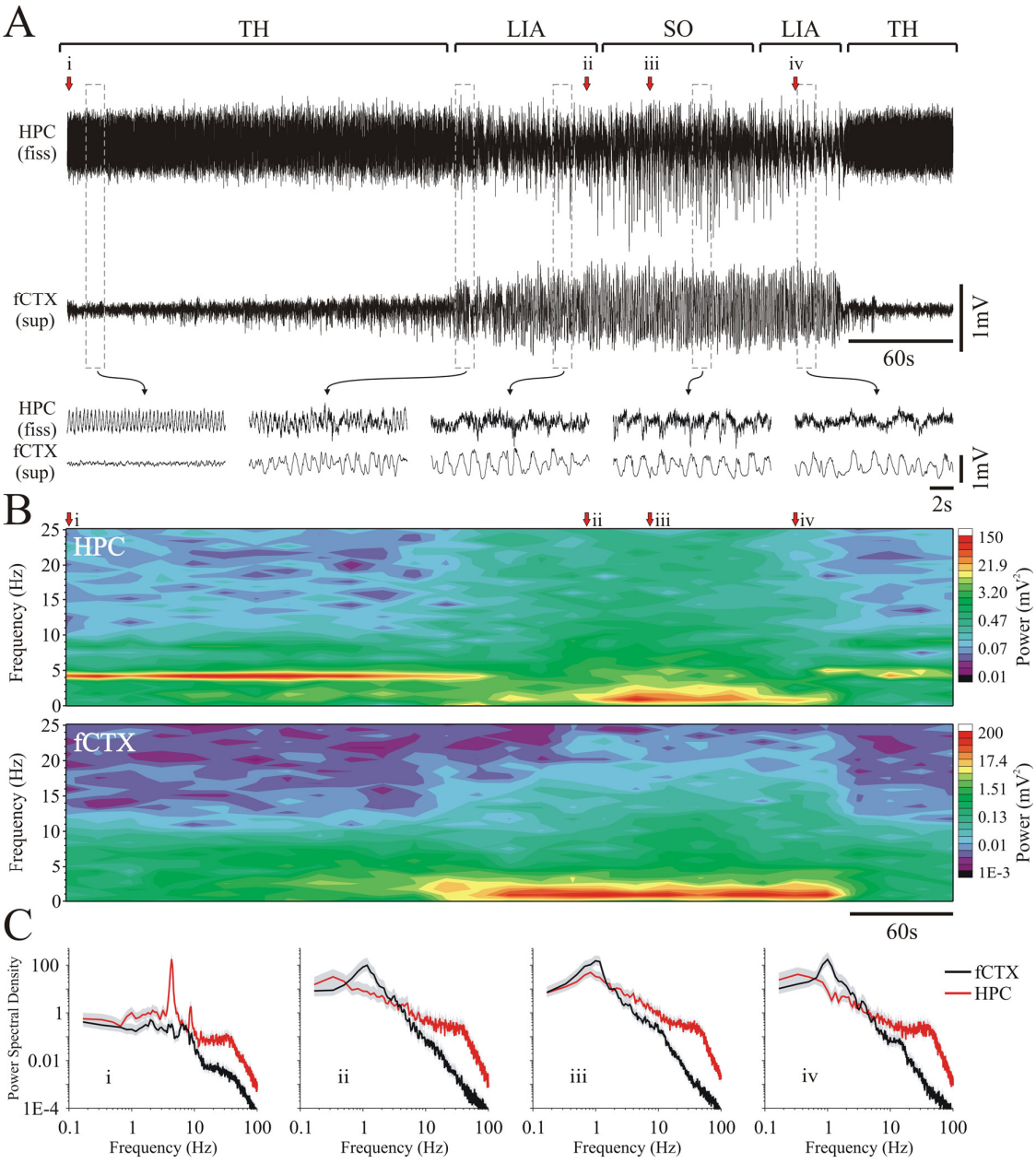

Figure 2-06 Caption:

(**A**) Simultaneous field recordings from the HPC and superficial fCTX during a spontaneous field state change. Bracketed segments (*top*) and expansions (*lower panel*) of the traces highlight the features of the transitive evolution of the hippocampal SO in comparison to the neocortical SO. The beginning (and end) of the episode was characterised by activated patterns in both hippocampal (theta) and neocortical (LVFA) traces. The transition to slower and larger amplitude rhythms (culminating in the SO) appeared first in the nCTX while the SO in the HPC appeared later, following an initial transition through LIA. This point is more clearly shown in the continuous spectrogram (**B**). (**C**) Power spectra for fixed 60s episodes beginning at points *i*, *ii*, *iii*, and *iv* as indicated in **A** and **B** (*grey shaded area* represents 95% confidence interval). Abbreviations: frontal cortex (fCTX), hippocampal fissure (fiss), hippocampus (HPC), large-amplitude irregular activity (LIA), low-voltage fast activity (LVFA), slow oscillation (SO), superficial (sup), theta (TH)

Figure 2-07:

Cortical – cortical, hippocampal – hippocampal, and cortical – hippocampal coherence of the slow oscillation during urethane anaesthesia

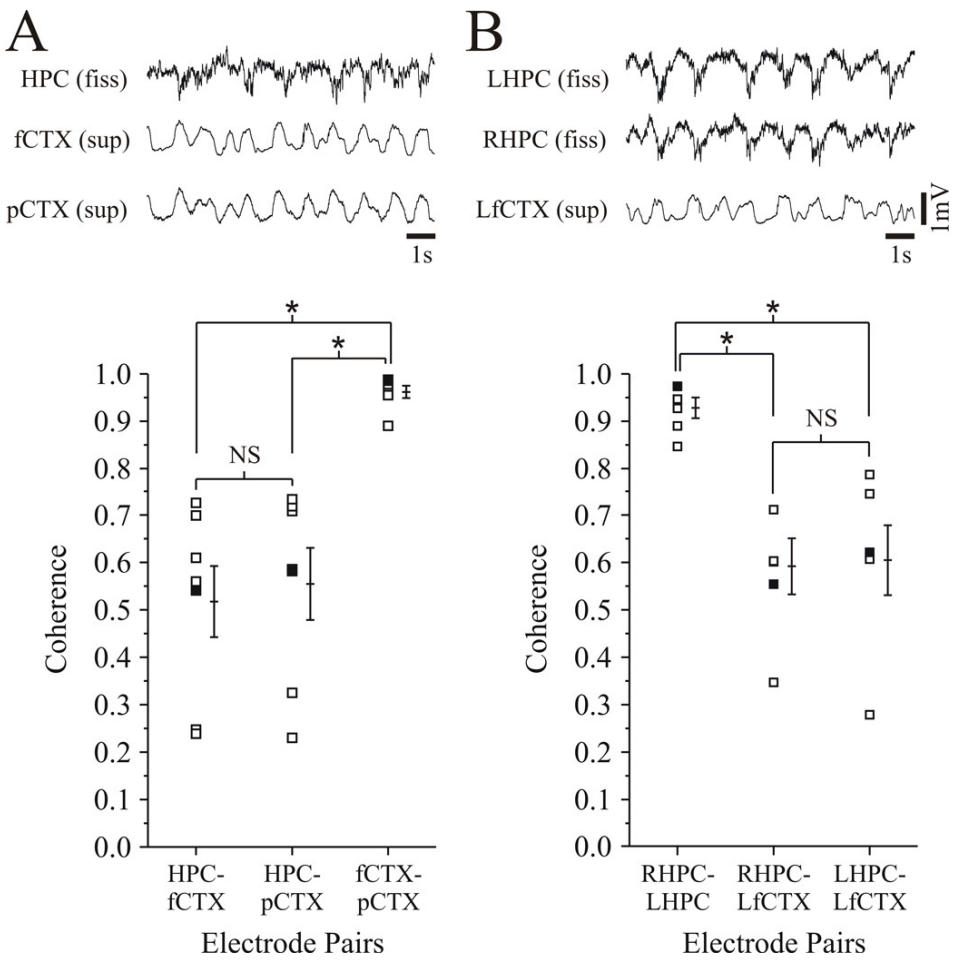

Figure 2-07 Caption:

Representative field recordings from the HPC and two distant cortical sites are shown in **A** and recordings from the fCTX and two isotypic points in the right and left HPC are shown in **B**. While cortical EEG traces in **A** and hippocampal EEG traces in **B** look almost identical, there is more variation between cortical and hippocampal field activity. Lower panel shows coherence measurements between the above sites for seven different experiments in **A** and six other experiments in **B** (filled squares represent measures for data shown in *top panel*). Averages and SEM are offset to the right of each pair-wise plot. These demonstrate that while cortical-cortical and hippocampal-hippocampal coherence of the SO is relatively invariable and extremely high, cortical-hippocampal coherence tends to be more variable and significantly lower. Abbreviations: frontal cortex (fCTX), hippocampus (HPC), left (L), not significant (NS), posterior cortex (pCTX), right (R), superficial layers (sup)

Figure 2-08:

Dynamic coordination of the hippocampal and neocortical slow oscillations during urethane anaesthesia

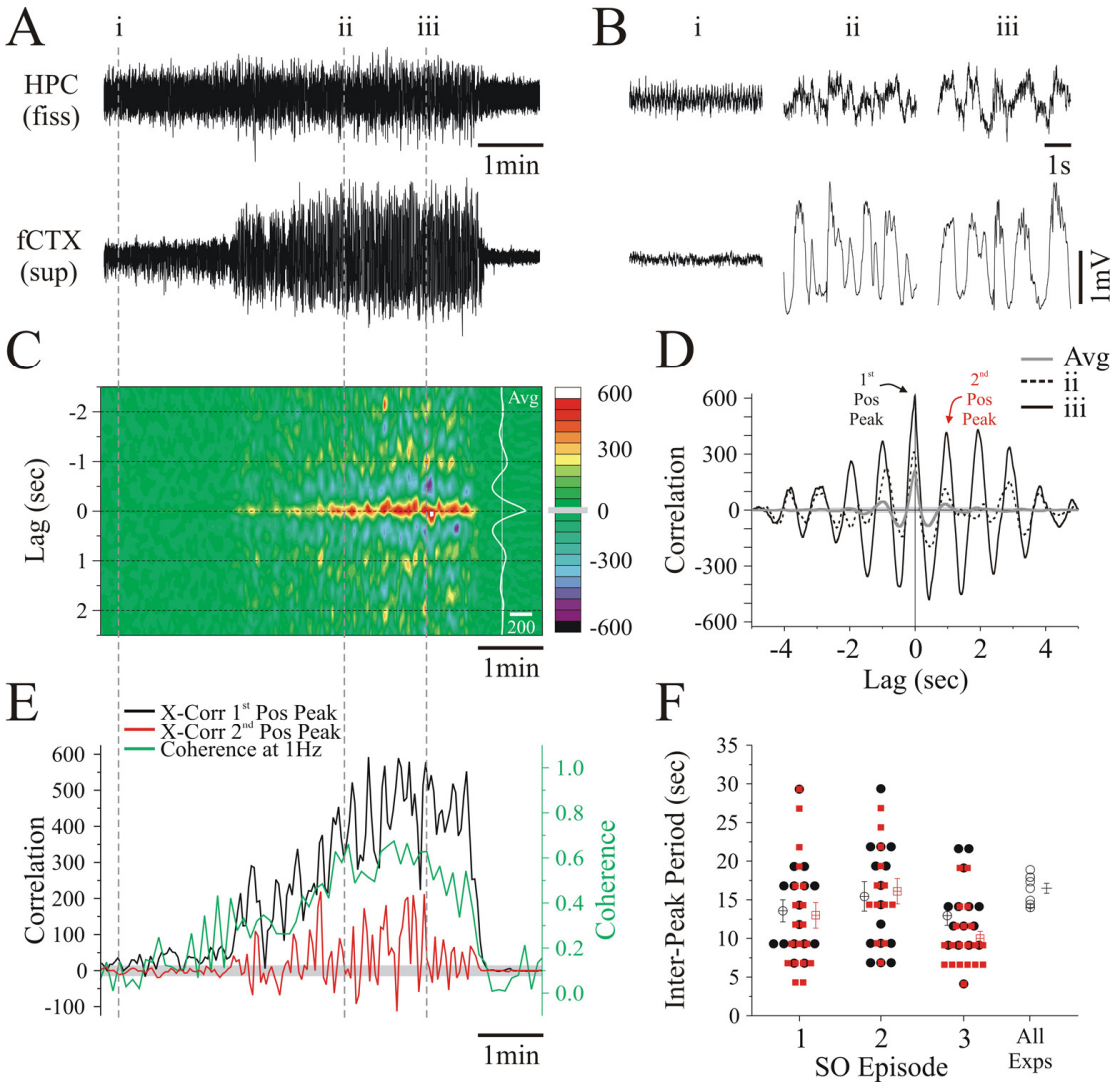

Figure 2-08 Caption:

(**A**) Simultaneous long term field recordings and expansions from indicated positions (**B**) from the HPC and deep fCTX (*note that signals are in phase*) during a spontaneous field state change. As previously shown (**Figure 3**), there is a lack of correlation between cortical and hippocampal SO early in the evolution of this activity. (**C**) Time-aligned sliding cross-correlogram of hippocampal and cortical signals shown in **A**. As suggested by the raw traces in **B**, there is a gradual increase of the rhythmic correlation of slow oscillatory activity through the episode as denoted by the development of positive peaks at lag intervals of ~1s (*hot colors*) centered around ~0s (*all colors other than green* represent significant changes; 95% confidence interval represented by *grey box* on color scale). The average cross-correlation function computed across the entire episode is shown in white at the right of the panel. (**D**) Individual cross-correlation functions computed at time points *ii* and *iii* in **A** (and **B**) are superimposed with the averaged cross-correlation function from **C** (95% confidence interval represented by *grey shaded area*). As suggested by the traces, the cross-correlation of the signals increases substantially when comparing time point *ii* to time point *iii*. This increase waxes and wanes, as observed by periodic increases and decreases of the peak values in **C** (95% confidence interval represented by *grey shaded area*). (**E**) Dynamics of the 1st (*black*: lag = -25ms) and 2nd (*red*: lag = 1000ms) positive peak values of the cross-correlation function and coherence values at 1Hz (*green*) across the entire episode (time-aligned to the raw data (**A**) and cross-correlogram (**C**)). Although the values of the cross-correlation peak

tend to increase across time (shown by a related increase in coherence), there is also a systematic and seemingly periodic fluctuation in these values every 10 to 20s. (**F**) The period of these fluctuations were plotted and averaged for the 1st (*black circles*) and 2nd (*red squares*) positive correlation peaks for multiple SO episodes in the same rat (*1*, *2*, and *3*; *unfilled squares* represent measures for data shown) and across all experiments. The period within and across experiments showed a high degree of overlap across all animals. Abbreviations: average (Avg), cross-correlation (X-Corr), experiments (Exps), frontal cortex (fCTX), hippocampal fissure (fiss), hippocampus (HPC), positive (Pos), slow oscillation (SO), superficial layers (sup)

Figure 2-09:

The slow oscillation is unrelated to the respiratory rhythm during urethane anaesthesia

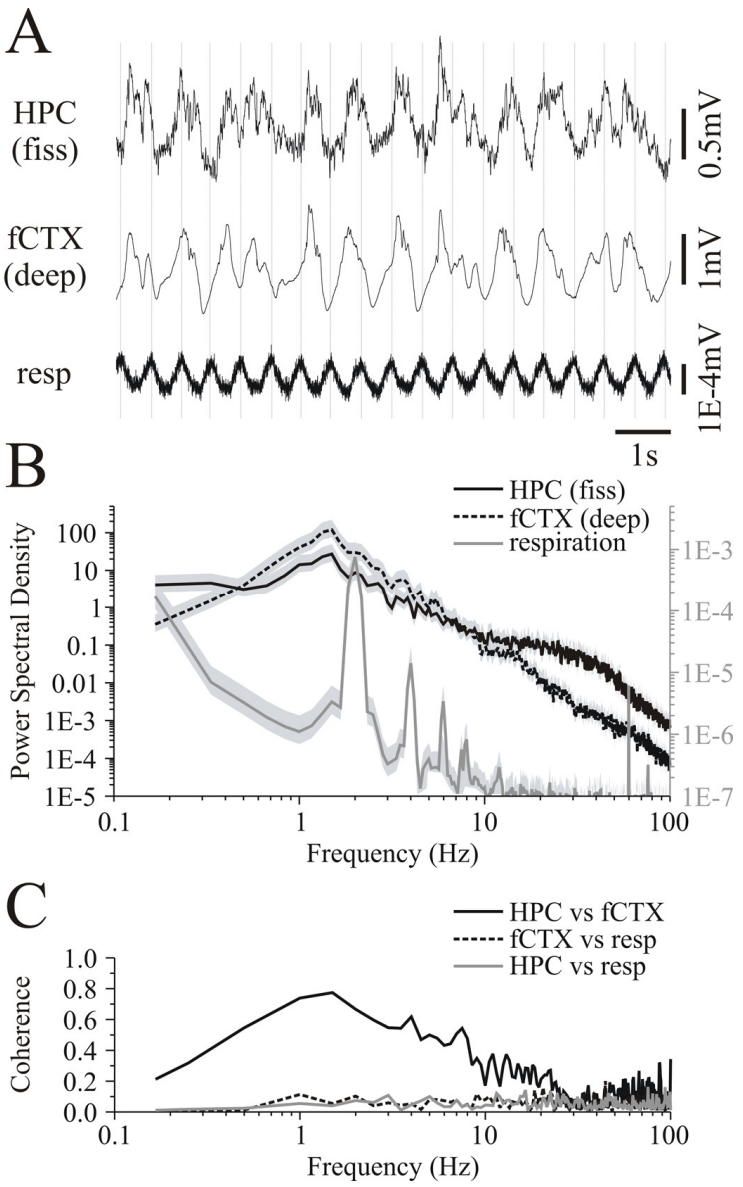

Figure 2-09 Caption:

(**A**) Simultaneously recorded field signal from the HPC, fCTX and respiration. Vertical lines aligned with the positive phase of the respiratory rhythm demonstrate that there is no phase relationship to hippocampal or neocortical slow oscillatory activity. Peak spectral frequencies of hippocampal (1.5Hz; 1.33 ± 0.08Hz) and neocortical (1Hz; 1.33 ± 0.08Hz) field are completely different from respiration (1.83Hz; 2.17 ± 0.15Hz; *grey shaded area* represents 95% confidence interval) (**B**). (**C**) No coherence was observed between respiration and SO field activity in the HPC (0.06; 0.19 ± 0.03) or fCTX (0.12; 0.14 ± 0.02), although hippocampal-neocortical coherence remained intact (0.74; 0.57 ± 0.03). Abbreviations: deep layers (deep), frontal cortex (fCTX), hippocampal fissure (fiss), hippocampus (HPC), respiration (resp), slow oscillation (SO)

Figure 2-10:

The slow oscillation is abolished by muscarinic agonism and enhanced by muscarinic antagonism during urethane anaesthesia

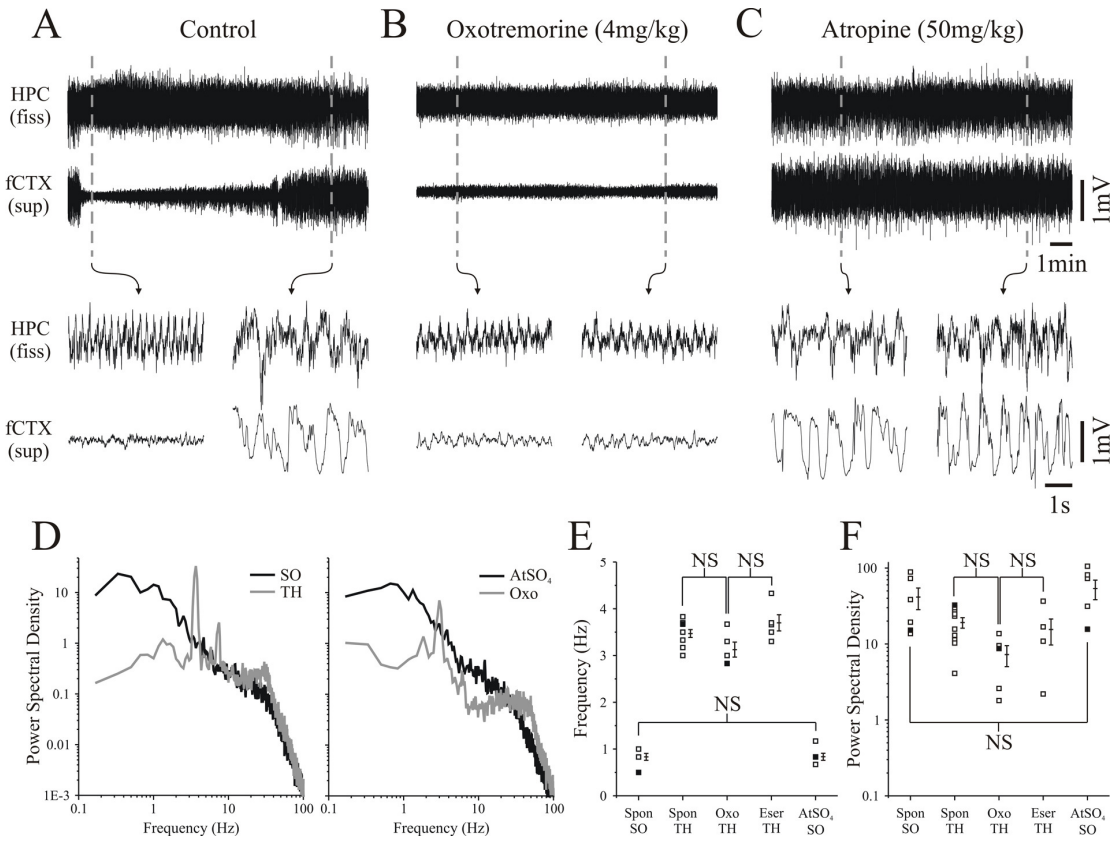

Figure 2-10 Caption:

(**A**) Simultaneously recorded field signals from the HPC and nCTX showing a spontaneous state change. (**B**) Following *i.p.* administration of 4mg/kg oxotremorine (Oxo), a continuously activated (theta and LVFA) state was elicited. (**C**) Conversely, subsequent *i.p.* administration of 50mg/kg atropine sulphate ($AtSO_4$) elicited a continuous deactivated (SO) state. (**D**) Spectra of spontaneous and pharmacologically induced states appeared highly similar in terms of peak frequencies (**E**) as well as peak power values (**F**) and statistical comparison verified that there was no significant difference. Abbreviations: eserine (eser), frontal cortex (fCTX), hippocampus (HPC), low-voltage fast activity (LVFA), not significant (NS), slow oscillation (SO), spontaneous (spon), superficial layers (sup), theta (TH)

Figure 2-11:

Spectral profile of the slow oscillation and theta during urethane anaesthesia

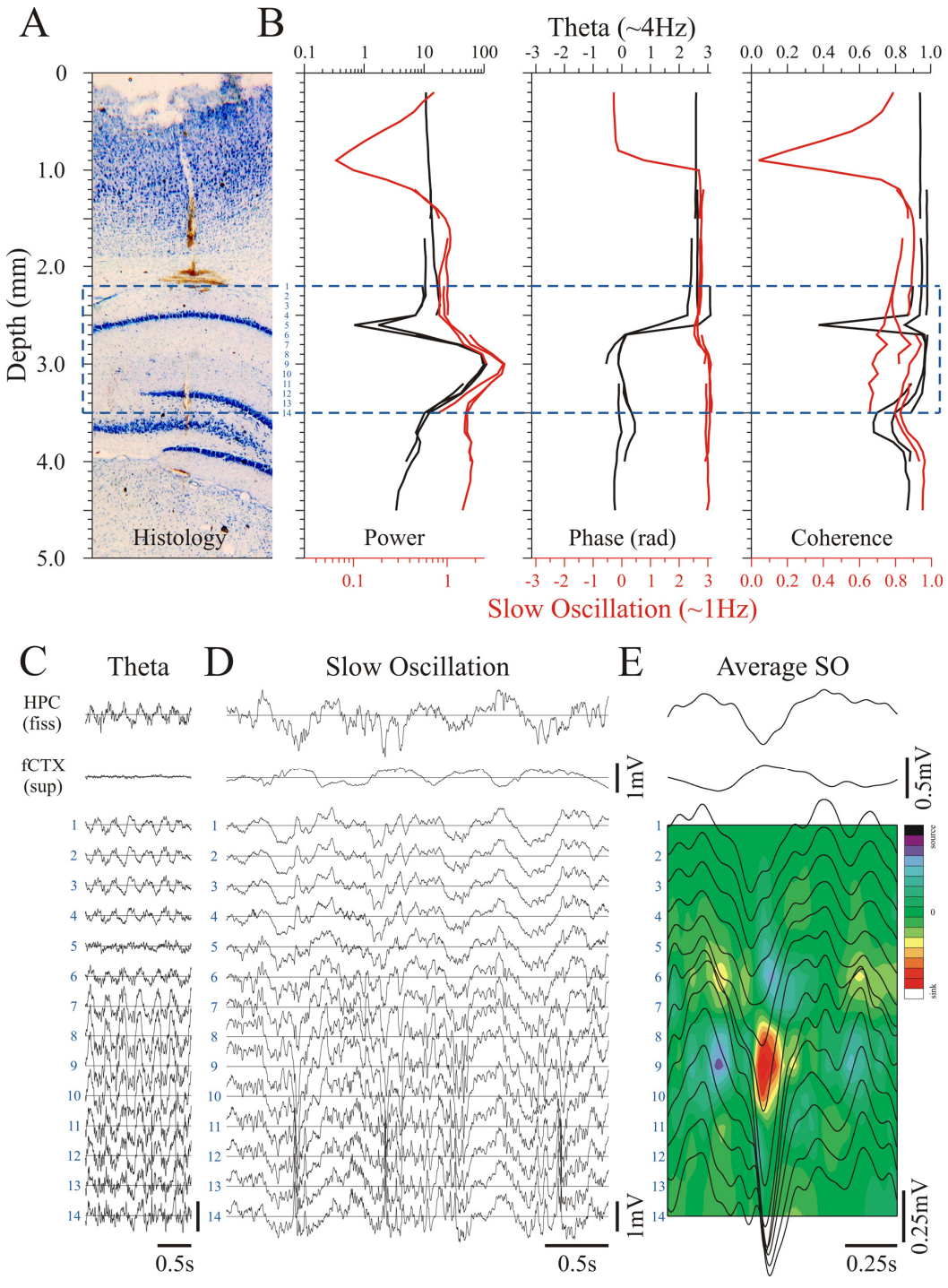

Figure 2-11 Caption:

Sequential laminar profiles of field activity were recorded in 0.5mm increments through the dorsal to ventral axis of the brain, to a final depth of 4.5mm using a multi-channel probe; each line represents one laminar recording spanning 1.4mm with the multiprobe. A histological photomicrograph of the multiprobe track is shown in **A**. Spectral analysis was performed on these signals in addition to simultaneously recorded field activity from fixed sites in the HPC and fCTX. (**B**) Average spectral values, including autopower, phase, and coherence are plotted as a function of depth and aligned to the histology in **A**. Phase and coherence were computed with respect to the fixed neocortical signal during the SO and the fixed hippocampal signal during theta. The SO (*red lines*) null zone occurred in the fCTX at a depth of 0.9mm (approximately layer V). It also showed a significant phase shift (~20º) aligned with a maximal value within the HPC. This depth coincided with the position of the theta (*black lines*) maximum (approximately at the level of the hippocampal fissure). Coherence for both the SO and theta remained high throughout the profile except at positions that corresponded to phase reversals. The coherence of the SO within the HPC, however, was more variable especially at locations near the power maximum. Raw field samples of theta (**C**) and the SO (**D**) from the numbered probe contacts are shown. Fast components of the SO, in addition to theta, reverse phase at a depth of 2.6mm (trace #5). (**E**) An average voltage profile clearly demonstrates the SO phase shift within the HPC. The corresponding average CSD shows a large sink at ~3.0mm and smaller sinks at ~2.7mm. CSD scale is -13.0 to 13.0mV/mm^2. Abbreviations:

current source density (CSD), frontal cortex (fCTX), hippocampal fissure (fiss), hippocampus (HPC), slow oscillation (SO), superficial layers (sup)

Figure 2-12:

Current source density analysis of theta and slow oscillatory activity during urethane anaesthesia

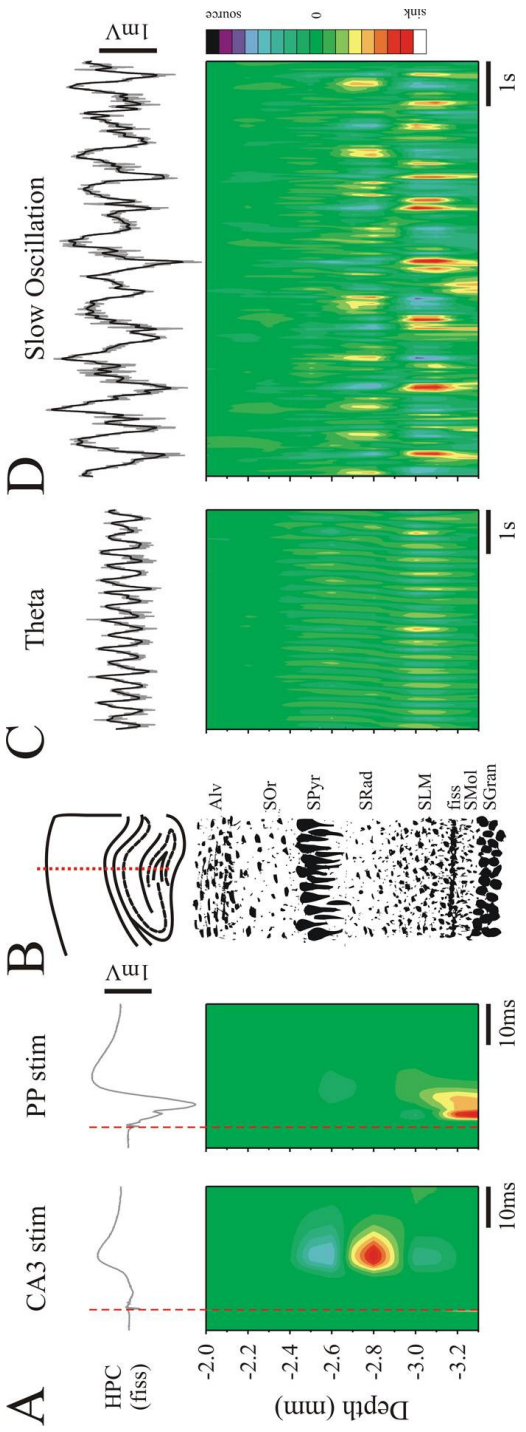

Figure 2-12 Caption:

CSD profiles of averaged evoked potentials in response to contralateral CA3 and ipsilateral perforant path (PP) stimulation (**A**) and 10Hz lowpass filtered, unaveraged, spontaneous theta (**C**) and SO field activity (**D**). For all profiles, the simultaneously recorded field potentials from contralateral fixed hippocampal sites are displayed (unfiltered potentials are shown in *grey* and lowpass filtered traces are shown in *black*). CSD profiles were computed from field potentials recorded through the dorsal to ventral axis of the brain using a multi-channel probe. (**A**) The CSD profile of unfiltered, averaged evoked potentials was used to estimate the anatomical location of recording sites and is aligned to a hand drawn representation of the cellular layers throughout the multiprobe track (**B**) (*see abbreviations below*). The most prominent sink after CA3 stimulation was observed in SRad, corresponding to excitatory input from commissural fibres of the contralateral CA3 and the most prominent sink after perforant path stimulation was observed in the molecular layer of the DG. (**C**) During theta, prominent rhythmic alternations of sinks and sources are observed at the level of SLM of hippocampal CA1 and paired with alternating sources and sinks at the levels of SRad. (**D**) During the SO, prominent and consistent sink-source alternations are also observed at the level of SLM, and are often matched with weaker current flow in SRad. CSD scales are -125.0 to 125.0mV/mm^2 for contralateral CA3 stimulation, -370.0 to 370.0mV/mm^2 for PP stimulation, and -18.0 to 18.0mV/mm^2 for spontaneous activity in **C** & **D**. Abbreviations: alveus (Alv), cornu ammonis 3 (CA3), current source density (CSD), hippocampal fissure

(fiss), hippocampus (HPC), perforant path (PP), slow oscillation (SO), stimulation (stim), stratum granulosum (SGran), stratum lacunosum moleculare (SLM), stratum moleculare (SMol), stratum oriens (SOr), stratum pyramidale (SPyr), stratum radiatum (SRad)

Figure 2-13:

The slow oscillation is a prominent feature of entorhinal activity during urethane anaesthesia

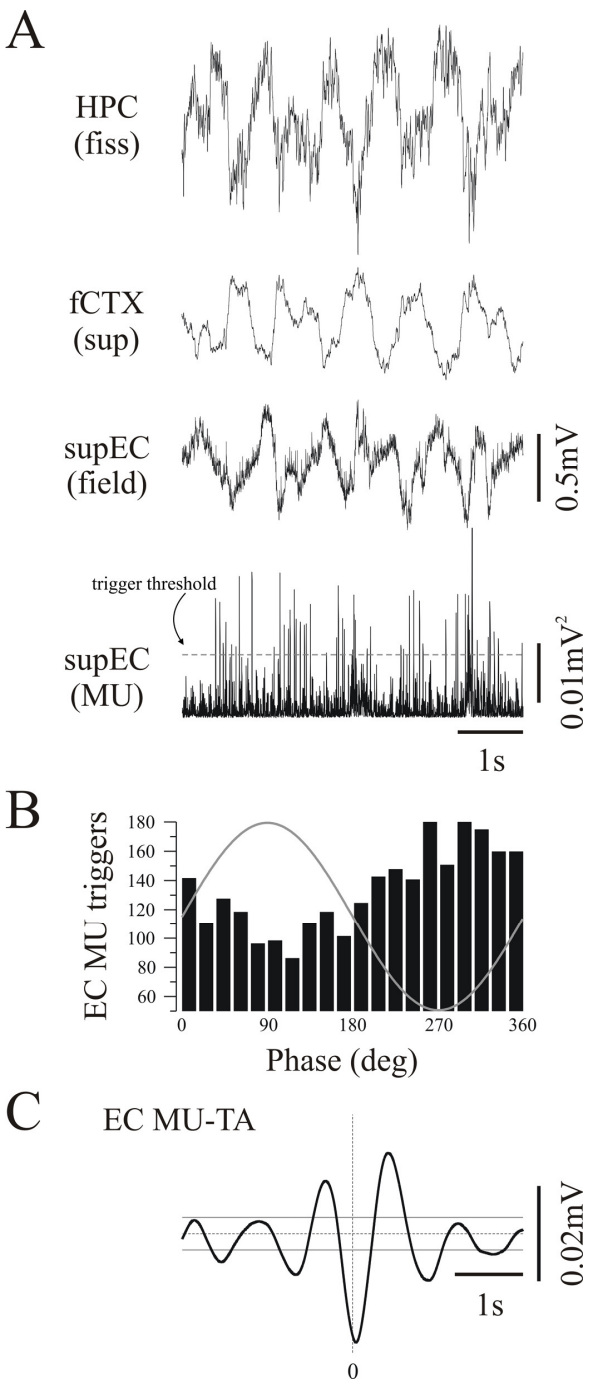

Figure 2-13 Caption:

(**A**) Simultaneously recorded hippocampal, neocortical, and superficial entorhinal field activity show that the SO is prominent in all three structures. Rectified supEC multiunit activity (supEC MU) was rhythmic (**A**) and was modulated by the ongoing SO (95% confidence interval represented by *grey lines*) (**C**). Phase histogram (**B**) was constructed using rectified supEC MU trigger (threshold represented by *grey line*) against supEC field and demonstrates that EC units tend to discharge just prior to the negative phase of the hippocampal field oscillation rhythmically at ~1Hz (**C**). Abbreviations: entorhinal cortex (EC), frontal cortex (fCTX), hippocampal fissure (fiss), hippocampus (HPC), multiunit (MU), superficial entorhinal cortex (supEC), superficial layers (sup), triggered-average (TA)

Figure 2-14:

The slow oscillation modulates other synchronised ensemble patterns in the hippocampus during urethane anaesthesia

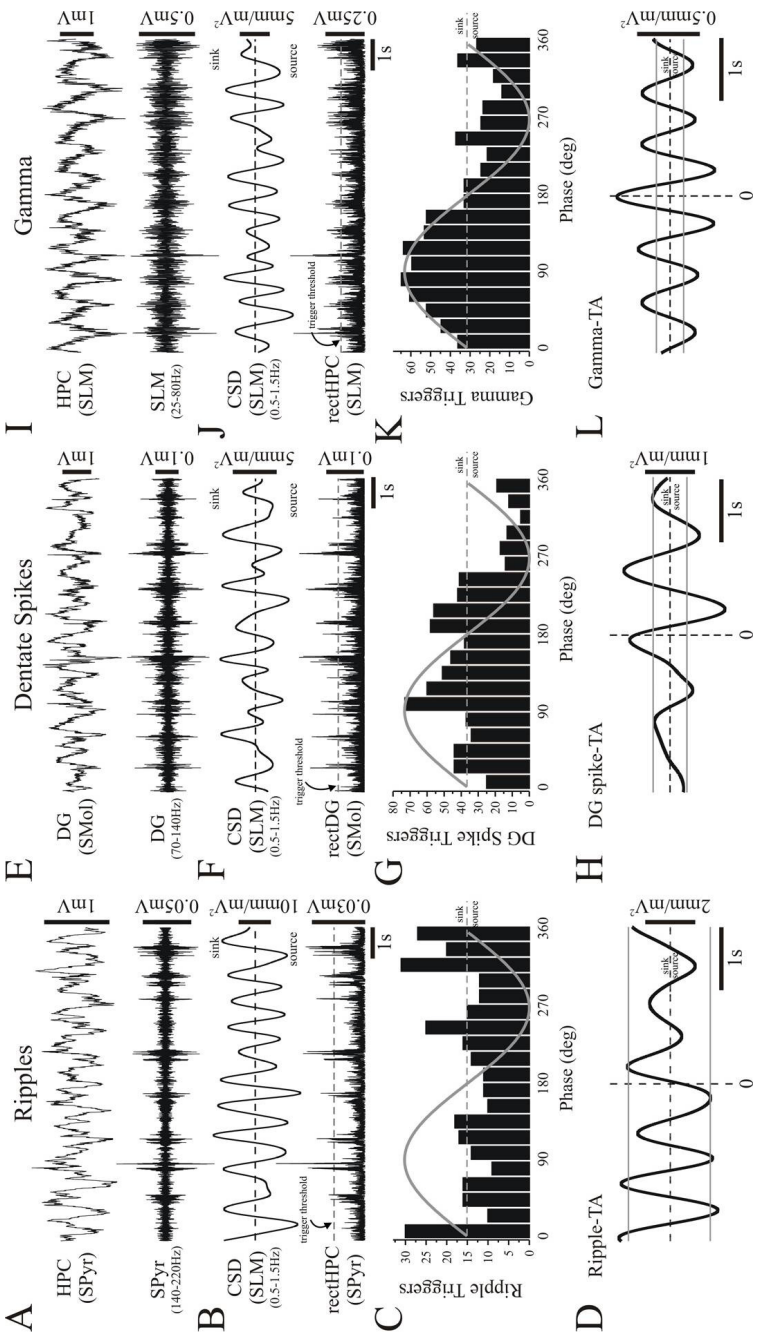

Figure 2-14 Caption:

(**A**, **E**, and **I**) Unfiltered slow oscillatory activity (*top*) and simultaneously recorded (**A**) ripples, (**E**) dentate spikes, and **(I)** gamma (*bottom panels*) recorded in SPyr, the inner molecular layer of the DG (SMol), and SLM, respectively. Traces are time-aligned to (**B**, **F**, and **I**) SO-filtered SLM CSD (*top*) and rectified (**B**) ripples, (**F**) dentate spikes and (**J**) gamma traces (*bottom panels*). Phase histograms were constructed using rectified trace trigger (threshold represented by *grey lines*) against respective SLM CSD. Phase histograms and event-triggered CSD averages demonstrate that (**G** and **H**) dentate spikes and (**K** and **L**) gamma rhythms were phase-modulated by the SLM SO CSD, and that (**C** and **D**) ripples were not phase-modulated by the SLM SO CSD. Dentate spikes tended to occur during or just after maximal SO sink at the level of SLM and gamma was maximal during the maximal SO sink in SLM. *Grey lines* in **D**, **H**, and **L** represent values for 95% confidence intervals. Abbreviations: current source density (CSD), dentate gyrus (DG), hippocampus (HPC), rectified (rect), stratum lacunosum moleculare (SLM), stratum moleculare (SMol), stratum pyramidale (SPyr), triggered-average (TA)

Chapter 2 References

Amzica F, Steriade M (1997) The K-complex: its slow (<1-Hz) rhythmicity and relation to delta waves. Neurology 49:952-959.

Amzica F, Steriade M (1998) Cellular substrates and laminar profile of sleep K-complex. Neuroscience 82:671-686.

Barrionuevo G, Brown TH (1983) Associative long-term potentiation in hippocampal slices. Proc Natl Acad Sci U S A 80:7347-7351.

Battaglia FP, Sutherland GR, McNaughton BL (2004) Hippocampal sharp wave bursts coincide with neocortical "up-state" transitions. Learn Mem 11:697-704.

Bertram EH, Zhang DX (1999) Thalamic excitation of hippocampal CA1 neurons: a comparison with the effects of CA3 stimulation. Neuroscience 92:15-26.

Bland BH (1986) The physiology and pharmacology of hippocampal formation theta rhythms. Prog Neurobiol 26:1-54.

Bland BH, Whishaw IQ (1976) Generators and topography of hippocampal theta (RSA) in the anaesthetized and freely moving rat. Brain Res 118:259-280.

Bland BH, Colom LV (1993) Extrinsic and intrinsic properties underlying oscillation and synchrony in limbic cortex. Prog Neurobiol 41:157-208.

Bland SK, Bland BH (1986) Medial septal modulation of hippocampal theta cell discharges. Brain Res 375:102-116.

Bragin A, Jando G, Nadasdy Z, van Landeghem M, Buzsáki G (1995a) Dentate EEG spikes and associated interneuronal population bursts in the hippocampal hilar region of the rat. J Neurophysiol 73:1691-1705.

Bragin A, Jandó G, Nádasdy Z, Hetke J, Wise K, Buzsáki G (1995b) Gamma (40-100 Hz) oscillation in the hippocampus of the behaving rat. J Neurosci 15:47-60.

Bramham CR, Srebro B (1987) Induction of long-term depression and potentiation by low- and high-frequency stimulation in the dentate area of the anesthetized rat: magnitude, time course and EEG. Brain Res 405:100-107.

Brankack J, Stewart M, Fox SE (1993) Current source density analysis of the hippocampal theta rhythm: associated sustained potentials and candidate synaptic generators. Brain Res 615:310-327.

Brun VH, Leutgeb S, Wu HQ, Schwarcz R, Witter MP, Moser EI, Moser MB (2005) Direct input from entorhinal cortex is necessary for spatial representation in hippocampal area CA1. In: Soc. Neuroci. Abstracts, p Program # 198.192: Society for Neuroscience.

Buzsáki G (1986) Hippocampal sharp waves: their origin and significance. Brain Research 398:242-252.

Buzsáki G (1989) Two-stage model of memory trace formation: A role for "noisy" brain states. Neurosci 31:551-570.

Buzsáki G (1996) The hippocampo-neocortical dialogue. Cerebral Cortex 6:81-92.

Buzsáki G (1998) Memory consolidation during sleep: a neurophysiological perspective. J Sleep Res 7 Suppl 1:17-23.

Buzsáki G (2002) Theta oscillations in the hippocampus. Neuron 33:325-340.

Buzsáki G, Leung LW, Vanderwolf CH (1983) Cellular bases of hippocampal EEG in the behaving rat. Brain Res 287:139-171.

Buzsáki G, Czopf J, Kondakor I, Kellenyi L (1986) Laminar distribution of hippocampal rhythmic slow activity (RSA) in the behaving rat: current-source density analysis, effects of urethane and atropine. Brain Res 365:125-137.

Buzsáki G, Horvath Z, Urioste R, Hetke J, Wise K (1992) High-frequency network oscillation in the hippocampus. Science 256:1025-1027.

Chaput M, Holley A (1980) Single unit responses of olfactory bulb neurones to odour presentation in awake rabbits. J Physiol (Paris) 76:551-558.

Cohen NJ, Squire LR (1980) Preserved learning and retention of pattern-analyzing skill in amnesia: dissociation of knowing how and knowing that. Science 210:207-210.

Collins DR, Lang EJ, Pare D (1999) Spontaneous activity of the perirhinal cortex in behaving cats. Neuroscience 89:1025-1039.

Collins DR, Pelletier JG, Pare D (2001) Slow and fast (gamma) neuronal oscillations in the perirhinal cortex and lateral amygdala. J Neurophysiol 85:1661-1672.

Corkin S, Amaral DG, Gonzalez RG, Johnson KA, Hyman BT (1997) H.M.'s medial temporal lobe lesion: Findings from magnetic resonance imaging. J Neurosci 17:3964-3979.

Dan Y, Poo MM (2004) Spike timing-dependent plasticity of neural circuits. Neuron 44:23-30.

Day J, Damsma G, Fibiger HC (1991) Cholinergic activity in the rat hippocampus, cortex and striatum correlates with locomotor activity: an in vivo microdialysis study. Pharmacol Biochem Behav 38:723-729.

Dickson CT, Wolansky TD, Kerber JW (2005) Neocortical modulation of the hippocampal slow oscillation via the entorhinal cortex. In: Soc. Neurosci. Abstracts, Program # 275.273: Society for Neuroscience.

Dolleman-Van der Weel MJ, Lopes da Silva FH, Witter MP (1997) Nucleus reuniens thalami modulates activity in hippocampal field CA1 through excitatory and inhibitory mechanisms. J Neurosci 17:5640-5650.

Eichenbaum H (2000) A cortical-hippocampal system for declarative memory. Nat Rev Neurosci 1:41-50.

Fontanini A, Bower JM (2005) Variable coupling between olfactory system activity and respiration in ketamine/xylazine anesthetized rats. J Neurophysiol 93:3573-3581.

Fontanini A, Spano P, Bower JM (2003) Ketamine-xylazine-induced slow (< 1.5 Hz) oscillations in the rat piriform (olfactory) cortex are functionally correlated with respiration. J Neurosci 23:7993-8001.

Frankland PW, Bontempi B (2005) The organization of recent and remote memories. Nat Rev Neurosci 6:119-130.

Freeman JA, Nicholson C (1975) Experimental optimization of current source-density technique for anuran cerebellum. J Neurophysiol 38:369-382.

Grams JD, Lamy AL, Wolansky TD, M.A. P, C.T. D (2003) Coordination of the slow rhythm in neo-, hippocampal and entorhinal cortices of the urethane anaesthetized rat. In: Soc. Neurosci. Abstracts, p Program # 932.932: Society for Neuroscience.

Hasselmo ME (1999) Neuromodulation: acetylcholine and memory consolidation. Trends Cogn Sci 3:351-359.

Huber R, Ghilardi MF, Massimini M, Tononi G (2004) Local sleep and learning. Nature 430:78-81.

Isomura Y, Sirota A, Ozen S, Buzsaki G (2005) Entorhino-hippocampal interactions during slow and theta network oscillations. In: Soc. Neurosci. Abstracts, p Program # 275.211: Society for Neuroscience.

Jasper HH, Tessier J (1971) Acetylcholine liberation from cerebral cortex during paradoxical (REM) sleep. Science 172:601-602.

Jouvet M, Michel F, Courjon J (1959a) L'activité électrique du rhinencéphale au cours du sommeil chez le Chat. C R Seances Soc Biol Fil 153:101-105.

Jouvet M, Michel F, Courjon J (1959b) Sur un stade d'activité électrique cérébrale rapide ou cours de sommeil physiologique. C R Seances Soc Biol Fil 153:1024-1028.

Kametani H, Kawamura H (1990) Alterations in acetylcholine release in the rat hippocampus during sleep-wakefulness detected by intracerebral dialysis. Life Sci 47:421-426.

Karni A, Tanne D, Rubenstein BS, Askenasy JJ, Sagi D (1994) Dependence on REM sleep of overnight improvement of a perceptual skill. Science 265:679-682.

Ketchum KL, Haberly LB (1993) Synaptic events that generate fast oscillations in piriform cortex. J Neurosci 13:3980-3985.

King C, Henze DA, Leinekugel X, Buzsáki G (1999) Hebbian modification of a hippocampal population pattern in the rat. J Physiol 521 Pt 1:159-167.

Lavenex P, Amaral DG (2000) Hippocampal-neocortical interaction: a hierarchy of associativity. Hippocampus 10:420-430.

Leung LW (1985) Spectral analysis of hippocampal EEG in the freely moving rat: effects of centrally active drugs and relations to evoked potentials. Electroencephalogr Clin Neurophysiol 60:65-77.

Leung LW, Lopes da Silva FH, Wadman WJ (1982) Spectral characteristics of the hippocampal EEG in the freely moving rat. Electroencephalogr Clin Neurophysiol 54:203-219.

Levy WB, Steward O (1979) Synapses as associative memory elements in the hippocampal formation. Brain Res 175:233-245.

Lynch GS, Dunwiddie T, Gribkoff V (1977) Heterosynaptic depression: a postsynaptic correlate of long-term potentiation. Nature 266:737-739.

Manns ID, Alonso A, Jones BE (2003) Rhythmically discharging basal forebrain units comprise cholinergic, GABAergic, and putative glutamatergic cells. J Neurophysiol 89:1057-1066.

Maquet P, Laureys S, Peigneux P, Fuchs S, Petiau C, Phillips C, Aerts J, Del Fiore G, Degueldre C, Meulemans T, Luxen A, Franck G, Van Der Linden M, Smith C, Cleeremans A (2000) Experience-dependent changes in cerebral activation during human REM sleep. Nat Neurosci 3:831-836.

Marr D (1970) A theory for cerebral neocortex. Proc R Soc Lond B Biol Sci 176:161-234.

Marr D (1971) Simple memory: a theory for archicortex. Philos Trans R Soc Lond B Biol Sci 262:23-81.

McGaugh JL (2000) Memory--a century of consolidation. Science 287:248-251.

McNaughton BL, Douglas RM, Goddard GV (1978) Synaptic enhancement in fascia dentata: cooperativity among coactive afferents. Brain Res 157:277-293.

Nadel L, Moscovitch M (1997) Memory consolidation, retrograde amnesia and the hippocampal complex. Curr Opin Neurobiol 7:217-227.

Nicholson C, Freeman JA (1975) Theory of current source-density analysis and determination of conductivity tensor for anuran cerebellum. J Neurophysiol 38:356-368.

Noda H, Manohar S, Adey WR (1969a) Correlated firing of hippocampal neuron pairs in sleep and wakefulness. Exp Neurol 24:232-247.

Noda H, Manohar S, Adey WR (1969b) Spontaneous activity of cat hippocampal neurons in sleep and wakefulness. Exp Neurol 24:217-231.

O'Keefe J, Nadel L (1978) The hippocampus as a cognitive map. Oxford: Oxford University Press.

Pavlides C, Winson J (1989) Influences of hippocampal place cell firing in the awake state on the activity of these cells during subsequent sleep episodes. J Neurosci 9:2907-2918.

Peigneux P, Laureys S, Delbeuck X, Maquet P (2001) Sleeping brain, learning brain. The role of sleep for memory systems. Neuroreport 12:A111-124.

Peigneux P, Laureys S, Fuchs S, Collette F, Perrin F, Reggers J, Phillips C, Degueldre C, Del Fiore G, Aerts J, Luxen A, Maquet P (2004) Are spatial memories strengthened in the human hippocampus during slow wave sleep? Neuron 44:535-545.

Peigneux P, Laureys S, Fuchs S, Destrebecqz A, Collette F, Delbeuck X, Phillips C, Aerts J, Del Fiore G, Degueldre C, Luxen A, Cleeremans A, Maquet P (2003) Learned material content and acquisition level modulate cerebral reactivation during posttraining rapid-eye-movements sleep. Neuroimage 20:125-134.

Plihal W, Born J (1997) Effects of early and late nocturnal sleep on declarative and procedural memory. J Cogn Neurosci 9:534–547.

Rauchs G, Desgranges B, Foret J, Eustache F (2005) The relationships between memory systems and sleep stages. J Sleep Res 14:123-140.

Remondes M, Schuman EM (2004) Role for a cortical input to hippocampal area CA1 in the consolidation of a long-term memory. Nature 431:699-703.

Ribeiro S, Nicolelis MA (2004) Reverberation, storage, and postsynaptic propagation of memories during sleep. Learn Mem 11:686-696.

Ribeiro S, Gervasoni D, Soares ES, Zhou Y, Lin SC, Pantoja J, Lavine M, Nicolelis MA (2004) Long-lasting novelty-induced neuronal reverberation during slow-wave sleep in multiple forebrain areas. PLoS Biol 2:E24.

Rimbaud L, Passouant P, Cadilhac J (1955) Participation de l'hippocampe a la regulation des etats de veille et de sommeil. Rev Neurol (Paris) 93:303-308.

Robinson TE (1980) Hippocampal rhythmic slow activity (RSA; theta): a critical analysis of selected studies and discussion of possible species-differences. Brain Res 203:69-101.

Robinson TE, Kramis RC, Vanderwolf CH (1977) Two types of cerebral activation during active sleep: relations to behavior. Brain Res 124:544-549.

Rodriguez R, Haberly LB (1989) Analysis of synaptic events in the opossum piriform cortex with improved current source-density techniques. J Neurophysiol 61:702-718.

Samonds JM, Bonds AB (2005) Gamma oscillation maintains stimulus structure-dependent synchronization in cat visual cortex. J Neurophysiol 93:223-236.

Sanchez-Vives MV, McCormick DA (2000) Cellular and network mechanisms of rhythmic recurrent activity in neocortex. Nat Neurosci 10: 1027-1034.

Scoville WB, Milner B (1957) Loss of recent memory after bilateral hippocampal lesions. J Neurol Neurosurg Psychiat 20:11-21.

Siapas AG, Wilson MA (1998) Coordinated interactions between hippocampal ripples and cortical spindles during slow-wave sleep. Neuron 21:1123-1128.

Siapas AG, Lubenov EV, Wilson MA (2005) Prefrontal phase locking to hippocampal theta oscillations. Neuron 46:141-151.

Sirota A, Csicsvari J, Buhl D, Buzsáki G (2003) Communication between neocortex and hippocampus during sleep in rodents. Proc Natl Acad Sci U S A 100:2065-2069.

Smith C, MacNeill C (1994) Impaired motor memory for a pursuit rotor task following Stage 2 sleep loss in college students. J Sleep Res 3:206-213.

Squire LR (1992) Memory and the hippocampus: a synthesis from findings with rats, monkeys, and humans. Psychol Rev 99:195-231.

Squire LR, Zola-Morgan S (1991) The medial temporal lobe memory system. Science 253:1380-1386.

Squire LR, Alvarez P (1995) Retrograde amnesia and memory consolidation: A neurobiological perspective. Curr Opin Neurobiol 5:169-177.

Stanton PK, Sejnowski TJ (1989) Associative long-term depression in the hippocampus induced by hebbian covariance. Nature 339:215-218.

Stefanacci L, Buffalo EA, Schmolck H, Squire LR (2000) Profound amnesia after damage to the medial temporal lobe: A neuroanatomical and neuropsychological profile of patient E. P. J Neurosci 20:7024-7036.

Steriade M (1999) Coherent oscillations and short-term plasticity in corticothalamic networks. Trends Neurosci 22:337-345.

Steriade M, Nunez A, Amzica F (1993a) Intracellular analysis of relations between the slow (< 1 Hz) neocortical oscillation and other sleep rhythms of the electroencephalogram. J Neurosci 13:3266-3283.

Steriade M, Amzica F, Nunez A (1993b) Cholinergic and noradrenergic modulation of the slow (approximately 0.3 Hz) oscillation in neocortical cells. Journal of Neurophysiology 70:1385-1400.

Steriade M, Nunez A, Amzica F (1993c) A novel slow (< 1 Hz) oscillation of neocortical neurons in vivo: depolarizing and hyperpolarizing components. J Neurosci 13:3252-3265.

Steriade M, Timofeev I, Grenier F (2001) Natural waking and sleep states: a view from inside neocortical neurons. J Neurophysiol 85:1969-1985.

Steriade M, Contreras D, Curro_Dossi R, Nunez A (1993d) The slow (< 1 Hz) oscillation in reticular thalamic and thalamocortical neurons: scenario of sleep rhythm generation in interacting thalamic and neocortical networks. J Neurosci 13:3284-3299.

Stewart DJ, Vanderwolf CH (1987) Hippocampal rhythmical slow activity following ibotenic acid lesions of the septal region. I. Relations to behavior and effects of atropine and urethane. Brain Res 423:88-100.

Suzuki SS, Smith GK (1987) Spontaneous EEG spikes in the normal hippocampus. I. Behavioral correlates, laminar profiles and bilateral synchrony. Electroencephalogr Clin Neurophysiol 67:348-359.

Suzuki SS, Smith GK (1988a) Spontaneous EEG spikes in the normal hippocampus. V. Effects of ether, urethane, pentobarbital, atropine, diazepam and bicuculline. Electroencephalogr Clin Neurophysiol 70:84-95.

Suzuki SS, Smith GK (1988b) Spontaneous EEG spikes in the normal hippocampus. II. Relations to synchronous burst discharges. Electroencephalogr Clin Neurophysiol 69:532-540.

Timofeev I, Steriade M (1996) Low-frequency rhythms in the thalamus of intact-cortex and decorticated cats. Journal of Neurophysiology 76:4152-4168.

Timofeev I, Grenier F, Steriade M (2001) Disfacilitation and active inhibition in the neocortex during the natural sleep-wake cycle: an intracellular study. Proc Natl Acad Sci U S A 98:1924-1929.

Timofeev I, Grenier F, Bazhenov M, Sejnowski TJ, Steriade M (2000) Origin of slow cortical oscillations in deafferented cortical slabs. Cereb Cortex 10:1185-1199.

Tononi G, Cirelli C (2001) Some considerations on sleep and neural plasticity. Arch Ital Biol 139:221-241.

Usui S, Iwahara S (1977) Effects of atropine upon the hippocampal electrical activity in rats with special reference to paradoxical sleep. Electroencephalogr Clin Neurophysiol 42:510-517.

Vanderwolf CH (1969) Hippocampal electrical activity and voluntary movement in the rat. Electroencephalogr Clin Neurophysiol 26:407-418.

Vanderwolf CH (1988) Cerebral activity and behavior: control by central cholinergic and serotoninergic systems. Int Rev Neurobiol 30:225-340.

Vanderwolf CH, Kramis R, Robinson TE (1977) Hippocampal electrical activity during waking behaviour and sleep: analyses using centrally acting drugs. Ciba Found Symp:199-226.

Vanderwolf CH, Kolb B, Cooley RK (1978) Behavior of the rat after removal of the neocortex and hippocampal formation. J Comp Physiol Psychol 92:156-175.

Vertes RP, Eastman KE (2000) The case against memory consolidation in REM sleep. Behav Brain Sci 23:867-876; discussion 904-1121.

Walker MP, Stickgold R (2004) Sleep-dependent learning and memory consolidation. Neuron 44:121-133.

Walker MP, Brakefield T, Morgan A, Hobson JA, Stickgold R (2002) Practice with sleep makes perfect: sleep-dependent motor skill learning. Neuron 35:205-211.

Whelan PJ (2003) Electromyogram recordings from freely moving animals. Methods 30:127-141.

Williams JA, Comisarow J, Day J, Fibiger HC, Reiner PB (1994) State-dependent release of acetylcholine in rat thalamus measured by in vivo microdialysis. J Neurosci 14:5236-5242.

Wilson MA, McNaugghton BL (1994) Reactivation of hippocampal ensemble memories during sleep. Science 265:676-679.

Winson J (1972) Interspecies differences in the occurrence of theta. Behav Biol 7:479-487.

Winson J (1974) Patterns of hippocampal theta rhythm in the freely moving rat. Electroencephalogr Clin Neurophysiol 36:291-301.

Witter MP, Wouterlood FG, Naber PA, Van_Haeften T (2000) Anatomical organization of the parahippocampal-hippocampal network. Ann N Y Acad Sci 911:1-24.

Wolansky TD, Clement EA, Richard AG, Ailon JI, Peters SR, Palczak MA, Dickson CT (2004) Extrinsic influences on the coordination of hippocampal and neocortical slow oscillations. In: Soc. Neurosci. Abstracts, p Program # 196.114: Society for Neuroscience.

Wouterlood FG, Saldana E, Witter MP (1990) Projection from the nucleus reuniens thalami to the hippocampal region: light and electron microscopic tracing study in the rat with the anterograde tracer Phaseolus vulgaris-leucoagglutinin. J Comp Neurol 296:179-203.

Ylinen A, Bragin A, Nadasdy Z, Jando G, Szabo I, Sik A, Buzsáki G (1995) Sharp wave associated high frequency oscillation (200Hz) in the intact hippocampus: network and intraellular mechanisms. J Neurosci 15:30-46.

Zar (1999) Biostatistical Analysis, 4th Ed. Prentice Hall Edition. Upper Saddle River, New Jersey, USA.

Zola-Morgan S, Squire L, Amaral DG (1986) Human amnesia and the medial temporal region: enduring memory impairment following a bilateral lesion limited to field CA1 of the hippocampus. J Neurosci 6:2950-2967.

Chapter 3:

The Slow Oscillation is a Feature of Both Hippocampal Input and Output Layers of the Entorhinal Cortex

Trish Wolansky[1] and Clayton T. Dickson[1, 2, 3]

[1]Centre for Neuroscience, [2]Department of Psychology, and [3]Department of Physiology

University of Alberta, Edmonton, Canada

Submitted to:

Journal of Neuroscience

Introduction

The HPC, at the hub of the MTL, receives highly processed multimodal sensory information from the nCTX. This information transfer occurs via parahippocampal structures, most prominently from the EC. Input is funnelled into the HPC via the supEC (Steward, 1976; Steward and Scoville, 1976; Dolorfo and Amaral, 1998) and hippocampal output is redistributed back to the nCTX (Insausti et al., 1997) via the deep EC (Kohler, 1985; Jones, 1993; Witter, 1993; Amaral and Witter, 1995; Kloosterman et al., 2003). Episodic memory is dependent on this MTL circuitry (Scoville and Milner, 1957; Squire and Zola-Morgan, 1991; Moser and Moser, 1998; Eichenbaum, 2000) and understanding the activity-dependent interactions between the MTL and its extended network will be an important step in understanding its role in mnemonic processing.

Synchronised brain activity during deep SWS is thought to play an important role in episodic memory consolidation (Buzsáki, 1989; Buzsáki, 1996; Siapas and Wilson, 1998; King et al., 1999; Steriade, 1999; Sirota et al., 2003; Siapas et al., 2005; Marshall et al., 2006; Ji and Wilson, 2007; Tsukamoto-Yasui et al., 2007). Recently, we described the hippocampal SO: a novel form of hippocampal network activity that occurs during SWS in the naturally-sleeping animal and also occurs during the deactivated state of urethane anaesthesia. We found that the hippocampal SO was coordinated with similar slow activity in the nCTX (Wolansky et al., 2006) and we speculated that this coordination may play a role in sleep-dependent plasticity and episodic memory consolidation.

Several lines of evidence have suggested that the synaptic connections between the nCTX, EC, and HPC could be involved in the coordination of the SO (Hahn et al., 2006; Isomura et al., 2006; Wolansky et al., 2006; Hahn et al., 2007). Spectral analysis of both field potentials and rhythmic current sink – source alternations revealed that SO power was maximal at the level of SLM – the lamina of CA1 where temporoammonic fibres from superficial entorhinal layer III terminate. Preliminary recordings in supEC also showed both the local SO field and supEC cellular activity was related to the ongoing hippocampal SO.

To more systematically investigate the interactions between the EC and HPC during the SO, we conducted single and multisite (laminar profile) LFP, multiunit, and single unit recordings in the EC simultaneously with neocortical and hippocampal LFP recordings. The SO was a prominent feature of the electrographic activity in both the superficial and deep layers of the EC. In fact, the strongest SO-related coupling was observed between the HPC and deep EC. Our data show that the SO is a prominent feature of both the cortical input and output pathways of the HPC.

Materials and Methods

Data were obtained from 32 male Sprague-Dawley rats weighing 155.60 to 384.60g (average ± SEM: 251.51 ± 11.44g). All methods conformed to the guidelines established by the Canadian Council on Animal Care, the Society for Neuroscience, and were approved by the Biosciences Animal Policy and Welfare Committee of the University of Alberta.

Anaesthesia and Surgery. Animals were initially anaesthetised with gaseous isoflurane at 4 MAC in an enclosed anaesthetic chamber. Following loss of righting reflexes, animals were maintained on isoflurane (2.0 to 2.5 MAC) via a nose cone and implanted with a jugular catheter. Isoflurane was discontinued and general anaesthesia was achieved using slow *i.v.* administration of urethane (0.8g/ml; final dosage 1.3 ± 0.01g/kg) via the jugular vein. Body temperature was maintained at 37°C using a servo driven system connected to a heating pad and rectal probe (FST) for the remainder of the surgical and recording procedures. Level of anaesthesia was assessed throughout the experiment by monitoring reflex withdrawal to a hindpaw pinch. If any visible withdrawal occurred, the animal was administered a supplemental dose (0.01ml) of urethane.

Using stereotaxic techniques, animals were implanted with monopolar electrodes constructed from Teflon-coated stainless steel wire (bare diameter 125µm: A-M Systems Inc.) in superficial frontal nCTX (from bregma: **AP**: +0.3, **ML**: +1.0, **DV**: surface to -0.2mm) and at the level of the hippocampal fissure of the dorsal HPC (from bregma: **AP**: -3.3, **ML**: +2.0, **DV**: -2.6 to -3.6mm; *HPC*).

Superficial entorhinal electrodes were implanted at a 40 degree angle below the horizontal (from bregma: **AP**: -4, **ML**: +4, **Depth**: -7.5 to -9.4mm; *supEC*) and lowered into the EC obliquely. Deep EC electrodes were implanted in the same manner (from bregma: **AP**: -4, **ML**: +4, **Depth**: -6.3 to -8.5mm; *deep EC*). In additional experiments, a silicon multiprobe with 16 contacts arranged in a linear array (contact separation of 100μm; Neuronexus Technologies; Ann Arbor, MI) was inserted in the EC using the same angled approach as above. Following implantation, all single pole electrodes were fixed to the skull using jeweller's screws and dental acrylic.

Recording Procedures

Single electrode field recordings. All single pole field potential recordings were amplified at a gain of 1000, filtered between 0.1 and 500Hz using a differential AC amplifier (Model 1700, A-M Systems Inc.), and were referenced to ground (stereotaxic apparatus). Following recording sessions, small lesions were made at the tips of active electrodes by passing 1mA of DC current for 5s using an isolated constant current pulse generator (Model 2100, A-M Systems Inc.). These lesions allowed us to specify their location during histological procedures (*see below*).

Linear multiprobe recordings. Signals from the probe were amplified at a final gain of 1000 and wide-band filtered between 0.7Hz to 10kHz via a 16-channel headstage (unity gain) and amplifier system (Plexon Inc.; Dallas, TX). All signals from the multiprobe were referenced to stereotaxic ground. The signal from the first (deepest) channel on the probe was audio amplified and sent to a

speaker. The electrophysiological profile of theta field activity (Alonso and Garcia-Austt, 1987b), as well as increases in multiunit activity, aided in the determination of the vertical position of the probe. Following recording sessions, the probe was moved slightly in two planes orthogonal to its long axis at its most ventral position in order to make a visible track for histological purposes. The position of the probe track in every experiment was verified by comparing the histology to the laminar profile of the ongoing field potentials. Both field and multiunit recordings were made using the linear multiprobe. Signals were lowpass filtered (software controlled- see below) at 2.5kHz. Offline digital filtering (*see below*) allowed us to extract both the LFPs and simultaneous multiunit activity from these latter traces. If only field recordings were being made, the signals were lowpass filtered (software controlled- see below) at 500Hz.

Single unit recordings. Entorhinal (**AP**: -8.5, **ML**: +4.5, **DV**: -1.8 to -6.0mm) single unit activity was recorded using fine glass micropipettes (inner diameter: 1.12mm; outer diameter: 1.5mm; A-M Systems Inc.) filled with 2.0M sodium acetate mixed with 2% methylene blue (resistance ranging from 3.5 to 12.4MΩ). Micropipettes were mounted on a single axis micropositioner (Model 2660; David Kopf Instruments; Tujunga, CA) that was positioned over the brain with a coarse 3-axis manipulator (FST). Glass pipette signals were initially amplified using a DC amplifier (Neurodata IR-283, Cygnus Technology, Inc.; Delaware Water Gap, PA) at a gain of 10, split, and further amplified using two channels of an AC amplifier (Model 2100, A-M Systems Inc.). One channel was amplified at a gain of 1000, and bandpass filtered between 0.5 to 10kHz for unit

activity, and the other channel was amplified at a gain of 100, and bandpass filtered between 0.1 to 500Hz for local field activity. The unit signal was also passed to an audio amplifier and speaker. As the pipette was advanced through the brain at a speed of 5 to 10μm per second, we were able to detect the spiking activity of neural units near the tip of the electrode. Then by advancing at 0.1μm per second, we were able to isolate the unit from the background activity. We ensured that the unit did not change its state-dependent spiking pattern which would have indicated that we were damaging the cell. At the end of the recording session, methylene blue was iontophoresed from the tip of the electrode by 250 to 300ms pulses of 1mA positive current applied at a frequency of 1Hz for 5 to 10 minutes.

Data storage. All signals were digitized with a Digidata 1322A A-D board connected to a Pentium PC running the AxoScope acquisition program (Axon Instruments; Union City, CA). All signals were acquired at sampling rates that were at least twice as high as the lowpass filter setting of the signals (software controlled).

Euthanasia and Histology

At the end of recording sessions, rats were perfused transcardially, initially with physiological saline, and then with 4% paraformaldehyde in saline. Brains were extracted and stored overnight in 30% sucrose in 4% paraformaldehyde. The tissue was frozen with compressed CO_2 and sectioned at 48μm with a rotary microtome (Leica 1320 Microtome; Vienna, Austria). Slices were then mounted

on gel-coated slides, allowed to dry for a minimum of 24 hours, subsequently stained using thionin, and cover-slipped. Microscopic inspection of stained slices was used to verify recording loci. Digital photomicrographs (Canon Powershot S45; Tokyo, Japan) were taken on a Leica DM LB2 (Buffalo, NY) microscope, imported using Canon Remote Capture 2.7 software (Tokyo, Japan) and processed with Corel PhotoPaint (Ottawa, ON, Canada).

Data Processing and Analysis

Raw signals were first examined visually using AxoScope (Axon Instruments) and segments for further analysis were chosen using visual, spectral and autocorrelational criteria. The theta state was characterised by a 3 to 4 Hz rhythm in the raw LFP and the autocorrelation function, in addition to a prominent spectral peak in this same range. The SO state was characterised by a clear ~1Hz rhythm in the raw LFP and the autocorrelation function, in addition to a prominent spectral peak in this same range. LIA tended to have a similar spectrum to the SO but showed an irregular non-rhythmic LFP and autocorrelation. All analyses were conducted using Matlab Version 5.3 (Mathworks; Natick, MA) and visualized using Origin Version 7.0 (Microcal Software Inc.; Northampton, MA). For field signals, these analyses included: digital resampling, digital filtering, single and dual-channel spectral analyses, autocorrelations, and CSD. For unit and multiunit signals, these analyses included: digital filtering, autocorrelation, and root mean square (RMS) calculations. We also computed STAs of field activity, and the oscillatory phase cycle preference of units. Details for all analyses are described below. Our digital

filtering technique was previously confirmed to elicit zero phase distortion by both spectral and cross-correlation analyses (Wolansky et al., 2006).

Field recordings. Autopower, crosspower, cross phase, and coherence spectra were computed and plotted for field signals and signal pair combinations. To ensure that all comparative analyses (e.g., coherence, cross phase) concerning the EC were consistent, the hippocampal or neocortical signal was "channel 1" (i.e., the reference signal). In instances where comparisons were made between the nCTX and HPC (e.g., SO coherence), the HPC was always the reference signal. Spectra were computed from data segments whose length depended upon the type and stationarity of the signal. For segments of activated patterns with higher frequency components such as theta, segments were at least 30s. For deactivated patterns with lower frequency such as the SO, segments were at least 60s. Using Welch's averaged periodogram method, spectra were estimated from a series of 6s long, sequential Hanning windowed samples from these data segments with 2s overlap. Spectral values were averaged across a peak frequency bandwidth (peak frequency ± 1/6Hz) and compared across brain states. Spectral profiles for theta and slow oscillatory activity recorded with the linear multiprobe were also constructed in this way by comparing each trace from the probe against a fixed (hippocampal) reference and extracting peak frequency values. Frequency-dependent phase distortion of the SO due to differential filtering of the two amplification systems was corrected using a spectral input/output analysis of a series of sine waves with frequencies ranging from 0.5 to 30Hz (Wolansky et al., 2006).

Spectrograms were computed from even longer data segments (several minutes) in which spontaneous state alternations took place. A sliding windowing procedure was adopted that allowed discrete spectra to be calculated for specific time points across the entire data segment. Windows were 24s in duration and were moved across the data segment in increments of 6s. Spectral analysis of these individual windows was identical to the methods described above.

To describe the evolution of the SO in each of the EC, HPC, and nCTX as a function of time, we used the ratio of normalized power values (to total spectral power) of the peak SO frequency to the peak theta frequency for field recordings in each location. When the value of this ratio was ≥ 1.0, SO activity dominated the field traces. By verifying that a spectral power peak and a rhythmic autocorrelation at ~1Hz were present at the same time points in the raw data, we ensured that this activity was indeed the SO. By plotting the value of this ratio across time and using 1 as a threshold, we could effectively describe when the SO state began in the neocortical, entorhinal, and hippocampal field traces and how it evolved with respect to the other field traces.

Autocorrelations were computed on data segments whose lengths were 30 to 60 seconds long, dependent upon the frequency of interest (i.e. theta or SO, respectively). The range of time lags for autocorrelations of field activity also depended on the peak power frequency as computed by autospectral analysis. For frequencies $\leq$ 1Hz, we used a window size of 2.5s while for frequencies $\geq$ 3Hz, we used a window size of 1s.

Multiunit activity. Multiunit activity was extracted from original signals recorded with the multiprobe by offline digital filtering (250Hz hipass). For multiunit analyses, we began by calculating the root mean square (RMS) of the multiunit traces. The RMS value was calculated at every time point using a 20ms time window and was plotted as a continuous trace. This provided a continuous function representing the positive envelope of the multiunit traces. Using the distribution of RMS values across time, we calculated a value corresponding to the upper confidence limit (95%). This value was used as a trigger to extract the time points corresponding to both the beginning and end of significant burst of multiunit activity (Molle et al., 2006). Finally, we calculated the time stamp of the midpoint between the beginning and end of these fluctuations and used these (hereafter referred to as "multiunit triggers") as a point process to perform time series analyses in the same manner as described below for single unit activity.

Single unit activity. Spike rates, inter-spike intervals, and autocorrelation histograms (10ms bin size) were computed to analyze spike train dynamics. The relationship between LFP and unit activity was assessed by spike-triggered averaging of simultaneously recorded field potentials. The preferred phase of unit spiking to rhythmic field activity was assessed separately by filtering the reference hippocampal field in a specific bandwidth (0.5 to 1.5Hz for the SO and 3 to 6Hz for theta) and then computing the time points of negative to positive zero crossings. Unit activity was binned (bin size: 18°) according to the phase of the field cycle from 0 to 360° (i.e., from one zero crossing to the next).

Current source density analysis. CSD analysis was conducted on spontaneous field profiles recorded using the linear multiprobe. The underlying assumptions for CSD followed those of prior work (Freeman and Nicholson, 1975; Nicholson and Freeman, 1975; Rodriguez and Haberly, 1989; Ketchum and Haberly, 1993). Briefly, spontaneous multiprobe LFPs were filtered (1.5Hz lowpass for the SO and 3 to 6Hz bandpass for theta) and CSD was computed by estimating the second spatial derivative of these filtered traces. This estimate was calculated using a three-point difference (differentiation grid size of 300μm) on the field potential values across spatially adjacent traces:

$$CSD = [f(p_{i-1})-2f(p_i)+f(p_{i+1})]/d^2 \qquad (\textit{Equation 1})$$

Where $f(p_i)$ is the field signal from probe channel i (i = 2, 3, …, 13) and d is the distance between adjacent channels (0.1mm). For traces from each end of the probe (i = 1 and 14), the differentiation grid was based only on the immediately adjacent channel. We confirmed that this latter procedure yielded similar, if not identical, CSD results as the 3-point differentiation method by successively eliminating probe end channels, then re-computing and comparing results.

Determination of the anatomical location of multiprobe channels. The laminar position of individual probe channels was estimated based on the histology, the theta profile in comparison to past studies, and the location and behavior of prominent multiunit activity. Layer I was easily determined due to 1) the complete reversal of local theta activity (Mitchell and Ranck, 1980; Alonso and Garcia-Austt, 1987b) and 2) the lack of multiunit activity. The approximate location of the border between layers II and III was demarked by the position of

the actual theta reversal (LFP null zone) in combination with prominent theta-related multiunit activity on either side (Mitchell and Ranck, 1980; Alonso and Garcia-Austt, 1987a, 1987b). The location of layers V and deeper were confirmed at positions having prominent multiunit activity that was only weakly theta-modulated and more strongly modulated during deactivated states (Alonso and Garcia-Austt, 1987a; Chrobak and Buzsáki, 1994; Dickson and Alonso, 1995; Frank et al., 2001).

Statistics. All comparisons across conditions for the same datasets were made using one-tailed pair-wise *t*-tests (significance was evaluated for $p < 0.05$). As all tests were specified *a priori*, this was also the case for datasets with more than two conditions.

The statistical significance of the time series analyses conducted were assessed through comparisons with the 95% confidence limits of randomized distributions computed on the same datasets. Autocorrelation function significance was assessed by comparison to a distribution of 100 different autocorrelograms computed on lowpass (3Hz) filtered noise. The spectrum of this filtered noise represents a random phase approximation of a typical LFP spectrum. The significance of STAs was computed by comparison to the distribution of STAs computed using a series (n = 100) of randomized (shuffled) spike trains derived from the original data. The shuffling of spike trains was conducted through random assignments based on the actual inter-spike intervals computed for the original spike train. The resulting distribution of STAs had a variance which was proportional to the amplitude of the original field signal but

which was lower than the original fluctuations for signals with a strong correspondence.

The significance of autocorrelation histograms derived from point processes (unit activity) was assessed by computing the average bin value and their fluctuations within a randomized distribution (random n = 100). Confidence limits were computed as the average value ± 2*SEM. Any units with autocorrelation histograms demonstrating systematic and periodic fluctuations beyond this window were classified as rhythmic. This technique has been noted to eliminate problems using either spectral or Gabor fitting analyses (Samonds and Bonds, 2005). Phase histograms were statistically evaluated using the Rayleigh statistic for circular data (Zar, 1999).

Drugs and Chemicals

Atropine methyl nitrate, lidocaine, thionin, methylene blue, and urethane were all purchased from Sigma (St. Louis, MO). Isoflurane was purchased from Bimeda-MTC (Animal Health Inc.; Cambridge, ON, Can) and paraformaldehyde from Fisher Scientific (Toronto, ON, Can).

Results

Spontaneous state-dependent field activity in the entorhinal cortex

As previously described (Wolansky et al., 2006; Clement et al., 2008), the spontaneous LFP activity in the HPC and nCTX of the urethane-anaesthetised rat consisted of systematic and cyclic alternations between activated and deactivated patterns. In the present study, we observed that similar state changes in the supEC co-occurred with those in the HPC and nCTX. The activated state was characterised by theta in the supEC and HPC, and LVFA in the nCTX. The deactivated state was characterised by the SO in all three structures. The gradual spontaneous progression from the activated state to the deactivated state occurred through a transition state that was characterised by LIA in the supEC and HPC and moderate-amplitude slow rhythms in the nCTX (**Figure 3-01**).

Evolution of the slow oscillation in the entorhinal cortex

After verifying that spontaneous state changes were a feature of the LFP in the supEC, we sought to characterize the dynamics of the activated and deactivated states across the supEC, HPC, and nCTX. We recorded spontaneous activity in all 3 structures simultaneously (n = 12); an example of one such recording is shown in **Figure 3-01**. By expanding segments of each long-duration recording (*bottom panel* of **Figure 3-01A**), and by examining spectrograms computed on each trace (**Figure 3-01B**) and the individual spectra that corresponded to the segments of data shown in the expansions (**Figure 3-01C**),

we were able to describe the evolution of theta, LIA, and the SO in the supEC in relation to that in the HPC and nCTX.

The LFPs and their transition from activated to deactivated patterns in the supEC and HPC were quite similar. Power at the peak theta frequency (3.39 ± 0.12Hz) in both the supEC and HPC was highest during the activated state, when LVFA dominated the neocortical trace (*leftmost expansion* in *bottom panel* of **Figure 3-01A**). In the experiment shown, power at the peak SO frequency (1.03 ± 0.064Hz) initially became prominent in the nCTX, concomitant with the appearance of LIA in both the supEC and HPC (*middle expansion* in *bottom panel* of **Figure 3-01A**). SO power subsequently increased in the supEC and HPC (*rightmost expansion* in *bottom panel* of **Figure 3-01A**).

By plotting the ratio of normalized SO power to normalized theta power over time (*see Methods section*), we could show that the pattern of SO evolution shown in **Figure 3-01** (nCTX – supEC – HPC) was a systematic feature in the majority of our experiments (8/12; 67%). In all cases, the onset of the hippocampal SO followed that in the nCTX and/or EC. This finding was consistent with our previous results (Wolansky et al., 2006). The relative latencies of the evolution of the SO in each region are shown in **Figure 3-02** with individual experiments in *black* and averages in *grey*. The average latency of SO onset in the nCTX (0.69 ± 0.44s) was significantly less (*t*-test: $p < 0.05$) than that in the HPC (2.65 ± 1.02s) confirming that the SO developed in the nCTX prior to the HPC. The latency of the SO onset in the supEC (1.44 ± 0.51s) was

intermediate with respect to both the nCTX and HPC but was not significantly different from either.

Laminar field potential profile in the entorhinal cortex

To characterize slow oscillatory activity in the superficial and deep EC (corresponding to the layers providing hippocampal input and receiving hippocampal output, respectively), we recorded spontaneous activity using the multiprobe (n = 6) at an angled approach that was oriented orthogonally to the entorhinal cell layers (*see Methods section for details*). This allowed us to record across a column of all entorhinal layers simultaneously. We used a combination of field activity, multiunit activity, and histology to physiologically determine the location of the various laminae (*see Methods section for details*).

Representative raw LFP traces during both theta (*left*) and SO (*right*) are shown in **Figure 3-03A**. The maximal theta amplitude was observed in the multiprobe contacts (*blue numbers*) closest to the pial surface and just superficial to the theta phase reversal (corresponding to the border of layers II and III). These are consistent with prior results (Mitchell and Ranck, 1980; Alonso and Garcia-Austt, 1987b). The SO, on the other hand, did not exhibit a complete phase reversal, although fast transient events associated with the negative phase of the SO cycle did reverse at the same position as the theta phase reversal (the border of layers II and III). The amplitude of the SO was maximal at about the same position as the theta maximum (layer I), although unlike theta, SO amplitude tended to be high throughout the depth of the profile.

Using LFP recordings from the multiprobe, we calculated and plotted state-dependent spectral power, phase, and coherence according to depth **(Figure 3-03B)**. Power values were averaged across a 0.3Hz bandwidth centered on the peak frequency (3.78 ± 0.15Hz for theta and 0.97 ± 0.08Hz for the SO). Phase and coherence values were calculated in reference to the contralateral hippocampal signal, and then averaged across the same frequency bandwidth as stated above. This allowed us to visualize the laminar distribution of theta and SO activity in alignment to each other and to the histological track.

Again, the laminar spectral profiles for entorhinal theta (*black lines*; **Figure 3-03B**) were consistent with previous research (Mitchell and Ranck, 1980; Alonso and Garcia-Austt, 1987b). Theta power was consistently greatest in the supEC, (specifically in layer I), as compared to deeper layers. The phase reversal of theta occurred approximately at the border of layers II and III, 0.62 ± 0.05mm from the pial surface on average, and also corresponded to the point at which both overall power and coherence sharply decreased. At deeper positions in the EC, theta power could increase at approximately layer IV, but thereafter decreased in a monotonic fashion.

The general shape of the SO power, phase, and coherence profiles constructed for each experiment were consistent with the one shown in **Figure 3-03B** (*red lines*). SO power was consistently large in layers I and the superficial portion of layer II and the profile showed two local minima: one at the pial surface and the other at the border of layers II and III. In contrast to the theta power profile, we observed a monotonic increase in SO power with increasing

depth (toward the deep EC and HPC). The SO field potential did not reverse in the EC, however, it consistently shifted phase (9.74 ± 2.35°) at the same level or near the depth of the theta phase reversal (between layers II and III; 0.62 ± 0.05mm from pial surface). The phase shift of the SO in the EC corresponded to an average time difference of 27.06 ± 6.53ms for hippocampal versus entorhinal activity at 1Hz, and is approximately half of the phase/time difference between neocortical and hippocampal activity at 1Hz that we reported previously (22.3 ± 1.1º or 56 ± 3ms) (Wolansky et al., 2006). Interestingly, the SO-related field potential power and coherence with the HPC appeared to have a reciprocal relationship: at points in the EC where the SO power was high, coherence with the HPC SO tended to be low. Coherence with the HPC also unexpectedly increased at the same level as the phase shift of the SO in the EC.

Current source density profile in the entorhinal cortex

Although the laminar voltage profile of EC SO is a relatively accurate approximation of the distribution of activity during this state, extracellular potentials can be influenced by volume conduction. To circumvent this potential issue, we computed the CSD for continuous field recordings of spontaneous theta and SO activity. We then performed spectral analysis on the CSD traces in the same manner as described above for voltage traces.

A representative example of a CSD profile for spontaneous theta and SO activity is shown in **Figure 3-04A**. The largest sink – source alternations during both theta and the SO occurred in layer I, along with phase-reversed alternations

of slightly lower amplitudes in layer II. During the SO, and in contrast to theta, weaker sink – source alternations could be observed at deeper sites (i.e., layers III and V).

Spectral analyses of the CSD profiles allowed us to isolate and compare the distribution of theta- and SO-related extracellular current fluctuations. **Figure 3-04B** shows a representative example of the average state-dependent CSD power, phase, and coherence for both theta (*black lines*) and the SO (*red lines*) plotted according to depth through the EC laminae. Theta CSD power was greatest in the supEC, specifically in layers I, II, and III, as compared to deeper layers. The phase reversal of the theta CSD (i.e., the separation of simultaneous sink – source pairs) occurred at the border of layers I and II and corresponded to a local minimum in both the overall CSD power and coherence with the HPC. Theta CSD coherence with the HPC was highest in layers I, II, and III, and was lowest in deep entorhinal layers.

Similarly to the theta profile, the SO CSD power was greatest in supEC, specifically in layers I and II and SO-related sink – source alternations reversed phase at the border between layers I and II. Additional sink – source alternations (phase reversals of SO CSD power) were also observed at deeper levels of the EC (i.e., layers III and V). Although CSD power at these locations was lower than that in the supEC, the coherence with the hippocampal SO was higher (especially in layer V).

To assess the dissociation between the SO-related CSD power and coherence across the superficial and deep layers of the EC, we compared the

coherence of the entorhinal CSD to the field signals generated in both the HPC and nCTX. Consistent with previous work (Mitchell and Ranck, 1980; Alonso and Garcia-Austt, 1987a, 1987b; Chrobak and Buzsáki, 1994; Dickson, 1994; Frank et al., 2001), theta coherence with the HPC was strong in the supEC (layers I and II) and weaker, but still significant in the deep EC (layer V) (**Figure 3-05A**). The SO coherence was surprisingly lower than the theta coherence overall (**Figure 3-05B**). In fact, the SO coherence to the HPC across EC laminae appeared higher in the deep EC than in the supEC (**Figure 3-05Bi**). The SO coherence between the nCTX and EC sites was even lower than the coherence with the HPC, but again coherence in the deep EC was slightly higher than in the supEC (**Figure 3-05Bii**).

Another surprising finding was that the coherence between the entorhinal CSD and hippocampal LFP (**Figure 3-05Bi**) was lower than the coherence between the neocortical and hippocampal LFPs (**Figure 3-05Biii**). Therefore, we conducted a similar coherence comparison between hippocampal CSD traces and neocortical LFP. The coherence between the hippocampal CSD and neocortical LFP (**Figure 3-05Biv**) was lower than the coherence between the LFP signals themselves (**Figure 3-05Biii**), but it was still higher than the coherence between the entorhinal CSD and neocortical LFP (**Figure 3-05Bii**).

Entorhinal multiunit activity during the slow oscillation

To further elucidate the fine structure of SO-related activity in the EC, we sampled multiunit activity simultaneously in both the superficial and deep layers

using the multiprobe in the same manner as described above for LFP recordings (n = 4). Rhythmic entorhinal multiunit activity was apparent during both theta (*not shown*) and the SO (**Figure 3-06A**). Multiunit activity in the supEC was prominently rhythmic during theta, however, theta-related rhythmicity was not as apparent in the deep EC (*not shown*). In contrast, SO-related rhythmicity was a robust feature in layer V multiunit activity and less consistent in layers II and III (**Figure 3-06A**).

We characterised the phase relationship of entorhinal multiunit activity to the ongoing hippocampal field using multiunit triggers (*see Methods section for details*). During theta, only the multiunit activity in the supEC tended to be rhythmic and phase-related to hippocampal LFP (*not shown*) whereas both sup- and deep EC multiunit activity tended to be related to the hippocampal LFP during the SO. **Figure 3-06B** shows the average phase distributions of the multiunit triggers in EC layers II, III, and V with respect to the hippocampal SO field for the experiment depicted in panel **A**; they were all distributed close to the negative phase of the hippocampal field. Group data are shown in **Figure 3-06C**: the average from the experiment depicted in panel **A** is displayed in *black* (layer II: angle: 282.86°, radius: 0.61; Rayleigh, z: $p < 0.05$; layer III: angle: 273.05°, radius: 0.60; Rayleigh, z: $p < 0.05$; layer V: angle: 273.26°, radius: 0.45; Rayleigh, z: $p < 0.05$), averages from other experiments are displayed in *grey*. Individual experiments with significant Rayleigh values are shown as *filled grey* and *filled black circles* and those with non-significant Rayleigh values are shown as *unfilled grey circles*. The group averages are shown as an *X* and were

computed across experiments with significant Rayleigh values only (layer II (3/4 significant): angle: 281.99°, radius: 0.40; $F_{(2, 1)} = 3.22$; $p = 0.37$; layer III (3/4 significant): angle: 282.37°, radius: 0.36; $F_{(2, 1)} = 5.04$; $p = 0.30$; layer V (2/4 significant): angle: 273.62°, radius: 0.41; $F_{(2, 0)} = 0$; $p = 1.00$).

The number of multiunit bursts, their duration and their amplitude appeared variable across the different layers of the EC. To assess whether any differences we observed between the layers were significant, we expressed the number of multiunit triggers (i.e., multiunit burst events) in each layer, during each state, per unit time (**Figure 3-07A**). Individual experiments are shown as *unfilled symbols* and layer averages across experiments are shown in *grey*. The number of bursts in layers II and III during both theta (*left panel*; 0.43 ± 0.091 bursts/s and 0.36 ± 0.11 bursts/s, respectively) and the SO (*right panel;* 0.45 ± 0.59 bursts/s and 0.44 ± 0.041 bursts/s, respectively) were similar. In layer V, we observed significantly fewer (*t*-test: $p < 0.05$) bursts during theta (0.26 ± 0.067 bursts/s) than during the SO (0.42 ± 0.039 bursts/s). This confirms that on average, layer V was more active during the SO.

We also measured the duration of the multiunit bursts in EC layers II, III, and V and compared them within each layer and across different states. In each experiment, including the one depicted in **Figure 3-06**, the duration of the multiunit bursts was not significantly different (*t*-test: $p > 0.05$) across theta (*left panel* of **Figure 3-07B**) and the SO (*right panel* of **Figure 3-07B**) in layers II and III, but it was (*t*-test: $p < 0.05$) in layer V. We further compared the duration of the multiunit bursts across different layers and within each state. Theta-related

multiunit bursts in layer III appeared longer than those in layers II and V and SO-related multiunit bursts appeared to increase in duration with increasing depth (towards the deep EC); neither of these differences were statistically significant (*t*-test: $p > 0.05$).

Finally, we assessed the amplitude of the multiunit bursts in each of the entorhinal layers across states. The amplitudes of the multiunit bursts in each layer during the SO were significantly larger than bursts in the same layer during theta (*comparison lines not shown*; *t*-test: $p < 0.05$; **Figure 3-07C**). Theta-related bursts (*left panel* of **Figure 3-07C**) in layer III were significantly larger in amplitude (*t*-test: $p < 0.05$) than those in layers II and V. SO-related bursts (*right panel* of **Figure 3-07C**) in layer III were also significantly larger in amplitude (*t*-test: $p < 0.05$) than those in layers II and V. In addition, SO-related multiunit bursts in layer II were significantly larger in amplitude (*t*-test: $p < 0.05$) than those in layer V. Despite the fact that SO-related multiunit bursts in layer V were smaller in amplitude than those in layers II and III, they were robustly phase-modulated by the SO (**Figure 3-06C**). Together with our CSD coherence data, this suggests that the deep EC is strongly influenced during the SO, likely via hippocampal output.

Entorhinal single unit activity during the slow oscillation

The multiunit data confirmed that the local networks in the superficial and deep EC were modulated by state in a differential fashion. To evaluate this at the single cell level, we recorded 43 entorhinal single units in 12 urethane-

anaesthetised rats and analysed their spike train dynamics during both theta and the SO. We characterised the location of each unit as layer II, layer III, or deep (layer V and/or VI) by: 1) histological verification of recording track and methylene blue injection site, 2) the phase of the entorhinal theta field in comparison to the hippocampal theta field, and 3) comparison to the depth measurements made for other confirmed units recorded in the same track. Based on these criteria, we collected data from 12 layer II units, 15 layer III units, and 16 deep units.

Every unit that we recorded showed either: 1) a significant change in the firing rate across theta and the SO, 2) a significant change in spike train dynamics across theta and the SO, or 3) both. **Figure 3-08** shows representative samples of hippocampal field activity (*bottom panels* of **A**, **D**, and **G**) along with simultaneously recorded entorhinal LFP (*top panels*) and single unit activity (*middle panels*) in layers II (**A**), III (**D**), and V (**G**). We found that the majority of neurons from each layer generated action potentials during the SO in a rhythmic and phase-related manner.

The firing rate of the layer II cell shown in **Figure 3-08A** was not significantly different (*t*-test: $p > 0.05$) across theta and the SO. The raw traces (**Figure 3-08A**), autocorrelation (*top panel* of **Figure 3-08B**), STA (*middle panel*), and field cycle preference histogram (*bottom panel*) demonstrate that this unit discharged rhythmically in a phase-related fashion during the SO. It did not discharge rhythmically during theta (*not shown*). On average, this unit fired

approximately 70ms prior to the negative peak of the hippocampal SO (angle: 254.41° radius: 0.71; Rayleigh z = 225.55, $p < 0.05$ n = 450).

Group data for all layer II neurons that generated rhythmic and phase-related (Rayleigh, z: $p < 0.05$) action potentials during the SO are shown in **Figure 3-08C**. The cell shown in the previous panels is represented in *black*, data from other rhythmic and phase-related layer II units are displayed in *grey*, and the group average is displayed in *white* (angle: 256.18°, radius: 0.34; $F_{(2, 6)} = 31.94$; $p = 0.00063$). Most layer II neurons discharged just before the negative peak of the hippocampal SO. **Table 3-01** is a summary of the spike train dynamics of all 12 layer II units recorded across theta and the SO. The majority of them (10/12; 83%) showed a significant change in spike rate across the two states (*t*-test: $p < 0.05$) and 9/12 (75%) were significantly rhythmic and phase related to the SO LFP.

The spike rate of the layer III cell shown in **Figure 3-08D** was significantly different (*t*-test: $p < 0.05$) across theta and the SO (it was silent during theta; *not shown*). The raw traces (**Figure 3-08D**), autocorrelation (*top panel* of **Figure 3-08E**), STA (*middle panel*), and field cycle preference histogram (*bottom panel*) demonstrate that it discharged rhythmically and in a phase-related fashion during the SO. On average, this unit fired approximately 179.5ms following the negative peak of the hippocampal SO (angle: 304.89°; radius: 0.55; Rayleigh z = 28.77, $p < 0.05$, n = 95).

Group data for all layer III neurons that generated rhythmic and phase-related (Rayleigh, z: $p < 0.05$) action potentials during the SO are shown in

Figure 3-08F. The cell shown in the previous panels is represented in *black*, data from other rhythmic and phase-related layer III units are displayed in *grey*, and the group average is displayed in *white* (angle: 303.14°, radius: 0.29; $F_{(2, 10)}$ = 14.01; $p = 0.0013$). Most layer III neurons tended to fire just after the negative peak of the hippocampal SO. **Table 3-02** is a summary of the spike train dynamics of all 15 layer III units recorded across theta and the SO. The majority of them (14/15; 93.3%) showed significant changes in spike rates across states (*t*-test: $p < 0.05$) and 12/15 (80%) were significantly rhythmic and phase related to the SO LFP.

The deep entorhinal unit shown in **Figure 3-08G** generated rhythmic action potentials during both theta (*not shown*) and the SO (**Figure 3-08H**, *top panel*) and its firing rate was significantly (*t*-test: $p < 0.05$) greater during the SO. It discharged in a phase-related fashion during the SO as shown in the raw traces (**Figure 3-08G**), autocorrelation (*top panel* of **Figure 3-08H**), STA (*middle panel*), and field cycle preference histogram (*bottom panel*). On average, action potentials occurred 24ms before the negative peak of the hippocampal field during theta (theta: angle: 201.74°, radius: 0.39; Rayleigh, z = 5.64, $p < 0.05$, n = 37) and 82ms after the negative peak of the hippocampal field during the SO (angle: 315.08°; radius: 0.23; Rayleigh, z = 11.73, $p < 0.05$, n = 213).

Group data for layer V neurons that generated rhythmic and phase-related (Rayleigh, z: $p < 0.05$) action potentials during the SO are shown in **Figure 3-08I**. The cell shown in the previous panels is represented in *black*, data from other deep units are displayed in *grey*, and the group average is displayed in *white*

(angle: 253.00°, radius: 0.16; $F_{(2, 10)} = 5.11$; $p = 0.030$). **Table 3-03** is a summary of all 16 units that we recorded during theta and the SO. The majority of them (15/16; 93.8%) showed significant changes in spike rates across states (*t*-test: $p < 0.05$) and13/16 (81.25%) were significantly rhythmic and phase related to the LFP during the SO.

Discussion

This series of experiments has conclusively shown that the SO is a prominent feature of entorhinal electrographic activity. It occurs in the superficial layers which give rise to the primary input of the HPC (i.e., II and III) as well as in the deep layers which receive the bulk of the output from the HPC. Two main observations are especially interesting in this respect. First, although the SO-related LFP and CSD were larger in the supEC (i.e., hippocampal input), the SO-related coherence with the HPC was largest in the deep layers (i.e., hippocampal output). Second, although we observed rhythmic modulation of superficial and deep multiunit and single unit activity during both states, the rhythmic modulation in the deep layers appeared to be significantly enhanced during the SO. This suggests that SO-related coupling in the entorhinal-hippocampal circuit occurs in a robustly bidirectional fashion. Given the recent attention on the relationship between non-REM sleep (specifically SWS and the SO) and the consolidation of episodic (i.e., hippocampal-dependent) memories (Hirase et al., 2001; Mednick et al., 2003; Huber et al., 2004; Marshall et al., 2004; Molle et al., 2004; Peigneux et al., 2004; Backhaus et al., 2006; Marshall et al., 2006; Takashima et al., 2006; Ji and Wilson, 2007; Rasch et al., 2007; Tse et al., 2007; Backhaus et al., 2008; Eschenko et al., 2008; Talamini et al., 2008; Wilhelm et al., 2008), the coordination of MTL and neocortical activity during the SO is a pertinent avenue of research.

Coordination of the slow oscillation across the neocortex and hippocampus

Previous evidence has suggested that during the SO, the nCTX entrains the HPC via the EC in a serial manner (Hahn et al., 2006; Isomura et al., 2006; Wolansky et al., 2006; Hahn et al., 2007). The latencies of the SO evolution in each of these structures generally supported this idea since the SO began in the EC at an intermediate latency relative to that in the nCTX and HPC on average. The presence of SO-related activity in the supEC (i.e., hippocampal input) is also consistent with this idea. However, even though the SO occurred in the supEC, its coherence with the HPC was very low; even lower than that between the HPC and nCTX. This may indicate that an alternate or additional circuit is involved in the coordination of SO activity across the nCTX and MTL.

We previously suggested that the NReu could be another source of SO coordination across the EC, HPC, and nCTX (Wolansky et al., 2006). Excitatory (Dolleman-Van der Weel et al., 1997; Bertram and Zhang, 1999) projections from the NReu terminate predominantly in layers I and III of the EC and at the level of SLM in the HPC (Wouterlood et al., 1990). These are the precise zones where the SO-related sink – source alternations are the largest in both structures. Since the NReu receives a prominent input from the prefrontal nCTX (Beckstead, 1979; Swanson, 1981; Ferino et al., 1987; Jay et al., 1989; Sesack et al., 1989; van Groen and Wyss, 1990; Wouterlood et al., 1990; Hurley et al., 1991; Jay and Witter, 1991; Vertes, 2002; Proulx and Timofeev, 2007) and the SO is thought to originate from frontal regions (Massimini et al., 2004; Murphy et al., 2009), it is

possible that the NReu also plays a role in the coordination of MTL structures with the nCTX during the SO. This remains to be tested experimentally.

Hippocampal SO output

One of the major implications of our present study is that hippocampal output during the SO is distinctly oscillatory and it produces a measurable impact on the cells in the deep EC. This is consistent with our previous work showing that the majority of units in the HPC, including CA1 are modulated by the SO. Others have demonstrated clear SO-related activity in the Subic (Isomura et al, 2006), which is the major output structure of the HPC. We also showed that other indicators of network activation (i.e., gamma activity) are present and phase-related to the SO (Wolansky et al., 2006) suggesting that the HPC exhibits network UP states similar to those in the nCTX (Mukovski et al., 2007). Other researchers have demonstrated clear membrane potential bistability (UP and DOWN states) in hippocampal interneurons (Hahn et al., 2006) and phasic modulation of membrane potentials in hippocampal principal neurons (Hahn et al., 2007) that were linked to the ongoing cortical SO. In addition, Ji and Wilson (2007) demonstrated that most hippocampal units demonstrate “frames” of activity that are coordinated with neocortical UP states expressed during SWS. Given our results, it is likely that deep EC SO reflects the synchronised rhythmic output of CA1 and subicular networks.

Functional significance of the slow oscillation

Recent work from our laboratory has shown that excitatory neurotransmission in region CA1 of the HPC is enhanced during the SO as compared to theta. This effect was independent of the source; occurring in both the contralateral CA3 and ipsilateral entorhinal inputs to the HPC (Schall et al., 2008). This implies that synaptic input to CA1 during theta may have less influence than the same input occurring during the SO. Schall et al. (2008) also showed that the strength of excitatory neurotransmission was significantly modulated across the phase of the SO cycle (maximal just after the positive peak of the LFP). Thus, both state and phase of ongoing field oscillations can influence transmission in the hippocampal circuit. The diverse SO phase relationships that we found in our multiunit and single unit data could represent an additional level of functional processing in the MTL circuitry.

It is widely accepted that synchronization is critical for changes in the synaptic efficacy between pre- and post-synaptic neurons (Lynch et al., 1977; McNaughton et al., 1978; Levy and Steward, 1979; Barrionuevo and Brown, 1983; Bramham and Srebro, 1987; Stanton and Sejnowski, 1989) and the transient synchronization of neurons and their networks during sleep could facilitate these synaptic modifications (Buzsáki, 1998; Hasselmo, 1999; Peigneux et al., 2001; Tononi and Cirelli, 2001; Ribeiro and Nicolelis, 2004; Walker and Stickgold, 2004; Rauchs et al., 2005). Tsukamoto-Yasui et al. (2007) recently showed that the expression of spontaneous and slow membrane potential UP and DOWN states (intracellular SO) in CA3 neurons from hippocampal slices could evoke, by

itself, changes in synaptic efficacy. These plastic changes were long-lasting, frequency-dependent, universal (all cells could express plasticity), and dynamic (each synaptic pathway could express either potentiation or depression). All of these characteristics would be adaptive in the context of physiological mnemonic processing. It would be interesting to demonstrate that slow synchronization across synaptically connected neurons by itself could significantly modify their connection strengths.

Conclusion

The current data demonstrate that the SO is a phenomenon of the parahippocampal region and is a feature of the activity in the cortical input and output pathways to and from the HPC. We suggest that the SO reflects a functional bidirectional interaction between the EC and HPC and potentially even larger tracts of the cortical mantle. The expression of this activity during SWS could create extended network activity patterns that facilitate episodic memory consolidation.

Table 3-01: Summary of entorhinal layer II state-dependent spike train dynamics

Layer II Units		SLOW OSCILLATION						TOTAL	
		Rhythmic		Non-rhythmic		Silent			
THETA	Rhythmic	6	50.0%	1	8.3%	--	--	7/12	58.3%
	Non-rhythmic	2	16.7%	1	8.3%	--	--	3/12	25.0%
	Silent	1	8.3%	1	8.3%	--	--	2/12	16.7%
TOTAL		9/12	75.0%	3/12	25.0%	--	--	12/12	100%

We recorded a total of 12 layer II EC units during both theta and the SO. Six of 12 generated rhythmic action potentials during both states and 1 of 12 was non-rhythmic during both states. Two of 12 units were silent during theta, but none were silent during the SO.

Table 3-02: Summary of entorhinal layer III state-dependent spike train dynamics

Layer III Units		SLOW OSCILLATION						TOTAL	
		Rhythmic		Non-rhythmic		Silent			
THETA	Rhythmic	7	46.7%	--	--	--	--	7/15	46.7%
	Non-rhythmic	--	--	2	13.3%	--	--	2/15	13.3%
	Silent	5	33.3%	1	6.67%	--	--	6/15	40.0%
TOTAL		12/15	80.0%	3/15	20.0%	--	--	15/15	100%

We recorded a total of 15 layer III EC units during both theta and the SO. Seven of 15 generated rhythmic action potentials during both states and 2 of 15 were non-rhythmic during both states. Six of 15 units were silent during theta, but none were silent during the SO.

Table 3-03: Summary of deep entorhinal state-dependent spike train dynamics

Deep Units		SLOW OSCILLATION						TOTAL	
		Rhythmic		Non-rhythmic		Silent			
THETA	Rhythmic	8	50.0%	2	12.5%	--	--	10/16	62.5%
	Non-rhythmic	3	18.75%	1	6.25%	--	--	4/16	25.0%
	Silent	2	12.5%	--	--	--	--	2/16	12.5%
TOTAL		13/16	81.25%	3/16	18.75%	--	--	16/16	100%

We recorded a total of 16 deep layer EC units during both theta and the SO. Eight of 16 generated rhythmic action potentials during both states and 2 of 16 were non-rhythmic during both states. Two of 14 units were silent during theta, but none were silent during the SO.

Figure 3-01:

Evolution of the slow oscillation in the entorhinal cortex

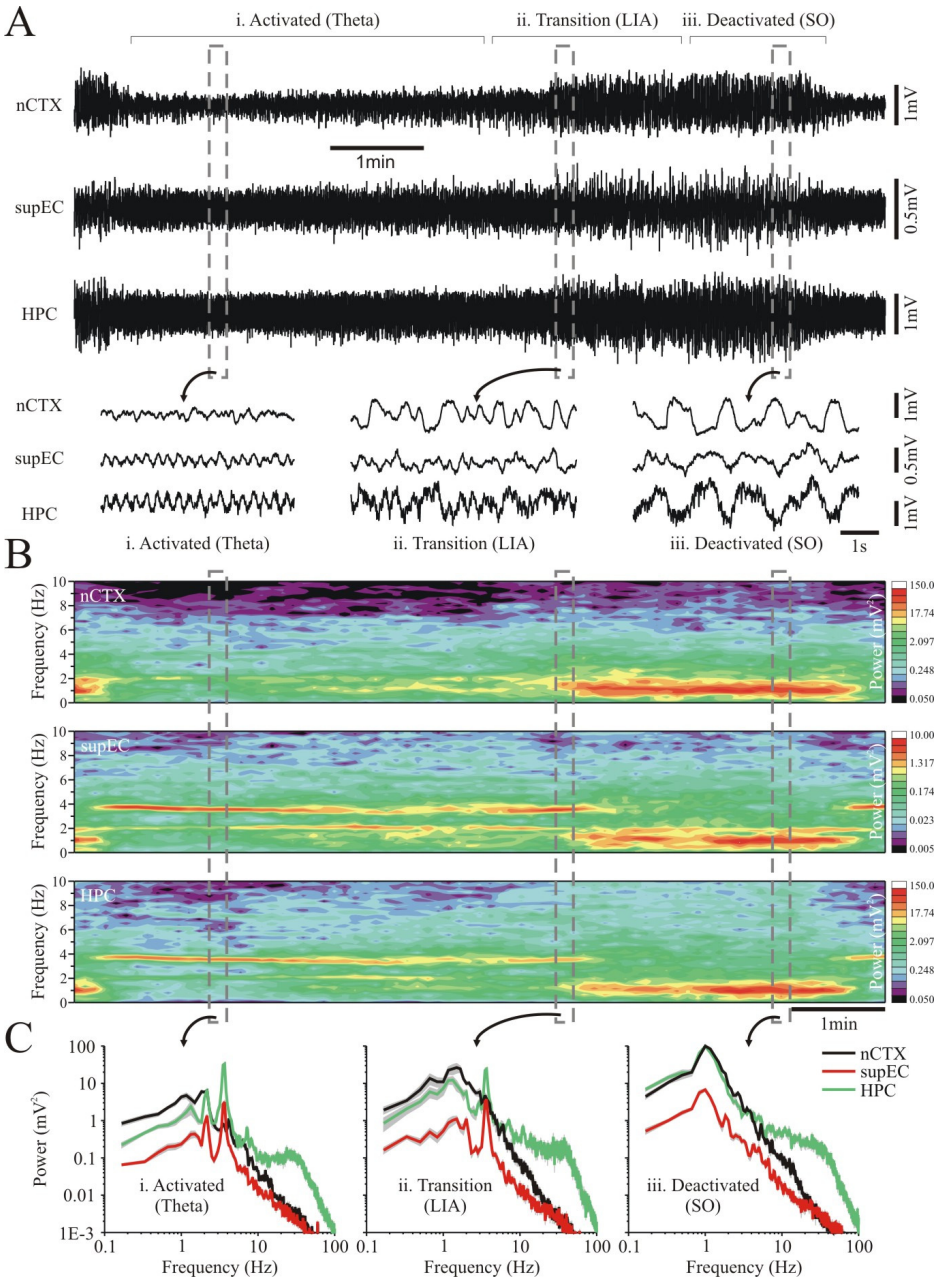

Figure 3-01 Caption:

(**A**) Simultaneously recorded field activity in the nCTX, the supEC, and the HPC show the progression from the activated state: characterised by LVFA in the nCTX and theta in the supEC and HPC (*left-most expansion* in the *lower panel*), to the deactivated state: characterised by the SO in all three structures (*right-most expansion* in the *lower panel*), through a transition state: characterised by slow rhythms in the nCTX and LIA in the supEC and HPC (*middle expansion* in *lower panel*). Time-aligned spectrograms in **B** and individual spectra in **C** show that theta power is greatest during the activated state and SO power is greatest during the deactivated state. *Grey shaded area* represents 95% confidence interval. The spectrograms also highlight how SO power becomes prominent in the nCTX prior to the supEC and HPC in this experiment. Abbreviations: hippocampus (HPC), large amplitude irregular activity (LIA), low-voltage fast activity (LVFA), neocortex (nCTX), slow oscillation (SO), superficial entorhinal cortex (supEC)

Figure 3-02:

Timing of the evolution of the slow oscillation

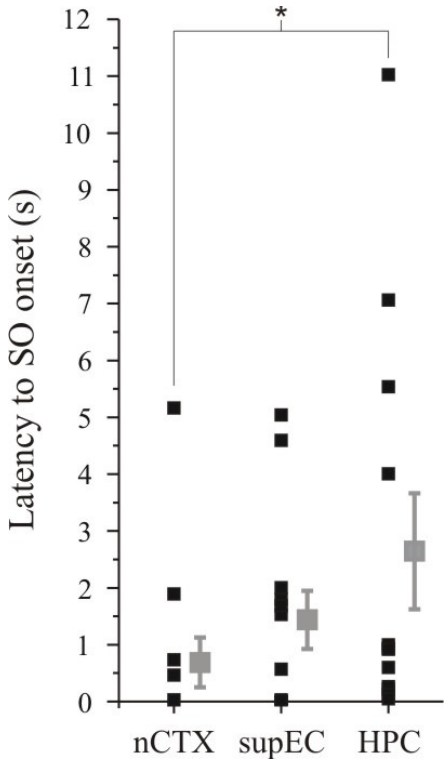

The average latency of SO onset in the nCTX was significantly different from that in the HPC (*t*-test: $p < 0.05$). The average latency of SO onset in the supEC was not significantly different from that in either of the nCTX and HPC. Individual experiments are shown in *black* and averages are shown in *grey*. Abbreviations: hippocampus (HPC), neocortex (nCTX), slow oscillation (SO), superficial entorhinal cortex (supEC)

Figure 3-03:

Laminar profile of theta and the slow oscillation in the entorhinal cortex

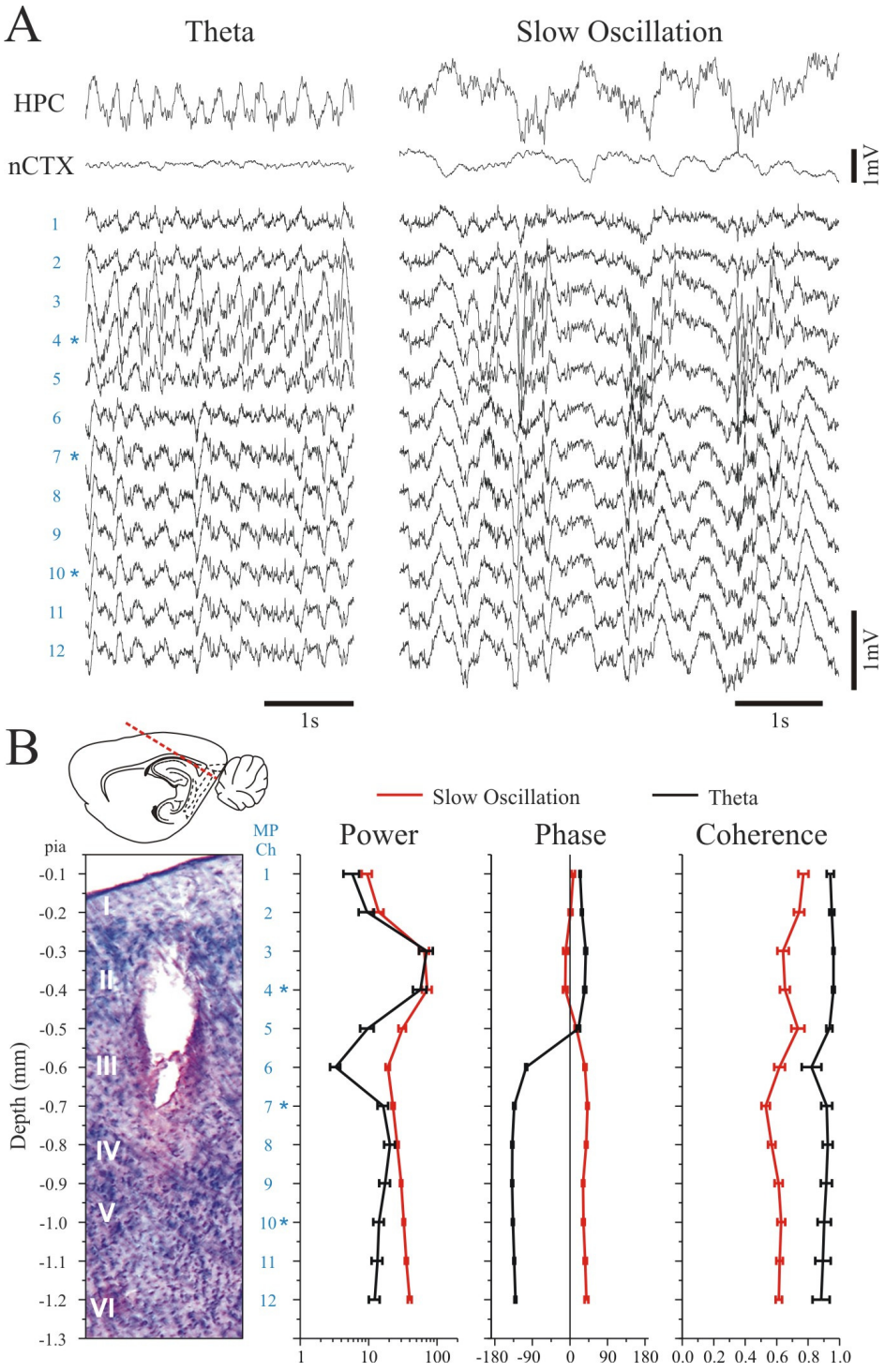

Figure 3-03 Caption:

(**A**) A sample of simultaneously recorded spontaneous LFPs across all layers of the EC (*blue numbers*; *blue asterisks* represent channels with maximal multiunit amplitude); compare to histology in the *left-most panel* of **B**) during theta (*left panel*) and the SO (*right panel*). The theta phase reversal can be seen across channels 5 (layer II) and 6 (layer III) while channels 3 and 4 (layers I and II) show maximal amplitudes. The amplitude of the SO was high throughout the profile and fast transient events were observed to reverse across channels 5 (layer II) and 6 (layer III). (**B**) State-dependent power, phase, and coherence during both theta (*black lines*) and the SO (*red lines*) aligned to the histology for the same experiment presented in **A**. Theta power was greatest in layers I and II and the phase reversal occurred at the border of layers II and III. The theta phase reversal consistently corresponded to a decrease in power and coherence. SO power was large in layers I and II and the profile showed two local minima: one at the pial surface and the other at the border of layers II and III. We observed a monotonic increase in SO power with depth (toward the deep EC and HPC). The SO field potential shifted phase between layers II and III (at or near the theta phase reversal). Abbreviations: deep entorhinal cortex (deep EC), hippocampus (HPC), local field potential (LFP), multiprobe channel (MP Ch), neocortex (nCTX), slow oscillation (SO)

Figure 3-04:

Laminar current source density profile of theta and the slow oscillation in the entorhinal cortex

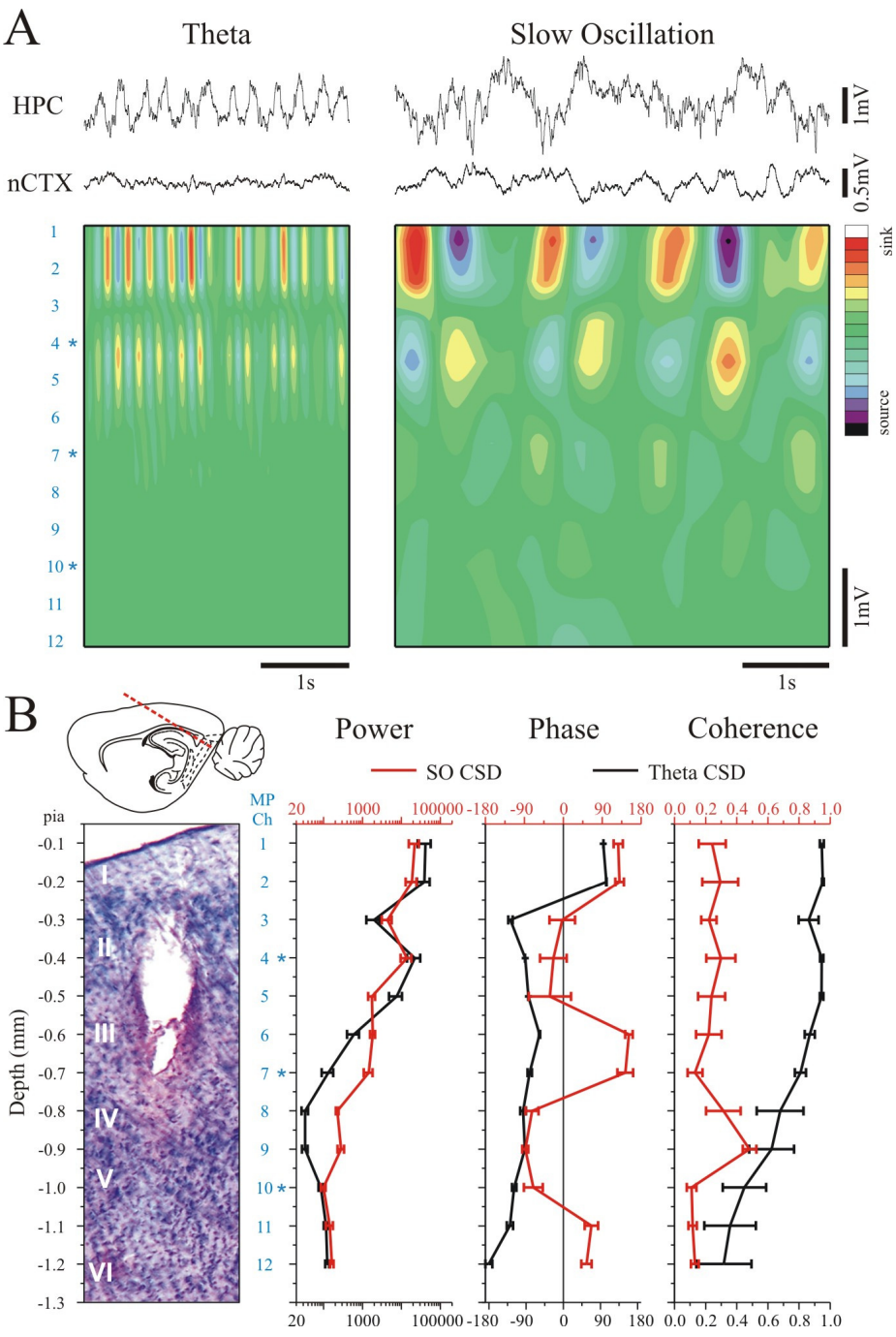

Figure 3-04 Caption:

(**A**) CSD profiles for spontaneous theta (*left panel*) and SO (*right panel*) activity time-aligned to simultaneously recorded hippocampal and neocortical potentials from the same experiment depicted in **Figure 3**. The multiprobe contacts are represented by the *blue numbers* to the left of the theta CSD profile (*blue asterisks* represent channels with maximal multiunit amplitude). The sink – source alternations during both theta and the SO reversed polarity across channel 3 (layer I/II border) and the amplitude of the superficial sink – source alternations was maximal in channels 2 and 4 (layers I and II). Additional sink – source alternations occurred in the deep EC during the SO and reversed across channel 11 (layer V/VI border); the amplitude for this deep entorhinal SO-related activity was maximal in channel 9 (layer V). (**B**) Average state-dependent CSD power, phase, and coherence for this experiment arranged according to depth through the EC laminae (aligned to multiprobe channels in *blue* and histology in *left-most panel*). Theta is represented by the *black lines* and the SO is represented by the *red lines*. Theta CSD power was greatest in layers I, II, and III, as compared to layer V. The theta CSD phase reversed at the border of layers I and II, which corresponded to a decrease in the overall CSD power and coherence with the HPC. Theta CSD coherence with the HPC was highest in layers I, II, and III, and decreased in deep entorhinal layers. The SO CSD power profile shows that power was greatest in layers I, II, and III. SO-related sink – source alternations also reversed at the border between layers I and II. Additional sink – source alternations reversed across layer V and these were accompanied by an increase in

coherence with hippocampal SO field activity. CSD scales for theta and the SO: -7.5 – 7.5. Abbreviations: current source density (CSD), entorhinal cortex (EC), hippocampus (HPC), multiprobe channel (MP Ch), neocortex (nCTX), slow oscillation (SO)

Figure 3-05:

Coherence of the entorhinal and hippocampal current source densities with hippocampal and neocortical field potentials

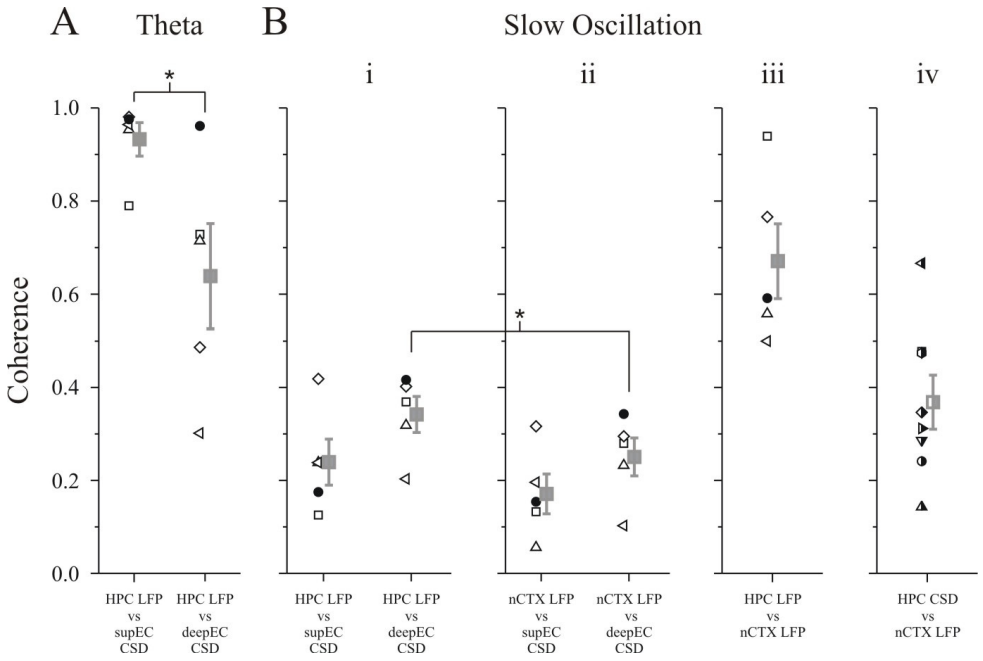

Figure 3-05 Caption:

The coherence values for individual experiments are shown as *unfilled symbols*, values for the experiment shown in **Figures 3** and **4** are shown in *black*, and averages across experiments are shown in *grey*. (**A**) The HPC vs supEC CSD coherence was greater than HPC vs deep EC CSD coherence during theta (*t*-test: $p < 0.05$). The HPC vs deep EC CSD coherence (**Bi**) was significantly greater than the nCTX vs deep EC CSD coherence (**Bii**) during the SO (*t*-test: $p < 0.05$). The HPC vs supEC coherence and the HPC vs deep EC coherence were both significantly different across theta (**A**) and the SO (**Bi**) (*comparison lines not shown*; *t*-test: $p < 0.05$). The coherence between hippocampal and neocortical LFPs (**Biii**) was greater than that with the entorhinal CSD (**Bi** and **Bii**). The coherence of hippocampal SO CSD traces from the level of SLM to the neocortical field potential traces is shown in **Biv** for comparison. The coherence values for individual experiments are shown as *half-filled black symbols* and averages across experiments are shown as *half-filled grey squares*. Abbreviations: current source density (CSD), deep entorhinal cortex (deep EC), hippocampus (HPC), local field potential (LFP), neocortex (nCTX), slow oscillation (SO), superficial entorhinal cortex (supEC)

Figure 3-06:

Entorhinal multiunit activity during the slow oscillation

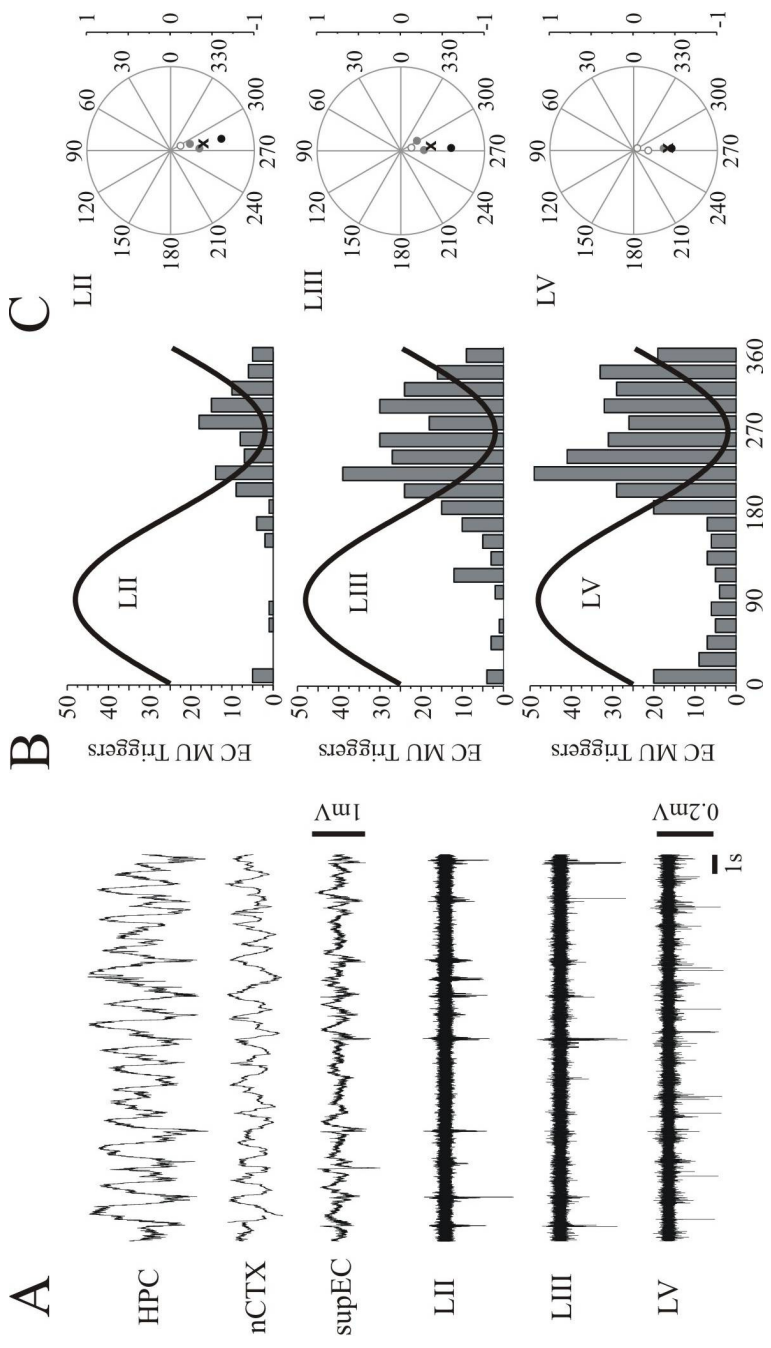

Figure 3-06 Caption:

(**A**) A representative sample of simultaneously recorded hippocampal and neocortical LFP and entorhinal multiunit activity during the SO. (**B**) The average distributions of the multiunit triggers in EC layers II, III, and V with respect to the phase of the hippocampal SO field activity for the experiment depicted in **A**. Group data is shown in **C**: the data from the experiment depicted in **A** is plotted in *black* and data from other experiments are displayed in *grey*, individual experiments with significant Rayleigh values are plotted as *filled grey* and *filled black circles*, those with non-significant Rayleigh values are shown as *unfilled grey* and *unfilled black circles*, and the group averages (computed across significant values only) are shown as an *X*. Abbreviations: entorhinal layer II (LII), entorhinal layer III (LIII), entorhinal layer V (LV), entorhinal multiunit (EC MU), hippocampus (HPC), local field potential (LFP), neocortex (nCTX), slow oscillation (SO), superficial entorhinal cortex (supEC)

Figure 3-07:

State-dependent entorhinal multiunit burst number, duration, and amplitude

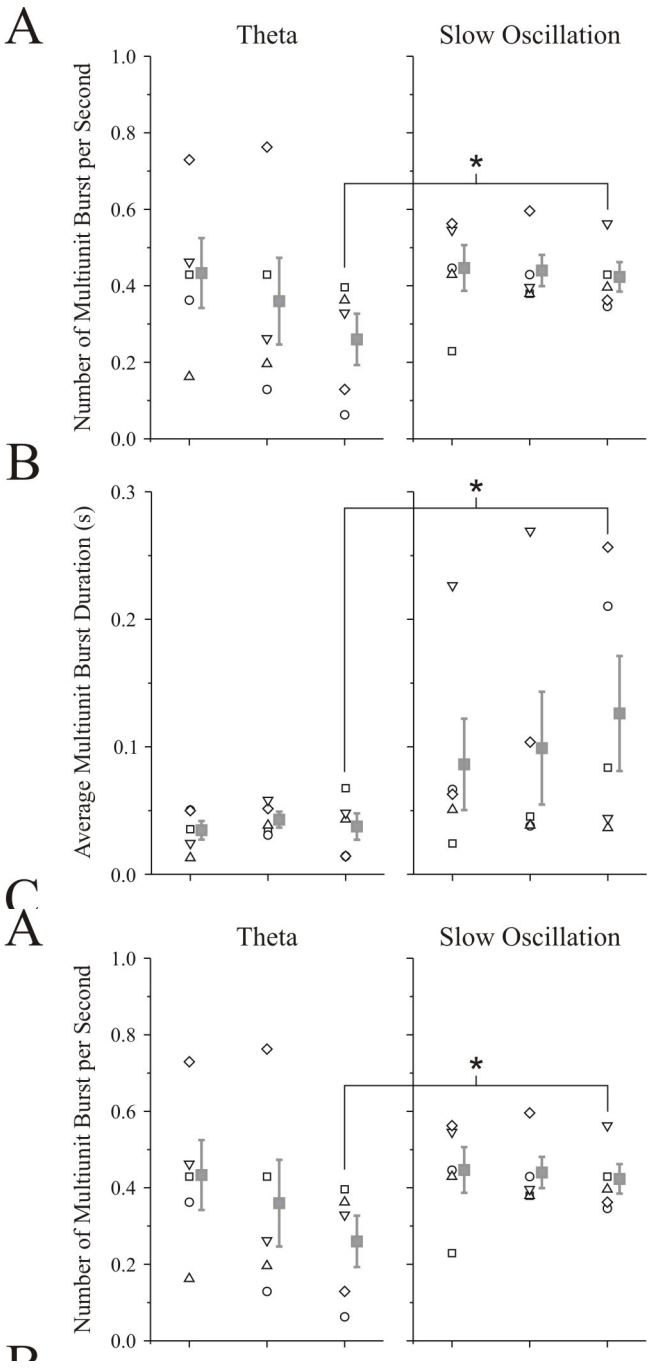

Figure 3-07 Caption:

(**A**) The number of triggered multiunit burst events in each layer per second during theta (*left panel*) and the SO (*right panel*). The number of bursts in layers II and III during both theta and the SO were similar (individual experiments shown as *unfilled symbols*, layer averages shown in *grey*). The number of multiunit bursts in layer V was significantly lower (*t*-test: $p < 0.05$) during theta. (**B**) The duration of the multiunit bursts was not significantly different (*t*-test: $p > 0.05$) across theta (*left panel*) and the SO (*right panel*) in layers II and III, but it was different in layer V. The duration of multiunit bursts was similar across the entorhinal layers within states. (**C**) The amplitude of the multiunit bursts within layers II, III, and V were significantly larger during the SO (*t*-test: $p < 0.05$; *comparison lines not shown*). The amplitude of theta-related bursts (*left panel*) in layer III were significantly larger (*t*-test: $p < 0.05$) than those in layers II and V. Similarly during the SO (*right panel*), multiunit bursts were larger (*t*-test: $p < 0.05$) in layer III as compared to those in layers II and V. SO-related multiunit bursts in layer II were significantly larger (*t*-test: $p < 0.05$) in amplitude than those in layer V. Abbreviations: slow oscillation (SO)

Figure 3-08:

Entorhinal single unit activity during the slow oscillation

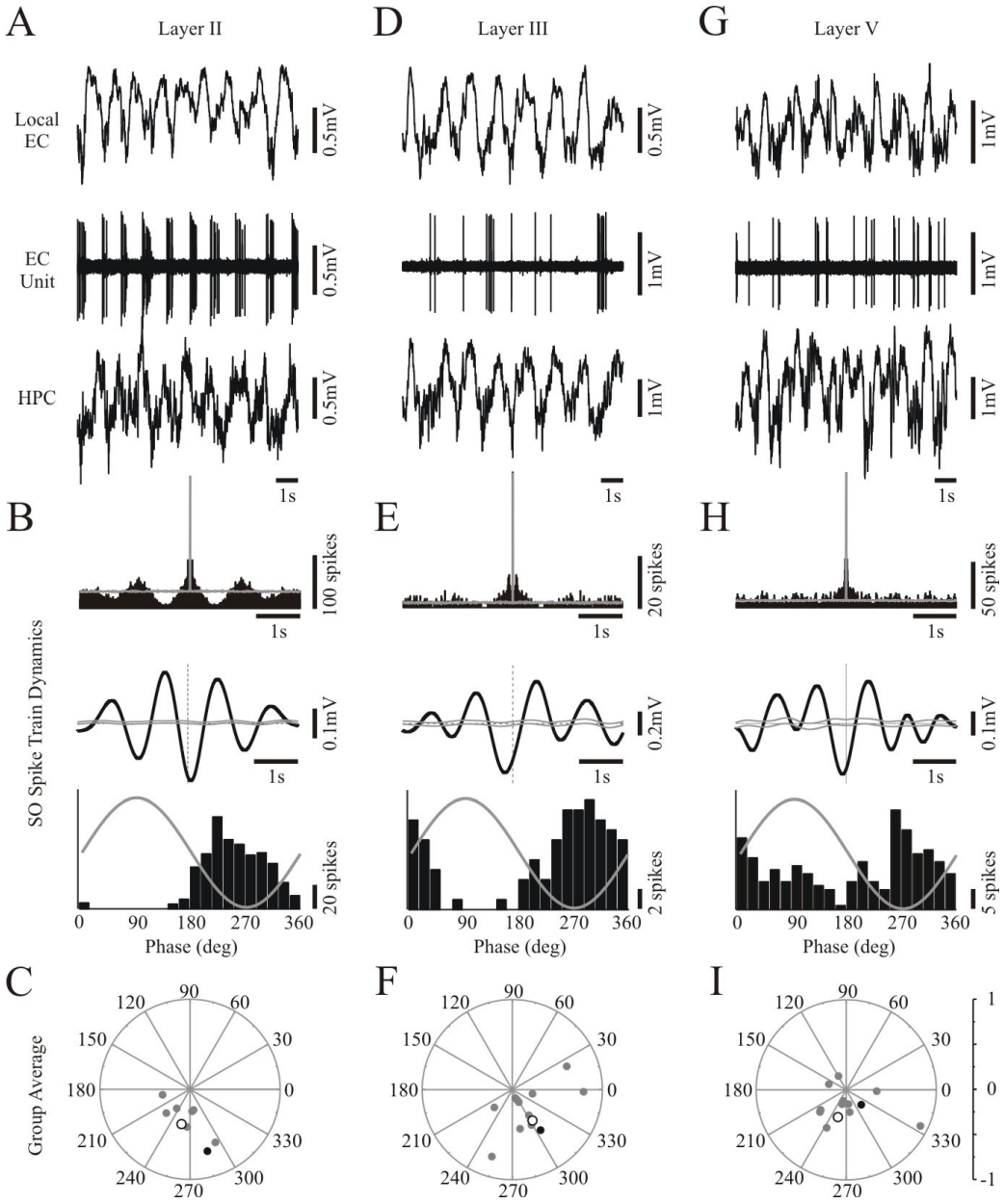

Figure 3-08 Caption:

(**A**) A sample of spontaneous field activity recorded in the supEC (*top panel*) and HPC (*bottom panel*) with simultaneously recorded layer II single unit activity (*middle panel*). This unit generated rhythmic action potentials (**B**, *top panel*) that occurred 70ms prior to the negative peak of the hippocampal SO (**B**, *middle* and *bottom panels*). Group data for all layer II neurons that generated significantly rhythmic (Rayleigh, z: $p < 0.05$) action potentials during the SO is shown in **C**: the data from this layer II unit is shown in *black*, data from other layer II units are shown in *grey*, and the group average is shown in *white*. (**D**) A sample of spontaneous field activity recorded in the supEC (*top panel*) and HPC (*bottom panel*) with simultaneously recorded layer III single unit activity (*middle panel*). (**E**) This layer III unit generated rhythmic action potentials during the SO (**E**, *top panel*) that occurred 179.5ms after the negative peak of the hippocampal SO (**E**, *middle* and *bottom panels*). Group data for all layer III neurons that generated significantly rhythmic (Rayleigh, z: $p < 0.05$) action potentials during the SO is shown in **F**: the data from this layer III unit is shown in *black*, data from other layer III units are shown in *grey*, and the group average is shown in *white*. The deep entorhinal unit shown in **G** (*middle panel*) along with samples of spontaneous SO activity in the deep EC (*top panel*) and HPC (*bottom panel*) generated rhythmic action potentials during the SO (**H**, *top panel*) that occurred 82ms after the negative peak of the hippocampal field (**H**, *middle* and *bottom panels*). Group data for layer V neurons that generated rhythmic action potentials (Rayleigh, z: $p < 0.05$) during the SO is shown in **I**: the data from this particular

deep unit is shown in *black*, data from other deep units are shown in *grey*, and the group average is shown in *white*. Abbreviations: deep entorhinal cortex (deep EC), entorhinal cortex (EC), entorhinal layer II (ECII), entorhinal layer III (ECIII), hippocampus (HPC), slow oscillation (SO), superficial entorhinal cortex (supEC)

Chapter 3 References

Alonso A, Garcia-Austt E (1987a) Neuronal sources of theta rhythm in the entorhinal cortex of the rat. II. Phase relations between unit discharges and theta field potentials. Exp Brain Res 67:502-509.

Alonso A, Garcia-Austt E (1987b) Neuronal sources of theta rhythm in the entorhinal cortex of the rat. I. Laminar distribution of theta field potentials. Exp Brain Res 67:493-501.

Amaral DG, Witter MP (1995) Hippocampal Formation. In: The Rat Nervous System, Second Edition (Paxinos G, ed), pp 443-493. USA: Academic Press.

Backhaus J, Hoeckesfeld R, Born J, Hohagen F, Junghanns K (2008) Immediate as well as delayed post learning sleep but not wakefulness enhances declarative memory consolidation in children. Neurobiol Learn Mem 89:76-80.

Backhaus J, Junghanns K, Born J, Hohaus K, Faasch F, Hohagen F (2006) Impaired declarative memory consolidation during sleep in patients with primary insomnia: Influence of sleep architecture and nocturnal cortisol release. Biol Psychiatry 60:1324-1330.

Barrionuevo G, Brown TH (1983) Associative long-term potentiation in hippocampal slices. Proc Natl Acad Sci U S A 80:7347-7351.

Beckstead RM (1979) An autoradiographic examination of corticocortical and subcortical projections of the mediodorsal-projection (prefrontal) cortex in the rat. J Comp Neurol 184:43-62.

Bertram EH, Zhang DX (1999) Thalamic excitation of hippocampal CA1 neurons: a comparison with the effects of CA3 stimulation. Neuroscience 92:15-26.

Bramham CR, Srebro B (1987) Induction of long-term depression and potentiation by low- and high-frequency stimulation in the dentate area of the anesthetized rat: magnitude, time course and EEG. Brain Res 405:100-107.

Buzsáki G (1989) Two-stage model of memory trace formation: A role for "noisy" brain states. Neurosci 31:551-570.

Buzsáki G (1996) The hippocampo-neocortical dialogue. Cerebral Cortex 6:81-92.

Buzsáki G (1998) Memory consolidation during sleep: a neurophysiological perspective. J Sleep Res 7 Suppl 1:17-23.

Chrobak JJ, Buzsáki G (1994) Selective activation of deep layer (V-VI) retrohippocampal cortical neurons during hippocampal sharp waves in the behaving rat. J Neurosci 14:6160-6170.

Clement EA, Richard A, Thwaites M, Ailon J, Peters S, Dickson CT (2008) Cyclic and sleep-like spontaneous alternations of brain state under urethane anaesthesia. PLoS ONE 3:e2004.

Dickson CT (1994) The Extrinsic Modulation of Entorhinal Cortex Theta: Field and Unit Activity Studies. In: Behavioral Neuroscience. Calgary: University of Calgary.

Dickson CT, Alonso A (1995) The entorhinal cortex contains two intrinsic pacemakers of epileptiform activity: An in vitro study. Epilepsia 36, suppl 4:87.

Dolleman-Van der Weel MJ, Lopes da Silva FH, Witter MP (1997) Nucleus reuniens thalami modulates activity in hippocampal field CA1 through excitatory and inhibitory mechanisms. J Neurosci 17:5640-5650.

Dolorfo CL, Amaral DG (1998) Entorhinal cortex of the rat: organization of intrinsic connections. J Comp Neurol 398:49-82.

Eichenbaum H (2000) A cortical-hippocampal system for declarative memory. Nat Rev Neurosci 1:41-50.

Eschenko O, Ramadan W, Molle M, Born J, Sara SJ (2008) Sustained increase in hippocampal sharp-wave ripple activity during slow-wave sleep after learning. Learn Mem 15:222-228.

Ferino F, Thierry AM, Glowinski J (1987) Anatomical and electrophysiological evidence for a direct projection from Ammon's horn to the medial prefrontal cortex in the rat. Exp Brain Res 65:421-426.

Frank LM, Brown EN, Wilson MA (2001) A comparison of the firing properties of putative excitatory and inhibitory neurons from CA1 and the entorhinal cortex. J Neurophysiol 86:2029-2040.

Freeman JA, Nicholson C (1975) Experimental optimization of current source-density technique for anuran cerebellum. J Neurophysiol 38:369-382.

Hahn TT, Sakmann B, Mehta MR (2006) Phase-locking of hippocampal interneurons' membrane potential to neocortical up-down states. Nat Neurosci 9:1359-1361.

Hahn TT, Sakmann B, Mehta MR (2007) Differential responses of hippocampal subfields to cortical up-down states. Proc Natl Acad Sci U S A 104:5169-5174.

Hasselmo ME (1999) Neuromodulation: acetylcholine and memory consolidation. Trends Cogn Sci 3:351-359.

Hirase H, Leinekugel X, Czurko A, Csicsvari J, Buzsaki G (2001) Firing rates of hippocampal neurons are preserved during subsequent sleep episodes and modified by novel awake experience. Proc Natl Acad Sci U S A 98:9386-9390.

Huber R, Ghilardi MF, Massimini M, Tononi G (2004) Local sleep and learning. Nature 430:78-81.

Hurley KM, Herbert H, Moga MM, Saper CB (1991) Efferent projections of the infralimbic cortex of the rat. J Comp Neurol 308:249-276.

Insausti R, Herrero MT, Witter MP (1997) Entorhinal cortex of the rat: cytoarchitectonic subdivisions and the origin and distribution of cortical efferents. Hippocampus 7:146-183.

Isomura Y, Sirota A, Ozen S, Montgomery S, Mizuseki K, Henze DA, Buzsaki G (2006) Integration and segregation of activity in entorhinal-hippocampal subregions by neocortical slow oscillations. Neuron 52:871-882.

Jay TM, Witter MP (1991) Distribution of hippocampal CA1 and subicular efferents in the prefrontal cortex of the rat studied by means of anterograde transport of Phaseolus vulgaris-leucoagglutinin. J Comp Neurol 313:574-586.

Jay TM, Glowinski J, Thierry AM (1989) Selectivity of the hippocampal projection to the prelimbic area of the prefrontal cortex in the rat. Brain Res 505:337-340.

Ji D, Wilson MA (2007) Coordinated memory replay in the visual cortex and hippocampus during sleep. Nat Neurosci 10:100-107.

Jones RSG (1993) Entorhinal-hippocampal connections: A speculative view of their function. Trends Neurosci 16:58-64.

Ketchum KL, Haberly LB (1993) Synaptic events that generate fast oscillations in piriform cortex. J Neurosci 13:3980-3985.

King C, Henze DA, Leinekugel X, Buzsáki G (1999) Hebbian modification of a hippocampal population pattern in the rat. J Physiol 521 Pt 1:159-167.

Kloosterman F, Witter MP, Van Haeften T (2003) Topographical and laminar organization of subicular projections to the parahippocampal region of the rat. J Comp Neurol 455:156-171.

Kohler C (1985) Intrinsic projections of the retrohippocampal region in the rat brain. I. The subicular complex. J Comp Neurol 236:504-522.

Levy WB, Steward O (1979) Synapses as associative memory elements in the hippocampal formation. Brain Res 175:233-245.

Lynch GS, Dunwiddie T, Gribkoff V (1977) Heterosynaptic depression: a postsynaptic correlate of long-term potentiation. Nature 266:737-739.

Marshall L, Molle M, Hallschmid M, Born J (2004) Transcranial direct current stimulation during sleep improves declarative memory. J Neurosci 24:9985-9992.

Marshall L, Helgadottir H, Molle M, Born J (2006) Boosting slow oscillations during sleep potentiates memory. Nature 444:610-613.

Massimini M, Huber R, Ferrarelli F, Hill S, Tononi G (2004) The sleep slow oscillation as a traveling wave. J Neurosci 24:6862-6870.

McNaughton BL, Douglas RM, Goddard GV (1978) Synaptic enhancement in fascia dentata: cooperativity among coactive afferents. Brain Res 157:277-293.

Mednick S, Nakayama K, Stickgold R (2003) Sleep-dependent learning: a nap is as good as a night. Nat Neurosci 6:697-698.

Mitchell SJ, Ranck JBJ (1980) Generation of theta rhythm in medial entorhinal cortex of freely moving rats. Brain Res 189:49-66.

Molle M, Marshall L, Gais S, Born J (2004) Learning increases human electroencephalographic coherence during subsequent slow sleep oscillations. Proc Natl Acad Sci U S A 101:13963-13968.

Molle M, Yeshenko O, Marshall L, Sara SJ, Born J (2006) Hippocampal sharp wave-ripples linked to slow oscillations in rat slow-wave sleep. J Neurophysiol 96:62-70.

Moser MB, Moser EI (1998) Functional differentiation in the hippocampus. Hippocampus 8:608-619.

Mukovski M, Chauvette S, Timofeev I, Volgushev M (2007) Detection of active and silent states in neocortical neurons from the field potential signal during slow-wave sleep. Cereb Cortex 17:400-414.

Murphy M, Riedner BA, Huber R, Massimini M, Ferrarelli F, Tononi G (2009) Source modeling sleep slow waves. Proc Natl Acad Sci U S A 106:1608-1613.

Nicholson C, Freeman JA (1975) Theory of current source-density analysis and determination of conductivity tensor for anuran cerebellum. J Neurophysiol 38:356-368.

Peigneux P, Laureys S, Delbeuck X, Maquet P (2001) Sleeping brain, learning brain. The role of sleep for memory systems. Neuroreport 12:A111-124.

Peigneux P, Laureys S, Fuchs S, Collette F, Perrin F, Reggers J, Phillips C, Degueldre C, Del Fiore G, Aerts J, Luxen A, Maquet P (2004) Are spatial memories strengthened in the human hippocampus during slow wave sleep? Neuron 44:535-545.

Proulx E, Timofeev I (2007) Medial prefrontal cortex intracellular and local field potential recordings provide evidence for a hippocampo-prefronto-thalamic relay: An in vivo study in the cat. In: Society for Neuroscience Abstracts, p Program # 792.799: Society for Neuroscience.

Rasch B, Buchel C, Gais S, Born J (2007) Odor cues during slow-wave sleep prompt declarative memory consolidation. Science 315:1426-1429.

Rauchs G, Desgranges B, Foret J, Eustache F (2005) The relationships between memory systems and sleep stages. J Sleep Res 14:123-140.

Ribeiro S, Nicolelis MA (2004) Reverberation, storage, and postsynaptic propagation of memories during sleep. Learn Mem 11:686-696.

Rodriguez R, Haberly LB (1989) Analysis of synaptic events in the opossum piriform cortex with improved current source-density techniques. J Neurophysiol 61:702-718.

Samonds JM, Bonds AB (2005) Gamma oscillation maintains stimulus structure-dependent synchronization in cat visual cortex. J Neurophysiol 93:223-236.

Schall KP, Kerber J, Dickson CT (2008) Rhythmic constraints on hippocampal processing: state and phase-related fluctuations of synaptic excitability during theta and the slow oscillation. J Neurophysiol 99:888-899.

Scoville WB, Milner B (1957) Loss of recent memory after bilateral hippocampal lesions. J Neurol Neurosurg Psychiat 20:11-21.

Sesack SR, Deutch AY, Roth RH, Bunney BS (1989) Topographical organization of the efferent projections of the medial prefrontal cortex in the rat: an anterograde tract-tracing study with Phaseolus vulgaris leucoagglutinin. J Comp Neurol 290:213-242.

Siapas AG, Wilson MA (1998) Coordinated interactions between hippocampal ripples and cortical spindles during slow-wave sleep. Neuron 21:1123-1128.

Siapas AG, Lubenov EV, Wilson MA (2005) Prefrontal phase locking to hippocampal theta oscillations. Neuron 46:141-151.

Sirota A, Csicsvari J, Buhl D, Buzsáki G (2003) Communication between neocortex and hippocampus during sleep in rodents. Proc Natl Acad Sci U S A 100:2065-2069.

Squire LR, Zola-Morgan S (1991) The medial temporal lobe memory system. Science 253:1380-1386.

Stanton PK, Sejnowski TJ (1989) Associative long-term depression in the hippocampus induced by hebbian covariance. Nature 339:215-218.

Steriade M (1999) Coherent oscillations and short-term plasticity in corticothalamic networks. Trends Neurosci 22:337-345.

Steward O (1976) Topographic organization of the projections from the entorhinal area to the hippocampal formation of the rat. J Comp Neurol 167:285-314.

Steward O, Scoville SA (1976) The cells of origin of entorhinal afferents to the hippocampus and fascia dentata of the rat. J Comp Neurol 169:347-370.

Swanson LW (1981) A direct projection from Ammon's horn to prefrontal cortex in the rat. Brain Res 217:150-154.

Takashima A, Petersson KM, Rutters F, Tendolkar I, Jensen O, Zwarts MJ, McNaughton BL, Fernandez G (2006) Declarative memory consolidation in humans: a prospective functional magnetic resonance imaging study. Proc Natl Acad Sci U S A 103:756-761.

Talamini LM, Nieuwenhuis IL, Takashima A, Jensen O (2008) Sleep directly following learning benefits consolidation of spatial associative memory. Learn Mem 15:233-237.

Tononi G, Cirelli C (2001) Some considerations on sleep and neural plasticity. Arch Ital Biol 139:221-241.

Tse D, Langston RF, Kakeyama M, Bethus I, Spooner PA, Wood ER, Witter MP, Morris RG (2007) Schemas and memory consolidation. Science 316:76-82.

Tsukamoto-Yasui M, Sasaki T, Matsumoto W, Hasegawa A, Toyoda T, Usami A, Kubota Y, Ochiai T, Hori T, Matsuki N, Ikegaya Y (2007) Active hippocampal networks undergo spontaneous synaptic modification. PLoS ONE 2:e1250.

van Groen T, Wyss JM (1990) Extrinsic projections from area CA1 of the rat hippocampus: olfactory, cortical, subcortical, and bilateral hippocampal formation projections. J Comp Neurol 302:515-528.

Vertes RP (2002) Analysis of projections from the medial prefrontal cortex to the thalamus in the rat, with emphasis on nucleus reuniens. J Comp Neurol 442:163-187.

Walker MP, Stickgold R (2004) Sleep-dependent learning and memory consolidation. Neuron 44:121-133.

Wilhelm I, Diekelmann S, Born J (2008) Sleep in children improves memory performance on declarative but not procedural tasks. Learn Mem 15:373-377.

Witter MP (1993) Organization of the entorhinal-hippocampal system: a review of current anatomical data. Hippocampus 3 Spec No:33-44.

Wolansky T, Clement EA, Peters SR, Palczak MA, Dickson CT (2006) Hippocampal slow oscillation: a novel EEG state and its coordination with ongoing neocortical activity. J Neurosci 26:6213-6229.

Wouterlood FG, Saldana E, Witter MP (1990) Projection from the nucleus reuniens thalami to the hippocampal region: light and electron microscopic tracing study in the rat with the anterograde tracer Phaseolus vulgaris-leucoagglutinin. J Comp Neurol 296:179-203.

Zar (1999) Biostatistical Analysis, 4th Ed. Prentice Hall Edition. Upper Saddle River, New Jersey, USA.

Chapter 4:

Low-Amplitude and Slow-Frequency Stimulation Entrains the Slow Oscillation in the Hippocampus

Trish Wolansky[1] and Clayton T. Dickson[1, 2, 3]

[1]Centre for Neuroscience, [2]Department of Psychology, and [3]Department of Physiology

University of Alberta, Edmonton, Canada

Submitting to:

Journal of Neuroscience

Introduction

Episodic memory is dependent on the bidirectional connections of the MTL memory system (Scoville and Milner, 1957; Squire and Zola-Morgan, 1991; Moser and Moser, 1998; Eichenbaum, 2000), at the centre of which is the HPC. Synchronised brain activity in this system during deep SWS is thought to play an important role in the processing of episodic mnemonic information (Buzsáki, 1989; Buzsáki, 1996; Steriade, 1999; Hirase et al., 2001; Mednick et al., 2003; Huber et al., 2004; Molle et al., 2004; Peigneux et al., 2004; Marshall et al., 2006; Takashima et al., 2006; Ji and Wilson, 2007; Rasch et al., 2007; Tse et al., 2007). Most studies of the HPC have focused on the production of sharp wave/ripple complexes which were thought to be the only oscillatory activity expressed during SWS (Buzsáki, 1986). We have recently shown that the SO (≤ 1Hz) is also a prominent feature of the electrographic activity of the HPC during both deep SWS and anaesthesia. We demonstrated that the SO is a distinct state in terms of its spectral components, cellular correlates (Wolansky et al., 2006), and with respect to its modulation of excitatory synaptic transmission in both the CA and DG subregions of the HPC (Schall et al., 2008). We also demonstrated that the hippocampal SO was dynamically coordinated with the SO in the nCTX suggesting that it may play a role in sleep-dependent neuronal plasticity in this extended MTL circuit (Wolansky et al., 2006).

The mechanism of SO coordination across the nCTX and HPC is of substantial interest for sleep-related mnemonic processing. The most prominent

SO-related inward (excitatory) synaptic currents in the HPC occur at the level of SLM (Isomura et al., 2006; Wolansky et al., 2006). This is where the temporoammonic pathway – the direct entorhinal input to CA1, terminates. The EC is the final synaptic convergence point for multimodal sensory information to gain access to the HPC (Steward, 1976; Steward and Scoville, 1976; Dolorfo and Amaral, 1998). Therefore, we and others hypothesised that the coordination of the SO across the HPC and nCTX was mediated by neocortical input via the EC (Hahn et al., 2006; Isomura et al., 2006; Wolansky et al., 2006; Hahn et al., 2007). It is also possible that SO coordination across the HPC and nCTX is mediated by another pathway: the mpfCTX to SLM of CA1 via the NReu (Swanson, 1981; Ferino et al., 1987; Jay et al., 1989; Wouterlood et al., 1990; Hurley et al., 1991; Jay and Witter, 1991; Vertes, 2002; Proulx and Timofeev, 2007).

Within the nCTX, the SO tends to originate in fCTX and propagate (presumably via cortico-cortical connections; Amzica and Steriade, 1995) as a traveling wave (Massimini et al., 2004; Murphy et al., 2009). In humans, the neocortical SO can be evoked and entrained by both transcranial electrical (Marshall et al., 2006) and magnetic (Massimini et al., 2004) stimulation of frontal regions. Recently, animal experiments have shown that weak and widespread electrical field stimulation (Ozen et al., 2007; Ozen et al., 2008) as well as more localised, direct electrical stimulation (Vyazovskiy et al., 2009) of fCTX appears to evoke and entrain the cortical SO during both anaesthesia and sleep.

The present study was designed to assess the effects of electrical stimulation on the hippocampal SO in the urethane-anaesthetised rat. We found that low-amplitude and slow-frequency stimulation delivered directly to the mpfCTX and NReu disrupted the hippocampal SO, but stimulation delivered across the fCTX did not. We also found that repeated low-amplitude and slow-frequency stimulation delivered to each of the fCTX, mpfCTX, and NReu entrained the hippocampal SO. Repeated stimulation delivered to the fCTX and mpfCTX enhanced the coordination between the nCTX and HPC, but repeated stimulation of the NReu did not. We suggest that entraining the hippocampal SO and enhancing its coordination are differentially mediated via a series of cortical pathways through both the EC and NReu.

Materials and Methods

Data were obtained from 9 male Sprague-Dawley rats weighing 189.5 to 264.6g (average ± SEM: 239.27 ± 8.58g). All methods conformed to the guidelines established by the Canadian Council on Animal Care, the Society for Neuroscience, and were approved by the Biosciences Animal Policy and Welfare Committee of the University of Alberta.

Anaesthesia and Surgery

Animals were initially anaesthetised with gaseous isoflurane (4 MAC) in an enclosed anaesthetic chamber. Following loss of righting reflexes, animals were maintained on isoflurane (2.0 to 2.5 MAC) via a nose cone and implanted with a jugular catheter. Isoflurane was discontinued and general anaesthesia was achieved using slow *i.v.* administration of urethane (0.8g/ml; final dosage 1.67 ± 0.007g/kg) via the jugular vein. Body temperature was maintained at 37°C using a servo driven system connected to a heating pad and rectal probe (FST) for the remainder of the surgical and recording procedures. Level of anaesthesia was assessed throughout the experiment by monitoring reflex withdrawal to a hindpaw pinch. If any visible withdrawal occurred, the animal was administered a supplemental dose (0.01ml) of urethane.

Using stereotaxic techniques, animals were implanted with monpolar electrodes constructed from Teflon-coated stainless steel wire (bare diameter 125µm: A-M Systems Inc.) in superficial fCTX (from bregma: **AP**: +0.3, **ML**: +1.0, **DV**: surface to -0.2mm) and in superficial posterior cortex (from bregma:

AP: **-**6.3, **ML**: +3.1, **DV**: surface to -0.2mm; *pCTX*). Following implantation, both single pole electrodes were fixed to the skull using jeweller's screws and dental acrylic. A 16-contact silicon multiprobe arranged in a linear array with a contact separation of 100µm (Neuronexus Technologies; Ann Arbor, MI) was inserted in the HPC (from bregma: **AP**: -3.3, **ML**: +2.0) such that the two most ventral channels were situated in the superficial blade of the DG (**DV**: -3.0 to **-** 3.9mm).

We conducted two series of experiments. In the first series, two monopolar electrodes constructed from thick Teflon insulated wire (200µm: A-M Systems Inc.) were positioned bilaterally across the surface of the fCTX (from bregma: **AP**: +3.7, **ML**: ±2.4, **DV**: surface). Stimulation was delivered across these two poles. In the second series of experiments, a bipolar stimulating electrode constructed from a twisted pair of thick Teflon insulated wires (200µm: A-M Systems Inc.) with tips vertically staggered by 0.2 to 0.5mm was implanted directly in the mpfCTX (from bregma: **AP**: +3.2, **ML**: +2.4, **DV**: -4.5 to -4.75) at a 25° angle below the horizontal and lowered into the mpfCTX obliquely. This approach allowed us to avoid damaging the superior sagittal sinus. Another bipolar stimulating electrode was implanted in the NReu (from bregma: **AP**: **-**1.6, **ML**: **-**3.2, **DV**: -7.55 to -7.8) at a 25° angle below the horizontal and lowered into the NReu obliquely. Visualising the electrical stimulation-evoked potentials in the HPC as this electrode was lowered aided in its placement (*see below*). All stimulation electrodes were fixed to the skull using jeweller's screws and dental acrylic after proper placement.

Following recording sessions, small lesions were made at the tips of active electrodes (recording and stimulating) by passing 1mA of DC current for 5s using an isolated constant current pulse generator (Model 2100, A-M Systems Inc.). This allowed us to specify their location during histological procedures (*see below*).

Stimulation Protocols

Evoked Potentials. Average profiles were generated by passing a biphasic pulse of 50 to 200µA of direct current for 0.5ms using an isolated constant current pulse generator (Model 2100, A-M Systems Inc.). Evoked potential averages were calculated from 16 independent stimulation sweeps (i.e., trials).

Stimulation trials. We delivered 0.5s duration biphasic pulses at 1/1.01Hz for 60s. Low intensity (10µA) stimulation across the fCTX (n = 5) generated a LFP that was essentially identical (aside from amplitude) to the spontaneous SO. We delivered 30µA (n = 4) directly to the mpfCTX and 10 to 30µA (n = 5) to the NReu. During the entraining stimulation protocol, we delivered and averaged 8 consecutive sweeps of stimulation.

Following NReu stimulation in our second series of experiments we electrolytically lesioned the NReu using 1mA of current for 5s. We then repeated the mpfCTX stimulation procedure to determine if its effect on the hippocampal SO was dependent on the integrity of the NReu.

Control trials. We recorded spontaneous LFPs that were similarly triggered using the same protocol as above but with the stimulation leads detached (i.e., without applying current).

Recording Procedures

Single electrode field recordings. The frontal and posterior neocortical single pole field potential recordings were amplified at a gain of 1000, filtered between 0.1 to 500Hz using a differential AC amplifier (Model 1700, A-M Systems Inc.), and were referenced to the stereotaxic apparatus.

Linear multiprobe recordings. Hippocampal signals from the probe were amplified at a final gain of 1000 and wide-band filtered between 0.7Hz to 10kHz via a 16-channel headstage (unity gain) and amplifier system (Plexon Inc.; Dallas, TX). All signals from the multiprobe were referenced to stereotaxic ground. The signal from the first (deepest) channel on the probe was audio amplified and sent to a speaker. The electrophysiological profile of theta field activity (Bland and Bland, 1986), SO field activity (Wolansky et al., 2006), as well as increases in multiunit activity, aided in the determination of the vertical position of the probe. Following recording sessions, the probe was moved slightly in two planes orthogonal to its long axis to make a visible track for histological purposes. The position of the probe track in every experiment was verified by comparing the histology to the laminar profile of the ongoing field potentials.

Data storage. All signals were digitised with a Digidata 1322A A-D board connected to a Pentium PC running the AxoScope acquisition program (Axon Instruments; Union City, CA). This system low pass filtered all field signals at 500Hz and sampled at a rate of 1000Hz.

Euthanasia and Histology

At the end of recording sessions, rats were perfused transcardially, initially with physiological saline, and then with 4% paraformaldehyde in saline. Brains were extracted and stored overnight in 30% sucrose in 4% paraformaldehyde. The tissue was frozen with compressed CO_2 and sliced at 48μm with a rotary microtome (Leica 1320 Microtome; Vienna, Austria). Slices were then mounted on gel-coated slides, allowed to dry for a minimum of 24 hours, subsequently stained using thionin, and cover-slipped. Microscopic inspection of stained slices was used to verify recording loci. Digital photomicrographs (Canon Powershot S45; Tokyo, Japan) were taken on a Leica DM LB2 (Buffalo, NY) microscope, imported using Canon Remote Capture 2.7 software (Tokyo, Japan) and processed with Corel PhotoPaint (Ottawa, ON, Canada).

Data Processing and Analysis

The stimulation field averages were computed from 8 consecutive sweeps of stimulation automatically in AxoScope (Axon Instruments). All analyses were conducted on both single sweeps and the average sweeps of stimulation (60s) using Matlab Version 5.3 (Mathworks; Natick, MA) and visualised using Origin Version 7.0 (Microcal Software Inc.; Northampton, MA). These analyses included: digital filtering, single and dual-channel spectral analyses, autocorrelation (AC), and CSD. Our digital filtering technique was previously confirmed to elicit zero phase distortion by both spectral and cross-correlation analyses (Wolansky et al., 2006).

Spectral analysis. Spectral analysis was computed on 60s LFP and/or CSD traces of either individual stimulation sweeps or sweep averages. Phase was computed across signal pair combinations on the neocortical LFPs and coherence was computed between both the neocortical LFPs and between neocortical LFPs and the hippocampal CSD traces. Spectra were estimated using Welch's averaged periodogram method, from a series of 6s long, sequential Hanning windowed samples from these data segments with 2s overlap. Spectral values were averaged across a peak frequency bandwidth (peak frequency ± 1/6Hz). ACs were computed on 60 second long data segments using a window size of 2.5s.

Current source density analysis. The underlying assumptions for CSD followed those of prior work (Freeman and Nicholson, 1975; Nicholson and Freeman, 1975; Rodriguez and Haberly, 1989; Ketchum and Haberly, 1993). Briefly, spontaneous multiprobe LFPs were 1.5Hz lowpass filtered for the SO and CSD was computed by estimating the second spatial derivative of these filtered traces. This estimate was calculated using a three-point difference (differentiation grid size of 300μm) on the field potential values across spatially adjacent traces:

$$CSD = [f(p_{i-1})-2f(p_i)+f(p_{i+1})]/d^2 \qquad (\textit{Equation 1})$$

Where $f(p_i)$ is the field signal from probe channel i (i = 2, 3, …, 13) and d is the distance between adjacent channels (0.1mm). For traces from each end of the probe (i = 1 and 14), the differentiation grid was based only on the immediately adjacent channel (i.e., i = 2 and 13). We confirmed that this latter procedure yielded similar, if not identical, CSD results as the 3-point differentiation method

by successively eliminating probe end channels, then re-computing and comparing results.

We have previously characterised the sink – source alternations that occur in the different hippocampal laminae during the SO and how they compare to the sink – source alternations that occur during theta (Wolansky et al., 2006). We used this schema to extract the data from the channels in SLM. If more than one channel was located within this layer of the HPC, we averaged the power, coherence, and AC values across those channels.

Statistics. All comparisons across conditions for the same datasets were made using one-tailed pair-wise *t*-tests (significance was evaluated at $p < 0.05$). We compared the power profiles of the hippocampal CSD under stimulation conditions to that under control conditions using linear regression (significance was evaluated at $p < 0.05$). AC function significance was assessed by comparison to the average AC under control conditions across all experiments. We compared the rhythmicity of the AC function in two ways. First, we assessed whether the AC values during stimulation fell outside the control condition average ± 1.96*SEM. Second, we calculated the spectral power of the AC functions, extracted the power values at the peak SO frequency in the same manner as described for raw traces (*see above*), and compared the values across control and stimulation conditions ($p < 0.05$).

Drugs and Chemicals

Atropine methyl nitrate, lidocaine, thionin, and urethane were all purchased from Sigma (St. Louis, MO). Isoflurane was purchased from Bimeda-

MTC (Animal Health Inc.; Cambridge, ON, Can) and paraformaldehyde from Fisher Scientific (Toronto, ON, Can).

Results

Propagation of the slow oscillation during urethane anaesthesia

As mentioned previously, the SO tends to originate in the fCTX and propagate as a traveling wave (Massimini et al., 2004; Murphy et al., 2009). To assess whether the SO propagates as a traveling wave under urethane anaesthesia, we calculated the phase of the SO between the two neocortical recording electrodes (fCTX and pCTX; *see Methods*). The coherence between the fCTX and pCTX was significant (0.65 ± 0.06) suggesting that the two signals had a relatively consistent phase relationship. The phase difference between the frontal and posterior neocortical recording sites was 16.04 ± 6.89deg (posterior lagging frontal) at the peak SO frequency (1.00 ± 0.096Hz) across all experiments. This corresponds to a time difference of 0.045 ± 0.019s at 1.00 ± 0.096Hz and suggests that similarly to sleep, the SO propagates across the nCTX in a frontal to posterior direction under urethane anaesthesia.

Low-amplitude and slow-frequency stimulation across the frontal cortex alters the spectral characteristics of the slow oscillation in the hippocampus.

In 2006, Marshall et al. showed that low-amplitude and slow-frequency stimulation across the human fCTX during early SWS selectively enhanced both the SO and performance on an episodic (i.e. hippocampal-dependent) memory task the day after learning. Their findings imply that some neocortical – hippocampal interaction was also enhanced and could be responsible for the

behavioural effect. Our first goal was to assess whether low-amplitude (10µA), slow-frequency (1Hz) stimulation of the fCTX influences the SO in the HPC.

Field potentials in the rodent nCTX and HPC during the spontaneous SO were characterised by a high amplitude ~1Hz rhythm (**Figure 4-01A**), consistent with our previous work (Wolansky et al., 2006; Wolansky and Dickson, 2009). During low-amplitude, slow-frequency stimulation of the fCTX, the field potentials in the nCTX and HPC appeared similar to those during spontaneous SO activity (**Figure 4-01B**) albeit higher in amplitude and more stereotyped. SO filtered (1.5Hz lowpass; *see Methods section*) traces from the fCTX, pCTX, and HPC at the level of SLM are plotted in *black* superimposed on the corresponding raw traces plotted in *grey*.

While the LFP is a reasonable representation of ongoing population activity in the HPC, it can be contaminated by volume conduction of potentials from closely opposed structures such as the overlying nCTX. To avoid this potential issue entirely, we used hippocampal CSD traces as our measure of ongoing hippocampal activity for all further analyses.

Low-amplitude, slow-frequency stimulation across the fCTX evoked a large rhythmic field potential in the fCTX (*top trace* in *top panel* of **Figure 4-02C**) that was similar to the spontaneous SO (*top trace* in *top panel* of **Figure 4-02B**). SO power in the pCTX was only slightly greater during fCTX stimulation (*bottom trace* in *top panel* of **Figure 4-02C**) as compared to control (*bottom trace* in *top panel* of **Figure 4-02B**). The raw CSD profiles of the SO (i.e., 1Hz activity) in the HPC (*color contour plots* in *bottom panels*) during both control (**Figure 4-**

02B) and stimulation (**Figure 4-02C**) conditions are shown aligned to the hippocampal laminae (**Figure 4-02A**). SO-related current flow in the HPC was greater during stimulation overall. This is reflected in the power profiles of 1Hz activity in the hippocampal CSD. The SO CSD power profile during fCTX stimulation (*black line* in *bottom panel* of **Figure 4-02C**) had the same general shape as the SO power profile during the spontaneous SO (*black line* in *bottom panel* of **Figure 4-02B**). We applied a linear regression to this data (i.e., control vs stimulation power values at each depth); this relationship was significant ($p < 0.05$) in 4/5 experiments, including the one shown in **Figure 4-02**. One of the obvious differences between the power profiles was the significant increase in SO-related activity in the dentate hilus.

We assessed the rhythmicity of SO activity by calculating ACs of both the neocortical LFPs and hippocampal CSD at the level of SLM during control and stimulation conditions (**Figure 4-02D**). ACs of spontaneous activity in this experiment are plotted as *solid black lines* and those during stimulation are plotted as *solid red lines*. The *dashed black* (control) and *dashed red* (stimulation) traces represent the average AC across experiments. The *grey regions* represent the average ± 1.96*standard error. The rhythmicity of the SO in both fCTX (*top panel*) and pCTX (*middle panel*) LFPs increased significantly during fCTX stimulation. The rhythmicity of the SO in the SLM CSD (*bottom panel*) also increased during stimulation, but this increase was not significant. These results are consistent with the average ACs during single sweeps of fCTX stimulation across all experiments (*dashed traces*). We also calculated the power spectrum of

the AC functions and extracted the power at the peak SO frequency (*see Methods*) during control (fCTX LFP: 0.97 ± 0.03Hz; pCTX LFP: 0.9 ± 0.07Hz; SLM CSD: 0.93 ± 0.08Hz) and stimulation (fCTX LFP: 1.0 ± 0.0Hz; pCTX LFP: 1.0 ± 0.0Hz; SLM CSD: 0.90 ± 0.04Hz) conditions. These values are plotted in **Figure 4-02E**. SO power in both the fCTX LFP (462.07 ± 1.68) and pCTX LFP (185.62 ± 59.38) ACs was significantly ($p < 0.05$) greater during stimulation as compared to control (fCTX LFP AC: 23.46 ± 4.13; pCTX LFP AC: 15.11 ± 3.39). SO power in the SLM CSD AC appeared to increase during stimulation, but this increase was not significant (control: 19.72 ± 3.51; stimulation: 52.62 ± 18.88).

We calculated the ratio between power and coherence values during stimulation with respect to the values during control (i.e., values expressed are a proportion of control). The average ratiometric power and coherence values during single 60s sweeps of low-amplitude, slow-frequency fCTX stimulation across all experiments are plotted in *red* in **Figure 4-02F**. The values from the experiment shown are plotted as *black symbols* and those from all other experiments are plotted as *unfilled symbols*. SO power (*left panel* of **Figure 4-02F**) increased significantly (*t*-test: $p < 0.05$) in both the fCTX (1564.73 ± 953.47) and pCTX (4.34 ± 1.58) LFPs during fCTX stimulation, however, SO power in the SLM CSD was not significantly different from control (1.51 ± 0.53).

SO coherence (*right panel* of **Figure 4-02F**) between the fCTX and pCTX LFPs (1.86 ± 0.42) almost doubled during stimulation. We used the pCTX LFP for neocortical – hippocampal coherence comparisons because the fCTX recording electrode was positioned in close proximity to the stimulation

electrodes (*see Methods*). The average ratiometric SO coherence between the pCTX LFP and SLM CSD was 1.27 ± 0.64. This value was not significantly different from control (i.e., 1.0).

Repeated stimulation across the frontal cortex entrains the slow oscillation in the hippocampus

The increase in rhythmicity of the neocortical LFPs and the hippocampal CSD at the level of SLM suggested that stimulation of fCTX was entraining the SO at distant hippocampal sites. First, we aligned and averaged 8 consecutive trials of stimulation. We were then able to compare the averaged neocortical LFPs and hippocampal CSD (computed on the averaged hippocampal LFP profile) across control and stimulation conditions. If the HPC was being entrained during repeated fCTX stimulation, we expected that the average SO power would increase during stimulation.

Repeated low-amplitude, slow-frequency stimulation across the fCTX evoked an average SO field potential in the fCTX and pCTX (*top panel* of **Figure 4-03C**) that was larger and more rhythmic than the control average (*top panel* of **Figure 4-03B**). The average CSD profiles of 1Hz activity in the HPC (*color contour plots* in *bottom panels* of **Figure 4-03 B** and **C**) during both control and stimulation conditions are shown aligned to the hippocampal laminae (**Figure 4-03A**). SO-related current flow in the HPC was greater during stimulation overall, especially in the dentate hilus. This is reflected in the average hippocampal CSD SO power profile during repeated fCTX stimulation (*black line* in *bottom panel* of

Figure 4-03C) as compared to that during control conditions (*black line* in *bottom panel* of **Figure 4-03**). Linear regression between control and stimulation averages revealed a significant correlation ($p < 0.05$) in 3/5 experiments, including the one depicted in **Figure 4-03**.

ACs of the averaged neocortical LFPs and sink – source alternations at the level of SLM during both control (*solid black lines*) and stimulation (*solid red lines*) conditions are shown in **Figure 4-03D**. The *dashed black* (control) and *dashed red* (stimulation) traces represent the average AC across experiments. The *grey regions* represent the average ± 1.96*standard error. The rhythmicity of the SO in the fCTX LFP (*top panel*), pCTX LFP (*middle panel*), and SLM CSD (*bottom panel*) increased markedly during repeated fCTX stimulation. These results are consistent with the average ACs during repeated sweeps of fCTX stimulation across all experiments (*dashed traces*). SO power at the peak SO frequencies in the fCTX LFP (0.97 ± 0.03Hz), pCTX LFP (0.9 ± 0.07Hz), and SLM CSD (0.93 ± 0.08Hz) ACs was significantly ($p < 0.05$) greater during stimulation (fCTX LFP: 407.68 ± 0.07; pCTX LFP: 1324.69 ± 27.82; SLM CSD: 213.49 ± 27.68) as compared to control (fCTX LFP: 108.87 ± 10.20; pCTX LFP: 126.19 ± 17.64; SLM CSD: 163.92 ± 18.30). These values are plotted in **Figure 4-03E**.

The average ratiometric power values from repeated 60s sweeps of low-amplitude, slow-frequency fCTX stimulation averaged across all experiments are plotted in *red* in **Figure 4-03F**. The values from the experiment shown are plotted as *black symbols* and those from all other experiments are plotted as *unfilled*

symbols. SO power was significantly (*t*-test: $p < 0.05$) greater than control at all sites (fCTX LFP: 20242.55 ± 10177.04; pCTX LFP: 31.35 ± 7.34; HPC CSD: 19.21 ± 14.90; SLM CSD: 2.43 ± 0.33). These data suggest that the hippocampal SO was entrained during repeated fCTX stimulation and that SO coordination across the nCTX and HPC was simultaneously enhanced.

Low-amplitude and slow-frequency stimulation of the medial prefrontal cortex alters the spectral characteristics of the slow oscillation in the hippocampus

Frontal field stimulation was highly effective at entraining and coordinating the hippocampal SO. As previously stated, there are two pathways by which neocortical – hippocampal SO coordination is likely to occur: 1) via intracortical connections that eventually converge in the HPC through the EC and 2) via the mpfCTX to the HPC through the NReu. It has previously been shown that more direct and localised stimulation of the mpfCTX induced individual slow waves in the nCTX (Vyazovskiy et al., 2009). Our next goal was to assess whether the effect that we observed during fCTX stimulation could be replicated by direct stimulation of the mpfCTX.

We first delivered repeated low-amplitude and slow-frequency stimulation directly to the mpfCTX. Similarly to our observations during fCTX stimulation, it evoked a large rhythmic field potential in both the fCTX (*top trace* in *top panel* of **Figure 4-04C**) and pCTX (*bottom trace* in *top panel* of **Figure 4-04C**) that appeared similar to the spontaneous SO (*top panel* of **Figure 4-04B**). The CSD profiles (*color contour plots* in *bottom panels*) during both stimulation (**Figure 4-**

04C) and control (**Figure 4-04B**) conditions aligned to the hippocampal laminae (**Figure 4-04A**) show that in this experiment, hippocampal SO-related current flow decreased during mpfCTX stimulation. Again similarly to fCTX stimulation, the SO CSD power profile during mpfCTX stimulation (*black line* in *bottom panel* of **Figure 4-04C**) had the same general shape as the SO power profile during the spontaneous SO (*black line* in *bottom panel* of **Figure 4-04B**). Linear regression revealed a significant correlation ($p < 0.05$) in 4/4 experiments.

As shown in the ACs in **Figure 4-04D**, the neocortical SO LFPs both appeared more rhythmic during single sweeps of mpfCTX stimulation (*solid red plots* in *top* and *middle panels*). This comparison was only significant ($p < 0.05$) in the fCTX. The rhythmicity of the hippocampal SLM SO CSD (*bottom panel*) during stimulation (*solid red plot*) was similar to control (*solid black plot*). We did observe slight increases in SO rhythmicity at the level of SLM during single sweeps of mpfCTX stimulation in some experiments. Across all experiments however, these increases were not significant (*dashed plots*). The *grey region* represents the average AC across experiments under control conditions ± 1.96*standard error. These results are reflected in the power at the peak SO frequencies (fCTX LFP: control: 0.92 ± 0.05Hz; stim: 1.0 ± 0.0Hz; pCTX LFP: control: 0.92 ± 0.05Hz; stim: 1.0 ± 0.0Hz; SLM CSD: control: 0.75 ± 0.14; stim: 0.96 ± 0.04) in the ACs of the fCTX LFP (440.44 ± 8.14), pCTX LFP (177.16 ± 90.99), and SLM CSD (61.93 ± 31.29) during stimulation as compared to control (fCTX LFP: 31.86 ± 6.50; pCTX LFP: 34.17 ± 10.91; SLM CSD: 44.29 ± 15.46) (**Figure 4-04E**).

The average ratiometric power and coherence values during single 60s sweeps of low-amplitude, slow-frequency mpfCTX stimulation across all experiments are plotted in *red* in **Figure 4-04F**. The values from the experiment shown are plotted as *black symbols* and those from all other experiments are plotted as *unfilled symbols*. SO power (*left panel*) in the fCTX LFP (48.82 ± 14.69) and pCTX LFP (11.73 ± 7.47) increased (*t*-test: $p < 0.05$), whereas SO power at the level of SLM (0.66 ± 0.27) decreased (*t*-test: $p < 0.05$) during stimulation. SO coherence (*right panel*) increased between the pCTX and fCTX (3.38 ± 2.25) but decreased at the level of SLM (0.64 ± 0.17).

Repeated stimulation of the medial prefrontal cortex entrains the slow oscillation in the hippocampus

Repeated low-amplitude, slow-frequency stimulation delivered to the mpfCTX evoked an average field potential in the fCTX and pCTX (*top panel* of **Figure 4-05C**) that was larger than the control average (*top panel* of **Figure 4-05B**). SO-related current flow in the HPC was also greater during repeated mpfCTX stimulation overall. This is reflected in the average hippocampal SO CSD power profile (*black lines* and *color contour plots* in *bottom panels* of **Figure 4-05 B** and **C**). Although the general shape of the power profiles were similar across experiments, only the experiment depicted in **Figure 4-05** showed a significant correlation between control and stimulation averages by linear regression ($p < 0.05$). Repeated stimulation also increased the rhythmicity of the activity we observed in the fCTX, pCTX, and SLM (*solid red* traces; **Figure 4-**

05D). These results are consistent with the average ACs during repeated sweeps of mpfCTX stimulation across all experiments (*dashed traces*). Power at the peak SO frequencies (fCTX LFP: control: 0.9 ± 0.06Hz; stim: 1.0 ± 0.0Hz; pCTX LFP: control: 0.7 ± 0.13Hz; stim: 1.0 ± 0.0Hz; SLM CSD: control: 0.8 ± 0.08; stim: 1.0 ± 0.0) in the ACs of each of the fCTX LFP (405.42 ± 0.97), pCTX LFP (366.15 ± 11.20), and SLM CSD (292.82 ± 45.35) during stimulation was significantly ($p < 0.05$) greater than control (fCTX LFP: 133.17 ± 14.65; pCTX LFP: 157.94 ± 18.69; SLM CSD: 152.46 ± 20.56) (**Figure 4-05E**).

The average ratiometric power values from repeated 60s sweeps of low-amplitude, slow-frequency mpfCTX stimulation averaged across all experiments are plotted in *red* in **Figure 4-05F**. The values from the experiment shown are plotted as *black symbols* and those from all other experiments are plotted as *unfilled symbols*. Similarly to our observations during repeated fCTX stimulation, SO power (fCTX: 663.37 ± 170.80; pCTX: 151.77 ± 107.67; HPC: 18.72 ± 6.24; SLM: 2.00 ± 0.31) was significantly (*t*-test: $p < 0.05$) greater than control at all sites. These data suggest that repeated mpfCTX stimulation also entrained and enhanced the coordination of the hippocampal SO.

Low-amplitude and slow-frequency stimulation of the nucleus reuniens thalami alters the spectral characteristics of the slow oscillation in the hippocampus

Both repeated fCTX and mpfCTX stimulation entrained the hippocampal SO and enhanced its coordination with the nCTX. To assess whether either of these effects could be mimicked by stimulation of the NReu – hippocampal

pathway, we stimulated the NReu directly. SO power and coherence were not significantly different across the varying intensities of stimulation (*see Methods*; *not shown*). Low-amplitude, slow-frequency stimulation delivered to the NReu evoked field potentials in the fCTX and pCTX (*top panel* of **Figure 4-06C**) that appeared very similar to spontaneous SO activity (*top panel* of **Figure 4-06B**) in shape and amplitude. SO power in the HPC was lower during stimulation in this experiment (*black lines* and *color contour plots* in *bottom panels* of **Figure 4-06 B** and **C**), but was higher on average across experiments (*not shown*). SO power at the level of SLM was consistently lower during stimulation across experiments (*see below*; **Figure 4-06F**). Three of 4 experiments, including the one depicted in **Figure 4-06**, had a significant ($p < 0.05$) linear regression.

We assessed the rhythmicity of the averaged evoked SO activity by calculating ACs of both the neocortical LFPs and the SLM CSD during control (*black*) and stimulation (*red*) conditions (**Figure 4-06D**). *Grey regions* represent the average AC across experiments under control conditions ± 1.96*standard error. The rhythmicity of the SO in the fCTX (*top panel*) and pCTX (*middle panel*) increased during NReu stimulation (*solid red traces*) similarly to mpfCTX stimulation except that this increase was significant at both sites (*see below*; **Figure 4-06F**). In this experiment and across all others, the rhythmicity of the SO CSD at the level of SLM (*bottom panel* of **Figure 4-06E**) during NReu stimulation (*dashed red trace*) was not significantly different from control (*dashed black trace*). Again, these results are reflected in the power at the peak SO frequencies (fCTX LFP: control: 0.92 ± 0.05Hz; stim: 1.0 ± 0.0Hz; pCTX

LFP: control: 0.92 ± 0.05Hz; stim: 0.96 ± 0.04Hz; SLM CSD: control: 0.75 ± 0.14; stim: 0.89 ± 0.04) in the ACs of the fCTX LFP (248.87 ± 62.98), pCTX LFP (178.30 ± 51.19), and SLM CSD (43.74 ± 10.86) during stimulation as compared to control (fCTX LFP: 31.86 ± 6.50; pCTX LFP: 34.17 ± 10.91; SLM CSD: 44.29 ± 15.46) (**Figure 4-06E**).

The average ratiometric power and coherence values during single 60s sweeps of low-amplitude, slow-frequency NReu stimulation across all experiments are plotted in **Figure 4-06F**. The pattern of ratiometric power (*left panel*) that we observed during single sweeps of NReu stimulation and mpfCTX stimulation was identical. SO power increased in the fCTX (8.46 ± 4.07) and pCTX (4.46 ± 1.99), but decreased at the level of SLM (0.57 ± 0.13). The pattern of SO coherence (*right panel*) that we observed was slightly different between the two stimulation conditions. During NReu stimulation, coherence between the fCTX and pCTX (1.04 ± 0.15) was similar to control and coherence between the pCTX and SLM (0.35 ± 0.18) decreased.

Repeated stimulation of the nucleus reuniens thalami entrains the slow oscillation in the hippocampus

Repeated low-amplitude, slow-frequency stimulation delivered to the NReu evoked an average field potential in the fCTX and pCTX (*top panel* of **Figure 4-07C**) that was only slightly larger than the control average (*top panel* of **Figure 4-07B**). SO power in the average hippocampal CSD was also greater during repeated NReu stimulation (*black lines* and *color contour plots* in *bottom*

panels of **Figure 4-07 B** and **C**). Linear regression analysis revealed that the correlation across depth between the control and stimulation averages was significant ($p < 0.05$) in 3/4 experiments, including the one depicted. As shown in **Figure 4-07D**, repeated NReu stimulation (*solid red traces*) appeared to increase the rhythmicity of the activity that we observed in the fCTX LFP (*top panel*), pCTX LFP (*middle panel*), and hippocampal CSD at the level of SLM (*bottom panel*). The increase in rhythmicity at the level of SLM was not significant. These results are consistent with the average ACs during repeated sweeps of NReu stimulation across all experiments (*dashed red traces*). **Figure 4-07E** shows the power at the peak SO frequencies (fCTX LFP: control: 0.90 ± 0.06Hz; stim: 1.0 ± 0.0Hz; pCTX LFP: control: 0.70 ± 0.13Hz; stim: 1.0 ± 0.0Hz; SLM CSD: control: 0.80 ± 0.08; stim: 0.95 ± 0.05) in the ACs of the fCTX LFP (380.10 ± 14.00), pCTX LFP (337.37 ± 45.11), and SLM CSD (240.67 ± 25.64) during stimulation as compared to control (fCTX LFP: 133.17 ± 14.65; pCTX LFP: 157.94 ± 18.69; SLM CSD: 152.46 ± 20.56).

The average ratiometric SO power during repeated NReu stimulation (*left panel* of **Figure 4-07F**) was significantly (*t*-test: $p < 0.05$) greater than control at all sites (fCTX LFP: 85.29 ± 45.16; pCTX LFP: 40.17 ± 18.89; SLM CSD: 1.64 ± 0.16). Therefore, our data show that the hippocampal SO is entrained during repeated stimulation of each of the fCTX, mpCTX, and NReu. They also show that neocortical stimulation enhances SO coordination across neocortical and hippocampal sites, but that NReu stimulation does not.

Lesioning the nucleus reuniens thalami abolishes the effect of medial prefrontal cortex stimulation on the slow oscillation in the hippocampus

Given that repeated stimulation of both the mpfCTX and NReu entrained the hippocampal SO but only mpfCTX stimulation enhanced its coordination with the nCTX, we wanted to directly test whether the effect of mpfCTX stimulation was mediated through engagement of the mpfCTX – NReu – HPC pathway. We electrolytically lesioned the NReu after we tested the effects of both mpfCTX and NReu stimulation. This allowed us to investigate whether the integrity of the NReu was central to the effects we observed during mpfCTX stimulation (**Figure 4-08**).

Stimulation of the mpfCTX evoked large rhythmic field potentials in the fCTX (*top trace*) and pCTX (*bottom trace*) LFPs both before (*mpfCTX Stim* 1; *top panel* of **Figure 4-08B**) and after (*mpfCTX Stim 2*; *top panel* of **Figure 4-08C**) NReu lesion. In fact, the field potentials in the nCTX were practically identical across the pre-lesion and post-lesion stimulation conditions. However, the same was not true in the hippocampal CSD. With the NReu intact, SO power was relatively low in the hippocampal CSD during mpfCTX stimulation (*black line* and *colour contour plot* in *bottom panel* of **Figure 4-08B**) as compared to control conditions (*dashed black line* in *bottom panel* of **Figure 4-08C**) consistent with the data presented previously (**Figure 4-04**). Following NReu lesion, the hippocampal SO CSD power profile (*solid black line* and *colour contour plot* in *bottom panel* of **Figure 4-08C**) was nearly identical to the profile during control conditions (*dashed black line* in *bottom panel* of **Figure 4-08C**). This effect was

observed despite the obvious discrepancy in neocortical LFPs across control and stimulation conditions shown previously (**Figure 4-04**). We applied a linear regression to the pre- and post-NReu lesion data; 3/4 experiments were significantly correlated ($p < 0.05$) including the one depicted in **Figure 4-08**. The effect of mpfCTX stimulation on the hippocampal CSD was essentially abolished suggesting that the NReu was responsible for it.

The ACs of SO activity in the fCTX (*top panel* of **Figure 4-08D**) and pCTX (*middle panel* of **Figure 4-08D**) LFPs were essentially identical both before (*solid black plot*) and after (*solid red plot*) NReu lesion; both were more rhythmic than ACs of activity during control conditions (*green dashed plots*). Prior to NReu lesion, single sweeps of mpfCTX stimulation also increased SO rhythmicity (*solid black plot*) in the SLM CSD in this experiment. This result was not typical. As shown in both **Figure 4-04D** and **E,** and in the *black dashed plot* in the *bottom panel* of **Figure 4-08D**, the rhythmicity of the SLM CSD did not increase during single sweeps of mpfCTX stimulation on average across all experiments. Following NReu lesion, the AC of SLM CSD activity (*solid red plot*) was more rhythmic than during control conditions (*green dashed plot*) in this experiment. Again, this result was an exception to the average ACs during single sweeps of mpfCTX stimulation following NReu lesion across all experiments (*dashed red plot*). These results are also consistent with the power at the peak SO frequencies (fCTX LFP: stim 1: 1.0 ± 0.0Hz; stim 2: 0.83 ± 0.0Hz; pCTX LFP: stim 1: 1.0 ± 0.0Hz; stim 2: 0.83 ± 0.0Hz; SLM CSD: stim 1: 0.96 ± 0.04Hz; stim 2: 0.83 ± 0.0Hz) in the ACs of the fCTX LFP (440.44 ± 8.14), pCTX LFP (177.16

± 90.99), and SLM CSD (61.93 ± 31.29) during mpfCTX stimulation prior to NReu lesion as compared to following NReu lesion (fCTX LFP: 395.37 ± 3.78; pCTX LFP: 237.41 ± 68.62; SLM CSD: 228.35 ± 70.78) (**Figure 4-08E**). Although the rhythmicity of the SLM CSD during mpfCTX stimulation prior to and following NReu lesion was similar to control on average (*bottom panel* of **Figure 4-08D**), the rhythmicity of the SLM CSD following NReu lesion was significantly ($p < 0.05$) greater than the rhythmicity prior to NReu lesion (*right panel* of **Figure 4-08E**).

Average ratiometric power and coherence values during single 60s sweeps of low-amplitude, slow-frequency stimulation delivered to the mpfCTX following NReu lesion across all experiments are plotted in *red* in **Figure 4-08F**. The values from this experiment are plotted as *black symbols* and those from all other experiments are plotted as *unfilled symbols*. SO power in the fCTX LFP (48.21 ± 13.22) increased (*t*-test: $p < 0.05$). SO power values in the pCTX LFP (10.72 ± 9.81) and the SLM CSD (1.47 ± 0.95) were not significantly different from control.

Lesioning the nucleus reuniens thalami has no effect on the entrainment of the hippocampal slow oscillation during repeated medial prefrontal cortex stimulation

SO activity was entrained across the nCTX and HPC during repeated mpfCTX (**Figure 4-05**) and repeated NReu (**Figure 4-07**) stimulation. To determine the role of the NReu in this entrainment, we delivered repeated 60s

sweeps of low-amplitude, slow-frequency stimulation to the mpfCTX in the same manner as described above both before and after NReu lesion.

Repeated stimulation of the mpfCTX resulted in large-amplitude rhythmic averaged field potentials in the fCTX and pCTX LFPs both before (*mpfCTX stim 1*; *top panel* of **Figure 4-09B**) and after (*mpfCTX stim 2*; *top panel* of **Figure 4-09C**) NReu lesion. Again, the average neocortical field potentials were nearly identical across the two conditions. With the NReu intact, SO power was greater than control (*not shown*) in the average hippocampal CSD (*black line* and *colour contour plot* in *bottom panel* of **Figure 4-09B**) consistent with the data presented previously (**Figure 4-05**). The same was generally true following NReu lesion (*black line* and *colour contour plot* in *bottom panel* of **Figure 4-09C**). Linear regression analysis showed that the correlation between the power profiles before and after NReu lesion was significant ($p < 0.05$) in all 4 experiments. We calculated the ratio between the SO power pre- and post-NReu lesion (**Figure 4-09F**); the ratio at each site was approximately equal to 1. This means that SO power in the fCTX LFP (732.76 ± 216.19), pCTX LFP (182.40 ± 169.24), and SLM CSD (2.49 ± 1.66) following NReu lesion was similar to SO power prior to NReu lesion (fCTX: 663.37 ± 170.80; pCTX: 151.77 ± 107.67; SLM CSD: 2.00 ± 0.31).

Consistent with the data presented above (**Figure 4-05**) and with averages across all experiments (*dashed plots*), the rhythmicity in the fCTX, pCTX, and SLM was stronger during stimulation than during control conditions (*dashed green plots*). ACs show that the rhythmicity of the neocortical LFPs and the SLM

CSD during repeated sweeps of mpfCTX stimulation were essentially identical before (*solid black plots* and *grey regions*) and after (*solid red plots* and *grey regions*) NReu lesion (**Figure 4-09D**). The power at the peak SO frequencies (fCTX LFP: Stim 1: 1.0 ± 0.0Hz; Stim 2: 1.0 ± 0.0Hz; pCTX LFP: Stim 1: 1.0 ± 0.0Hz; Stim 2: 1.0 ± 0.0Hz; SLM CSD: Stim 1: 1.0 ± 0.0Hz; Stim 2: 1.0 ± 0.0Hz) in the ACs during mpfCTX stimulation prior to NReu lesion (fCTX LFP: 405.42 ± 0.97; pCTX LFP: 366.15 ± 11.20; SLM CSD: 292.82 ± 45.35) were similar to values following NReu lesion (fCTX LFP: 406.75 ± 0.58; pCTX LFP: 326.56 ± 41.49; SLM CSD: 321.64 ± 29.87) (**Figure 4-09E**). These data suggest that SO entrainment across the nCTX and HPC is not directly dependent on the integrity of the NReu.

Discussion

The SO is a feature of the electrographic activity in the nCTX (Steriade et al., 1993a, 1993b; Steriade et al., 2001; Timofeev et al., 2001), HPC, and the EC (Wolansky et al., 2006; Wolansky and Dickson, 2009), all of which are included in the MTL memory system for episodic memories (Squire and Zola-Morgan, 1991). The SO occurs during deep SWS and the deactivated state of urethane anaesthesia. We suggest that the coordination of this activity across these structures could play a role in the processing and consolidation of episodic mnemonic information.

Repeated low-amplitude, slow-frequency stimulation entrains the hippocampal slow oscillation

A recent study done by Marshall et al. (2006) showed that enhancing the neocortical SO through electrical stimulation selectively enhanced performance on an episodic task the next day. We were curious to see if enhancing the neocortical SO also enhanced the hippocampal SO, including: 1) a concomitant entrainment of the hippocampal SO as measured by SO power in averaged CSD profiles, and 2) an enhancement of SO coordination as measured by rhythmicity at the level of SLM. In this study we showed that repeated low-amplitude (10μA) and slow-frequency (1Hz) stimulation delivered across the surface of the fCTX of urethane-anaesthetised rats both entrained the hippocampal SO and enhanced its coordination with the nCTX.

The mpfCTX is considered one of the main regions of the brain where slow waves originate (Massimini et al., 2004; Murphy et al., 2009; Vyazovskiy et al., 2009). In a second series of experiments, we delivered similar low-amplitude, slow-frequency stimulation locally to the mpfCTX. We found that this stimulation protocol was also effective at entraining the hippocampal SO and enhancing its coordination with the nCTX.

There are two main synaptic pathways from the fCTX to the HPC: 1) via the supEC, and 2) via the NReu. There is substantial evidence that the supEC is involved in the coordination of the SO across the nCTX and HPC (Hahn et al., 2006; Isomura et al., 2006; Wolansky et al., 2006; Hahn et al., 2007). However, we have recently shown that the actual SO-related coupling between the supEC and HPC is surprisingly low (Wolansky and Dickson, 2009).

The mpfCTX and HPC are interconnected via the NReu (Beckstead, 1979; Swanson, 1981; Ferino et al., 1987; Jay et al., 1989; Sesack et al., 1989; van Groen and Wyss, 1990; Wouterlood et al., 1990; Hurley et al., 1991; Jay and Witter, 1991; Vertes, 2002; Proulx and Timofeev, 2007). NReu afferents terminate at the level of SLM in the HPC and mainly in layers I and III of the supEC (Wouterlood et al., 1990); where the largest spontaneous SO-related sink – source alternations occur (Isomura et al., 2006; Wolansky et al., 2006; Wolansky and Dickson, 2009). SLM was also where we observed large rhythmic sink – source alternations during repeated fCTX surface, mpfCTX, and NReu stimulation in this study. It seemed very likely that if the supEC was not responsible for SO coordination, the NReu would be. Repeated low-amplitude,

slow-frequency stimulation delivered locally to the NReu entrained the hippocampal SO but did not enhance its coordination with the nCTX.

Coordination of the neocortex and hippocampus during the slow oscillation

An important finding from this study is that entraining the hippocampal SO is not the same as enhancing its coordination with the nCTX; SO power at the level of SLM was dissociable from SO rhythmicity during repeated NReu stimulation. By analysing the differences in our findings across stimulation protocols, we can hypothesise about the mechanisms of SO coordination. First, SO rhythmicity in the SLM CSD increased during repeated fCTX and mpfCTX (prior to and following NReu lesion) stimulation but not during repeated NReu stimulation. In addition, although rhythmicity of the SLM CSD increased following NReu lesion, coherence with the pCTX decreased. These data suggest that SO coordination between the nCTX and HPC does not occur solely via the NReu. If SO coordination occurred mainly via the mpfCTX – NReu – HPC circuit, we would also expect that: 1) repeated stimulation of the NReu would have also increased the rhythmicity of the SLM CSD, and 2) the coordination between the nCTX and HPC during repeated mpfCTX stimulation post-NReu lesion would have decreased as compared to pre-NReu lesion. As stated above, the other likely pathway for SO coordination across the nCTX and HPC is via the supEC. Therefore, these implications seem surprising based on our recent findings regarding the SO-related coupling between the EC and the HPC (Wolansky and Dickson, 2009).

Second, the hippocampal SO was entrained by repeated stimulation of the fCTX, mpfCTX, and NReu stimulation. However, lesioning the NReu had no effect on its entrainment during repeated mpfCTX stimulation post-NReu lesion. These data imply that the hippocampal SO can be entrained via both the mpfCTX – NReu – HPC and the fCTX – EC – HPC circuits. Third, single sweeps of stimulation across the fCTX did not affect hippocampal SO power or coherence with the pCTX whereas single sweeps of stimulation delivered to the mpfCTX and NReu decreased hippocampal SO power and coherence with the pCTX. Combined with our findings above, perhaps our data indicate that driving the mpfCTX – NReu – HPC pathway with electrical stimulation without regard for ongoing spontaneous activity in the fCTX – supEC – HPC pathway disrupts the SO in the HPC – the final common endpoint of both circuits. Therefore, we hypothesise that both the fCTX – supEC – HPC and mpfCTX – NReu – HPC synaptic pathways are differentially involved in the entrainment and coordination of the hippocampal SO. Driving one pathway more than the other appears to disrupt the balance between the two and ultimately disrupt the hippocampal SO.

A final important implication of this study is that field stimulation across the fCTX appears to be the most robust protocol to simultaneously entrain the hippocampal SO and enhance its coordination with the nCTX. This combination of effects during repeated low-amplitude and slow-frequency stimulation across the fCTX may be responsible for the behavioural effects observed by Marshall et al. (2006).

Conclusion

Our data show that low-amplitude and slow-frequency stimulation across the surface of the fCTX is an effective and naturalistic method to entrain the hippocampal SO and enhance its coordination with the nCTX. Based on this and our previous work, we conclude that low-amplitude, slow-frequency stimulation across the fCTX recruits *both* the neocortical – entorhinal – hippocampal and neocortical – thalamic – hippocampal pathways equally and that these pathways collectively, but differentially, mediate the entrainment and coordination of the SO across the nCTX and HPC.

Figure 4-01:

Spontaneous versus stimulation-induced slow oscillation

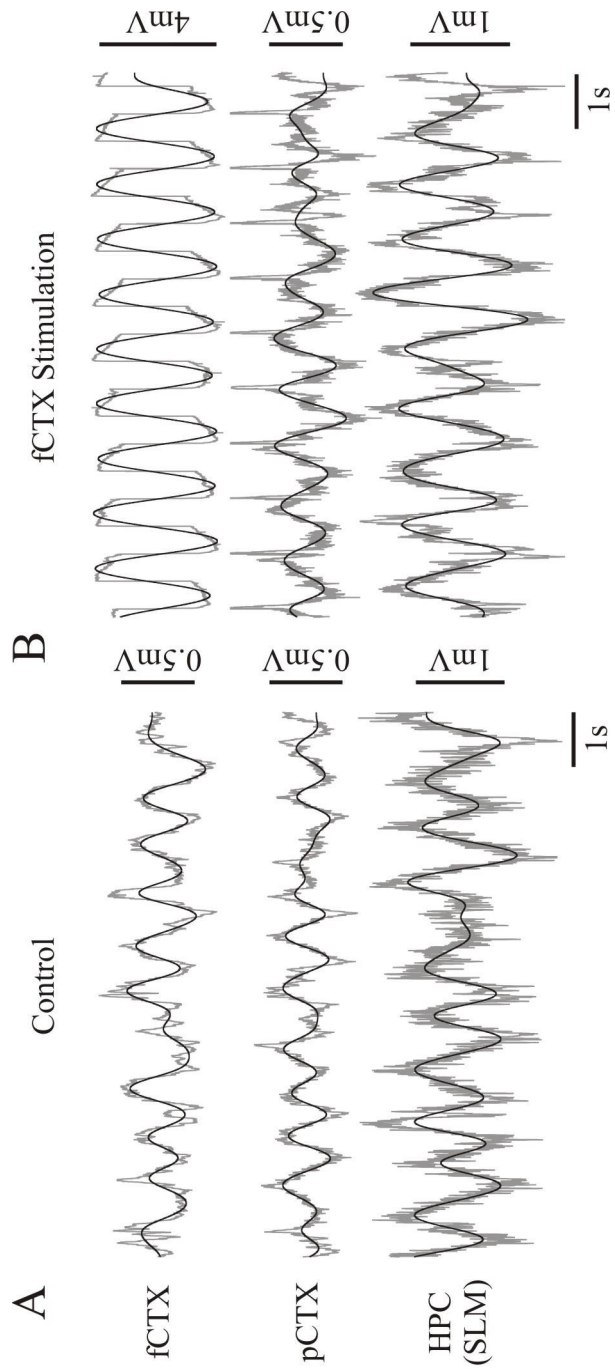

Figure 4-01 Caption:

(**A**) The field potentials in the fCTX, pCTX, and HPC were characterised by a high amplitude, ~1Hz rhythm during the spontaneous SO. During low-amplitude, slow-frequency stimulation of the fCTX (**B**), field potentials appeared similar to those during spontaneous SO activity except they were higher in amplitude and more stereotyped. 1.5Hz lowpass filtered traces from the fCTX, pCTX, and HPC at the level of SLM are plotted in *black* superimposed on the corresponding raw traces plotted in *grey*. Abbreviations: frontal cortex (fCTX), hippocampus (HPC), posterior cortex (pCTX), slow oscillation (SO), stratum lacunosum-moleculare (SLM)

Figure 4-02:

Low-amplitude, slow-frequency stimulation across the surface of the frontal cortex enhances slow power in the hippocampus

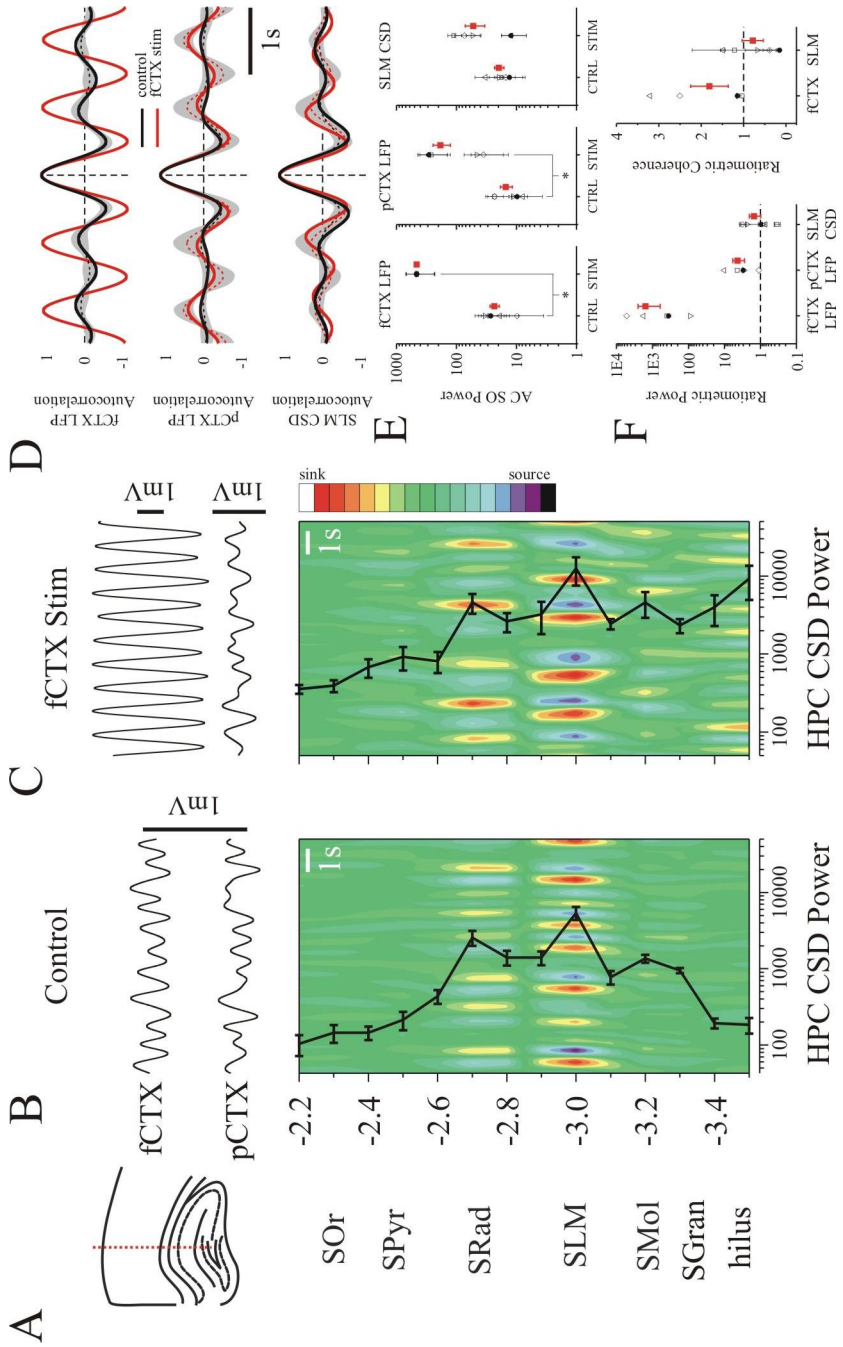

Figure 4-02 Caption:

(**A**) Diagrammatical representation of histological multiprobe track in this experiment and the hippocampal laminae aligned to the hippocampal CSD profiles filtered for SO activity (1.5Hz lowpass) during control (**B**) and stimulation (**C**) conditions. The *top panels* of **B** and **C** show the SO filtered LFPs recorded in the fCTX and pCTX during each condition, time-aligned to the hippocampal CSDs. The power profiles of 1Hz activity in the hippocampal CSDs are plotted as *black lines* superimposed on the hippocampal CSDs. (**D**) The rhythmicity of the SO in both fCTX (*top panel*) and pCTX (*middle panel*) LFPs increased significantly during fCTX stimulation. The rhythmicity of the SO in the SLM CSD (*bottom panel*) did not. These results are also reflected in the power at the peak SO frequency in the ACs plotted in **E**. (**F**) Ratiometric SO power (*left panel*) increased in the fCTX and pCTX during fCTX stimulation but was not significantly different from control at the level of SLM. Ratiometric SO coherence (*right panel*) between the fCTX and pCTX increased during stimulation but that between the pCTX and SLM was not significantly different from control. In **E** and **F**, the values from this experiment are plotted as *black symbols* and those from all other experiments are plotted as *unfilled symbols*. The averages across experiments are plotted in *red*. CSD scales in **C** and **D** are: 12 to -12. Abbreviations: control (CTRL), current source density (CSD), frontal cortex (fCTX), hippocampus (HPC), local field potential (LFP), posterior cortex (pCTX), slow oscillation (SO), stimulation (STIM), stratum lacunosum-moleculare (SLM)

Figure 4-03:

Repeated stimulation across the frontal cortex entrains the hippocampal slow oscillation and enhances its coordination with the neocortex

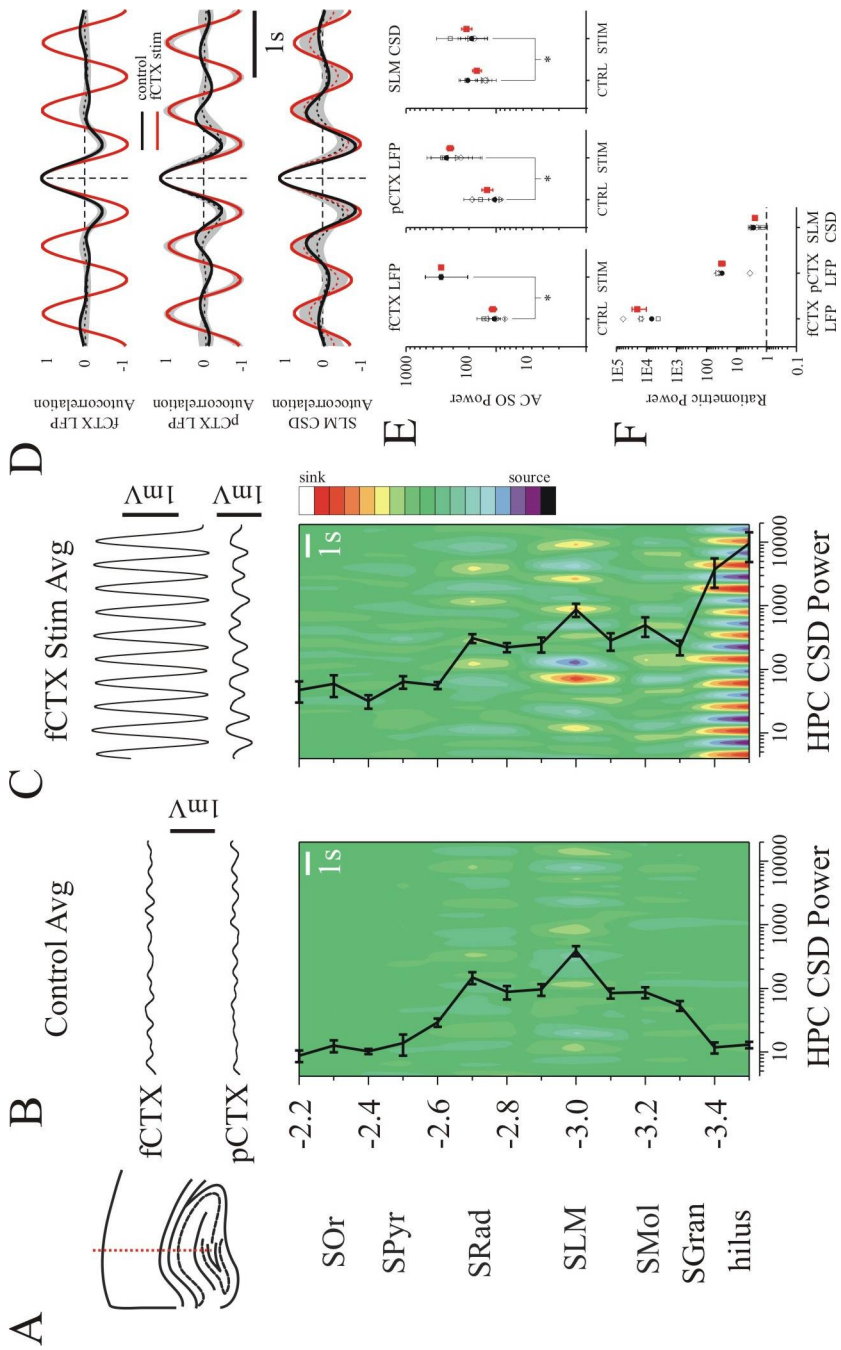

Figure 4-03 Caption:

(**A**) Diagrammatical representation of histological multiprobe track in this experiment and the hippocampal laminae aligned to the average hippocampal CSD profiles filtered for SO activity (1.5Hz lowpass) during control (**B**) and stimulation (**C**) conditions. The *top panels* of **B** and **C** show the average SO filtered LFPs recorded in the fCTX and pCTX during each condition, time-aligned to the average hippocampal CSDs. The power profiles of 1Hz activity in the average hippocampal CSDs are plotted as *black lines* superimposed on the hippocampal CSDs. (**D**) The rhythmicity of the SO in the fCTX (*top panel*) and pCTX (*middle panel*) LFPs, as well as in the SLM CSD (*bottom panel*), increased significantly during repeated fCTX stimulation. These results are also reflected in the power at the peak SO frequency in the ACs plotted in **E**. (**F**) SO ratiometric power (*left panel*) increased at all sites during repeated fCTX stimulation. In **E** and **F**, the values from this experiment are plotted as *black symbols* and those from all other experiments are plotted as *unfilled symbols*. The averages across experiments are plotted in *red*. CSD scales in **C** and **D** are: 5 to -5. Abbreviations: control (CTRL), current source density (CSD), frontal cortex (fCTX), hippocampus (HPC), local field potential (LFP), posterior cortex (pCTX), slow oscillation (SO), stimulation (STIM), stratum lacunosum-moleculare (SLM)

Figure 4-04:

Stimulation directly to the medial prefrontal cortex disrupts the hippocampal slow oscillation and its coordination with the neocortex

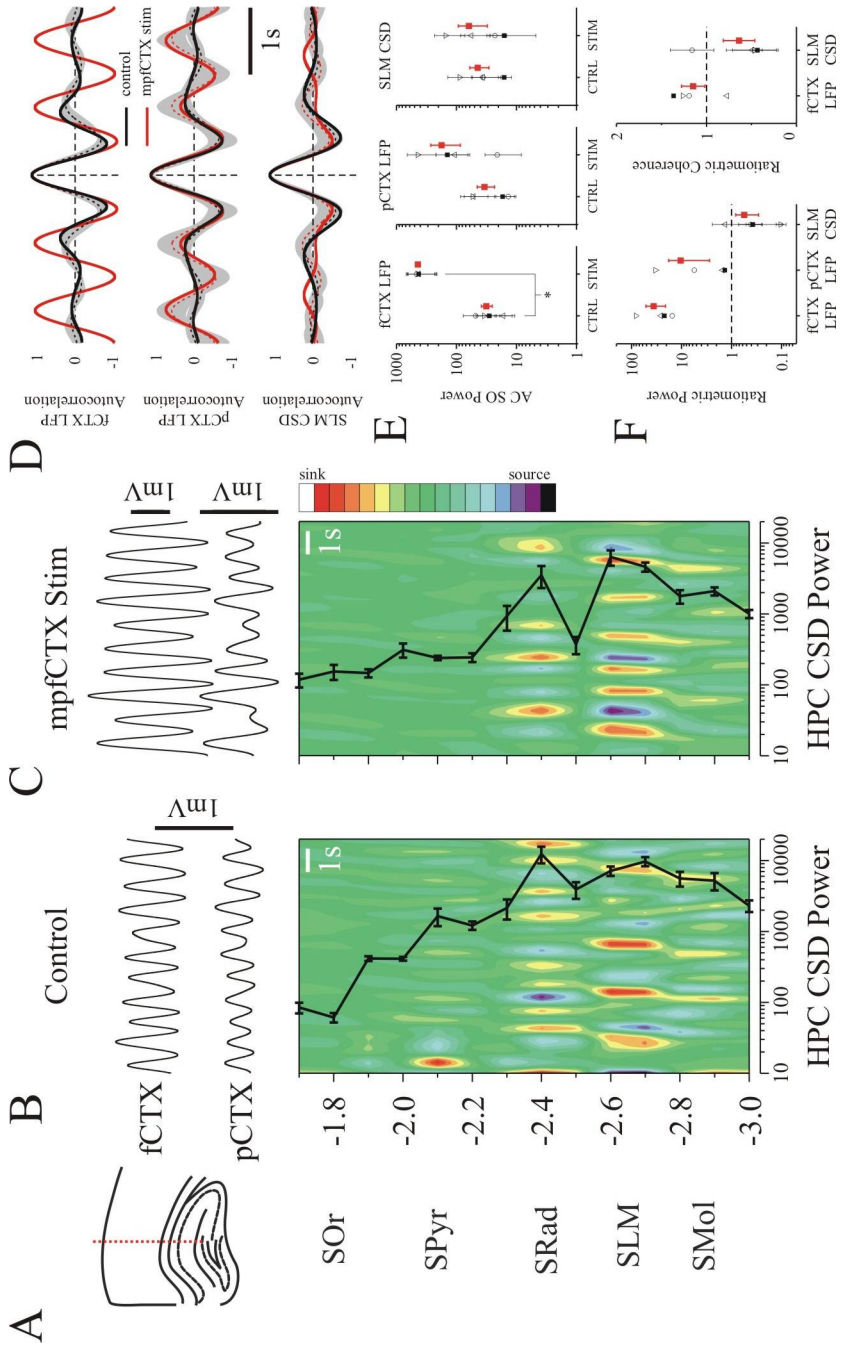

Figure 4-04 Caption:

(**A**) Diagrammatical representation of histological multiprobe track in this experiment and the hippocampal laminae aligned to the hippocampal CSD profiles filtered for SO activity (1.5Hz lowpass) during control (**B**) and stimulation (**C**) conditions. The *top panels* of **B** and **C** show the SO filtered LFPs recorded in the fCTX and pCTX during each condition, time-aligned to the hippocampal CSDs. The power profiles of 1Hz activity in the hippocampal CSDs are plotted as *black lines* superimposed on the hippocampal CSDs. (**D**) The rhythmicity of the SO in both fCTX (*top panel*) increased significantly during mpfCTX stimulation. The rhythmicity of the SO in the pCTX and at the level of SLM was similar to control. These results are reflected in the power at the peak SO frequency in the ACs plotted in **E**. (**F**) Ratiometric SO power (*left panel*) increased in the fCTX and pCTX LFPs during fCTX stimulation and decreased in the SLM CSD. Ratiometric SO coherence (*right panel*) between the fCTX and pCTX increased during stimulation, however, that between the pCTX and the HPC decreased. In **E** and **F**, the average values from this experiment are plotted as *black symbols* and those from all other experiments are plotted as *unfilled symbols*. The averages across experiments are plotted in *red*. CSD scales in **C** and **D** are: 11 to -11. Abbreviations: control (CTRL), current source density (CSD), frontal cortex (fCTX), hippocampus (HPC), local field potential (LFP), posterior cortex (pCTX), slow oscillation (SO), stimulation (STIM), stratum lacunosum-moleculare (SLM)

Figure 4-05:

Repeated stimulation of the medial prefrontal cortex entrains the hippocampal slow oscillation and enhances its coordination with the neocortex

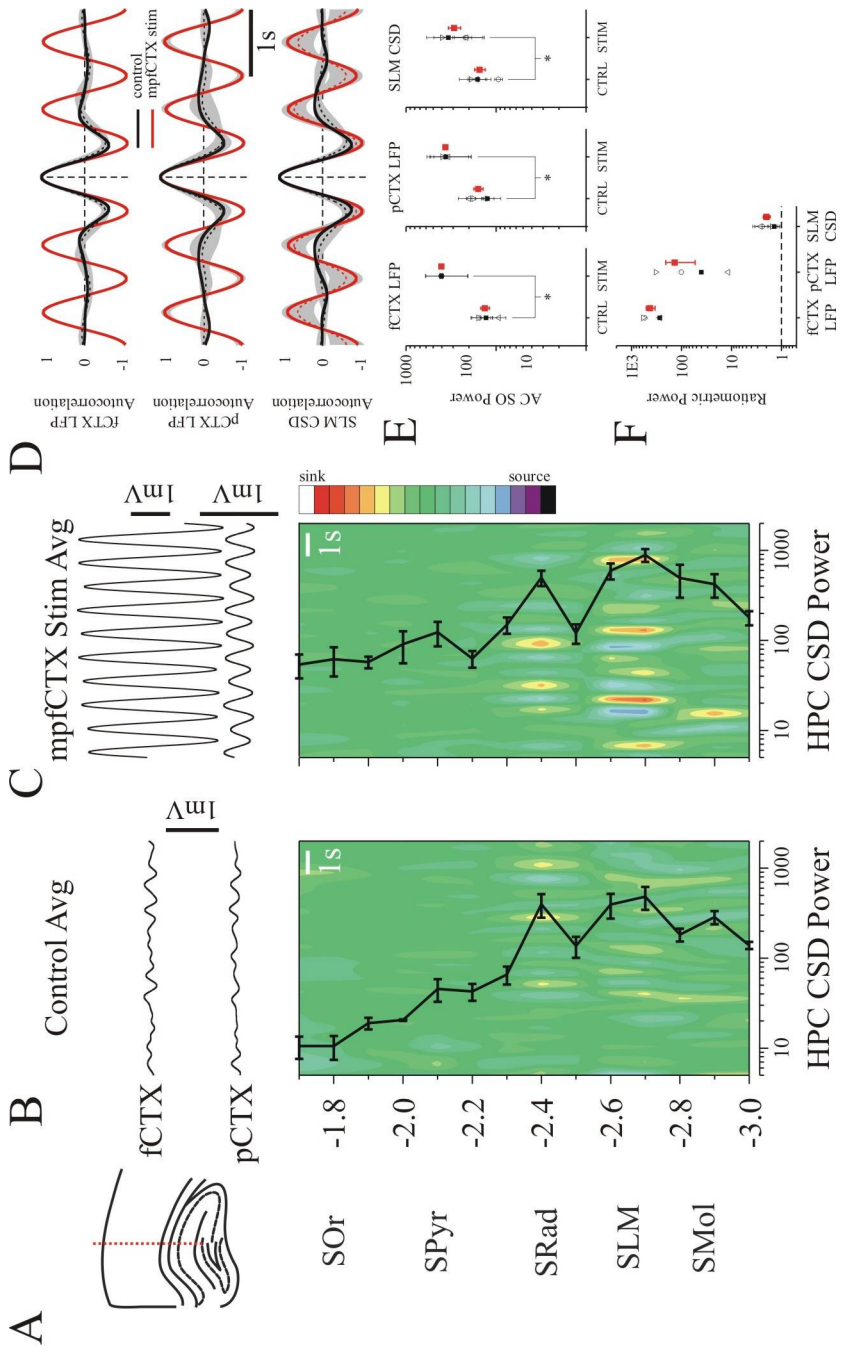

Figure 4-05 Caption:

(**A**) Diagrammatical representation of histological multiprobe track in this experiment and the hippocampal laminae aligned to the average hippocampal CSD profiles filtered for SO activity (1.5Hz lowpass) during control (**B**) and stimulation (**C**) conditions. The *top panels* of **B** and **C** show the average SO filtered LFPs recorded in the fCTX and pCTX during each condition, time-aligned to the average hippocampal CSDs. The power profiles of 1Hz activity in the average hippocampal CSDs are plotted as *black lines* superimposed on the hippocampal CSDs. (**D**) The rhythmicity of the SO in the fCTX (*top panel*), pCTX (*middle panel*), and at the level of SLM (*bottom panel*) increased significantly (**E**) during repeated mpfCTX stimulation. (**F**) SO power increased at all sites during repeated mpfCTX stimulation. In **E** and **F**, the average values from this experiment are plotted as *black symbols* and those from all other experiments are plotted as *unfilled symbols*. The averages across experiments are plotted in *red*. CSD scales in **C** and **D** are: 5 to -5. Abbreviations: control (CTRL), current source density (CSD), frontal cortex (fCTX), hippocampus (HPC), local field potential (LFP), posterior cortex (pCTX), slow oscillation (SO), stimulation (STIM), stratum lacunosum-moleculare (SLM)

Figure 4-06:

Stimulation directly to the nucleus reuniens thalami disrupts the hippocampal slow oscillation and its coordination with the neocortex

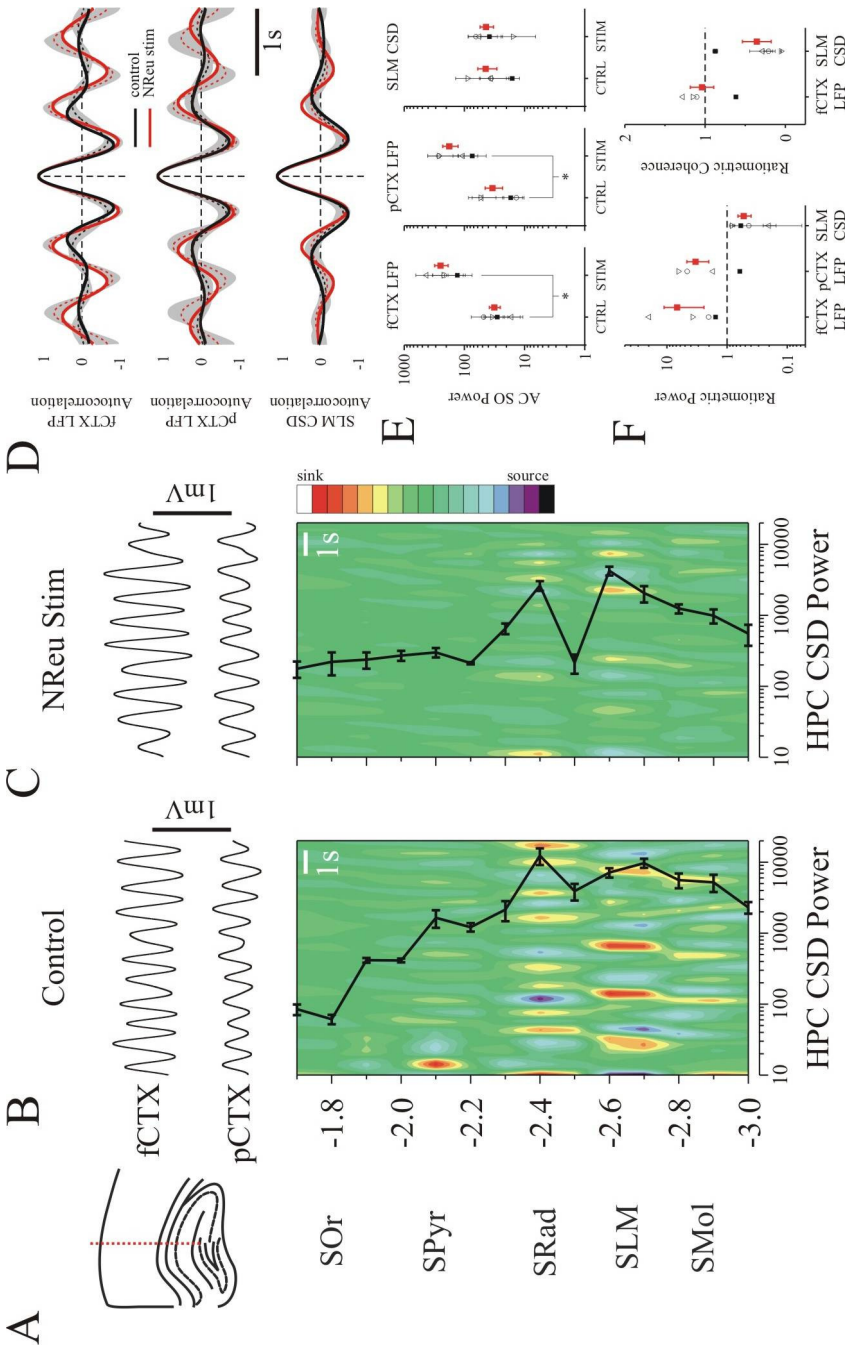

Figure 4-06 Caption:

(**A**) Diagrammatical representation of histological multiprobe track in this experiment and the hippocampal laminae aligned to the hippocampal CSD profiles filtered for SO activity (1.5Hz lowpass) during control (**B**) and stimulation (**C**) conditions. The *top panels* of **B** and **C** show the SO filtered LFPs recorded in the fCTX and pCTX during each condition, time-aligned to the hippocampal CSDs. The power profiles of 1Hz activity in the hippocampal CSDs are plotted as *black lines* superimposed on the hippocampal CSDs. (**D**) The rhythmicity of the SO in both fCTX (*top panel*) and pCTX (*middle panel*) increased during NReu stimulation. The rhythmicity of the SO at the level of SLM was similar to control. These results are reflected in the power at the peak SO frequency in the ACs plotted in **E**. (**F**) SO power (*left panel*) increased in the fCTX and pCTX during NReu stimulation and decreased at the level of SLM. SO coherence (*right panel*) between the fCTX and pCTX was not significantly different from control during NReu stimulation and decreased between the pCTX and SLM. In **E** and **F**, the average values from this experiment are plotted as *black symbols* and those from all other experiments are plotted as *unfilled symbols*. The averages across experiments are plotted in *red*. CSD scales in **C** and **D** are: 11 to -11. Abbreviations: control (CTRL), current source density (CSD), frontal cortex (fCTX), hippocampus (HPC), local field potential (LFP), posterior cortex (pCTX), slow oscillation (SO), stimulation (STIM), stratum lacunosum-moleculare (SLM)

Figure 4-07:

Repeated stimulation of the nucleus reuniens thalami entrains the hippocampal slow oscillation but does not enhance its coordination with the neocortex

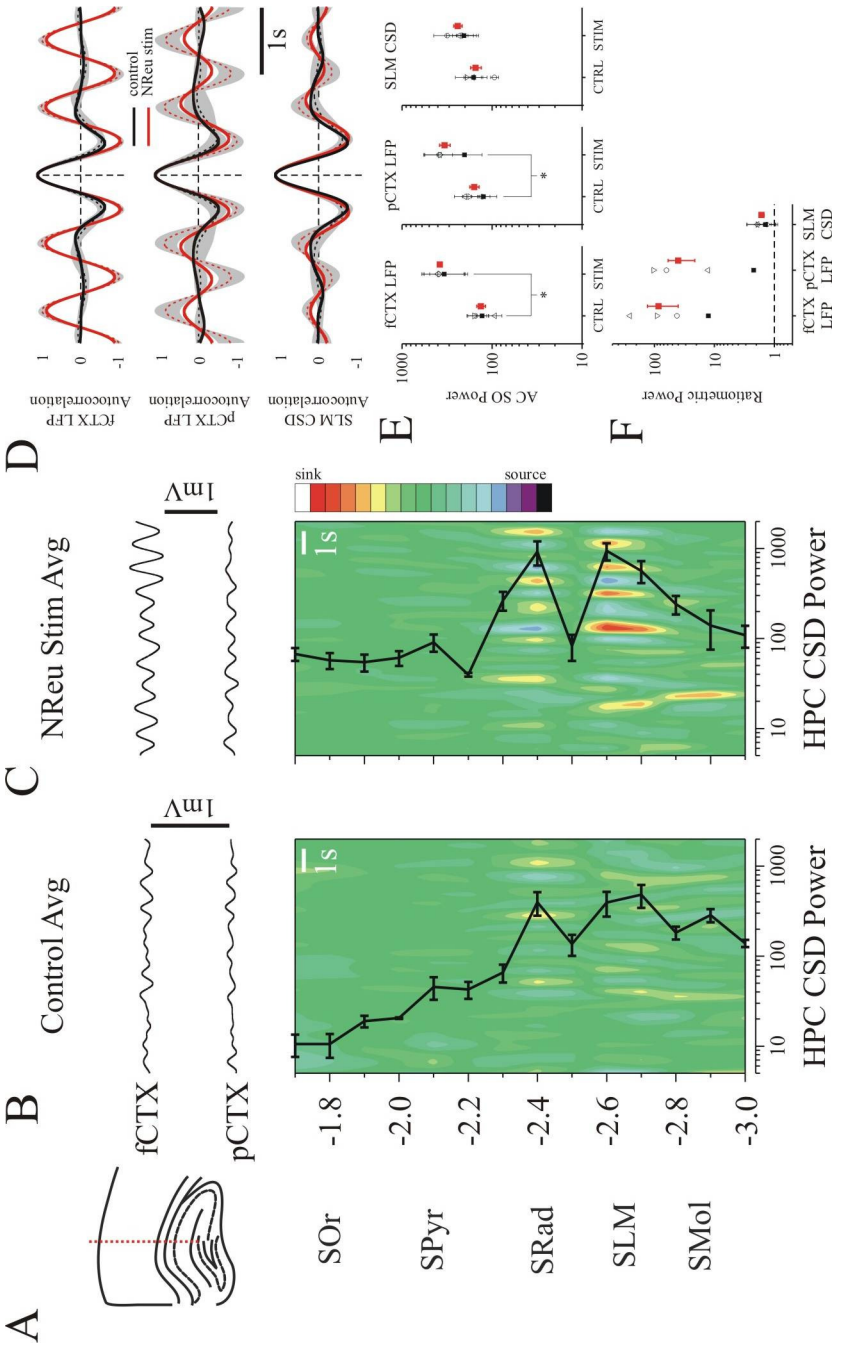

Figure 4-07 Caption:

(**A**) Diagrammatical representation of histological multiprobe track in this experiment and the hippocampal laminae aligned to the average hippocampal CSD profiles filtered for SO activity (1.5Hz lowpass) during control (**B**) and stimulation (**C**) conditions. The *top panels* of **B** and **C** show the average SO filtered LFPs recorded in the fCTX and pCTX during each condition, time-aligned to the average hippocampal CSDs. The power profiles of 1Hz activity in the average hippocampal CSDs are plotted as *black lines* superimposed on the hippocampal CSDs. (**D**) The rhythmicity of the SO in the fCTX (*top panel*) and pCTX (*middle panel*) increased significantly during repeated NReu stimulation but the rhythmicity of the SO at the level of SLM did not. These results are reflected in the power at the peak SO frequency in the ACs plotted in **E**. (**F**) SO power increased at all sites during repeated NReu stimulation. The average values from this experiment are plotted as *black symbols* and those from all other experiments are plotted as *unfilled symbols*. The averages across experiments are plotted in *red*. CSD scales in **C** and **D** are: 5 to -5. Abbreviations: control (CTRL), current source density (CSD), frontal cortex (fCTX), hippocampus (HPC), local field potential (LFP), posterior cortex (pCTX), slow oscillation (SO), stimulation (STIM), stratum lacunosum-moleculare (SLM)

Figure 4-08:

Lesioning the nucleus reuniens thalami has differential effects on the hippocampal slow oscillation

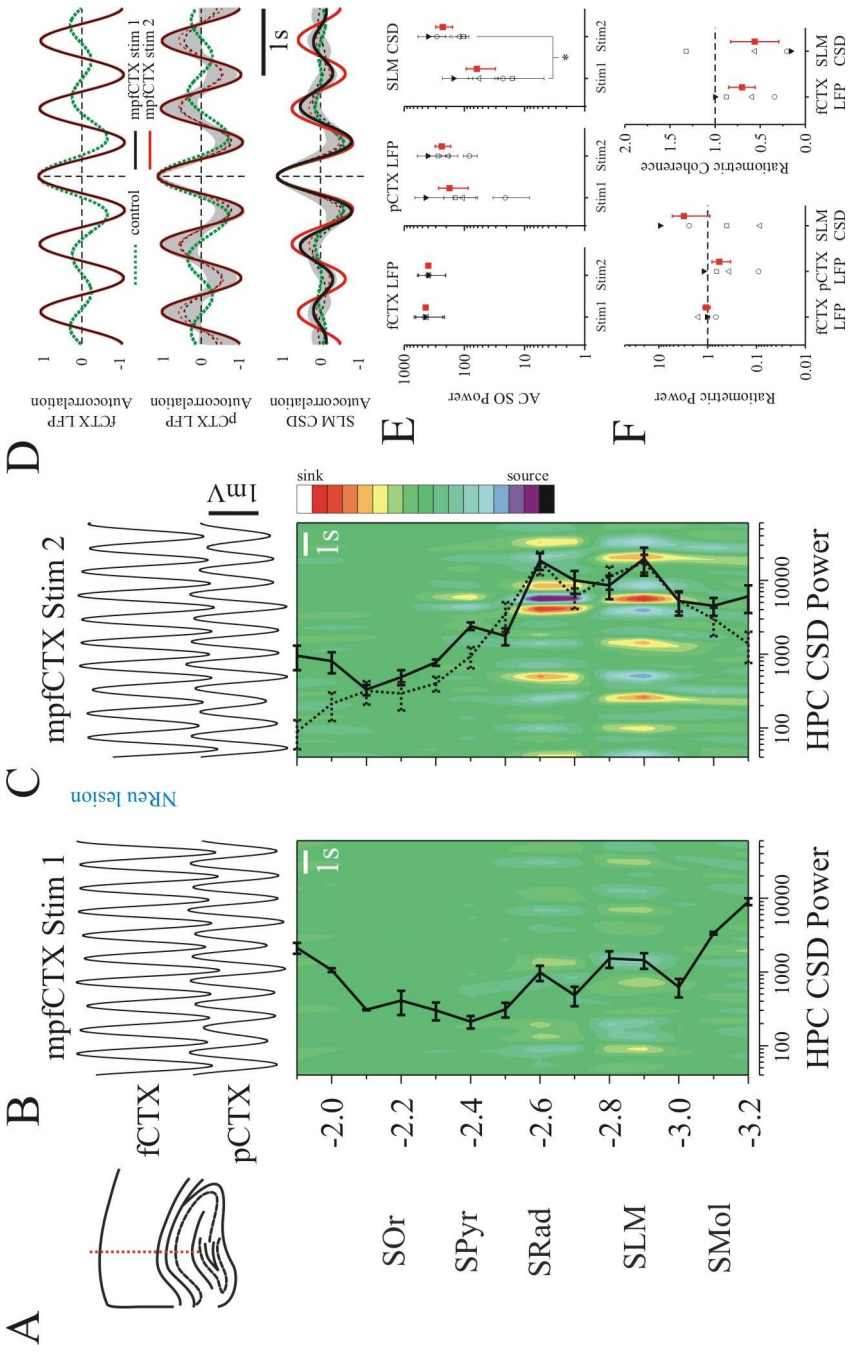

Figure 4-08 Caption:

(**A**) Diagrammatical representation of histological multiprobe track in this experiment and the hippocampal laminae aligned to the hippocampal CSD profiles filtered for SO activity (1.5Hz lowpass) during single sweeps of mpfCTX stimulation both before (**B**) and after (**C**) NReu lesion. The *top panels* of **B** and **C** show the SO filtered LFPs recorded in the fCTX and pCTX during each condition, time-aligned to the hippocampal CSDs. The power profiles of 1Hz activity in the hippocampal CSDs are plotted as *black lines* superimposed on the hippocampal CSDs. (**D** and **E**) The rhythmicity of the SO in the fCTX (*top panel*) and pCTX (*middle panel*) was similar during mpfCTX stimulation both before (*solid black plot*) and after (*red plot*) NReu lesion. The rhythmicity of the SLM CSD (*bottom panel* of **D**) was greater following NReu lesion as compared to pre-NReu lesion (*right panel* of **E**). (**F**) Post-NReu lesion ratiometric SO power (*left panel*) decreased in the pCTX LFP as compared to pre-NReu lesion values. Post-NReu lesion ratiometric SO coherence (*right panel*) decreased across all sites as compared to pre-NReu lesion values. The average values from this experiment are plotted as *black symbols* and those from all other experiments are plotted as *unfilled symbols*. The averages across experiments are plotted in *red*. CSD scales in **C** and **D** are: 20 to -20. Abbreviations: control (CTRL), current source density (CSD), frontal cortex (fCTX), hippocampus (HPC), local field potential (LFP), posterior cortex (pCTX), slow oscillation (SO), stimulation (STIM), stratum lacunosum-moleculare (SLM)

Figure 4-09:

Entrainment of the hippocampal slow oscillation is not dependent on the integrity of the nucleus reuniens thalami

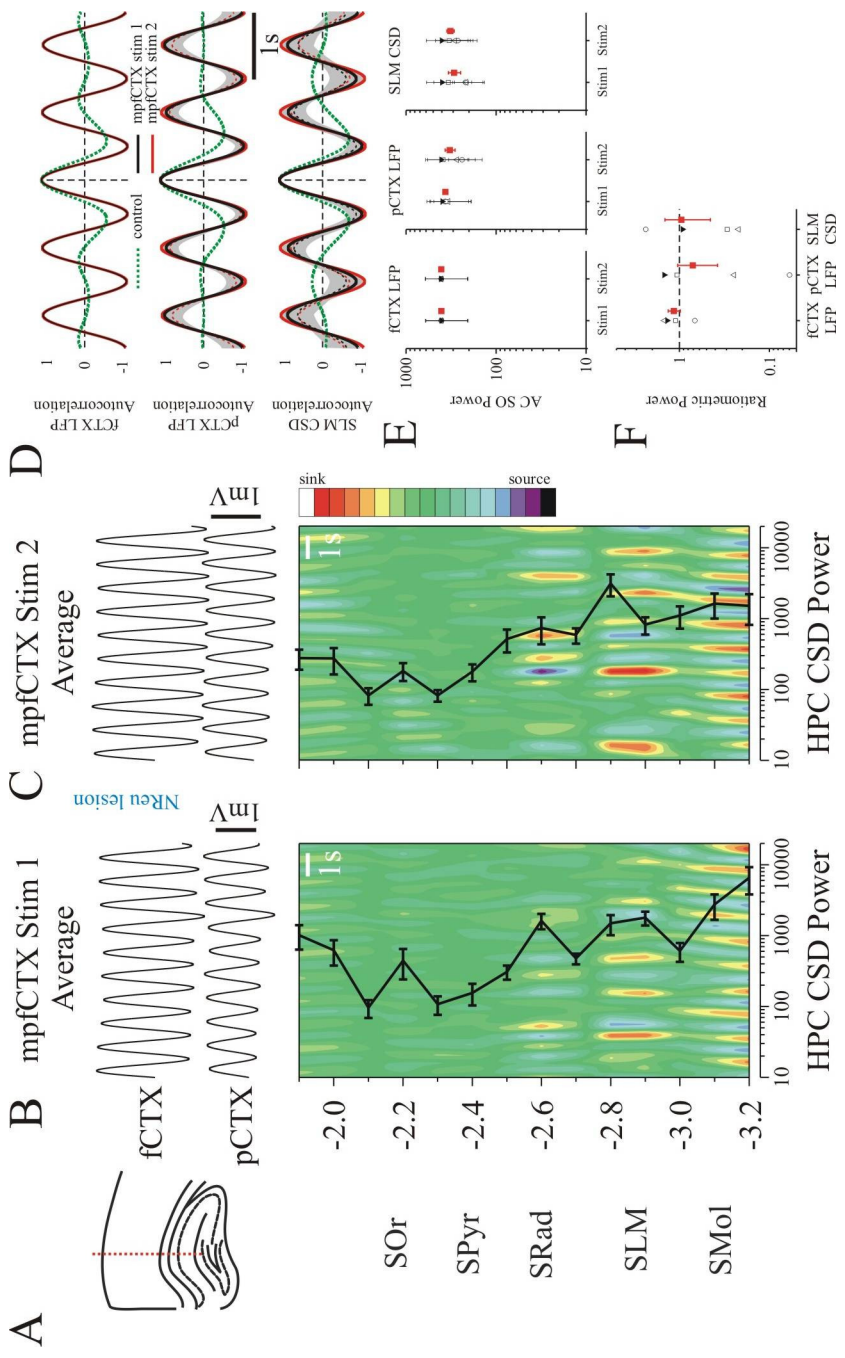

Figure 4-09 Caption:

(**A**) Diagrammatical representation of histological multiprobe track in this experiment and the hippocampal laminae aligned to the average hippocampal CSD profiles filtered for SO activity (1.5Hz lowpass) during repeated sweeps of mpfCTX stimulation both before (**B**) and after (**C**) NReu lesion. The *top panels* of **B** and **C** show the average SO filtered LFPs recorded in the fCTX and pCTX during each condition, time-aligned to the average hippocampal CSDs. The power profiles of 1Hz activity in the average hippocampal CSDs are plotted as *black lines* superimposed on the hippocampal CSDs. (**D**) The rhythmicity of the SO in the fCTX (*top panel*), pCTX (*middle panel*), and in SLM (*bottom panel*) increased as compared to control (*dashed green plot*) during mpfCTX stimulation both before (*solid black plot*) and after (*red plot*) NReu lesion. (**E**) The rhythmicity was similar in both pre- and post-NReu lesion conditions. (**F**) There was no significant difference in average ratiometric SO power across pre- and post-NReu lesion conditions. The average values from this experiment are plotted as *black symbols* and those from all other experiments are plotted as *unfilled symbols*. CSD scales in **C** and **D** are: 5 to -5. Abbreviations: control (CTRL), current source density (CSD), frontal cortex (fCTX), hippocampus (HPC), local field potential (LFP), posterior cortex (pCTX), slow oscillation (SO), stimulation (STIM), stratum lacunosum-moleculare (SLM)

Chapter 4 References

Amzica F, Steriade M (1995) Disconnection of intracortical synaptic linkages disrupts synchronization of a slow oscillation. Journal of Neuroscience 15:4658-4677.

Beckstead RM (1979) An autoradiographic examination of corticocortical and subcortical projections of the mediodorsal-projection (prefrontal) cortex in the rat. J Comp Neurol 184:43-62.

Bland SK, Bland BH (1986) Medial septal modulation of hippocampal theta cell discharges. Brain Res 375:102-116.

Buzsáki G (1986) Hippocampal sharp waves: their origin and significance. Brain Research 398:242-252.

Buzsáki G (1989) Two-stage model of memory trace formation: A role for "noisy" brain states. Neurosci 31:551-570.

Buzsáki G (1996) The hippocampo-neocortical dialogue. Cerebral Cortex 6:81-92.

Dolorfo CL, Amaral DG (1998) Entorhinal cortex of the rat: organization of intrinsic connections. J Comp Neurol 398:49-82.

Eichenbaum H (2000) A cortical-hippocampal system for declarative memory. Nat Rev Neurosci 1:41-50.

Ferino F, Thierry AM, Glowinski J (1987) Anatomical and electrophysiological evidence for a direct projection from Ammon's horn to the medial prefrontal cortex in the rat. Exp Brain Res 65:421-426.

Freeman JA, Nicholson C (1975) Experimental optimization of current source-density technique for anuran cerebellum. J Neurophysiol 38:369-382.

Hahn TT, Sakmann B, Mehta MR (2006) Phase-locking of hippocampal interneurons' membrane potential to neocortical up-down states. Nat Neurosci 9:1359-1361.

Hahn TT, Sakmann B, Mehta MR (2007) Differential responses of hippocampal subfields to cortical up-down states. Proc Natl Acad Sci U S A 104:5169-5174.

Hirase H, Leinekugel X, Czurko A, Csicsvari J, Buzsaki G (2001) Firing rates of hippocampal neurons are preserved during subsequent sleep episodes and modified by novel awake experience. Proc Natl Acad Sci U S A 98:9386-9390.

Huber R, Ghilardi MF, Massimini M, Tononi G (2004) Local sleep and learning. Nature 430:78-81.

Hurley KM, Herbert H, Moga MM, Saper CB (1991) Efferent projections of the infralimbic cortex of the rat. J Comp Neurol 308:249-276.

Isomura Y, Sirota A, Ozen S, Montgomery S, Mizuseki K, Henze DA, Buzsaki G (2006) Integration and segregation of activity in entorhinal-hippocampal subregions by neocortical slow oscillations. Neuron 52:871-882.

Jay TM, Witter MP (1991) Distribution of hippocampal CA1 and subicular efferents in the prefrontal cortex of the rat studied by means of anterograde transport of Phaseolus vulgaris-leucoagglutinin. J Comp Neurol 313:574-586.

Jay TM, Glowinski J, Thierry AM (1989) Selectivity of the hippocampal projection to the prelimbic area of the prefrontal cortex in the rat. Brain Res 505:337-340.

Ji D, Wilson MA (2007) Coordinated memory replay in the visual cortex and hippocampus during sleep. Nat Neurosci 10:100-107.

Ketchum KL, Haberly LB (1993) Synaptic events that generate fast oscillations in piriform cortex. J Neurosci 13:3980-3985.

Marshall L, Helgadottir H, Molle M, Born J (2006) Boosting slow oscillations during sleep potentiates memory. Nature 444:610-613.

Massimini M, Huber R, Ferrarelli F, Hill S, Tononi G (2004) The sleep slow oscillation as a traveling wave. J Neurosci 24:6862-6870.

Mednick S, Nakayama K, Stickgold R (2003) Sleep-dependent learning: a nap is as good as a night. Nat Neurosci 6:697-698.

Molle M, Marshall L, Gais S, Born J (2004) Learning increases human electroencephalographic coherence during subsequent slow sleep oscillations. Proc Natl Acad Sci U S A 101:13963-13968.

Moser MB, Moser EI (1998) Functional differentiation in the hippocampus. Hippocampus 8:608-619.

Murphy M, Riedner BA, Huber R, Massimini M, Ferrarelli F, Tononi G (2009) Source modeling sleep slow waves. Proc Natl Acad Sci U S A 106:1608-1613.

Nicholson C, Freeman JA (1975) Theory of current source-density analysis and determination of conductivity tensor for anuran cerebellum. J Neurophysiol 38:356-368.

Ozen S, Sirota A, Buzsaki G (2007) Effects of weak electrical fields on single cell and network activity in vivo. In: Society for Neuroscience 2007. San Diego, California.

Ozen S, Sirota AM, Anastassiou CA, Koch C, Buzsaki G (2008) Entrainment of the cortical slow oscillation by extra-cranial weak electric fields. In: Society for Neuroscience. Washington, D.C.

Peigneux P, Laureys S, Fuchs S, Collette F, Perrin F, Reggers J, Phillips C, Degueldre C, Del Fiore G, Aerts J, Luxen A, Maquet P (2004) Are spatial memories strengthened in the human hippocampus during slow wave sleep? Neuron 44:535-545.

Proulx E, Timofeev I (2007) Medial prefrontal cortex intracellular and local field potential recordings provide evidence for a hippocampo-prefronto-thalamic relay: An in vivo study in the cat. In: Society for Neuroscience Abstracts, p Program # 792.799: Society for Neuroscience.

Rasch B, Buchel C, Gais S, Born J (2007) Odor cues during slow-wave sleep prompt declarative memory consolidation. Science 315:1426-1429.

Rodriguez R, Haberly LB (1989) Analysis of synaptic events in the opossum piriform cortex with improved current source-density techniques. J Neurophysiol 61:702-718.

Schall KP, Kerber J, Dickson CT (2008) Rhythmic constraints on hippocampal processing: state and phase-related fluctuations of synaptic excitability during theta and the slow oscillation. J Neurophysiol 99:888-899.

Scoville WB, Milner B (1957) Loss of recent memory after bilateral hippocampal lesions. J Neurol Neurosurg Psychiat 20:11-21.

Sesack SR, Deutch AY, Roth RH, Bunney BS (1989) Topographical organization of the efferent projections of the medial prefrontal cortex in the rat: an anterograde tract-tracing study with Phaseolus vulgaris leucoagglutinin. J Comp Neurol 290:213-242.

Squire LR, Zola-Morgan S (1991) The medial temporal lobe memory system. Science 253:1380-1386.

Steriade M (1999) Coherent oscillations and short-term plasticity in corticothalamic networks. Trends Neurosci 22:337-345.

Steriade M, Nunez A, Amzica F (1993a) Intracellular analysis of relations between the slow (< 1 Hz) neocortical oscillation and other sleep rhythms of the electroencephalogram. J Neurosci 13:3266-3283.

Steriade M, Nunez A, Amzica F (1993b) A novel slow (< 1 Hz) oscillation of neocortical neurons in vivo: depolarizing and hyperpolarizing components. J Neurosci 13:3252-3265.

Steriade M, Timofeev I, Grenier F (2001) Natural waking and sleep states: a view from inside neocortical neurons. J Neurophysiol 85:1969-1985.

Steward O (1976) Topographic organization of the projections from the entorhinal area to the hippocampal formation of the rat. J Comp Neurol 167:285-314.

Steward O, Scoville SA (1976) The cells of origin of entorhinal afferents to the hippocampus and fascia dentata of the rat. J Comp Neurol 169:347-370.

Swanson LW (1981) A direct projection from Ammon's horn to prefrontal cortex in the rat. Brain Res 217:150-154.

Takashima A, Petersson KM, Rutters F, Tendolkar I, Jensen O, Zwarts MJ, McNaughton BL, Fernandez G (2006) Declarative memory consolidation in humans: a prospective functional magnetic resonance imaging study. Proc Natl Acad Sci U S A 103:756-761.

Timofeev I, Grenier F, Steriade M (2001) Disfacilitation and active inhibition in the neocortex during the natural sleep-wake cycle: an intracellular study. Proc Natl Acad Sci U S A 98:1924-1929.

Tse D, Langston RF, Kakeyama M, Bethus I, Spooner PA, Wood ER, Witter MP, Morris RG (2007) Schemas and memory consolidation. Science 316:76-82.

van Groen T, Wyss JM (1990) Extrinsic projections from area CA1 of the rat hippocampus: olfactory, cortical, subcortical, and bilateral hippocampal formation projections. J Comp Neurol 302:515-528.

Vertes RP (2002) Analysis of projections from the medial prefrontal cortex to the thalamus in the rat, with emphasis on nucleus reuniens. J Comp Neurol 442:163-187.

Vyazovskiy VV, Faraguna U, Cirelli C, Tononi G (2009) Triggering slow waves during NREM sleep in the rat by intracortical electrical stimulation: effects of sleep/wake history and background activity. J Neurophysiol 101:1921-1931.

Wolansky T, Dickson CT (2009) The slow oscillation is a feature of both hippocampal input and output layers of the entorhinal cortex. Submitted to the Journal of Neuroscience.

Wolansky T, Clement EA, Peters SR, Palczak MA, Dickson CT (2006) Hippocampal slow oscillation: a novel EEG state and its coordination with ongoing neocortical activity. J Neurosci 26:6213-6229.

Wouterlood FG, Saldana E, Witter MP (1990) Projection from the nucleus reuniens thalami to the hippocampal region: light and electron microscopic tracing study in the rat with the anterograde tracer Phaseolus vulgaris-leucoagglutinin. J Comp Neurol 296:179-203.

Chapter 5:

Conclusion

Chapter Review

Introduction

The nCTX, EC, and HPC are all part of the MTL memory system (Squire and Zola-Morgan, 1991). Extensive damage to the MTL can result in both a severe anterograde and a temporally-graded retrograde amnesia for facts and events or episodic information but does not impair short-term or other forms of long-term memory. Therefore, the mnemonic function of the MTL is limited to the long-term episodic type. The synaptic interconnections between the structures of the MTL memory system (i.e., the nCTX, EC, and HPC) are the anatomical basis for its function.

The long-term consolidation of episodic memories mediated by the MTL memory system is thought to be dependent on SWS (reviewed in: Buzsáki, 1998; Hasselmo, 1999; Peigneux et al., 2001; Tononi and Cirelli, 2001; Ribeiro and Nicolelis, 2004; Walker and Stickgold, 2004; Rauchs et al., 2005). The synchronised interactions that occur across the nCTX, EC, and HPC during SWS could be a suitable platform for synaptic plasticity and possibly episodic memory consolidation. Using urethane anaesthesia as a model of brain activity during sleep (specifically SWS), I characterised slow oscillatory brain rhythms and their coordination across the nCTX, EC, and HPC.

Highly processed, multimodal information is transmitted from the nCTX to the supEC and then into the HPC via the perforant and temporoammonic pathways. Information flow through this circuit is essentially unidirectional – from the DG to CA3 via the mossy fibre pathway and from CA3 to CA1 via the

Schaffer collateral pathway. Following hippocampal processing, output is transmitted to the deep EC where it is either redirected back into the supEC and HPC via entorhinal association connections (Kohler, 1986, 1988; Dolorfo and Amaral, 1998) or sent back to the nCTX where it originated (Swanson and Cowan, 1977; Finch and Babb, 1980, 1981; Witter et al., 1988; van Groen and Wyss, 1990; Naber et al., 2001; Kloosterman et al., 2003).

We can make certain assumptions about the information processing that is occurring in a neural network based on its ongoing state – dependent activity. Theta is a 3 to 12Hz rhythm that occurs in the EC and HPC during exploratory movements and REM sleep. LIA is a broadband, non-rhythmic signal that occurs during stereotypical behaviours and during non-REM sleep.

The SO in the nCTX was first described by Steriade et al. (1993a). It only occurred during deep SWS and deep anaesthesia, consisted of ≤ 1Hz alternating periods of action potential generation and neuronal silence, which are generally referred to as UP and DOWN states, respectively. The SO has since been described in several other regions of the brain, including subcortical structures (Mahon et al., 2001; Tseng et al., 2001; Isomura et al., 2006; Crane et al., 2009). Individual slow waves are often generated in the prefrontal cortical region and propagate across the nCTX (Massimini et al., 2004; Murphy et al., 2009). Other sleep-related rhythms such as K-complexes, spindles, and delta, are grouped by the SO (Steriade et al., 1993b).

The Hippocampal Slow Oscillation- A Novel EEG State and Its Coordination with Ongoing Neocortical Activity

This was the first description of the SO in the HPC. Similarly to the SO in the nCTX, it is a rhythmic ≤ 1Hz oscillation that occurs in the HPC during deep SWS and the deactivated state of urethane anaesthesia. Classically, LIA has been considered the deactivated state of hippocampal activity. We concluded that the SO is a different and more deactivated state than LIA based on its temporal and spectral characteristics, differential activity in hippocampal units, and differential relationship(s) with other hippocampal ensemble patterns.

The hippocampal SO was dynamically coordinated with the previously described neocortical SO (Steriade et al., 1993a). Although the hippocampal SO always evolved following that in the nCTX, the coupling between the two structures was not consistently strong. We showed that the SO was dependent on the ascending cholinergic activating system but was not directly paced from this system. We suggested that the coordination of the SO was likely mediated by some external mechanism; potentially the EC and/or the NReu.

The Slow Oscillation is a Feature of Both Hippocampal Input and Output Layers of the Entorhinal Cortex

The rhythmicity of dentate spikes and the prominent sink-source alternations at the level of SLM in the HPC, as well as the timing of the evolution of SO and rhythmic unit activity in the EC all suggested that it was important for the coordination of the SO across the HPC and nCTX. Spectral and CSD analyses

confirmed that the SO occurred in both the superficial and deep layers of the EC; both the LFP and sink-source alternations were the largest in the supEC. A surprising finding was that the coherence between the supEC and the hippocampal SO was very low. The SO coherence between the supEC and the nCTX was also very low. This is exactly the opposite of what we would expect if the SO was being coordinated across all 3 structures in a serial synaptic manner (i.e., nCTX – EC – HPC).

Unit activity in the deep EC, a major target of hippocampal output, was significantly rhythmic during the SO. In addition, the SO coherence between the HPC, nCTX, and deep EC was higher than that in the supEC. We concluded that the coordination of the SO in the neocortical – entorhinal – hippocampal circuit is bidirectional and may not be solely dependent on the synaptic interconnections via the EC.

Low-Amplitude and Slow-Frequency Stimulation Entrains the Slow Oscillation in the Hippocampus

Marshall et al. (2006) showed that enhancing the neocortical SO during early SWS by applying stimulation across the frontal lobes selectively enhanced episodic memory performance the next day. Because the HPC is critical to episodic memory (Scoville and Milner, 1957; Squire and Zola-Morgan, 1991; Moser and Moser, 1998; Eichenbaum, 2000), their findings implied that fCTX stimulation may have engaged the HPC at SO frequencies.

Repeated low-amplitude 1Hz stimulation delivered across the fCTX, and directly to the mpfCTX and NReu entrained the SO in the HPC. Single sweeps of stimulation across the fCTX enhanced the SO and its coordination across the nCTX and HPC. Similar stimulation delivered to the mpfCTX and the NReu actually disrupted the hippocampal SO and its coordination with the nCTX. We concluded that both the fCTX – EC – HPC and mpfCTX – NReu – HPC circuitry are differentially involved in the entrainment and coordination of the hippocampal SO.

Discussion

UP – DOWN states in hippocampal neurons

The UP – DOWN state transitions in membrane potential that generate the SO LFP have been observed in the nCTX (Steriade et al., 1993a) and in several other regions of the brain (Mahon et al., 2001; Tseng et al., 2001; Crane et al., 2009), including the EC (Isomura et al., 2006). Shortly after *Chapter 2: The Hippocampal Slow Oscillation* was published, Hahn et al. (2006) showed that the membrane potential of interneurons situated at the border of SRad and SLM in CA1 of the dorsal HPC (R-LM interneurons) showed UP – DOWN state bistability. Moreover, these UP – DOWN state transitions and corresponding action potential generation occurred consistently after the UP – DOWN state transitions in the nCTX. It is interesting that R-LM interneurons receive substantial input from the nCTX via the supEC (Amaral and Witter, 1989). Similarly to our speculation (*Chapter 2*), Hahn et al. (2006) suggested that the SO could be coordinated across the nCTX and HPC via the supEC.

Support for the nCTX – EC – HPC serial synaptic hypothesis of SO coordination strengthened when Isomura et al. (2006) showed that current sinks occurred at the level of SLM following neocortical DOWN – UP state transitions in both the urethane-anaesthetised and naturally-sleeping rat. They did not observe significant membrane potential bimodality in hippocampal principal neurons. Their findings lead them to suggest that the SO was not a phenomenon that engaged neuronal activity in the HPC. Rather that the synaptic transmission

of rhythmic DOWN – UP transitions arriving from the EC were responsible for generating the SO LFP in the HPC.

Interestingly, Hahn et al. (2007) reported shortly thereafter that granule cells and some CA3 neurons exhibited membrane potential bistability, but that CA1 pyramids did not. They also showed that the activity in hippocampal principal neurons was modulated by the UP – DOWN state transitions in the nCTX. Granule cells in the DG rapidly depolarised following the DOWN – UP transition in the nCTX with a slight phase lag and CA1 pyramids tended to show a net hyperpolarisation. CA3 pyramids showed a mixed response: some depolarised, some hyperpolarised, and some did not respond following the neocortical DOWN – UP transition.

We were unable to comment on membrane potential bimodality because we did not perform intracellular recordings. Regardless, the majority of single units that we recorded (i.e., extracellular) in the HPC (*Chapter 2*) and EC (*Chapter 3*), in addition to hippocampal gamma activity (*Chapter 2*), were phasically modulated by the SO.

We presented several issues with respect to SO detection in *Chapter 2*, one of which was the transient nature of the hippocampal SO as compared to the neocortical SO. Isomura et al (2006) used the DOWN – UP shift in the nCTX as a trigger to investigate activity in the HPC without regard of the hippocampal LFP. As we showed in *Chapter 2*, the neocortical LFP has high power at ~1Hz during both LIA and the SO states (Wolansky et al., 2006). Therefore, it is not appropriate to use high SO power in the neocortical LFP as the only measure of

high SO power in the hippocampal LFP. The neocortical and hippocampal LFPs must both be monitored for periods of simultaneous high SO power and rhythmicity.

Another potential issue resides in the ongoing field activity they classified as SO. Recall that state – dependent activity is generated by individual neurons and the activity of individual neurons is constrained by state – dependent activity (*Chapter 2* and *Chapter 3*). The hippocampal LFP shown with simultaneously recorded intracellular unit activity (Isomura et al., 2006) does not visually appear to be a SO LFP; it appears more visually similar to LIA (*Chapter 2*). This could be due to their choice of data segments or it could be due to their filter settings. It is common practise to hipass filter electrophysiological recordings at ≥ 1Hz (Steriade et al., 1993a); Isomura et al. (2006) used filter settings of 1Hz to 5kHz. However, if one wishes to study a 1Hz oscillation, 1Hz hipass filter settings are not appropriate.

Underlying cellular mechanisms of the slow oscillation

Membrane potential bistability is inherently composed of two phases; the depolarised or UP state and the hyperpolarised or DOWN state. In the nCTX, excitatory post-synaptic potentials mediated by both the persistent sodium channel and the N-methyl D-aspartate (NMDA) receptor keep the membrane potential depolarised during the UP state. The UP state was shown to be independent of non-NMDA receptors (e.g., kainate) (Steriade et al., 1993a; Sanchez-Vives and McCormick, 2000). The prolonged hyperpolarisation during

the DOWN state is dependent on increased potassium conductance (Sanchez-Vives and McCormick, 2000).

Cunningham et al. (2006) showed that the interaction between kainate receptor-mediated activity and the metabolic needs of entorhinal pyramidal neurons was sufficient to generate membrane potential bistability *in vitro*. In addition, they showed that the SO in the EC (*in vitro*) was independent of the NMDA receptor.

Granule cells in the DG, pyramidal neurons in region CA, and many hippocampal interneurons express both NMDA (Laurie and Seeburg, 1994) and kainate receptors (Werner et al., 1991; Wisden and Seeburg, 1993; Paternain et al., 2000). Tsukamoto-Yasui et al. (2007) showed that CA3 pyramidal neurons *in vitro* expressed slow UP – DOWN oscillations in the presence of physiological artificial cerebrospinal fluid. Blocking glutamatergic and fast GABAergic transmission slowed the frequency of the UP states, but did not abolish them. UP states were eliminated following the pipette application of a calcium chelator. These data suggest that UP states in CA3 are not strictly dependent on glutamatergic or fast GABAergic transmission, but are dependent on intracellular calcium dynamics. Understanding the cellular mechanism(s) of the SO in the HPC will certainly provide insight into the role of the SO in hippocampal function. To date, there have been no reports of a network SO in the LFP recorded from hippocampal slices, the isolated HPC, or from the isolated whole brain.

Pharmacological modulation of the slow oscillation

In *Chapter 2*, we demonstrated the dependence of this activity on the ascending cholinergic activating system. Further work from our lab has continued to assess this dependence. Lidocaine inactivation of the medial septum – the main cholinergic input to the MTL, essentially eliminated the hippocampal sink – source alternations related to theta and the SO (Wolansky et al., 2004). This effect could have been due to the inactivation of septal neurons or inactivation of other fibres *en passant*. Muscimol inactivation (which only affects cell bodies) of the medial septum revealed slow ~0.5Hz sink – source alternations in the HPC during the activated state (i.e., when LVFA dominated the neocortical LFP). During the deactivated state, the SO was apparent and unaffected in both the hippocampal CSD and neocortical LFP (Padamsey, Z. and Dickson, C.T., unpublished data). In addition, we have made extracellular recordings of single septal neurons. We found that their discharge properties were phasically related to both ongoing theta and SO activity in the HPC (Nummi, M., Clair, J., and Dickson, C.T., unpublished data). The ascending neuromodulatory inputs from the medial septum (including cholinergic projection neurons) may not be involved in the active generation of the hippocampal SO per se, but perhaps they play a role in coordinating activity throughout the HPC with other subcortical structures at SO frequencies. Further research is necessary to determine the role of the cholinergic (and other) ascending activating systems during the SO.

Coordination of the slow oscillation

Several preliminary experiments were performed in our lab prior to my work in *Chapters 3* and *4*. First, we eliminated the perforant path input to the HPC (i.e., from the supEC) by severing the angular bundle. Complete transection of the perforant path eliminated the SO in the HPC. Second, we delivered electrical stimulation to the perforant path to attempt phase reset of the theta and slow rhythms. The hippocampal theta rhythm was successfully reset but not the SO (Dickson et al., 2005). It is possible that SO phase reset failed because of the stimulation protocols were not appropriate.

We entrained the SO in the HPC using repeated 60s sweeps of low-amplitude and slow-frequency stimulation in *Chapter 4*. Delivering the same stimulation to the perforant path could potentially entrain and enhance the coordination of the hippocampal SO. It would be valuable to know whether low-amplitude slow-frequency stimulation across the surface of the fCTX, or directly to the mpfCTX, and/or NReu (*Chapter 4*) also entrains the SO in the EC. In addition, it would be of interest to assess whether stimulation of CA1 entrains the SO in the deepEC and/or whether stimulation of CA1 has any effect on activity in the supEC. Several series of stimulation and lesion experiments across the fCTX, mpfCTX, NReu, CA1, and EC may elucidate how this circuitry is bound during the SO and yield more clues towards the mechanisms of its coordination.

Functional relevance of the slow oscillation

Throughout my thesis I have alluded to the relationship between episodic memory and SWS. We cannot make any definite conclusions regarding the role that the hippocampal SO could play in episodic memory because we have not performed any behavioural experiments. We can however, generate theories of its role based on ours and others' findings. For instance: Molle et al. (2004) showed that coherence of the neocortical SO during SWS in humans increased following an episodic memory task. In *Chapters 2*, *3*, and *4* we assessed the coherence of the spontaneous and stimulation-enhanced SO across the nCTX, EC, and HPC. Our coherence measurements suggested that coordination between the nCTX and HPC existed during the spontaneous SO but also that this coordination was only moderate. Marshall et al. (2006) showed that using electrical stimulation to enhance the SO also enhanced performance on a hippocampal-dependent task. In *Chapter 4*, we assessed the effects of electrical stimulation on the SO and we found that power, rhythmicity, and coherence with the nCTX all increased. Therefore, we might reason that the stimulation-induced enhancement in entrainment and coordination of the hippocampal SO may be analogous to the occurrence of hippocampal-dependent learning. Any suppositions of this kind still need to be formally tested. However, it is interesting to postulate that enhancing slow oscillatory activity and its coordination within and across the nCTX and HPC could be a SWS-dependent electrophysiological mechanism for behavioural improvement on episodic memory tasks.

Key future directions

I have already mentioned several paths that my research could take in the future. As stated in the section entitled *"Underlying cellular mechanisms of the slow oscillation"*, the hippocampal SO as a network phenomenon has not been reported in hippocampal slices, in the isolated HPC, nor in the isolated whole brain. Whether it does not exist as a network phenomenon *in vitro* or whether the experiment has not been performed is not clear. It would be very interesting if the hippocampal SO could be observed as a network phenomenon *in vitro*. This would suggest that the HPC is capable of generating the SO independently of the nCTX.

The neuromodulatory inputs from the medial septum appear to modulate the hippocampal SO as opposed to be responsible for generating it. As stated in the section entitled *"Pharmacological modulation of the slow oscillation"*, the generation of the hippocampal SO does not appear to be dependent on cholinergic, glutamatergic, or fast GABAergic mechanisms. Stimulation of serotonergic fibres from the median raphé desynchronises the hippocampal LFP and median raphé lesions generate a state of constant theta. Serotonergic fibres from the median raphé pass through the medial septum on their way to the HPC (reviewed in: Vertes and Kocsis, 1997). It would be interesting to investigate the effects of serotonin and manipulations of the serotonergic ascending system on the hippocampal SO.

As a follow up to our data in *Chapter 4*, low-amplitude and slow-frequency stimulation of the perforant path or supEC may entrain the

hippocampal SO. As stated in the section entitled *"Coordination of the slow oscillation"*, it would be very useful to expand on our series of stimulation experiments. For instance, assessing the effects of stimulation in the fCTX, mpfCTX, or the NReu on the SO in the EC. With respect to the hippocampal output during the SO, it would be interesting if we could drive SO activity in the deep EC using low-amplitude, slow-frequency stimulation of CA1.

The temporoammonic path is the projection from entorhinal layer III to hippocampal SLM. Du and Schwarcz (1992) demonstrated that aminooxyacetic acid selectively lesions layer III neurons in the EC. Assessing the differences in spontaneous hippocampal (and entorhinal) SO activity with and without entorhinal layer III may also aid in our understanding of the mechanisms of SO coordination.

Ultimately, we need to determine whether the hippocampal SO is actually involved in the long-term consolidation of episodic mnemonic information. This would require several experiments. First, is hippocampal SO activity during SWS following training on a hippocampal-dependent task different from hippocampal SO activity during SWS prior to training? If it is different, do these differences coincide with any changes in behavioural performance on the task? Can we use low-amplitude, slow-frequency stimulation to enhance the hippocampal SO during natural sleep and simultaneously enhance behavioural performance?

Concluding statement

Based on the current literature, it seems very probable that the hippocampal SO will be significant in the field of hippocampal mnemonic information processing. Someone once asked me what it would mean if this turned out not to be the case. My reply was that the hippocampal SO and its dynamic coordination with the nCTX are very real phenomena in both the naturally-sleeping and urethane-anaesthetised animal. This in itself implies functionality. If that function is not hippocampal-dependent memory consolidation, then future research on sleep-related slow oscillations in the neocortical – entorhinal – hippocampal bidirectional circuit should proceed accordingly.

Conclusion References

Amaral DG, Witter MP (1989) The three-dimensional organization of the hippocampal formation: a review of anatomical data. Neurosci 31:571-591.

Buzsáki G (1998) Memory consolidation during sleep: a neurophysiological perspective. J Sleep Res 7 Suppl 1:17-23.

Crane JW, Windels F, Sah P (2009) Oscillations in the basolateral amygdala: aversive stimulation is state dependent and resets the oscillatory phase. J Neurophysiol.

Cunningham MO, Pervouchine DD, Racca C, Kopell NJ, Davies CH, Jones RS, Traub RD, Whittington MA (2006) Neuronal metabolism governs cortical network response state. Proc Natl Acad Sci U S A 103:5597-5601.

Dickson CT, Wolansky TD, Kerber JW (2005) Neocortical modulation of the hippocampal slow oscillation via the entorhinal cortex. In: Soc. Neurosci. Abstracts, Program # 275.273: Society for Neuroscience.

Dolorfo CL, Amaral DG (1998) Entorhinal cortex of the rat: organization of intrinsic connections. J Comp Neurol 398:49-82.

Du F, Schwarcz R (1992) Aminooxyacetic acid causes selective neuronal loss in layer III of the rat medial entorhinal cortex. Neurosci Lett 147:185-188.

Eichenbaum H (2000) A cortical-hippocampal system for declarative memory. Nat Rev Neurosci 1:41-50.

Finch DM, Babb TL (1980) Neurophysiology of the caudally directed hippocampal efferent system in the rat: projections to the subicular complex. Brain Res 197:11-26.

Finch DM, Babb TL (1981) Demonstration of caudally directed hippocampal efferents in the rat by intracellular injection of horseradish peroxidase. Brain Res 214:405-410.

Hahn TT, Sakmann B, Mehta MR (2006) Phase-locking of hippocampal interneurons' membrane potential to neocortical up-down states. Nat Neurosci 9:1359-1361.

Hahn TT, Sakmann B, Mehta MR (2007) Differential responses of hippocampal subfields to cortical up-down states. Proc Natl Acad Sci U S A 104:5169-5174.

Hasselmo ME (1999) Neuromodulation: acetylcholine and memory consolidation. Trends Cogn Sci 3:351-359.

Isomura Y, Sirota A, Ozen S, Montgomery S, Mizuseki K, Henze DA, Buzsaki G (2006) Integration and segregation of activity in entorhinal-hippocampal subregions by neocortical slow oscillations. Neuron 52:871-882.

Kloosterman F, Witter MP, Van Haeften T (2003) Topographical and laminar organization of subicular projections to the parahippocampal region of the rat. J Comp Neurol 455:156-171.

Kohler C (1986) Intrinsic connections of the retrohippocampal region in the rat brain. II. The medial entorhinal area. J Comp Neurol 246:149-169.

Kohler C (1988) Intrinsic connections of the retrohippocampal region in the rat brain. III. The lateral entorhinal area. J Comp Neurol 271:208-228.

Laurie DJ, Seeburg PH (1994) Regional and developmental heterogeneity in splicing of the rat brain NMDAR1 mRNA. J Neurosci 14:3180-3194.

Mahon S, Deniau JM, Charpier S (2001) Relationship between EEG potentials and intracellular activity of striatal and cortico-striatal neurons: an in vivo study under different anesthetics. Cereb Cortex 11:360-373.

Marshall L, Helgadottir H, Molle M, Born J (2006) Boosting slow oscillations during sleep potentiates memory. Nature 444:610-613.

Massimini M, Huber R, Ferrarelli F, Hill S, Tononi G (2004) The sleep slow oscillation as a traveling wave. J Neurosci 24:6862-6870.

Molle M, Marshall L, Gais S, Born J (2004) Learning increases human electroencephalographic coherence during subsequent slow sleep oscillations. Proc Natl Acad Sci U S A 101:13963-13968.

Moser MB, Moser EI (1998) Functional differentiation in the hippocampus. Hippocampus 8:608-619.

Murphy M, Riedner BA, Huber R, Massimini M, Ferrarelli F, Tononi G (2009) Source modeling sleep slow waves. Proc Natl Acad Sci U S A 106:1608-1613.

Naber PA, Lopes da Silva FH, Witter MP (2001) Reciprocal connections between the entorhinal cortex and hippocampal fields CA1 and the subiculum are in register with the projections from CA1 to the subiculum. Hippocampus 11:99-104.

Paternain AV, Herrera MT, Nieto MA, Lerma J (2000) GluR5 and GluR6 kainate receptor subunits coexist in hippocampal neurons and coassemble to form functional receptors. J Neurosci 20:196-205.

Peigneux P, Laureys S, Delbeuck X, Maquet P (2001) Sleeping brain, learning brain. The role of sleep for memory systems. Neuroreport 12:A111-124.

Rauchs G, Desgranges B, Foret J, Eustache F (2005) The relationships between memory systems and sleep stages. J Sleep Res 14:123-140.

Ribeiro S, Nicolelis MA (2004) Reverberation, storage, and postsynaptic propagation of memories during sleep. Learn Mem 11:686-696.

Sanchez-Vives MV, McCormick DA (2000) Cellular and network mechanisms of rhythmic recurrent activity in neocortex. Nat Neurosci 10: 1027-1034.

Scoville WB, Milner B (1957) Loss of recent memory after bilateral hippocampal lesions. J Neurol Neurosurg Psychiat 20:11-21.

Squire LR, Zola-Morgan S (1991) The medial temporal lobe memory system. Science 253:1380-1386.

Steriade M, Nunez A, Amzica F (1993a) A novel slow (< 1 Hz) oscillation of neocortical neurons in vivo: depolarizing and hyperpolarizing components. J Neurosci 13:3252-3265.

Steriade M, Nunez A, Amzica F (1993b) Intracellular analysis of relations between the slow (< 1 Hz) neocortical oscillation and other sleep rhythms of the electroencephalogram. J Neurosci 13:3266-3283.

Swanson LW, Cowan WM (1977) An autoradiographic study of the organization of the efferent connections of the hippocampal formation in the rat. J Comp Neurol 172:49-84.

Tononi G, Cirelli C (2001) Some considerations on sleep and neural plasticity. Arch Ital Biol 139:221-241.

Tseng KY, Kasanetz F, Kargieman L, Riquelme LA, Murer MG (2001) Cortical slow oscillatory activity is reflected in the membrane potential and spike trains of striatal neurons in rats with chronic nigrostriatal lesions. J Neurosci 21:6430-6439.

Tsukamoto-Yasui M, Sasaki T, Matsumoto W, Hasegawa A, Toyoda T, Usami A, Kubota Y, Ochiai T, Hori T, Matsuki N, Ikegaya Y (2007) Active hippocampal networks undergo spontaneous synaptic modification. PLoS ONE 2:e1250.

van Groen T, Wyss JM (1990) Extrinsic projections from area CA1 of the rat hippocampus: olfactory, cortical, subcortical, and bilateral hippocampal formation projections. J Comp Neurol 302:515-528.

Vertes RP, Kocsis B (1997) Brainstem-diencephalo-septohippocampal systems controlling the theta rhythm of the hippocampus. Neuroscience 81:893-926.

Walker MP, Stickgold R (2004) Sleep-dependent learning and memory consolidation. Neuron 44:121-133.

Werner P, Voigt M, Keinanen K, Wisden W, Seeburg PH (1991) Cloning of a putative high-affinity kainate receptor expressed predominantly in hippocampal CA3 cells. Nature 351:742-744.

Wisden W, Seeburg PH (1993) A complex mosaic of high-affinity kainate receptors in rat brain. J Neurosci 13:3582-3598.

Witter MP, Griffioen AW, Jorritsma-Byham B, Krijnen JLM (1988) Entorhinal projections to the hippocampal CA1 region in the rat: an underestimated pathway. Neurosci Lett 85:193-198.

Wolansky T, Clement EA, Peters SR, Palczak MA, Dickson CT (2006) Hippocampal slow oscillation: a novel EEG state and its coordination with ongoing neocortical activity. J Neurosci 26:6213-6229.

Wolansky, T., Clement, E.A., Richard, A.G., Ailon, J.I., Peters, S.R., Palczak, M.A., Dickson, C.T. (2004). Cholinergic coordination of the slow rhythm in neo-, and hippocampal cortices of the urethane-anaesthetized rat. In: Soc. Neurosci. Abstracts, Program # 932.2.